

Stochastic modeling of intracellular processes: Bidirectional transport and microtubule dynamics

Dissertation

zur Erlangung des Grades
des Doktors der Naturwissenschaften

der Naturwissenschaftlich-Technischen Fakultät II
- Physik und Mechatronik -
der Universität des Saarlandes

und

der Université Paris-Sud 11
École Doctorale de Physique de la Région Parisienne - ED 107

von

Maximilian Ebbinghaus

Saarbrücken
2010

Tag des Kolloquiums: 21.04.2011

Dekan: Univ.-Prof. Dr. Helmut Seidel

Mitglieder des
Prüfungsausschusses: Dr. Cécile Appert-Rolland
Ass.-Prof. Dr. Enrico Carlon
Prof. Dr. Martin R. Evans
Prof. Dr. Hendrik-Jan Hilhorst
Dr. Christian Hoffmann
Prof. Dr. Albrecht Ott
Prof. Dr. Ludger Santen

THÈSE

Présentée pour obtenir

LE GRADE DE DOCTEUR EN SCIENCES
Spécialité: Physique

DE L'UNIVERSITÉ PARIS-SUD 11
École Doctorale de Physique de la Région Parisienne - ED 107

et

DE LA NATURWISSENSCHAFTLICH-TECHNISCHE FAKULTÄT II
- Physik und Mechatronik -
UNIVERSITÄT DES SAARLANDES

par
Maximilian EBBINGHAUS

Stochastic modeling of intracellular processes: Bidirectional transport and microtubule dynamics

Soutenue le 21 avril 2011 devant la Commission d'examen:

Dr. Cécile Appert-Rolland	Directrice de thèse
Ass.-Prof. Dr. Enrico Carlon	Rapporteur
Prof. Dr. Martin R. Evans	Rapporteur
Prof. Dr. Hendrik-Jan Hilhorst	Examineur
Dr. Christian Hoffmann	Examineur
Prof. Dr. Albrecht Ott	Examineur
Prof. Dr. Ludger Santen	Directeur de thèse

Thèse préparée aux

Département de Physique Théorique
Université de la Sarre
Campus - Geb. E2 6
D-66123 Saarbrücken
ALLEMAGNE

et

Laboratoire de Physique Théorique (UMR 8627)
Université Paris-Sud 11
Bâtiment 210
F- 91405 Orsay CEDEX
FRANCE

Abstract

This thesis uses methods and models from non-equilibrium statistical physics to describe intracellular processes. Bidirectional microtubule-based transport within axons is modeled as a quasi-one-dimensional stochastic lattice gas with two particle species moving in opposite directions under mutual exclusion interaction. Generically occurring clusters of particles in current models for intracellular transport can be dissolved by additionally considering the dynamics of the transport lattice, i.e., the microtubule. An idealized model for the lattice dynamics is used to create a phase transition toward a homogenous state with efficient transport in both directions. In the thermodynamic limit, a steady state property of the dynamic lattice limits the maximal size of clusters. Lane formation mechanisms which are due to specific particle-particle interactions turn out to be very sensitive to the model assumptions. Furthermore, even if some particle-particle interaction is considered, taking the lattice dynamics into account almost always improves transport. Thus the lattice dynamics seems to be the key aspect in understanding how nature regulates intracellular traffic. The last part introduces a model for the dynamics of a microtubule which is limited in its growth by the cell boundary. The action of a rescue-enhancing protein which is added to the growing tip of a microtubule and then slowly dissociates leads to interesting aging effects which should be experimentally observable.

Keywords: stochastic modeling, non-equilibrium systems, intracellular transport, microtubule dynamics.

Kurzzusammenfassung

Diese Dissertation wendet Methoden aus dem Bereich der Statistischen Physik des Nichtgleichgewichts an, um intrazelluläre Prozesse zu beschreiben. Bidirektionaler Transport auf Mikrotubuli wird als quasi-eindimensionales stochastisches Gittergas mit zwei Teilchensorten modelliert, die sich unter Volumenausschluss in entgegengesetzte Richtung bewegen. In bisherigen Modellen für intrazellulären Transport kommt es zu Staubildung. Die Staus lösen sich jedoch auf, wenn die Dynamik des Gitters, also des Mikrotubulus, berücksichtigt wird. Ein vereinfachtes Modell für die Gitterdynamik wird verwendet, um einen Phasenübergang zu einem homogenen Zustand zu erzeugen, der effizienten Transport in beide Richtungen erlaubt. Im thermodynamischen Limit begrenzt eine Eigenschaft des stationären Zustands des Gitters die maximale Länge von Staus. Spurbildung kann durch zusätzliche Teilchen-Teilchen-Wechselwirkungen erreicht werden, erweist sich jedoch als sehr empfindlich hinsichtlich der Modellannahmen. Darüber hinaus ist der positive Effekt der Gitterdynamik auf den Transport immer vorhanden. Folglich scheint die Dynamik des Gitters für das Verständnis der Regulierung des intrazellulären Transports besonders wichtig zu sein. Im letzten Teil wird ein Modell für Mikrotubuli-Dynamik eingeführt. Die Wirkung eines *Rescue*-fördernden Proteins, das dynamisch an der Spitze eingebaut wird, führt zu interessanten Alterungsphänomenen, die experimentell beobachtbar sein sollten.

Stichworte: stochastische Modellierung, Nicht-Gleichgewichtssysteme, intrazellulärer Transport, Mikrotubuli-Dynamik.

Résumé

Dans cette thèse, des méthodes de la physique statistique hors équilibre sont utilisées pour décrire deux processus intracellulaires. Le transport bidirectionnel sur les microtubules est décrit à l'aide d'un gaz sur réseau stochastique quasi-unidimensionnel. Deux espèces de particules sautent dans des directions opposées en interagissant par exclusion. La présence habituelle d'accumulations de particules peut être supprimée en rajoutant la dynamique du réseau, c'est-à-dire de la microtubule. Un modèle simplifié pour la dynamique du réseau produit une transition de phase vers un état homogène avec un transport très efficace dans les deux directions. Dans la limite thermodynamique, une propriété de l'état stationnaire limite la longueur maximale des accumulations. La formation de voies peut être causée par des interactions entre particules. Néanmoins, ces mécanismes s'avèrent peu robustes face à une variation des paramètres du modèle. Dans presque tous les cas, la dynamique du réseau a un effet positif et bien plus important sur le transport que la formation de voies. Par conséquent, la dynamique du réseau semble un point-clé pour comprendre la régulation du transport intracellulaire. La dernière partie introduit un modèle pour la dynamique d'une microtubule sous l'action d'une protéine qui favorise les sauvetages. Des phénomènes intéressants de vieillissement apparaissent alors, et devraient être observables dans des expériences.

Mots-clés : modélisation stochastique, systèmes hors équilibre, transport intracellulaire, dynamique de microtubules.

Summary

In this thesis, we consider molecular motor-driven transport phenomena and microtubule dynamics which we examine by means of non-equilibrium stochastic modeling.

The first part deals with the efficiency of bidirectional transport in axons. Long-range transport within this quasi-one-dimensional geometry is carried out along a network of dynamic microtubules on which molecular motors move. Different species of molecular motors carry intracellular cargo in different directions. In addition to transport being hindered by encounters of oppositely moving motors on the same track, the geometry of the axon is extremely elongated and therefore diffusion as transport mechanism is very weak.

Models based on cellular automata have turned out to be relevant tools to model the unidirectional transport of molecular motors on microtubules, and have been successful in explaining some experimental *in vitro* results. However, attempts – including ours – to extend this class of models to (*in vivo*) bidirectional transport have faced robust difficulties. Macroscopic jams are formed, that prevent efficient transport as soon as the number of motors is large (which is the case for intracellular transport). Several mechanisms can be invoked that play a role in intracellular transport. However, at this stage, no clear picture emerges that would explain how bidirectional transport is regulated within living cells.

In order to contribute to this debate, we have considered a model that should retain some basic characteristics of axonal transport. It is derived from the totally asymmetric simple exclusion process with periodic boundary conditions and two species of particles which hop in opposite directions on a quasi-one-dimensional lattice, in this context called filament. All particles interact via hard-core exclusion such that position exchanges of oppositely moving particles can only happen through detachment of one of the particles from the filament and diffusion in the surroundings. The model is analyzed mostly by means of Monte Carlo simulations and mean field approximations.

First, it is argued by a comparison of the cluster properties of this basic model with those of a two-species zero-range process that systems with the characteristics mentioned above exhibit macroscopic clustering with vanishing current in the limit of infinite system sizes. The current is actually limited by the efficiency of diffusional processes around the cluster which become less and less efficient with increasing cluster size.

We have proposed that, as a remedy to this jam formation, the dynamics of the filament itself should be taken into account. It is shown that already a very simple and idealized lattice dynamics is able to dissolve the generically occurring macroscopic

clusters in finite systems. As a result of the dissolution of large clusters, the system undergoes a transition to a state with density-dependent current which is characterized by a homogenous distribution of particles throughout the system. The transition is also present in other classes of lattice dynamics and seems to rely on a finite lifetime of individual sites. The strength of lattice dynamics needed to bring the system into the homogenous state shifts positively with the system size. This could suggest that the transition would not be present in infinitely long systems. However, in the case of intracellular transport, only finite systems should be considered, meaning that such a transition could indeed take place.

Apart from biological motivations, this result is interesting also from the point of view of out-of-equilibrium statistical physics, as it points out a new type of dynamic transition. In this context, it is of interest to decide whether the transition survives in the thermodynamic limit. In spite of the above remark on the shift of the transition with the system size, cluster sizes are constrained by a different effect caused by the chosen lattice dynamics. By eliminating lattice sites, the lattice is cut into several segments on which clusters can form. The steady state distribution of segment lengths is exponentially decaying, leading to a characteristic length scale for the upper bound of the possible cluster lengths, independent of the considered total system size.

As a conclusion, though the lattice dynamics considered here are quite far idealizations from the real microtubule dynamics, we have illustrated a mechanism through which the microtubule dynamics could be an important ingredient to make bidirectional axonal transport efficient. Of course, some other mechanisms could also play a role, and we shall discuss some of them now.

As an alternative mechanism for efficient bidirectional transport, two qualitatively different particle-particle interactions are considered which eventually lead to lane formation: preferential adsorption and dynamical demixing. The first type, which was proposed by Klumpp and Lipowsky, has formerly been shown to lead to lane formation for strong enough attractive interactions between particles of the same species and repulsive interactions between particles of opposite species. The new result here is the discovery that the lane formation states cannot always be associated to efficient transport as they lead to excessive occupation of the transport lattice. Furthermore, lane formation vanishes if the diffusion rate in the surroundings of the lattice is taken to be finite.

The second type of particle-particle interaction describes particles that push against each other and drive an obstacle to a neighboring filament. This type of interaction is able to induce lane formation only if diffusion is not too strong. It is therefore qualitatively different from the first type of interaction as the demixing is driven by direct filament changes and not by different affinities for the attachment to the filament from the reservoir.

Both lane formation mechanisms are also combined with the simple lattice dynamics treated in the first part, showing that the lattice dynamics has a stronger influence on the transport capacity of the model than the additional particle-particle interactions. Additionally, the latter are heavily influenced by the lattice dynamics. While the affinity-driven lane formation is suppressed by a dynamic lattice, lane formation

caused by mutual sideward pushing of particles is enhanced.

Taken together, the results indicate the importance of considering the dynamics of the underlying microtubule network in models describing intracellular transport in confined geometries as it might dramatically change the system's behavior. As a challenge for future models, a more realistic model for the dynamics of the axonal microtubule network would have to be designed in order to get closer to a quantitative description of intracellular transport. However, to do so, some further experimental work would be required, as the picture of the microtubule network dynamics that can be obtained today is far from being complete. Some projects with experimental teams are currently being started in Saarbrücken in order to gain insight into this direction.

The last part of the thesis introduces a new model for the dynamics of microtubules in a non-circular model cell. The model assumes the macroscopically observed behavior of *dynamic instability* and combines it with a finite cell geometry and the action of a rescue-enhancing protein which is dynamically added to a growing plus end of the microtubule. By choosing parameters from experiments, the model achieves a good agreement with those experiments. It also shows that the combination of rescue-enhancing protein and confinement by the cell boundary leads to an increase of the microtubule tip distribution which is stronger than exponential close to the boundary. The strong influence of the boundary is furthermore represented by the quantitative and most notably qualitative differences in the distributions of some quantities such as the shortening lengths according to the cell geometry.

The most important result from the microtubule model is the appearance of aging. Dynamical inclusion of a rescue factor in growth phases and constant loss of the rescue factor at any time leads to a destabilization of the filament while it is in a paused state at the cell boundary. As a consequence, the filament has different survival probabilities depending on the number of times it came in contact with the cell boundary. This aging effect should be observable experimentally and thus shed some light on the plus-end tracking mechanisms of proteins of the +TIP family.

Zusammenfassung

Die vorliegende Dissertation wendet Methoden und Modelle der statistischen Physik des Nichtgleichgewichts auf intrazellulären Transport durch molekulare Motoren und Mikrotubuli-Dynamik an.

Im ersten Teil wird die Effizienz des bidirektionalen Transports in Axonen untersucht. Innerhalb dieser quasi-eindimensionalen Systeme wird Transport durch molekulare Motoren über große Distanzen entlang eines Netzwerks von dynamischen Mikrotubuli betrieben. Unterschiedliche Motorspezies transportieren dabei intrazelluläre Fracht in unterschiedliche Richtung. Der Transport wird einerseits durch Begegnungen von Motoren auf dem Filament behindert, die in unterschiedliche Richtungen wandern. Andererseits führt die extrem gestreckte Geometrie des Axons dazu, dass Diffusion als Transportmechanismus ausscheidet.

Auf zellulären Automaten basierende Modelle konnten als Werkzeuge für die Modellierung von unidirektionalem Transport durch molekulare Motoren auf Mikrotubuli eingesetzt werden und waren in der Lage, einige experimentelle *in vitro*-Ergebnisse zu erklären. Allerdings stießen Versuche – unsere eigenen eingeschlossen –, diese Modellklasse auf bidirektionalen Transport (*in vivo*) zu erweitern, auf hartnäckige Schwierigkeiten. Makroskopische Staus treten auf, die effizienten Transport unmöglich machen, sobald eine große Anzahl von molekularen Motoren im System ist (wie es für intrazellulären Transport der Fall ist). Verschiedene Mechanismen können in Betracht gezogen werden, eine Rolle für intrazellulären Transport zu spielen. Im Moment existiert jedoch kein klares Bild, das erklären könnte, wie bidirektionaler Transport in einer lebenden Zelle genau reguliert wird.

Diese Arbeit trägt zu dieser Diskussion bei, indem ein Modell behandelt wird, das die grundlegenden Eigenschaften von axonalem Transport aufweist. Das Modell ist eine Weiterentwicklung des total asymmetrischen simplen Exklusionsprozesses (TASEP) mit periodischen Randbedingungen und zwei Teilchenspezies, die in entgegengesetzte Richtungen auf einem quasi-eindimensionalen Gitter (hier: Filament) hüpfen. Alle Teilchen interagieren über Volumenausschluss, sodass ein Platztausch von Teilchen mit entgegengesetzter Vorzugsrichtung nur möglich ist, wenn sich ein Teilchen vom Filament löst und in der Umgebung diffundiert.

Zunächst werden durch einen Vergleich der Stauereigenschaften dieses grundlegenden Modells mit denen eines Zero-Range-Prozesses mit zwei Spezies starke Indizien dafür gesammelt, dass Systeme mit den oben genannten Eigenschaften tatsächlich makroskopische Staubildung aufweisen mit verschwindendem Teilchenstrom für unendlich große Systeme. Der Teilchenstrom wird durch die Effizienz von Diffusionsprozessen um den Stau herum begrenzt. Diese Diffusionsprozesse werden umso ineffizienter, je länger der Stau auf dem Filament ist.

Als Lösung für das Stauprobblem wird vorgeschlagen, dass die Dynamik des Gitters mit in das Modell integriert werden muss. Es wird gezeigt, dass eine vereinfachte und idealisierte Gitterdynamik in der Lage ist, die generisch auftretenden Staus in endlichen System aufzulösen. In der Folge zeigt das System einen Phasenübergang zu einem Zustand mit dichteabhängigem Strom, der durch eine gleichmäßige Verteilung der Teilchen über das gesamte System charakterisiert wird. Dieser Übergang kann für unterschiedliche Arten von Gitterdynamik beobachtet werden und scheint von der endlichen Lebensdauer eines Bindungsplatzes auf dem Filament abzuhängen. Die Stärke der Gitterdynamik, bei der der Übergang stattfindet, verschiebt sich für größere System zu höheren Werten. Dies könnte darauf hinweisen, dass der Übergang in unendlich langen System nicht stattfindet. Für die Anwendung auf intrazellulären Transport ist eine Einschränkung auf endliche Systeme angebracht, sodass der Übergang im realen System in der Tat stattfinden könnte.

Abgesehen von der biologischen Motivation ist dies auch ein interessantes Ergebnis für die statistische Physik des Nichtgleichgewichts, da es eine neue Art eines dynamischen Phasenübergangs aufdeckt. In diesem Zusammenhang ist es interessant zu bestimmen, ob der Übergang im thermodynamischen Grenzwert noch existiert. Auch wenn der Übergang sich für größere Systeme verschiebt, sind die Staulängen im unendlichen System dennoch begrenzt, allerdings durch einen anderen Effekt, der durch die gewählte Gitterdynamik verursacht wird. Durch das Eliminieren von Bindungsplätzen wird das Gitter in Segmente unterteilt, auf denen sich Staus bilden können. Die stationäre Verteilung der Segmentlängen fällt exponentiell schnell ab, sodass es eine charakteristische Längenskala gibt, die eine obere Grenze für die möglichen Staulängen darstellt. Diese Längenskala ist unabhängig von der betrachteten Systemgröße.

Zusammenfassend wird festgestellt, dass der vorgestellte Mechanismus durchaus in der Lage ist, über die Dynamik von Mikrotubuli den bidirektionalen Transport in Axonen effizient zu machen, auch wenn die betrachtete Gitterdynamik eine starke Idealisierung der tatsächlichen Mikrotubuli-Dynamik ist. Natürlich könnten auch noch andere Mechanismen eine Rolle spielen, von denen einige jetzt vorgestellt werden.

Als alternativen Mechanismus für bidirektionalen Transport werden zwei qualitativ unterschiedliche Teilchen-Teilchen-Wechselwirkungen untersucht, die zu Spurbildung führen können: präferentielle Adsorption und dynamische Entmischung. Die erste Ausführung wurde von Klumpp und Lipowsky vorgeschlagen. Von ihnen wurde bereits gezeigt, dass Spurbildung für starke attraktive Wechselwirkungen zwischen Teilchen der gleichen Spezies und repulsive Wechselwirkungen für Teilchen unterschiedlicher Spezies tatsächlich zu Spurbildung führt. Als neues Ergebnis wird hier dargestellt, dass diese Zustände mit Spurbildung nicht immer mit effizientem Transport assoziiert werden können, da sie zu exzessiv hohen Dichten auf dem Filament führen. Darüber hinaus verschwindet jedwede Spurbildung, wenn die Diffusionsrate im Reservoir nicht unendlich ist.

Die zweite Ausführung von Teilchen-Teilchen-Wechselwirkungen beschreibt gegeneinander schiebende Teilchen. Durch sterische Wechselwirkungen ist es dann

möglich, ein Teilchen der anderen Spezies auf ein benachbartes Filament zu schieben. Diese Art der Wechselwirkung kann Spurbildung induzieren, allerdings nur wenn die Diffusionsrate nicht zu hoch ist. Der Mechanismus ist folglich qualitativ anders als der erste, da die Entmischung durch direkte Filamentwechsel stattfindet und nicht durch veränderte lokale Affinitäten zum Filament.

Beide Spurbildungsmechanismen werden ebenfalls mit der einfachen Gitterdynamik kombiniert, die im ersten Teil der Dissertation behandelt wurde. Es zeigt sich, dass die Gitterdynamik die Transportkapazität stärker beeinflusst als die obigen Teilchen-Teilchen-Wechselwirkungen. Außerdem werden Letztere in ihrer Wirkung selbst stark beeinflusst durch die Gitterdynamik. Während die affinitätsgetriebene Spurbildung von einem dynamischen Gitter unterdrückt wird, wird Spurbildung durch Ausweichen auf benachbarte Filamente sogar verstärkt.

Insgesamt ergibt sich, dass die Berücksichtigung der Gitterdynamik von großer Wichtigkeit für die Beschreibung intrazellulären Transports in beschränkten Geometrien ist, da die Gitterdynamik das Verhalten des Systems in dramatischer Weise verändern kann. Zukünftige Modelle müssten also eine realistischere Beschreibung des axonalen Mikrotubuli-Netzwerks beinhalten, um einer quantitativen Beschreibung des intrazellulären Transport näher zu kommen. Um dies zu erreichen, bedarf es weiterer experimenteller Anstrengungen, da das derzeitige Verständnis des Mikrotubuli-Netzwerks noch lange nicht als vollständig angesehen werden kann. Einige Projekte mit Experimentatoren in Saarbrücken befinden sich gerade in der Anlaufphase und werden zu einem besseren Verständnis in dieser Richtung führen.

Der letzte Teil der Dissertation führt ein neues Modell für Mikrotubuli-Dynamik in einer Modellzelle ein. Das Modell basiert auf dem makroskopischen Phänomen der *dynamischen Instabilität*, das mit einer beschränkten Zellgeometrie und der Wirkung eines *Rescue*-fördernden Proteins kombiniert wird. Letzteres wird dynamisch an wachsenden Enden von Mikrotubuli in diese eingebaut und dissoziiert schließlich. Mit Parametern aus experimentellen Daten erreicht das Modell eine gute Übereinstimmung mit ebendiesen Experimenten. Die Kombination des *Rescue*-fördernden Proteins mit der Beschränkung durch die Zellgeometrie führt zu einem Anstieg der Verteilung der Mikrotubuli-Spitzen in der Nähe des Zellrands, der stärker als exponentiell ist. Der starke Einfluss des Zellrands drückt sich außerdem in quantitativen und, vor allem, qualitativen Unterschieden in den Verteilungen einiger Größen aus wie zum Beispiel der Schrumpflängen.

Das wichtigste Ergebnis des Mikrotubuli-Modells ist das Auftreten von Alterung. Das dynamische Hinzufügen des *Rescue*-fördernden Proteins in Wachstumsphasen und dessen permanente Dissoziation vom Filament führen zu einer Destabilisierung des Filaments, wenn es am Zellrand pausiert. Dies führt dazu, dass das Filament unterschiedliche Überlebenswahrscheinlichkeiten hat, die davon abhängen, wie oft das Filament bereits Kontakt mit dem Zellrand hatte. Dieser Alterungseffekt sollte auch experimentell beobachtbar sein und somit dazu beitragen, die Frage zu klären, durch welchen Mechanismus Proteine der +TIP-Familie in der Lage sind, das Ende von Mikrotubuli zu finden.

Résumé substantiel

Dans cette thèse, nous considérons des phénomènes de transport par des moteurs moléculaires et la dynamique de microtubules. Les deux processus sont examinés à l'aide de modèles stochastiques hors équilibre.

La première partie considère l'efficacité du transport bidirectionnel dans les axones. Dans cette géométrie quasi-unidimensionnelle, le transport sur des longues distances est effectué par des moteurs moléculaires le long de microtubules dynamiques. Différentes espèces de moteurs moléculaires portent des cargos intracellulaires dans des directions différentes. Le transport n'est pas seulement encombré par la rencontre de moteurs qui bougent préférentiellement dans des directions opposées sur la même voie, mais la géométrie de l'axone est également très élonguée de sorte que la diffusion ne représente qu'un moyen de transport peu efficace.

Des modèles basés sur des automates cellulaires se sont avérés utiles pour la modélisation de transport unidirectionnel de moteurs moléculaires sur des microtubules. Ils ont également réussi à expliquer certains résultats expérimentaux *in vitro*. Cependant, les tentatives entreprises – la nôtre incluse – entreprises pour étendre cette classe de modèles à la description du transport bidirectionnel (*in vivo*) se sont heurtées à de sérieux problèmes. En fait, des embouteillages macroscopiques de particules se forment sur le filament, empêchant un transport efficace aussitôt qu'il y a un nombre considérable de moteurs dans le système (comme c'est le cas pour le transport intracellulaire). Plusieurs mécanismes ont été invoqués pour jouer un rôle dans le transport intracellulaire. Il n'y a toutefois pas d'image nette à présent qui permettrait d'expliquer comment le transport bidirectionnel s'effectue au sein d'une cellule vivante.

Pour contribuer à cette discussion, nous avons considéré un modèle qui comprend les propriétés de base du transport axonal. Le modèle est dérivé du processus d'exclusion simple totalement asymétrique (TASEP) avec des conditions aux bords périodiques et deux espèces de particules qui sautent dans des directions opposées sur un réseau quasi-unidimensionnel qu'on appelle filament dans ce contexte. Toutes les particules interagissent par exclusion de volume de sorte que des échanges de positions de deux particules sur le filament ne se fait que par détachement d'une des particules du filament, avec diffusion subséquente dans les environs.

D'abord, on montre que des systèmes avec les propriétés mentionnées ci-dessus présentent une formation d'embouteillages macroscopiques avec un courant qui tend vers zéro pour des systèmes de taille infinie. Ce résultat s'obtient par une comparaison des propriétés des embouteillages dans notre modèle avec ceux du processus zéro-range (ZRP) à deux espèces de particules. Le courant dans notre modèle est limité par l'efficacité de la diffusion autour d'un embouteillage. Celle-ci diminue avec une taille croissante de ce dernier.

Pour remédier à cette formation d'embouteillages, nous avons proposé que la dynamique du filament devrait aussi être incluse dans le modèle. On montre qu'une dynamique du réseau idéalisée peut, dans les systèmes finis, dissoudre les embouteillages macroscopiques qui apparaissent génériquement. Comme résultat, le système présente une transition de phase vers un état avec un courant qui ne dépend que de la densité de particules et qui est caractérisé par une distribution homogène de particules à travers tout le système. La transition est également présente pour d'autres types de dynamique du réseau et semble reposer sur un temps de vie fini de sites individuels du filament. L'amplitude de la dynamique du réseau qui est nécessaire pour arriver à la transition devient de plus en plus grande avec une taille croissante du système. Ceci pourrait suggérer que la transition ne serait pas existante dans des systèmes de taille infinie. Le transport intracellulaire a cependant lieu dans des systèmes finis, impliquant que la transition proposée pourrait réellement exister.

Au delà de la motivation biologique, le résultat est aussi intéressant du point de vue de la physique statistique hors équilibre, car il met en jeu une nouvelle sorte de transition dynamique. Dans ce contexte, il est d'intérêt de décider si la transition existe aussi dans la limite thermodynamique. Malgré la remarque sur le déplacement de la transition avec la taille du système, les tailles des embouteillages sont bornées par un effet différent qui est causé par la dynamique du réseau choisie. En éliminant des sites du réseau, on coupe le réseau en plusieurs segments sur lesquels les embouteillages peuvent se former. La distribution stationnaire des longueurs de segments décroît exponentiellement, impliquant une longueur caractéristique qui sert comme borne supérieure pour les longueurs possibles des embouteillages et qui est indépendant de la taille du système.

En conclusion, bien que la dynamique du réseau qu'on considère ici soit une idéalisation de la vraie dynamique des microtubules, nous avons présenté un mécanisme par lequel la dynamique des microtubules pourrait jouer un rôle important en rendant le transport bidirectionnel dans les axones efficace. Bien sûr, d'autres mécanismes peuvent également y contribuer et nous allons brièvement exposer ci-dessous les résultats détaillés dans le présent manuscrit.

Comme mécanismes alternatifs pour du transport bidirectionnel efficace, l'adsorption préférentielle et la ségrégation dynamique sont considérées par deux sortes d'interactions entre particules. Les deux interactions ont en commun qu'elles peuvent mener à la formation de voies. Le premier choix a été introduit par Klumpp et Lipowsky et il a été montré qu'il mène à la formation de voies pour une interaction attractive assez forte entre particules de même espèce et répulsive entre particules d'espèces différentes. Le résultat nouveau décrit ici est que les états avec une formation de voies ne peuvent pas nécessairement être associés à du transport efficace puisqu'ils exposent une densité excessive de particules sur le filament. De plus, la formation de voies disparaît si le taux de diffusion dans le réservoir n'est pas infini.

Le deuxième choix d'interactions décrit des particules d'espèces différentes qui exercent des forces l'une sur l'autre et réussissent éventuellement pousser une particule sur un filament adjacent. Ce type d'interaction induit la formation de voies seulement si la diffusion n'est pas trop forte. Par conséquent, il est qualitativement

différent du premier choix : l'organisation spontanée se fait par des changements de filaments et non pas par une modification locale d'affinité pour le filament.

Les deux mécanismes sont examinés simultanément avec la dynamique du réseau simple de la première partie. Les résultats montrent que la dynamique du réseau a une influence plus importante sur le transport que les interactions supplémentaires entre particules. En outre, ces dernières sont affectées gravement par la dynamique du réseau. La formation de voies reposant sur la modification de l'affinité est supprimée par un réseau dynamique, tandis que la formation de voies par des changements de filaments induits est même favorisée par un réseau dynamique.

En résumé, ces résultats indiquent l'importance de considérer la dynamique du réseau de microtubules parce que la dynamique peut modifier le comportement du système d'une manière dramatique. Dans des modèles futurs, une représentation plus réaliste de la dynamique du réseau de microtubules axonales sera essentielle pour s'approcher d'une description quantitative du transport intracellulaire. Plus de travail expérimental sera également indispensable pour affiner l'image actuelle de la dynamique des microtubules, loin d'être complète à l'heure actuelle. Des projets de collaboration avec des groupes expérimentaux à Sarrebruck visent à combler ces lacunes et à améliorer la compréhension mutuelle de ces mécanismes.

La dernière partie de cette thèse introduit un nouveau modèle pour la dynamique des microtubules dans une cellule non-circulaire. Le modèle prend comme hypothèse l'observation macroscopique de l'*instabilité dynamique* et la combine avec une géométrie finie de la cellule ainsi que l'action d'une protéine qui favorise les sauvetages et est rajoutée au filament au bout d'une microtubule dans des phases de croissance. En choisissant des paramètres en fonction des données expérimentales, le modèle reproduit certains résultats de ces expériences d'une manière satisfaisante. De plus, la combinaison d'une protéine qui favorise les sauvetages avec du confinement par le bord de la cellule cause un accroissement de la distribution des bouts de microtubules proche du bord de la cellule qui est plus fort qu'une exponentielle. L'influence prononcée du bord de la cellule se reflète aussi par les différences quantitatives et surtout qualitatives dans les distributions de certaines quantités comme par exemple les longueurs de raccourcissement.

Le résultat le plus important de ce modèle de microtubules est l'apparence de vieillissement. L'inclusion dynamique d'une protéine favorisant les sauvetages pendant la croissance de la microtubule et la perte continue de cette protéine causent une déstabilisation du filament lorsqu'il est arrêté en bord de cellule. Par conséquent, les probabilités de survie d'un filament dépend du nombre de contacts que ce filament a eu avec le bord de la cellule. Cet effet de vieillissement devrait être observable expérimentalement et pourrait ainsi contribuer à la compréhension des mécanismes par lesquels les protéines de la famille des +TIP trouvent l'extrémité des microtubules.

Contents

Nomenclature	29
List of Figures	31
List of Tables	33
1 Introduction	35
2 Biological background	39
2.1 Chapter introduction	39
2.2 Microtubules	39
2.2.1 Structure	39
2.2.2 Dynamics	40
2.2.3 Cytoskeletal interactions (MAPs)	43
2.3 Molecular motors	45
2.3.1 Kinesin	45
2.3.2 Dynein	47
2.3.3 Transport by multiple motors	47
2.4 The axon	49
2.4.1 Axonal microtubule network	49
2.4.2 Axonal transport and neuronal diseases	51
2.5 Chapter summary	52
3 State of the art in modeling intracellular transport	53
3.1 Chapter introduction	53
3.1.1 Modeling stochastic systems	53
3.1.2 Stochastic lattice gases for modeling of intracellular transport	55
3.2 Unidirectional transport	56
3.2.1 Totally asymmetric simple exclusion process (TASEP)	56
3.2.2 TASEP with finite resources	60
3.2.3 Bulk reservoir with infinite diffusion rates	61
3.2.4 Bulk reservoir with finite diffusion rates	64
3.2.5 Defects	67
3.3 Bidirectional transport	68
3.3.1 Site-exchange models	69
3.3.2 Multi-lane models	72
3.4 Chapter summary	78

4	Efficient transport in intracellular transport models I – Lattice dynamics	79
4.1	Chapter introduction	79
4.1.1	Basic model	79
4.1.2	Simulation method	80
4.2	Macroscopic clustering	82
4.2.1	Previous results	82
4.2.2	General idea	83
4.2.3	Numerical data	84
4.2.4	ZRP hopping rates	86
4.2.5	Condensation criterion	87
4.2.6	Discussion	90
4.3	Transport on a dynamic lattice	91
4.3.1	Motivation	91
4.3.2	Model definition	91
4.3.3	Phase transition to a homogenous state	93
4.3.4	Constraints on maximum cluster lengths	98
4.3.5	Different lattice dynamics	107
4.3.6	Discussion	108
4.4	Chapter conclusion	108
5	Efficient transport in intracellular transport models II – Lane formation	111
5.1	Chapter introduction	111
5.2	Attractive/repulsive particle-particle interactions	112
5.2.1	Model definition	112
5.2.2	Static lattice	113
5.2.3	Dynamic lattice	118
5.2.4	Summary	120
5.3	Lane change through steric interactions	121
5.3.1	Model definition	121
5.3.2	Static lattice	122
5.3.3	Dynamic lattice	123
5.3.4	Summary	128
5.4	Chapter conclusion	128
6	Modeling of microtubule dynamics	131
6.1	Chapter introduction	131
6.2	Existing models	131
6.2.1	Two-state model	132
6.2.2	Length regulation	133
6.2.3	GTP cap	134
6.3	Theoretical modeling of aging effects in microtubule dynamics	135
6.3.1	Motivation	135
6.3.2	Model	136
6.3.3	Methods	139

6.3.4	Choice of parameters	140
6.3.5	Steady state solution without +TIPs	140
6.3.6	Simulation results	142
6.4	Chapter conclusion	147
7	Conclusion & Outlook	151
A	Dynamics of maximum cluster lengths	157
A.1	Rates of length change	157
A.1.1	Fusion of segments	157
A.1.2	Splitting of segments	158
A.2	Flux of probability mass	161
A.2.1	Flux towards higher lengths	161
A.2.2	Flux towards shorter lengths	162
A.2.3	Balance of fluxes	163
A.3	Survival times of segments	164
B	Simulated microtubule distribution on a real cell geometry	167
	Own publications	169
	Bibliography	171

Table des matières

Nomenclature	29
Liste des figures	31
Liste des tables	33
1 Introduction	35
2 Motivation biologique	39
2.1 Introduction du chapitre	39
2.2 Microtubules	39
2.2.1 Structure	39
2.2.2 Dynamique	40
2.2.3 Interactions du cytosquelette (MAPs)	43
2.3 Moteurs moléculaires	45
2.3.1 Kinésine	45
2.3.2 Dynéine	47
2.3.3 Transport par plusieurs moteurs	47
2.4 L'axone	49
2.4.1 Réseau axonal de microtubules	49
2.4.2 Transport axonal et maladies neuronales	51
2.5 Résumé du chapitre	52
3 État de l'art de la modélisation du transport intracellulaire	53
3.1 Introduction du chapitre	53
3.1.1 Modélisation de systèmes stochastiques	53
3.1.2 Gaz sur réseaux stochastiques pour la modélisation du transport intracellulaire	55
3.2 Transport unidirectionnel	56
3.2.1 Processus d'exclusion simple totalement asymétrique (TASEP)	56
3.2.2 TASEP avec ressources finies	60
3.2.3 Réservoir avec taux de diffusion infini	61
3.2.4 Réservoir avec taux de diffusion fini	64
3.2.5 Défauts	67
3.3 Transport bidirectionnel	68
3.3.1 Modèles avec échange de position	69
3.3.2 Modèles à plusieurs voies	72

3.4	Résumé du chapitre	78
4	Transport efficace dans des modèles de transport intracellulaire I – Dynamique du réseau	79
4.1	Introduction du chapitre	79
4.1.1	Modèle de base	79
4.1.2	Méthode de simulation	80
4.2	Embouteillages macroscopiques	82
4.2.1	Résultats préalables	82
4.2.2	Idée générale	83
4.2.3	Données numériques	84
4.2.4	Taux de saut du ZRP	86
4.2.5	Critère de condensation	87
4.2.6	Discussion	90
4.3	Transport sur un réseau dynamique	91
4.3.1	Motivation	91
4.3.2	Définition du modèle	91
4.3.3	Transition de phase vers un état homogène	93
4.3.4	Contraintes sur les longueurs maximales des embouteillages	98
4.3.5	Dynamiques alternatives du réseau	107
4.3.6	Discussion	108
4.4	Conclusion du chapitre	108
5	Transport efficace dans des modèles de transport intracellulaire II – Formation de voies	111
5.1	Introduction du chapitre	111
5.2	Interactions attractives/répulsives entre particules	112
5.2.1	Définition du modèle	112
5.2.2	Réseau statique	113
5.2.3	Réseau dynamique	118
5.2.4	Résumé	120
5.3	Changement de voie par interactions stériques	121
5.3.1	Définition du modèle	121
5.3.2	Réseau statique	122
5.3.3	Réseau dynamique	123
5.3.4	Résumé	126
5.4	Conclusion du chapitre	128
6	Modélisation de la dynamique des microtubules	131
6.1	Introduction du chapitre	131
6.2	Modèles existants	131
6.2.1	Modèles à deux états	132
6.2.2	Régulation des longueurs	133
6.2.3	GTP cap	134

6.3	Modélisation théorique des effets de vieillissement dans la dynamique de microtubules	135
6.3.1	Motivation	135
6.3.2	Modèle	136
6.3.3	Méthodes	139
6.3.4	Choix de paramètres	140
6.3.5	Solution de l'état stationnaire sans +TIPs	140
6.3.6	Résultats des simulations	142
6.4	Conclusion du chapitre	147
7	Conclusion & Perspectives	151
A	Dynamique des longueurs maximales d'embouteillages	157
A.1	Taux de changement de longueur	157
A.1.1	Fusion de segments	157
A.1.2	Séparation de segments	158
A.2	Courant de probabilité	161
A.2.1	Flux vers des longueurs plus grandes	161
A.2.2	Flux vers des longueurs plus petites	162
A.2.3	Équilibre des flux	163
A.3	Temps de survie des segments	164
B	Distribution de microtubules simulées dans une géométrie de cellule réelle	167
	Publications	169
	Bibliographie	171

Nomenclature

$\bar{\alpha}$	entrance rate (chapter 3)
α	probability of filament change in front of obstacle (chapter 5)
β	exit rate
Δt	time increment between subsequent steps
δ	MT subunit length
γTuRC	γ -tubulin-containing ring complex
\mathbf{q}, \mathbf{q}'	states of stochastic system
ν_c	MT catastrophe rate
ν_d	+TIP dissociation rate
ν_g	MT growth rate
ν_r	MT rescue rate
ν_s	MT shortening rate
ω	transition rate between states
ω_a	attachment rate
ω_d	detachment rate
ρ	density of particles per lattice unit
ρ_b	density of particles on the filament
ρ_{tot}	total density of particles (= number of particles divided by system length L)
ρ_u	density of particles in the reservoir
τ_i	occupation of site i (chapter 3)
$\tilde{\tau}_i$	state of lattice site i (chapter 4)
$\tilde{\nu}_r$	MT rescue rate in presence of a rescue-enhancing +TIP
a, b	half-axes of elliptical cell
b_i^\pm	occupation variable of site i of the filament for positive/negative particles
c_R	reservoir coupling rate
D	diffusion rate
J, J_b	current along lattice/filament
k_d	rate of site elimination
k_p	rate of site recreation
L	length of lattice
l	length of MT
l^*	maximum length of MT
L_{Cl}	length of cluster
m	magnetization of the filament
N^\pm	number of positive/negative particles

N_{Cl}	number of particles in largest cluster
p	forward hopping rate
$p_{\pm}(l, t)$	probability for MT to have length l and to be in growing/shrinking state at time t
p_{ind}	probability for boundary-induced catastrophe
q	strength of interaction
t	time
t_N	time of N -th contact between filament and cell boundary
$u(n, m), v(n, m)$	ZRP hopping rates for positive and negative particles
u_i^{\pm}	occupation variable of site i of the reservoir for positive/negative particles
+TIP	plus-end tracking protein
AAA	ATPases associated with diverse cellular activities
AD	Alzheimer's disease
ADP	adenosine diphosphate
ASEP	asymmetric simple exclusion process
ATP	adenosine triphosphate
CLIP-170	cytoplasmic linker protein-170
EB1	end-binding protein 1
GDP	guanosine diphosphate
GFP	green fluorescing protein
GTP	guanosine triphosphate
MAP	microtubule-associated protein
MC	Monte Carlo
MT	microtubule
MTOC	microtubule-organizing centre
TASEP	totally asymmetric simple exclusion process
ZRP	zero range process

List of Figures

2.1	Microtubule structure and dynamic instability.	41
2.2	Stepping cycle of kinesin.	46
2.3	Possible mechanisms for bidirectional transport.	48
2.4	Neuron and MT spacing by tau proteins in axons.	49
3.1	The TASEP with open boundary conditions.	57
3.2	Phase diagram and density profiles of the TASEP with open boundary conditions.	59
3.3	TASEP with Langmuir kinetics.	62
3.4	Model with explicit consideration of the bulk reservoir.	65
3.5	Two-species TASEP coupled to a diffusive lane.	74
3.6	Cluster properties of a two-species TASEP with a diffusive lane.	75
3.7	Average current in a two-species TASEP with a diffusive lane.	76
3.8	Particle-particle interactions in a two-species TASEP.	77
4.1	Domain current in the basic model.	83
4.2	Composition of largest cluster.	85
4.3	Positive particle current along the filament.	86
4.4	Dependence of the fitting parameters.	87
4.5	Basic model with additional lattice dynamics.	92
4.6	Cluster distribution and current with lattice dynamics.	94
4.7	Space-time plots on a static and a dynamic filament.	94
4.8	Comparison of the current of positive particles along the filament for static and dynamic lattices.	95
4.9	Comparison of the current of positive particles along the filament for static and dynamic lattices.	96
4.10	Time evolution of current along the filament.	97
4.11	Critical depolymerization rate $k_{d,crit}$ as a function of the system size L	98
4.12	Critical depolymerization rate $k_{d,crit}$ as a function of the system size L	99
4.13	Properties of the conditioned Bernoulli process.	103
4.14	Comparison of cluster length decay and maximum cluster length decay.	104
5.1	Space-time plots of the filament with a grand-canonical reservoir on a static filament.	114
5.2	Current along a static filament with a grand-canonical reservoir on a static filament.	114
5.3	Magnetization and current in the canonical setup with a static lattice.	116

5.4	Comparison of the current in a one-species TASEP and the current along the filament in the two-species system.	117
5.5	Phase diagram of a system with a canonical reservoir and a static lattice.	117
5.6	Sketch of the system with two filaments and explicit positions in the reservoir.	118
5.7	Magnetization and current in the setup with a finite diffusion rate and a static lattice.	119
5.8	Magnetization and current in the setup with an infinite diffusion rate and a dynamic lattice.	120
5.9	Lane changes through steric interactions.	122
5.10	Magnetization and current for ‘two obstacles’ lane changes.	124
5.11	Magnetization and current for ‘single obstacle’ interaction on a dynamic lattice.	125
5.12	Dependence of lane formation in ‘single obstacle’ scenario on the reservoir coupling.	126
5.13	Magnetization and current for ‘two obstacles’ interaction on a dynamic lattice.	127
6.1	Schematic representation of the MT model.	136
6.2	Life history plots with and without +TIPs.	142
6.3	Distributions of shortening lengths.	143
6.4	Histograms of the distribution of active plus ends.	144
6.5	Distribution of active plus ends.	144
6.6	Evolution of a filament.	146
6.7	Survival probability of an MT.	146
6.8	Survival probability of MTs with altered rescue factor dynamics.	148
A.1	Fusion of two adjacent segments.	158
A.2	Modification of a segment of length $L_1 = 3$	159
A.3	Modification of a segment of length $L_1 = 4$	160
A.4	Modification of a segment of length $L_1 \geq 5$	161
A.5	Comparison of characteristic segment lengths.	164
A.6	Time before shortening.	165
B.1	Approximation of real cell geometry.	167
B.2	Histograms of the distribution of active plus ends in a real cell geometry.	168
B.3	Distribution of active plus ends in a real cell geometry.	168

List of Tables

- 5.1 Overview of results for attractive/repulsive particle-particle interactions. 121
- 5.2 Overview of results for lane formation through direct filament changes. 127
- 6.1 Standard set of parameters derived from experimental data. 140

Chapter 1

Introduction

The fundamental unit of life, the cell, is a perfect example for a naturally arisen complex system. In the course of evolution, a large number of biochemical processes assembled forming the smallest of any living organisms' subunits. As evidenced by the immense diversity of life forms on earth, there exist more than one possible combination of these processes fulfilling the basic criteria for life such as reproduction and the existence of a metabolism [1]. The metabolism is the sum of processes which maintain the cell out of equilibrium or – to put it in the words of Erwin Schrödinger [2] – “It feeds on negative entropy.” In fact, reproduction involves the transmission of the genetic information stored in the cell's DNA and as is well known from thermodynamics, information transmission is impossible in thermal equilibrium implying that free energy must constantly be imported into the cell. Using the energy directly or indirectly derived from solar radiation to keep the cell in a non-equilibrium state therefore prevents an organism from dying.

The sizes of cells are typically in the micrometer range with eukaryotic cells being larger than prokaryotic ones. The larger size of eukaryotes comes along with a compartmentalization of the cell's interior with distinct organelles which have different functions. The spatially distant organelles have to be connected in order to create the complete metabolic chain [3]. This explains the presence of a cytoskeleton in almost all eucaryotes. The cytoplasm being rather crowded, diffusion turns out to be a highly inefficient medium for transportation. Instead, active intracellular transport of metabolic products is necessary. Molecular motors walk along filaments of the cytoskeleton while carrying intracellular cargo from the site of supply to the site of demand. This type of intracellular transport of metabolic products is crucial for the cell's survival and makes the spatial organization possible in the first place. This is all the more true as in this thesis, we are particularly interested in axonal transport, where axons have a quasi-one-dimensional structure with a dense microtubule network.

This thesis treats two components of this non-equilibrium intracellular transport machinery: the active transport by molecular motors along microtubules and the dynamics of microtubules. As mentioned above, the well-functioning of both is a necessary condition for the survival of the cell. Different diseases in multi-cellular organisms, amongst them humans, can be attributed to the failure of intracellular transport. Understanding how the transport works is thus a necessary precondition for understanding why it fails.

Apart from the obvious physiological interest, the out-of-equilibrium nature of intracellular transport provides a platform for studying interesting problems of statistical physics. While the well established Boltzmann-Gibbs formalism exists for equilibrium systems, there is nothing similar at hand for non-equilibrium systems. The treatment of these is therefore generally a challenging task leading to compelling non-trivial phenomena. The interest of statistical physics in intracellular processes is not restricted to intracellular transport but has also provoked work on other topics as for example gene expression [4,5], metabolic pathways [6,7] or the gel-like properties of the cytoskeleton [8]. These processes usually involve a great number of interactions, some of which still unknown, prohibiting a detailed modeling. Statistical physics provides tools that allow one to deal with aggregated information, hence rendering it particularly suited for the analysis of the aforementioned complex systems. Although a modeled description within the framework provided by statistical physics may not deliver a description in every detail, it achieves a high degree of agreement between model and experiment and has proven successful in identifying those elements most crucial for the system's behavior.

In this thesis, we are especially interested in the collective effects created by the motion of molecular motors which move along the same filaments and drive the intracellular transport. Some molecular motors move into one direction while others move in the opposite direction. This bidirectionality of long-range transport along microtubules creates frequent encounters of oppositely moving molecular motors. The obvious question in this context is how intracellular transport can be coordinated in order to maintain a stable and efficient transport in both directions instead of forming jams. This question is actually not limited to intracellular transport but always exists if agents moving in different directions have to use the same tracks, e.g., in crowds of people, car traffic or driven colloids. The convention to use only one side of a road significantly increases the efficiency of road traffic. Within the cell, however, such conventions between individual molecules are impossible and an efficient transport state has to come about by local interactions on the molecular scale. The most intuitive solution is the formation of lanes, leading to self-organized states with a high transport efficiency. It will be shown that this mechanism – which actually is not always so easy to enforce – is actually not the only solution to this problem.

As an alternative, we propose that a *dynamic* transport network is able to create efficient transport in opposite directions. Here, dynamic network means a constant remodeling of the network through a double process of creation and elimination of sites. Conceptually, this effect is all but intuitive if one thinks of moving on a path that can be altered at any instant. Intuition fails because of our tendency to consider the consequences of the dynamics of the transport network on a single motor. Indeed, the dynamics would have a negative effect on the efficiency of its displacement. The overall advantage comes into play when considering collective motion which is considerably modified by the network dynamics as will be seen. Our model is inspired by bidirectional transport within axons. These are extremely elongated and can therefore be suitably modeled by derivatives of the totally asymmetric simple exclusion process (TASEP), a model which serves as paradigm for non-equilibrium

systems. Despite an extremely simple structure, it is able to reproduce observable properties of microtubule-based transport. It will be shown in chapter 4 that, while a straightforward generalization of these models to bidirectional transport generically leads to jam formation, considering a dynamic lattice allows to inhibit jam formation and obtain efficient bidirectional transport by inducing a transition to a homogenous state with a stable current of motors.

As mentioned before, another efficient self-organized transport state that can be imagined would involve lane formation. Lanes could form due to appropriate local interactions which will be investigated in chapter 5. Here, the intuitive reasoning is mainly right when predicting efficient transport: If all molecular motors on one microtubule move in the same direction, there can be no blocking encounters of oppositely moving motors. One problem here is to identify the mechanisms which could induce lane formation. Intracellular transport is complex enough to imagine different possibilities to achieve this feature. The choice of interactions should therefore – as always – be guided by experimental facts. However, with microtubules being 25 nm wide and having binding sites for molecular motors with 8 nm spacing, the direct observation of the interactions between different components in intracellular transport for the moment remains experimentally inaccessible. In this thesis, we shall present two mechanisms leading to lane formation which are inspired by experimental facts though quite arbitrarily defined. Of course, they cannot be considered an exhaustive list of possible interactions, but rather as two specific examples among many other possibilities. However, these two examples will allow us to show that, first, not only the type and strength of the interaction is important to obtain lane formation, but also other features such as for example the amount of space available for diffusion around the microtubule. This could orient experiments in the future by indicating the most relevant questions that should be answered. Second, these examples will allow us to study how the effects of interactions and of network dynamics combine when both effects are present. Having established the improvement of the transport by the lattice dynamics, it will be shown that this dominates, and sometimes even enhances, the improvements caused by lane formation.

Our results have led us to an enhanced interest for the microtubule dynamics. Actually, though the microtubule dynamics is very likely an essential feature for motor transport, it also plays an essential role as part of the cytoskeleton, i.e., it sustains and adapts the shape of the cell. In the following, we shall consider microtubule networks in rounded cells and evidence some aging phenomenon (chapter 6). First, we recall that microtubule filaments exhibit *dynamic instability*, i.e., a stochastic switching between phases of growth and shrinkage. Furthermore, the microtubule cannot traverse the cell membrane, it therefore exists in a confined environment. Microtubules interact with a large number of proteins which influence their dynamics, thus allowing it to serve as track for intracellular transport and stabilize the cell shape by extended contacts with the cell membrane. At the same time the microtubule is dynamic enough to quickly adapt to a changing environment. In particular, phases of shrinkage are reduced by the presence of certain proteins which are added to the tip of the filament in growth phases. We show that the subtle interplay between this

dynamic inclusion and the stabilization of the filament leads to aging of the filament whenever it does not grow. It will also be shown that this sort of aging leads to prolonged lifetimes and to increasing number of contacts with the cell boundary, thus fulfilling both tasks addressed above. In addition, after some time it renders the filament unstable and thus provides it with the desired ability to collapse and re-grow.

Due to the non-equilibrium nature and the complexity of the models considered in this thesis, an exact treatment is out of reach. Most results rely on extensive Monte Carlo simulations, complemented by analytical results obtained in the frame of a mean field hypothesis.

The overall goal of this thesis is not to achieve a quantitative agreement between the presented models and experiments. Instead, we propose two qualitative mechanisms which we believe to be relevant for the living cell: 1. the improvement of intracellular transport due to the microtubule dynamics and 2. aging of microtubules at the cell boundary. Both features should be experimentally observable, and moreover have an important impact on the understanding of the corresponding intracellular processes. More refined models would be needed in order to confirm the relevance for intracellular traffic and to go beyond qualitative statements.

The rest of this thesis is organized as follows: In chapter 2, the current knowledge about intracellular transport will be presented from the perspective of molecular cell biology, referring to important experimental results which will form the boundary conditions of the modeling in the following chapters. The state of the art in modeling intracellular transport will be presented in chapter 3 with a focus on the evolution of the models from the simple unidirectional TASEP to the more complicated bidirectional transport model considered here. Chapter 3 will also contain an analysis of the jamming transition that occurs in such a bidirectional model. The transition toward an efficient transport state due to the lattice dynamics is presented in chapter 4. Chapter 5 reports on possible lane formation mechanisms and their interference with the lattice dynamics. A model for microtubule dynamics involving a dynamically included rescue factor is presented in chapter 6 with special attention paid to the aging behavior, before we conclude with chapter 7.

Chapter 2

Biological background

2.1 Chapter introduction

By reviewing relevant parts of the current knowledge on intracellular transport processes from the perspective of molecular cell biology, this second chapter aims at establishing the basis for the rest of the present thesis. This is accomplished by reviewing relevant parts of the current knowledge from molecular cell biology about intracellular transport processes. I will focus on those biological facts which are necessary to motivate the subsequent models and to understand the problems this thesis is attempting to solve. Therefore, I will not insist on experimental techniques but present generally accepted results.

First, I concentrate on the 'roads' along which long-range transport within cells is performed: Microtubules (MTs) are presented with their structure, dynamics and some of the microtubule-associated proteins (MAPs) which considerably influence the MT properties. The ensuing section is dedicated to the 'trucks', i.e., the molecular motors, dragging intracellular cargo such as organelles and vesicles along the MTs. After having introduced roads and trucks, the two are linked when taking a look at the transport network and defects which possibly lead to impeded traffic. The last part will be dedicated to the axon and its structure as well as the particular properties of intracellular transport in axons and its failure under given defects.

2.2 Microtubules

Microtubules are one of the three major components of the cytoskeleton in eukaryotic cells and play a role in multiple cellular processes [3]. For example, microtubules support the cell shape with their long filamentous structure and are therefore implied in cell motility. At the same time, the microtubule filaments serve as tracks for long-range transport by motor proteins which is the function most relevant for the models in this thesis.

2.2.1 Structure

Microtubules are polymers whose fundamental subunit is a α/β -tubulin heterodimer of 8 nm length [3]. The globular α - and β -tubulin molecules differ slightly but offer both a binding site for nucleotides. While α -tubulin always incorporates a non-

exchangeable guanosine triphosphate (GTP), β -tubulin might also take up guanosine diphosphate (GDP) [9]. These nucleotides have an influence on the dynamics of MTs (see section 2.2.2).

The tubulin dimers are able to spontaneously assemble along their long axis into protofilaments (figure 2.1 A). Usually twelve to fourteen of these protofilaments wrap into a helical cylinder of approximately 25 nm diameter [9] which is then called microtubule. The helical pitch adds up to 12 nm, resulting in an imperfect wrapping and a distinguishable seam in the surface lattice (figure 2.1 B).

Due to the asymmetry of the dimer subunit, MTs are locally polar but also as a whole in the sense that the two ends of the filament are chemically different and can therefore be distinguished. The common convention is to define the filament end which exposes β -tubulin to be the plus end of the MT.

2.2.2 Dynamics

Dynamic instability

Microtubules exhibit a characteristic dynamic behavior, termed *dynamic instability*, characterized by a stochastic switching between phases of persistent growth (= polymerization) or shrinkage (= depolymerization) [10]. A transition from growth to shrinkage is called *catastrophe* and a transition from shrinkage to growth is called *rescue*. *In vitro*, both transitions are independent from the time spent in the respective states [11]. Furthermore, the speed of depolymerization does not depend on the concentration of tubulin in solution, whereas the speed of polymerization on the other hand depends linearly on the amount of tubulin [11]. The rescue and catastrophe frequencies *in vivo* are usually rather low such that MTs exhibit persistent growth and shortening on the typical length scales of the cell diameter [12], thus increasing the influence of the cell boundary on the MT dynamics.

The plus and minus ends of microtubules obey different kinetics [13]. This is only of limited importance for *in vivo* systems, because the minus end of the MT is usually attached to a microtubule-organizing centre (MTOC) (see section 2.2.2), inhibiting any dynamics at the minus end. Even if MTs are not attached to the MTOC like in axons, the minus end is supposed to be stable (section 2.4.1). Hence, the very special dynamic regime of *treadmilling*¹ is mostly observed *in vitro* [12].

Growth at the plus end occurs in form of an open sheet structure to which single tubulin dimers or small oligomers are added (figure 2.1 C). Shrinking MTs have single protofilaments curling outward which peel off the filament and eventually detach from it. The existence of a third intermediate state has been hypothesized which corresponds to a pausing MT with a closed sheet at its plus end [9].

The MT dynamics is influenced by a wide range of microtubule-associated proteins (see section 2.2.3) and the nucleotide which is bound to the tubulin subunits near the plus end. Free tubulin dimers are included into the MT with GTP molecules bound to

¹A treadmilling filament polymerizes at its one end while it depolymerizes at the other, thus moving in one direction as a whole filament while every single subunit is immobile.

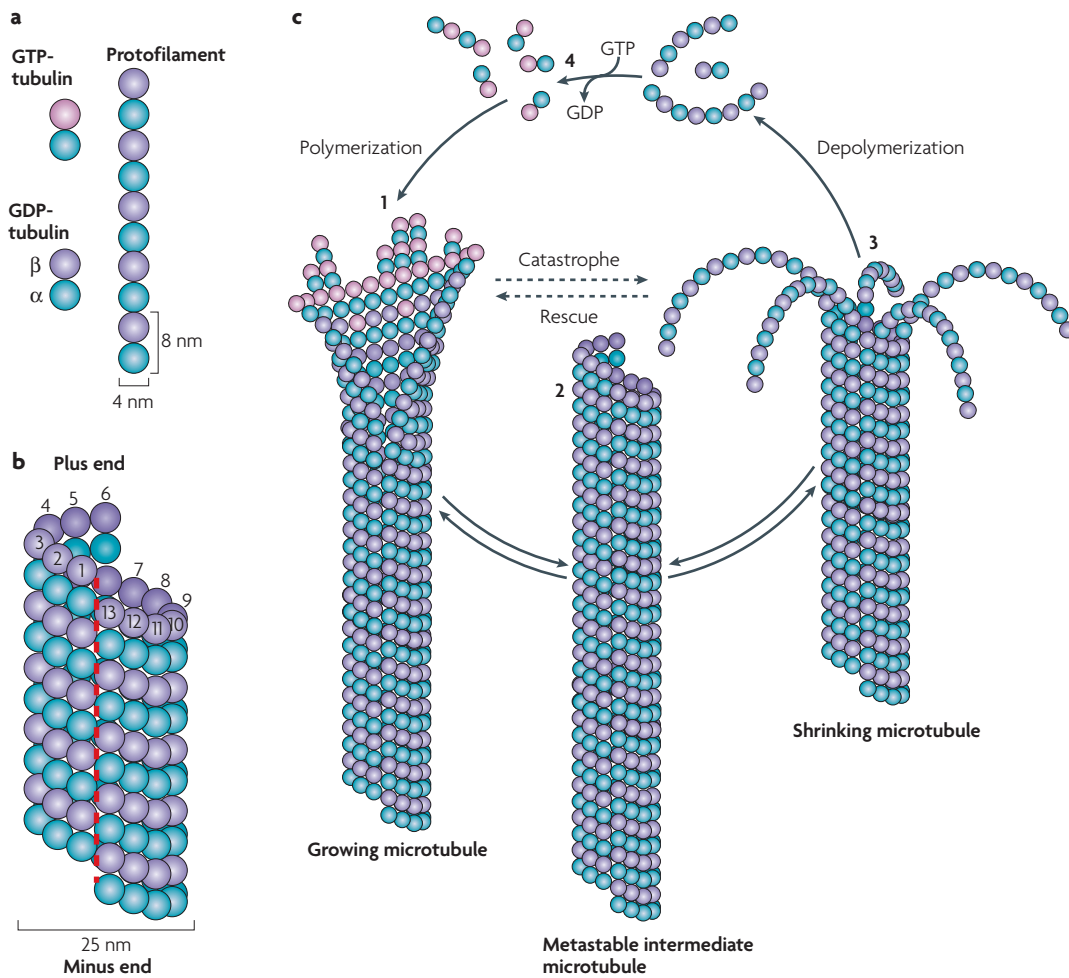


Figure 2.1: Microtubule structure and dynamic instability. (A) The α/β -tubulin heterodimers, either associated to GTP or GDP, assemble into protofilaments of 8 nm periodicity. (B) About thirteen protofilament helically wrap into a hollow cylinder. The helical pitch is 12 nm and therefore longer than the periodicity of the MT lattice in axial direction, resulting in a seam (red dashed line). (C) MTs switch between phases of growth and shrinkage. A transition from the polymerizing to the depolymerizing state is called *catastrophe* whereas the inverse transition is called *rescue*. 1. In the growing state, the plus end is in the form of an open sheet with GTP-bound tubulin at its end. At further growth, the MT closes along the seam and the GTP in the bulk of the lattice hydrolyzes to GDP. 2. The existence of a metastable state is possible in which the MT is completely closed and pauses. 3. The protofilaments have lost their lateral contacts at the plus ends and peel off. 4. Tubulin dimers or small oligomers have their GDP replaced by GTP in solution and are ready to be reincorporated into another growing MT. Reprinted by permission from Macmillan Publishers Ltd.: Nature Reviews Molecular Cell Biology 9:309–322, ©2008.

the α - and β -tubulin. The GTP bound to the β -tubulin then hydrolyzes to GDP after polymerization [14]. This process generically leads to a so-called *GTP cap* at the plus ends of growing MTs, i.e., a ring of dimers with GTP at both their α - and β -tubulin. The exact structure of the GTP cap as well as the conditions for GTP hydrolysis are unknown [15]. Furthermore, ‘islands’ of GTP can be found inside polymerized MTs *in vivo* [16]. This indicates that the stochastic process of GTP hydrolysis occurs on different time scales if the associated tubulin subunit is exposed at the plus end or if it is buried in the MT lattice.

The presence of GTP has been related to rescues of MT as well for the GTP cap [10] as for the GTP remnants inside the MT lattice [16]. The loss of the protecting GTP cap consequently leads to a destabilization of the MT. It is assumed that this is due to the more curved equilibrium conformation of the GDP-bound tubulin dimer [17]. In the bulk of the lattice, the curvature of GDP-tubulin can be compensated by the lateral bonds to the neighboring subunits, but when exposed at the end of the filament, the lateral bindings are not strong enough so that the protofilaments start to peel off (see figure 2.1).

Post-translational modifications² possibly also have an influence on the dynamics of MTs [19] although this is under debate [20]. The most likely scenario is that post-translational modifications lead to modified interactions with MAPs (see section 2.2.2) which then have an effect on MT dynamics [21]. Nevertheless, it is well established that younger MTs or the younger parts thereof are rich in tyrosine and much more dynamic than older detyrosinated MTs [22]. For the axons of rat sympathetic neurons, this is expressed by the very different half-lives of complete depolymerization for tyrosinated (5 minutes) and detyrosinated (240 minutes) MTs under the action of the MT destabilizing drug nocodazole [19]. The detyrosination does however seem to be rather a consequence of than the cause for the observed stabilization [20].

Nucleation

Microtubules are able to assemble spontaneously *in vitro* in the presence of soluble tubulin and GTP [23], but do so preferentially at a microtubule-organizing center (MTOC) such as centrosomes [24, 25]. A third tubulin subspecies, γ -tubulin, was shown to form a γ -tubulin-containing ring complex (γ TuRC) which is highly implicated in MT nucleation [26–28]. This complex is formed by approximately 13 γ -tubulin subunits which form a ring on the centrosome that has almost the same diameter as a MT. The ring is not completely closed but exhibits a helical pitch, which is also recovered in the polymerized MT structure (see section 2.2.1). Hundreds of γ TuRC are found on centrosomes *in vivo* where they cap the minus end of single MTs

²Post-translational modification is the term used for different types of chemical modification of a protein after its translation. This includes the attachment of further biochemical functional groups or structural changes, e.g., the formation of disulfide bridges. The removal of amino acids by enzymes or phosphorylation are also grouped in this class. All post-translational modifications have in common that they alter the chemical behavior of the protein and typically also the conformation. [18]

which nucleated from these ring complexes. They thus prevent the addition or loss of tubulin subunits at the minus end of nucleated MTs [28,29].

Release of MTs from the centrosome may occur in interphase, followed by depolymerization from the minus end as required in certain phases of the cell cycle [30]. A free minus end allows a MT to treadmill (see section 2.2.2) toward the cell membrane as has been observed *in vivo* in different cell types [12,31].

2.2.3 Cytoskeletal interactions (MAPs)

A large number of proteins interact with the MT and are consequently classed in the broad family of microtubule-associated proteins (MAPs). These MAPs are very diverse in structure and function and interact very differently with MTs. While some modify the dynamics of MTs, others do not exert an influence on the MTs but rather need the MT lattice to carry out their function. For the following chapters, only three sorts of MAPs will be of importance: Tau proteins and plus-end tracking proteins (+TIPs) will be presented in this section whereas molecular motors will be treated in section 2.3 because of their distinctive function for intracellular transport.

Tau and MAP2

Tau proteins and the related MAP2 proteins influence the MT dynamics as well as the dynamics of molecular motors and therefore have an important impact on intracellular transport. This is especially true in axons as the two proteins are very characteristic for neurons with tau being present in axons and MAP2 being tau's counterpart in the dendrites [32,33].

The structure of both proteins possesses a MT binding domain and a hydrophobic part which extends into the surrounding cytosol [34]. The MT binding domain is able to bind on the outside of the MT cylinder as well along as across protofilaments [35,36]. Tau binds in a phosphorylation-dependent way to MTs, i.e., it dissociates from the MT after phosphorylation and has a low affinity to tubulin in solution [37,38]. The hydrophobic parts of bound tau molecules are able to dimerize and in the consequence lead to bundling of MTs [39].

Tau furthermore has a stabilizing effect on MTs by modifying parameters of the dynamic instability of MTs [37]. In the presence of tau, the speed of polymerization is increased while that of depolymerization is decreased. Also, the frequency of catastrophes is lowered and the frequency of rescues is increased. *In vitro* grown MTs thus reach much higher maximum lengths as a consequence of the action of tau.

MTs in axons have been found to be particularly densely decorated by tau proteins at regions of high curvature, suggesting an influence of the mechanical properties [40]. It was also hypothesized that tau has a protective function for MTs against the action of the MT-severing protein katanin which forms a hexamer around the MT and uses the energy from ATP hydrolysis to break the filament [41].

+TIPs

Certain MAPs are able to track the (growing) plus ends of MTs, commonly referred to as plus-end tracking proteins (+TIPs). A non-negligible part of the research interest in +TIPs arises due to the fact that these proteins are highly conserved over large evolutionary distances and because of the question how the members of this protein class are able to find the end of the MT [9, 15, 42–45]. The following mechanisms for plus-end tracking are usually proposed in the literature [9]:

1. A +TIP might be able to bind to a specific structure at the plus end of MTs. Since a growing MT presents its lattice at the end as an open sheet (see figure 2.1), it is conceivable that interactions with MAPs are different in this part compared to the bulk of the MT lattice where the sheet has already closed.
2. In a very similar way to the previous mechanism, a +TIP might have a high affinity for a feature at the plus end but be nevertheless able to bind to the bulk of the MT lattice on which the +TIP performs two-dimensional diffusion until it arrives at the plus end.
3. Since several members of the kinesin protein family move on MTs to the plus end (see section 2.3.1), a +TIP could be carried by a kinesin to the plus end of the MT.
4. +TIPs might be added to the MT through a co-polymerization mechanism, i.e., tubulin dimers or oligomers associate in solution with the +TIP before these tubulin subunits are added to the filament.
5. Some +TIPs might themselves not be able to find the plus end but bind to another +TIP which is able to do so, a scenario which is termed *hitchhiking*.

Specific +TIPs have been found for each of these mechanisms and consequently, no single mechanism for plus-end tracking can be identified. The recognition of a specific structure at the plus end and the co-polymerization mechanism (scenarios 1 and 3) have in common that they lead to treadmilling of +TIPs: The +TIPs themselves do not move but are added at the tip and then released deeper down in the lattice without performing lateral motion.

Certain +TIPs have received particular attention, because of the experimental possibility to fuse them to green fluorescing protein (GFP) and hence visualize growing MTs. One prominent example is the cytoplasmic linker protein-170 (CLIP-170) which has been shown to increase the rescue frequency of MTs *in vivo* and therefore positively influence the average lifetime of MTs [46]. Later, it was shown that CLIP-170 is not capable of finding the MT plus end on its own but needs to be in a complex with end-binding protein 1 (EB1) which binds at high frequency to a binding site at the MT tip [47–51]. This binding site is added on MT polymerization and slowly decays as the MT lattice matures and thus reduces the binding of the CLIP-170-EB1 complex over time. The existence of the binding site has been linked to the GTP cap, the open sheet

structure or post-translational modifications such as detyrosination [15,43,45,52] but no clear picture so far emerges from the experimental evidence.

EB1 can find the MT tip independently of interactions with other +TIPs [48, 49] and is also acting positively on the lifetime of MTs by suppressing catastrophes *in vivo* [53]. Its effect on *in vitro* MT dynamics is in contrast to the *in vivo* results indicating a high number of interactions with other +TIPs which acquire their tracking capability due to the association with EB1.

The functions of other +TIPs can be found in numerous reviews [9, 15, 42–45] and will not be treated here as they are of minor importance for the remaining thesis.

2.3 Molecular motors

Molecular motors – also known as motor proteins – are molecules which are able to move along polar cytoskeletal filaments such as MTs or actin filaments by using the energy derived from hydrolysis of adenosine triphosphate (ATP). These proteins usually consist of at least two parts: the motor and the cargo domain. The motor domain is able to bind to the polar filament on which it can exert a directed force, the cargo domain binds to intracellular cargo such as organelles and vesicles or other elements of the cytoskeleton [3].

On large time scales, however, molecular motors perform random walks on a disordered MT network as they undergo cycles of directed motion along a filament and diffusion in the cytoplasm that surrounds the cytoskeleton while the motor is detached from the filament.

In the following, the two most important protein families for MT-based transport are presented, kinesins and dyneins. Both families are heterogenous in the sense that the cargo which they are able to carry as well as the type of motion along the filament varies within the same family despite similar structures of the motor domains.

2.3.1 Kinesin

The kinesin superfamily is subdivided into 14 families of kinesins which share an identical motor domain and therefore are all able to exert force on MTs [54]. Due to the different structure of the rest of the molecule, motion patterns vary: While most of the kinesins move toward the plus end of a MT, called anterograde movement, there are some motors which move in the opposite or retrograde direction. Also, many but not all kinesins perform *processive* motion, i.e., they go through multiple mechanochemical working cycles before detaching from the filament [55].

A representative member of the kinesin superfamily implicated in long-range transport is kinesin-1 (or conventional kinesin) which consists of two motor heads. The two motor heads are linked by a long neck to the cargo domain and step in an alternating hand-over-hand pattern on the MT [56]. The stepping is triggered by the hydrolysis of ATP (figure 2.2): An ATP-bound kinesin head has a high affinity to the MT lattice and binds strongly to it. When the ATP is hydrolyzed to adenosine

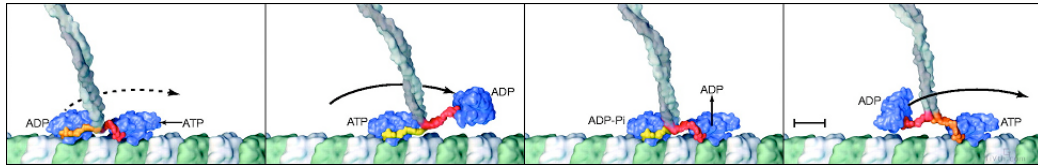


Figure 2.2: Stepping cycle of kinesin. From left to right: An ATP-bound head induces a conformational change which the other weakly-bound head containing ADP to the front. The ATP gets hydrolyzed to ADP and inorganic phosphate. After the release of the inorganic phosphate, the rear head unbinds from the filament and is brought to the front as soon as the other head exchanges its ADP by ATP. From R. D. Vale and R. A. Milligan, *The Way Things Move: Looking Under the Hood of Molecular Motor Proteins*, Science 288, 88–95, 2000. Reprinted with permission from AAAS and G. Johansson (fiVth media: www.fiVth.com).

diphosphate (ADP) and inorganic phosphate, the binding of that head gets weaker and the motor eventually detaches from the filament. Meanwhile, the other motor head was able to take up an ATP and bind to the MT, inducing a conformational change bringing the recently detached motor head to the front. As soon as this motor head replaces its ADP by ATP and re-attaches to the filament, the cycle starts over again. The step size of kinesin has been shown to be exactly one tubulin subunit, i.e., 8 nm [57].

Several of these cycles occur one after the other before detachment from the MT, leading to finite run lengths of this molecular motor along the MT between phases of diffusion in the cytosol. Typical run lengths are of the order of one hundred steps [58] which in combination with the step size of 8 nm gives runs of about 1 μm in length. This property of motion of some molecular motors is called *processivity* and is not affected by crowding of the filament, since it has been shown that kinesins stay tightly bound to the MT when being blocked by an obstacle [58]. Although the general direction of kinesin motion is along individual protofilaments [59], occasional side steps onto neighboring protofilaments of the same MT are possible [60, 61] and may even lead to bypassing of an obstacle in rare cases [62].

For conventional kinesin, there is evidence for a mutual attractive interaction between motor proteins, so that a kinesin preferentially binds to the MT in the vicinity of other kinesins [63–65]. The strength of the interaction between two kinesin-1 molecules has been estimated at $1.6 \pm 0.5 k_B T$ [65].

Since kinesins and tau proteins both bind on the outside of the MT cylinder, it is not unlikely that both proteins interfere with each other. In fact, it has been shown *in vitro* that kinesin's attachment to the MT is hindered by tau, whereas kinesin is not affected in its motion along the filament once it is bound, i.e., processivity and walking speeds are unaffected [66]. On the other hand, another study found that kinesin had a higher probability of detachment when encountering tau patches on the MT [67].

Other kinesins than kinesin-1 have been shown to be less implicated in intracellular

transport but to have an influence on the MT dynamics: For example, members of the kinesin-13 family are able to find the plus end of MTs (and are therefore considered as +TIPs [9]) where they destabilize MTs and promote depolymerization by using the energy from ATP hydrolysis to deform the MT lattice until it breaks [68–70].

2.3.2 Dynein

In contrast to the kinesin family, there is only a single cytoplasmic dynein carrying out most of the minus-end directed long-range transport along MTs. The attachment to the wide variety of different cargos is probably assured by different multifunctional adaptors such as dynactin which regulate dynein function [71]. The structure of cytoplasmic dynein is more complicated than those of kinesins which is also reflected in the very high molecular weight of 1.2 MDa [72]. The dynein head comprises six non-identical AAA (ATPases associated with diverse cellular activities) of which four are able to hydrolyze ATP and produce the necessary mechanical energy for motion. The binding to the MT is made by a stalk which stretches out from the head. The cargo is attached by a long tail pointing away from the MT in the bound state.

Dynein is able to perform processive motion if it is in dimerized form [73] and is then imagined to walk in a hand-over-hand mechanism with alternating steps of the two heads [74] similar to the motion of kinesin (section 2.3.1). The run lengths of the processive motion are of the order of 1 μm and thus comparable to those of kinesin [73,74]. However, step sizes of dynein can be multiples of the tubulin dimer length of 8 nm and depend on the load with higher forces leading to smaller steps, suggesting a sort of gear mechanism [75,76]. Single dynein motors mostly follow individual protofilaments on the MT surface but sometimes also exhibit non-directed diffusive motion on the whole two-dimensional MT lattice, therefore allowing the motor to change the protofilament [77,78]. The varying step size and the side steps have been hypothesized to allow the motor to bypass obstacles [79].

The binding site of dynein on the MT surface overlaps with the binding site of kinesin [80]. Both motor species thus compete for binding sites on the filament and probably block each other on encounters in bidirectional transport on MTs. The interaction with tau proteins are similar to those reported for kinesin: Run lengths are decreased at high concentrations of tau on the MT [66]. In contrast to kinesin, dynein does not detach at encounters of tau but tends to reverse direction, maybe by switching to the diffusive state of motion described above [67]. Altogether, dynein is much less affected by the presence of tau than kinesin is and is only seriously impeded in its motion at overexpression of tau [67,81].

2.3.3 Transport by multiple motors

Intracellular cargo such as organelles and vesicles are usually not transported by single molecular motors but instead have multiple motors attached to their surface. These motors bind individually to the MT [82,83]. Cooperative effects of the motor proteins are thus observable, leading to increased processivity of a transported cargo

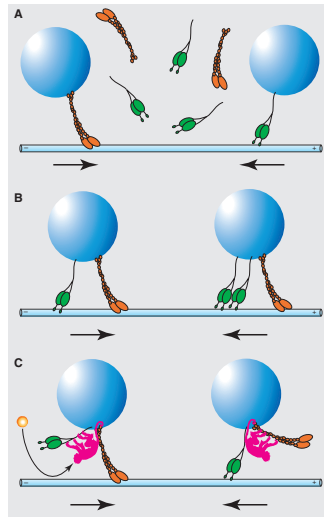


Figure 2.3: Possible mechanisms for bidirectional transport. Plus-end directed motors (orange) and minus-end directed motors (green) move a cargo (dark blue) along a MT (light blue). (A) A single motor species can be attached. (B) Tug-of-war of different motor species. (C) A coordination machinery determines moving direction. Reprinted from *Current Biology*, Vol. 14, M. A. Welte, *Bidirectional Transport along Microtubules*, R525–R537, ©2004, with permission from Elsevier.

and higher stalling forces than for individual motors which has been shown as well experimentally [84, 85] as in a theoretical model [86]. Cooperation between motors thus enhances long-range transport of individual cargos.

Different intracellular cargos have been observed to perform bidirectional motion [87]. For some, it was shown that the cargo motion involved two species of motors which move in opposite directions, e.g., in [88]. Different mechanisms of coordination are discussed to explain this type of motion (figure 2.3) [87]: A first scenario assumes a replacement of one motor species by the other on the cargo upon reversal of the direction, but this scenario could be ruled out for several systems [89]. In the second scenario, motors of both species are simultaneously attached to the cargo and pull on it, similar to a tug-of-war. The third mechanism involves a coordination machinery which turns off one motor species while activating the other on change of direction.

The tug-of-war is the most appealing scenario due to its simplicity and thanks to a theoretical investigation showing convincingly that such a simple mechanism is able to produce an efficient coordination between different teams of motors [90]. The motors reach in fact some sort of coordination by forcing the minority motor species to detach from the filament without the action of an external factor. Different states of motion can be obtained in this model by tuning the dynamic parameters of single motors as has also been evidenced for τ which decreases the number of attached motors [81]. Therefore, the cell would have the possibility to regulate the intracellular

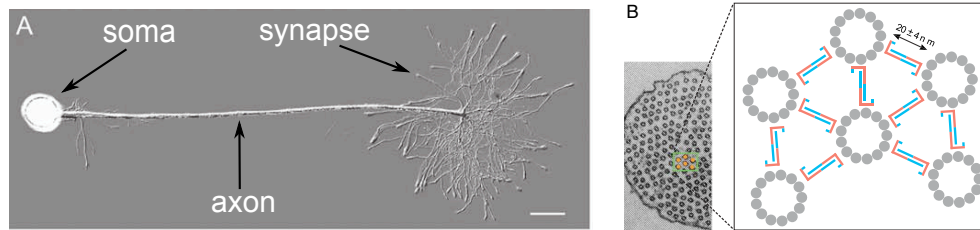


Figure 2.4: Neuron and MT spacing by tau proteins in axons. (A) Neuron in culture with clearly distinguishable soma (left), axon (middle) and synapse (right). The shorter dendrites starting at the soma cannot be seen in this image. Scale bar: 100 μm . Modified from Traffic, Vol. 9, O. A. Shemesh *et al.*, *Tau-Induced Traffic Jams Reflect Organelles Accumulation at Points of Microtubule Polar Mismatching*, 458–471, ©2008, with permission from John Wiley & Sons, Inc. (B) Cross-section of an axon. Tau dimers (blue and red) bundle MTs (grey rings) and induce a hexagonal structure of the axonal MT network. Reprinted from Proc. Nat. Acad. Sci. 105:7445–7450, ©2008. Electron micrograph (left) by permission from Macmillan Publishers Ltd.: Nature 360:674–677, ©1992.

transport by locally varying the concentration of proteins which affect the properties of individual motors.

2.4 The axon

The axon is one of the neurites of a neuron and as such connecting the distant synapse with the cell body or soma (figure 2.4 A). In vertebrates, axons are among the longest structures at the level of individual cells with lengths of up to 1 m in humans while having thicknesses typically not exceeding the micrometer scale [91]. The axon therefore presents a quasi-one-dimensional system within which intracellular cargos are bidirectionally transported from the soma to the synapse and vice versa.

2.4.1 Axonal microtubule network

Structure

The axonal MT network is highly polarized and consists of many MTs of different lengths. The MTs are longitudinally arranged and point almost uniformly with their plus end in distal direction [92]. Individual MTs may be as long as $\sim 100 \mu\text{m}$ [93, 94]. The bundling function of tau (see section 2.2.3) leads to a parallel arrangement of the axonal MTs in an imperfect lattice with spacing of $26.4 \pm 9.5 \text{ nm}$ [95] (figure 2.4 B).

In contrast to non-neuronal cells, the minus ends of axonal MTs are not attached to the centrosome or one of the other common nucleating structures. Instead, axonal MTs exhibit a stable detyrosinated region of tubulin at their proximal end [19] serving exclusively as nucleation seed for a more dynamic tyrosinated region with higher

turnover of tubulin subunits [96, 97]. More recently, γ -tubulin has been found to be present in the axon and might thus play a role in the nucleation of axonal MTs and serve as cap on the minus end [98].

Dynamics

Just as in most of the cells, only the plus end of axonal MTs is dynamic while the minus end seems to be stable [96], probably due to some capping protein [21] which might be the γ -tubulin addressed above [98]. Polymerization and depolymerization of the plus end is about a factor two slower in mature axons than in non-neuronal cells and occurs along the main axis of the axon [99, 100].

Since old MTs in the axon eventually depolymerize completely and since it is unclear whether there is a nucleating structure allowing for free tubulin to assemble into MTs directly in the axon, the so-called *Cut-and-run* model has been conceived by Baas *et al.* [101] to explain the maintenance of the stationary state of the axonal MT network: MTs nucleate and polymerize at the centrosome in the soma and are then cut by a MT-breaking protein such as katanin (see section 2.2.3). Katanin has indeed been shown to be located in higher concentrations near the centrosome [102]. Short MT pieces are then transported through the axon with their plus end pointing in distal direction [103, 104]. The motility is achieved through molecular motors which are anchored on actin filaments or longer MTs and exert forces on the transported MT by walking on it. It has in fact been shown that dynein and the actin cortex are responsible for half of the anterograde MT transport in axons while the rest depends on kinesin [105, 106]. One thus finds two populations of MTs in the axon: short and mobile MTs which are transported and perform bidirectional motion and long and immobile MTs which serve as structures along which the short MTs can be transported. The long MTs are imagined to be immobile because of a large number of crosslinks to other axonal structures such as the neighboring MTs via tau [106, 107], though actually they are still active at their plus end and might depolymerize at any moment. Experiments are contradictory whether the short MTs undergo dynamic instability during transport [104, 108] or whether they are stable [106, 109]. Furthermore, it is an open question if and how tubulin is transported retrogradely. Such motion has not been observed yet, but might be needed to balance the constant influx of tubulin in form of anterogradely transported MTs. Alternatively, tubulin might degrade at the synapse or be released to the extracellular space from there [110].

Katanin is also found in axons in regions of higher MT polymerization activity, e.g., in branching regions or at the tip of growing axons [102]. The action of katanin is able to locally promote the restructuring of the MT network: First, by cutting longer MTs, the resulting short MTs can be transported due to fewer crosslinks to other structures. Second, since free MT plus ends serve as nucleation points for further polymerization, breaking a long MT into many short MTs allows the growth of several long MTs and thus to expand the MT network as necessary in axonal outgrowth [107]. This hypothesis is supported by the observation that katanin concentrations decrease when axons become stationary [111].

The axonal MT network has been shown to be more dynamic far away from the cell body, i.e., in distal regions [109]. At the same time, these dynamic regions appear to be correlated to elevated tau concentrations [112], thus raising the question of tau's function in these parts of the axon. Tau is known to stabilize MTs and protect them from severing by katanin (section 2.2.3) but also has an influence on molecular motors (section 2.3). The purpose of tau's presence in these regions might be either one or even both of these two functions, i.e, the protection from katanin and the regulation of transport.

2.4.2 Axonal transport and neuronal diseases

Axonal transport has received a lot of attention because of its implication in several neurological diseases. The most prominent example in this respect is Alzheimer's Disease (AD) [113]. Axonal swellings caused by accumulations of MAPs, molecular motors, organelles and vesicles have been found in early stages of AD, suggesting failure of axonal transport to be linked to the progress of the disease [114]. Furthermore, accumulations of tau in neurofibrillary tangles is a hallmark pathology of AD so that overexpression of tau is hypothesized to be implicated in the failure of axonal transport.

A model of the cascade leading from tau overexpression to neuronal degeneration has been proposed by Baas and Qiang [115]. In this model, the overexpression of tau inhibits axonal transport by interfering with kinesin-driven transport along MTs as has been shown, e.g., in [116, 117]. MT-bound tau interferes with the attachment of both motor families, kinesin and dynein, but the effect is more pronounced for kinesin (section 2.3). Transport velocities on the other hand are independent of tau concentrations for both transport directions [66, 118]. The regulation of the directionality of axonal transport by tau has been proposed for example in [67]. In the case of abnormal tau overexpression, this proposed regulation fails and anterograde transport is almost completely suppressed.

Mandelkow *et al.* [117] propose that the neuron reacts to this blocking of the anterograde transport by hyperphosphorylation of tau which causes it to dissociate from the MT filament and thus clears a path for kinesin-driven transport. The hyperphosphorylated tau eventually forms the abnormal filaments mentioned above as a hallmark of AD. Additionally to restoring the axonal transport, the loss of tau on the MT makes it more susceptible to severing by katanin (see section 2.2.3) causing a disruption of the MT network and neuronal degeneration.

In line with this model, a massive reorientation of the MT network was identified under overexpression of tau in *Aplysia* neurons [119]. The reorientation might be caused by the elongation of shorter MTs which have been cut by katanin and are brought out of the parallel orientation by steric interaction or molecular motors which pull on the MT fragments. As a consequence of the MT network reorientation, axonal transport is impaired in both directions as swirls in the MT network act as attractive regions for molecular motors so that accumulations of axonal cargos occur as is observed in AD.

On the other hand, it is unclear whether the reorientation of MT filaments is really due to the cascade proposed above because tau might also impede axonal transport simply by stabilizing MTs if, as we suggest in this thesis, MT dynamics is necessary to sustain efficient bidirectional transport. Support for this hypothesis comes from an experiment in which axonal MTs have been stabilized with paclitaxel (also known as taxol) causing a reorientation of the MT network similar to the effects of tau overexpression [100]. The reorientation of MTs might therefore not be the consequence of an increased susceptibility of MTs to severing by katanin, but rather an effect of the stabilization effect of tau on MTs. The idea is that axonal transport fails due to MT stabilization and the whole machinery of MT transport as described in section 2.4.1 being de-balanced so that the initial stationary state of the MT network cannot be maintained.

In medicine, a possible neuropathy following the treatment of cancer by MT-stabilizing drugs such as paclitaxel or docetaxel is a well-known phenomenon [120] and presumably linked to the breakdown of axonal transport [121], also indicating a certain importance of MT dynamics for axonal transport.

2.5 Chapter summary

The key players in axonal transport are molecular motors which move stochastically along microtubule filaments while dragging intracellular cargo along with them. This type of transport of the molecular motors is characterized by alternating phases of processive motion and undirected diffusion in the cytoplasm. At the same time, the microtubule network undergoes constant remodeling: individual filaments elongate, shrink or even disappear completely; crosslinks between neighboring MTs are created which tend to align as a consequence.

Axonal transport *in vivo* is a result of these two dynamics together which undergo on their part a lot of external influences by numerous MAPs which modify as well the motor properties as the whole MT network by influencing the dynamic instability of MTs. The machinery of MAPs seems to be finely tuned to allow for stable axonal transport and may lead to serious neuronal diseases in the case of malfunction.

As for the purposes of this thesis, the question of interest is how the cell organizes the collective transport of various motor proteins such that efficient bidirectional transport is possible even over the very long distances found in axons. Kinesin and dyneins bind to overlapping binding site on the filament and therefore interact at least via exclusion. Additionally, the comparatively large size of the transported cargos in the dense environment of the axon adds another steric interaction between the cargos, indicating the possible emergence of collective phenomena. A few models have been developed to describe these collective phenomena involving motor proteins of different species. Specific interactions between molecular motors might be a solution to blocking situations between oppositely moving motors but the MT dynamics also seems to play a role in achieving efficient transport.

Chapter 3

State of the art in modeling intracellular transport

3.1 Chapter introduction

3.1.1 Modeling stochastic systems

When trying to model such complex systems as intracellular transport, one is usually confronted with several difficulties. First of all, there is the huge complexity of the problem. As has been shown in chapter 2, axonal transport is a result of the dynamics of many different proteins interacting in ways which are not fully understood. This lack of knowledge makes modeling a challenging task but even if we had a perfect knowledge about the intracellular processes, it would still be hopeless to model motor-driven transport in every detail. In any case, incorporating every detail cannot be desirable as one of the purposes of modeling consists of simplifying a system as much as possible while keeping enough of the complexity to reproduce interesting effects observed in the real system. At best, the outcome is a model which is tractable by analytical and numerical methods but still exhibits the basic features of the original system. The crucial task thus consists in identifying the most important elements of the system which dominate the collective behavior and determine the macroscopic features. A successful model is able to reproduce observable effects but also to predict new ones which might eventually be verified by experiments. In a next step, a further refinement of the model can be done by including more and more elements in order to achieve a better agreement with the quantities of interest.

Stochastic modeling has proven itself as a powerful tool in systems with complex interactions on a microscopic scale. A convenient example is the Brownian motion of a small particle in a suspension. Although the collisions between the molecules of the liquid and the particle are not explicitly considered, the stochastic treatment of the random motion of the particle describes well the real system. By describing the dynamics of the system in terms of stochastic transitions between different states, the microscopic interactions are characterized only by giving the transition rates. This approach hence corresponds to a treatment on a coarse-grained scale and overcomes the problem of lacking knowledge or extreme complexity.

In this thesis, all processes will be assumed to fulfill the *Markov property*, i.e., transitions between states depend exclusively on the current state of the system and not on

the whole history of states. This assumption is useful because it simplifies the problem, but also because there is no obvious reason for any memory effects on molecular scale which might introduce an explicit history-dependence. Markov processes are defined by their transition rules and the whole information on their time evolution is contained in the *master equation* [122]:

$$P(\mathbf{q}, t + \Delta t) - P(\mathbf{q}, t) = \sum_{\mathbf{q}' \neq \mathbf{q}} [\omega(\mathbf{q}' \rightarrow \mathbf{q}, \Delta t)P(\mathbf{q}', t) - \omega(\mathbf{q} \rightarrow \mathbf{q}', \Delta t)P(\mathbf{q}, t)]. \quad (3.1)$$

The expression $P(\mathbf{q}, t)$ gives the probability to find the system in state \mathbf{q} at time t . The transition from state \mathbf{q}' to state \mathbf{q} is given by the rate $\omega(\mathbf{q}' \rightarrow \mathbf{q})$. Thus, the left side of (3.1) corresponds to the net flow of probability mass into state \mathbf{q} between times t and $t + \Delta t$. The right side is the balance of probability mass flowing into and out of state \mathbf{q} from and to other states \mathbf{q}' . By conservation of probability, one must have $\sum_{\mathbf{q}} P(\mathbf{q}, t) = 1$ for all t . The time scale Δt links the transition rate ω to a probability p which describes the probability for the specific transition to occur during the next interval of time Δt . The probability to switch from state \mathbf{q} to state \mathbf{q}' in the time interval Δt is given by

$$p(\mathbf{q} \rightarrow \mathbf{q}') = \omega(\mathbf{q} \rightarrow \mathbf{q}')\Delta t. \quad (3.2)$$

It is rather obvious to see that the time interval in discrete Markov processes has to be chosen small enough in order to assure that the sum of all possible transition probabilities does not exceed 1. In this case, one can also use the formulation in (3.1) to approximate continuous-time systems which lack an intrinsic time scale and for which infinitesimal time increments $\Delta t \rightarrow dt$ have to be considered. In intracellular transport processes, the time a molecular motor needs to make a step is negligible compared to the waiting time between steps. As a result, no intrinsic time scale can be observed at the level of description in our models so that continuous-time models are considered throughout the rest.

If the considered system exhibits *ergodicity*, i.e., any state can be reached from any other state by a finite number of transition steps, the probability distribution from (3.1) reaches a unique long-time limit

$$\lim_{t \rightarrow \infty} P(\mathbf{q}, t) := P(\mathbf{q}) = \text{const.}, \quad (3.3)$$

called the stationary state [122]. The left side of (3.1) consequently vanishes in the stationary state as there is no more variation over time of the probability distribution. A special solution of a stationary state is obtained if every term in the sum on the right side of the master equation cancels:

$$\omega(\mathbf{q}' \rightarrow \mathbf{q})P(\mathbf{q}') = \omega(\mathbf{q} \rightarrow \mathbf{q}')P(\mathbf{q}). \quad (3.4)$$

This property is referred to as *detailed balance* and is a sufficient condition to have an equilibrium system, i.e., a system which is not subject to external driving forces. In

intracellular transport, however, there is a constant input of energy by the hydrolysis of ATP by the motors and GTP by microtubules which maintains the system out of equilibrium. The stationary state of such a non-equilibrium system exhibits net current from q to q' on the scale of individual states but also shows a macroscopic current on the scale of the whole system which is the characteristic feature of non-equilibrium systems.

Equilibrium systems are well understood and there exists a standard formalism with which one is able to analyze these systems. For non-equilibrium systems on the other hand, several approaches to the master equation exist, but one is still missing a generalized approach, making the analytical solution of driven systems a challenging task. The total number of non-equilibrium systems for which an exact solution can be found, even in the stationary state, is very limited. In the other cases, one has to resort to approximations in order to gain some information on non-equilibrium systems. In general, a numerical approach by Monte Carlo (MC) simulations is relatively straightforward for most systems, including the models which are discussed in this thesis. The simulation method will briefly be presented in section 4.1.2 along with the definition of the model where it is first used.

3.1.2 Stochastic lattice gases for modeling of intracellular transport

In the past, stochastic lattice gas models have been used in a wide range of active transport phenomena, e.g., pedestrian dynamics [123], car traffic [124, 125] and intracellular processes [126–128]. Lattice gas models are composed of a lattice with discrete sites and particles which occupy these sites and stochastically hop from one site to another depending on hopping rules and rates which are chosen to mimic the properties of the modeled system. In active transport models, these hopping rates depend on the direction so that the particles are driven to one direction on average, creating a macroscopic current. All the models in this thesis are thus non-equilibrium models.

In the case of intracellular transport, stochastic lattice gases are an appropriate choice because the hopping of particles on the lattice can be directly understood as a step of a molecular motor like kinesin or dynein along the MT. The different steps of the mechanochemical cycle during which ATP is converted to ADP and inorganic phosphate and mechanical work is produced (see section 2.3.1) is summarized in a single hopping rate, hence drastically simplifying the problem.¹ At the same time, driven stochastic lattice gases have proven to exhibit a rich phenomenology already in one-dimensional systems making them an interesting object of study. In fact, phase transitions in one-dimensional systems without long-range interactions can only be observed in non-equilibrium systems. Furthermore, the transitions from one state to the other in the stochastic lattice gases considered here are local which allows for a subdivision of the state q into substates τ_i which correspond to the occupation of

¹Simulations of single proteins at atomistic level are unfortunately still not accessible with current computing technologies if the molecule undergoes large conformational changes.

site i . The update scheme of the local states has to be chosen appropriately to the considered problem [129]. For systems with continuous time which lack an intrinsic time scale, a *random sequential update* is a convenient choice. In this case, the local states are not updated all at once. Instead, single transitions are chosen sequentially and at random.

In the present chapter, several lattice gas models are presented with a focus on models which have been proposed to describe intracellular transport. The self-evident starting point is the totally asymmetric simple exclusion process (TASEP) as the prototypical model of this class. It has the appealing property that it can be solved exactly. In the subsequent sections, modifications of the TASEP will be treated which add several details of transport by molecular motors and thus are important contributions in the understanding of unidirectional (section 3.2) and bidirectional (section 3.3) transport.

3.2 Unidirectional transport

Different lattice gas models have been introduced in order to understand the collective effects arising from the basic properties of individual molecular motors. Although intracellular long-range transport is bidirectional in most of the cases, a lot of insight can already be gained by considering only a single particle species as will be shown in this section.

3.2.1 Totally asymmetric simple exclusion process (TASEP)

Model

The TASEP is defined on a one-dimensional lattice with L discrete sites that can either be vacant or occupied by a particle (figure 3.1). A particle stochastically hops to a site on its right with rate p if that site is vacant, i.e., no site can be occupied by more than one particle at a time. The hopping rate p is typically set to unity so that all other rates in the system are expressed in terms of p . Hopping to the left is prohibited in this model but possible in other simple exclusion processes as the symmetric simple exclusion process or the asymmetric simple exclusion process. For the purposes of transport by molecular motors, the totally asymmetric variant is appropriate because backward steps of motors as kinesin-1 are rare and can be neglected (see section 2.3).

Two different boundary conditions are usually considered: Under *periodic boundary conditions*, the system is closed into a ring so that a particle which hops from site L arrives at site 1. This choice obviously exhibits conservation of particles and it can be shown that every allowed configuration has the same probability of occurrence [130].

Current-density relation

Investigating on the efficiency of axonal transport, the current across a bond between two neighboring sites is a quantity of high interest and is defined as the number of

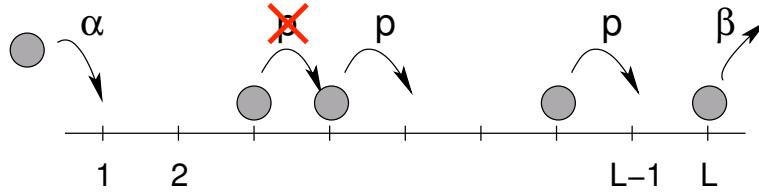


Figure 3.1: The TASEP with open boundary conditions. A particle hops to the next site on the right if that site is empty at rate p . If vacant, the first site of the system is filled from the reservoir at rate α and a particle on the last site can leave the system at rate β .

particles crossing that bond on average in one unit of time. Since the TASEP obeys local conservation of particles, the average current is also conserved throughout the system and thus equal for all bonds:

$$J := J_{i,i+1} = p\langle\tau_i(1 - \tau_{i+1})\rangle, \quad (3.5)$$

where i denotes the starting site of the hopping move and τ_i the occupation of site i taking values 0 or 1 if that site is vacant or occupied, respectively. In a product-state or mean field approximation, the averages over products of state variables are assumed to factorize $\langle\tau_i\tau_j\rangle \approx \langle\tau_i\rangle\langle\tau_j\rangle$. Additionally, the periodically closed system exhibits translational invariance so that $\rho := \langle\tau_i\rangle \approx \langle\tau_{i+1}\rangle$. Applying the mean field approximation and translational invariance to (3.5), the unique current-density relation

$$J(\rho) = p\rho(1 - \rho) \quad (3.6)$$

is obtained which is actually exact in the continuum limit [131] and identical to the one obtained for the system with open boundaries discussed hereafter. Its maximum is at $\rho = 1/2$ where the corresponding current is $J = 1/4$, a value which may serve as benchmark to evaluate the current in other models.

The second choice of hopping rules on the boundary sites is *open boundary conditions* which will be considered in the rest of this section. In that case, two infinitely large particle reservoirs are imagined at both ends of the lattice with density $\rho_0 = \alpha/p$ for the reservoir on the left and density $\rho_{L+1} = (1 - \beta)/p$ for the reservoir on the right. The first site of the lattice can hence be filled at rate α if it is empty and a particle on the last site leaves the lattice at rate β (figure 3.1). The system with open boundary conditions has been solved by Derrida *et al.* using a matrix product ansatz [131] and simultaneously by Schütz and Domany [132] by solving the exact recursion relations found in [133].

Phase diagram

An important property of the TASEP is its particle-hole-symmetry, i.e., the identical behavior of the model under certain symmetry operations:

$$\tau_i \leftrightarrow 1 - \tau_i, \quad \alpha \leftrightarrow \beta, \quad i \leftrightarrow L + 1 - i. \quad (3.7)$$

These symmetry operations also imply a symmetry of the density profile:

$$\rho_{L+1-i}(\alpha, \beta) = 1 - \rho_i(\beta, \alpha). \quad (3.8)$$

Thanks to this property, the whole phase diagram can be deduced from considering only half of the parameter space (α, β) .

In contrast to the system with periodic boundary conditions, the TASEP with open boundary conditions shows interesting non-trivial behavior. Depending on the entrance and exit rates α and β , three different phases can be reached [134]:

- **Low-density phase (LD):** For $\alpha < \beta$ and $\alpha < 1/2$, the entry rate dominates the system's behavior and determines current and density far from the boundaries:

$$J = \alpha(1 - \alpha), \quad \rho = \alpha, \quad \text{for } \alpha < \beta \text{ and } \alpha < 1/2. \quad (3.9)$$

At the right boundary, the system exhibits a *boundary layer* which decays exponentially to α . If $\beta > 1/2$ the exponential decay is additionally modulated by a power law.

- **High-density phase (HD):** For $\alpha > \beta$ and $\beta < 1/2$, the exit rate limits the current in the system and creates a queue of particles in front of the exit which extends through the whole system except for the boundary layer on the left end of the system.

$$J = \beta(1 - \beta), \quad \rho = 1 - \beta, \quad \text{for } \alpha > \beta \text{ and } \beta < 1/2. \quad (3.10)$$

Again, the boundary layer decays to the bulk value, with the characteristic of the decay depending on the value of α analogous to the low-density phase.

- **Maximal-current phase (MC):** For $\alpha > 1/2$ and $\beta > 1/2$, a maximal current is reached which is independent of the exact values of α and β .

$$J = 1/4, \quad \rho = 1/2, \quad \text{for } \alpha > 1/2 \text{ and } \beta > 1/2. \quad (3.11)$$

The boundary layers in this phase decay algebraically toward a density of $\rho = 1/2$, leading to long-range boundary layers from both sides.

The phase diagram of the TASEP is shown in figure 3.2 A and typical density profiles of the three phases can be seen in figure 3.2 B.

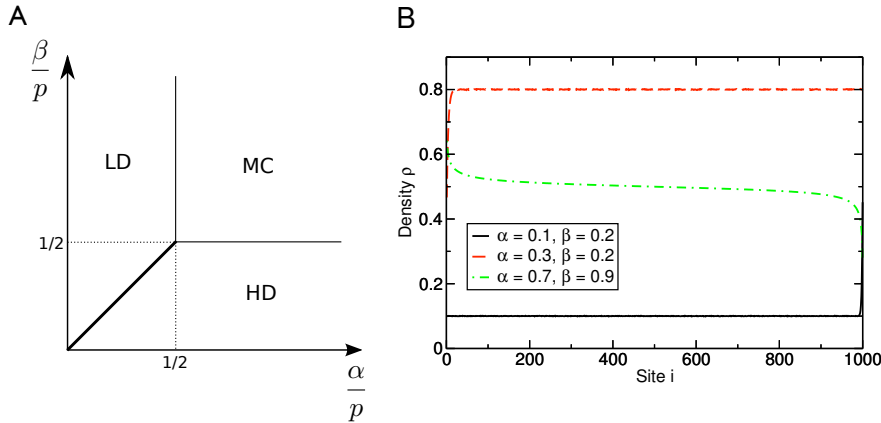


Figure 3.2: Phase diagram and density profiles of the TASEP with open boundary conditions. (A) Phase diagram of the TASEP with its three phases: low-density (LD), high-density (HD) and maximal-current (MC). The thick line between LD and HD indicates a first order transition, thin lines at the HD/MC and LD/MC interfaces are second order. The thin dotted lines indicate changes of the boundary layer while the bulk behavior remains unchanged. (B) Representative density profiles for a TASEP of system size $L = 1000$ for the three phases with $p = 1$. LD at $\alpha = 0.1, \beta = 0.2$ (solid black line), HD at $\alpha = 0.3, \beta = 0.2$ (red dashed line) and MC at $\alpha = 0.7, \beta = 0.9$ (green dash-dotted line).

The properties of the maximal-current phase and a part of the low-density phase² can be derived from a maximum current principle postulated by Krug for a continuous system of length L [135]:

$$J = \max_{\rho \in [\rho_{L+1}, \rho_0]} J(\rho). \quad (3.12)$$

This principle applies for monotonously decreasing density profiles, i.e., $\rho_0 > \rho_{L+1} \Leftrightarrow \beta > 1 - \alpha$ and is able to explain half of the LD phase and the whole MC phase. The reasoning is as follows: Since the density profile passes from ρ_0 on the left boundary to ρ_{L+1} on the right boundary, it must at some point reach the density ρ^* which maximizes the current. If that density ρ^* was not assumed in the bulk, it lies in the boundary layers where, in addition to the current due to driving, an excess current is created which is caused by the important density gradient in the boundary layer. The current in that boundary layer would therefore exceed the current in the bulk which is not possible in the stationary state. Hence, the density ρ^* leading to the maximum current value must be assumed in the bulk already. Krug is able with this reasoning to correctly predict the density profiles and the transition along the line $\beta = 1$.

The transitions from the low/high-density to the maximal-current phase are continuous: The bulk density approaches $1/2$ when arriving at the transition line from the low/high-density phase. In contrast, the transition line separating low-density

²Due to the symmetry, this also explains a part of the high-density phase.

from high-density phase is a first-order transition: The density changes abruptly from α to $1 - \beta$ when crossing the transition line thus giving a total density change of $1 - 2\alpha$. The current nevertheless is continuous upon crossing of the transition line. On the transition line at $\alpha = \beta < 1/2$, both reservoirs try to impose their density on the system leading to flat profiles emanating from both ends of the system which are connected by a shock front. This shock diffuses through the system, i.e., it performs a random walk along the lattice, leading to a linear averaged density profile.

In the LD and the HD phase, the shock connecting the densities of the two reservoirs has a non-zero average velocity causing it to be driven to the right and left boundary, respectively, where it forms the boundary layers mentioned above.

In summary, due to the conservation of particles and current, the boundaries are able to determine the bulk properties in the TASEP. It is remarkable to observe this rich phase diagram despite the simple structure of the model. This is a direct consequence of the driving which keeps the system out of equilibrium.

3.2.2 TASEP with finite resources

Model

With respect to the biological motivation of the TASEP, a reasonable extension is the consideration of finite resources as the number of proteins within the cell is naturally limited. This has first been done by Ha and den Nijs³ [136] who fixed the total density of particles ρ_{tot} in the system and defined it as

$$\rho_{\text{tot}} = \rho_{\text{b}} + \rho_{\text{u}}, \quad (3.13)$$

where ρ_{b} is the density of particles on the lattice and ρ_{u} the density of particles outside the lattice in the boundary reservoirs. The boundary reservoirs share a common pool of particles at density ρ_{u} so that the total density ρ_{tot} influences the reachable states of the system. Furthermore, the effective entrance rate α_{eff} depends on the density of particles in the reservoir:

$$\alpha_{\text{eff}}(\rho_{\text{u}}) = \alpha f(\rho_{\text{u}}). \quad (3.14)$$

The function $f(\rho_{\text{u}})$ satisfies the conditions $f(0) = 0$, $f(\infty) = 1$ and is monotonously increasing in order to respect the availability of particles in the reservoir. In [136], the case $\beta = 1$ was considered, whereas Adams et al. [137] had a more complete look at the modifications brought about to the whole phase diagram by the finite resources.

Modification of TASEP phases

It is easy to see that for $\rho_{\text{tot}} \rightarrow \infty$ the standard TASEP as presented in section 3.2.1 is recovered with $\alpha_{\text{eff}} = \alpha$. Interesting effects therefore arise when the total density

³Ha and den Nijs actually motivated their model with the *garage parking problem* instead of intracellular processes, but the model is nevertheless the same.

is chosen low enough in order to constrain the number of particles on the lattice and induce feedback mechanisms between the densities on the lattice and in the reservoir.

The LD phase is governed by the entrance rate α and so there is no dramatic change of behavior when the total density is low: The system behaves exactly like a standard TASEP in the LD phase with entrance and exit rates α_{eff} and β , respectively.

Alike, the MC phase behaves like a TASEP in the LD phase for low values of ρ_{tot} until the total density is high enough to have $\alpha_{\text{eff}} \geq 1/2$ where the system transits to the known MC state.

A more interesting behavior can be observed if α and β are chosen such that the unconstrained TASEP would be in the HD phase. Increasing the total density starting from $\rho_{\text{tot}} = 0$, the system first is in the LD phase, as the effective entrance rate is close to zero and therefore necessarily smaller than the fixed exit rate β . The bulk density in the system then increases with increasing α_{eff} until $\alpha_{\text{eff}} = \beta$. In the unconstrained TASEP, this corresponds to a point on the coexistence line. Increasing the density further leaves the reservoir density unchanged but fills the lattice more and more until the typical HD density profile is reached. The system thus stays at constant α_{eff} for different total densities ρ_{tot} . Here, a new type of behavior occurs: Although the system is on the line of coexistence, the shock or domain wall between the low and high density domain has a localized position on the lattice which is a result of a feedback mechanism [138]. If the shock from the low to the high density domain is to the right of its stationary position, more particles are driven to the reservoir, thus increasing the effective entrance rate α_{eff} such that the current in the low density domain to the left of the shock increases and drives the shock back to the left. The inverse happens for a fluctuation of the shock position to the left. After having reached the unconstrained HD-TASEP profile, any further increase of ρ_{tot} adds only to the reservoir density, thus being reminiscent of Bose-Einstein condensation.

For $\alpha = \beta < 1/2$, the shock is also localized for densities which are not too high and other highly non-trivial behavior emerges [137, 138].

The minimal modification of introducing a global conservation of particles and occupation-dependent entrance rates thus leads to a qualitatively different behavior of the system with interesting feedback mechanisms causing localized domain walls, a feature which will also be observed in the model of the following section.

3.2.3 Bulk reservoir with infinite diffusion rates

Model

Molecular motors switch between phases of directed and diffusive motion. During the latter, they are not attached to filament but move randomly through the cytoplasm under the constraints of other cytoskeletal elements (see section 2.3). This detachment and attachment of motors to the MT leads to a local non-conservation of particles and current in the bulk and has been considered in the most simple way in a model by Parmeggiani *et al.* [139] who coupled the open-boundary TASEP of section 3.2.1 with

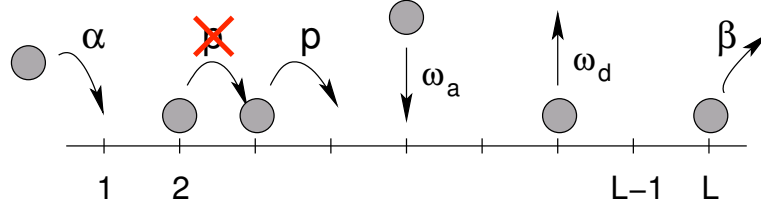


Figure 3.3: TASEP with Langmuir kinetics. In addition to the usual TASEP hopping rules, particles are also exchanged with a reservoir in the bulk of the system: A particle detaches from the lattice at rate ω_d and an empty site is occupied by a particle at rate ω_a .

Langmuir kinetics in the bulk. This means that a particle detaches from any lattice site at rate ω_d . Furthermore, an empty site becomes occupied by a particle at rate ω_a (figure 3.3). This corresponds to a coupling of the bulk of the system to a grand-canonical reservoir with constant density. Particles within the bulk reservoir have an infinite diffusion rate since a detached particle loses any memory of the site of previous attachment. The model exhibits the same type of particle-hole symmetry as the TASEP under the additional symmetry operation $\omega_d \leftrightarrow \omega_a$.

From a theoretical point of view, the model is interesting in that it combines the non-equilibrium TASEP with the equilibrium Langmuir kinetics. While the behavior of the former is boundary-driven (section 3.2.1), the latter controls the density in the bulk of the filament which in absence of any non-equilibrium process would take the value $\rho_{\text{eq}} = \omega_a / (\omega_a + \omega_d)$.⁴ The two processes thus compete and interesting effects are found due to this coupling. However, the rates which determine the model have to be chosen appropriately in order to observe this competition. The average time of attachment to the lattice is ω_d^{-1} which determines the average number of steps a particle performs between two phases of diffusion. Let n be the number of steps a particle makes during ω_d^{-1} . Then n remains constant in the continuum limit $L \rightarrow \infty$, while the fraction of the lattice which is visited by a particle before detachment tends to zero: $n/L \rightarrow 0$. This would effectively inhibit any influence of boundaries on the bulk of the system and, to avoid that, the coupling to the bulk reservoir is usually taken to scale inversely with the system size so that a particle always visits a finite fraction of the lattice [139, 140]:

$$\omega_a = \frac{\Omega_a}{L}; \quad \omega_d = \frac{\Omega_d}{L}; \quad \text{with } \Omega_a, \Omega_d = \text{const.} \quad (3.15)$$

This can also be understood by looking at the continuous mean field equation which describes the system in leading order L^{-1} [140]:

$$\frac{\partial \rho}{\partial \tau} = -(1 - 2\rho) \frac{\partial \rho}{\partial x} + \omega_d L \left[\frac{\omega_a}{\omega_d} - \left(1 + \frac{\omega_a}{\omega_d} \right) \rho \right], \quad (3.16)$$

⁴This density would be obtained for example when considering this model with periodic boundary conditions.

where $x = i/L$ and $\tau = t/L$. If the rates ω_a, ω_d were chosen to be constant, the second term in (3.16) would dominate for large systems. Actually, this is what occurs in systems with many exchanges, as the lane changes on a highway [141]. However, in the case of intracellular transport, it is generally considered that it is the weak coupling in the sense of (3.15) that is relevant.

Stationary states and phase diagram

When searching the stationary state $\partial\rho/\partial\tau = 0$ of this model, equation (3.16) obviously leads to a first-order differential equation. The couplings to the boundary reservoirs on the left and right end of the lattice impose two boundary conditions ($\rho(x = 0) = \alpha$ and $\rho(x = 1) = 1 - \beta$) on the differential equation. In other words, the problem is over-determined. The overall solution consists of the two individual solutions resulting from integration of the differential equation from the left and the right side of the system. The transition point from one solution to the other can be determined in the framework of kinematic wave theory. If the densities of the two solutions do not match at the point of transition, a shock (or domain wall) occurs which depends on higher orders of L^{-1} . Consequently, this shock gets sharper the longer the system is.

In contrast to the TASEP, the shock front does not move within the system, once the system has reached its stationary state. Instead, the shock is driven to the position in the system where the mass current through the shock front is zero, so that localization of the shock occurs [140]. This phenomenon is interesting in so far as no defects on the lattice are implicated and the particle dynamics is homogenous in the bulk of the system. Surprisingly, the localization effect persists for $\alpha = \beta < 1/2$ if the bulk reservoir density vanishes with increasing system size, i.e., $\omega_d, \omega_a \propto L^{-a}$ with $1 \leq a < 2$ [142].

Because the system can be controlled by both boundaries at the same time, the number of qualitatively different density profiles is much higher than for the TASEP and depends strongly on the attachment and detachment rates [140, 143]. In particular, the phase diagrams exhibit more different phases than for the TASEP. In addition to the three phases already known from the TASEP (see section 3.2.1), there is also a phase with a localized shock within the system as discussed above. Furthermore, there are several states in which two or all three TASEP phases coexist. In these phases, no shock is observed and the partial profiles are continuously connected with a cusp in the density profile. If $\Omega_a \neq \Omega_d$, the maximal-current phase is suppressed since the Langmuir kinetics tries to bring the bulk of the system to a density $\rho_{\text{eq}} \neq 1/2$, thus driving it away from the maximal-current density.

Altogether, the Langmuir kinetics brings about some very interesting effects despite it being an equilibrium process and as such not capable of exhibiting phase transitions on its own. In combination with a non-equilibrium process, the Langmuir kinetics nevertheless modifies the phase transitions found in the TASEP and leads to qualitatively new behavior. The results are qualitatively the same if two parallel lat-

tices are considered instead of one which are both affected by Langmuir kinetics and are additionally able to exchange particles between filaments [144]. The qualitative behavior also remains unaltered, if particles are considered to be dimers whose two heads individually bind to two neighboring sites and walk in the hand-over-hand fashion described for kinesin in section 2.3.1 [145].

Regarding the relevance for intracellular transport, the model includes one of the characteristic properties of molecular motors moving along MTs, i.e., processivity (section 2.3.1). It is therefore a step toward a more accurate description of MT-driven transport. The variety of different states demonstrate that a high degree of complexity can be achieved even with very basic ingredients. In fact, the predicted shock formation has been observed in experiments with a single-headed kinesin [128].

The next logical step toward a more accurate model of intracellular transport is the explicit consideration of the bulk reservoir. In the current model, particles in the bulk reservoir can attach to any vacant site on the filament, implying an infinite diffusion rate. The total number of particles in the system is not limited either. In a living cell, the cytoplasm is filled with structures of different sizes such that diffusion is limited and actually dependent on the size of the diffusing object [146, 147]. Furthermore, vesicles in axonal transport usually originate at the synapse or in the cell body, so that conservation of transported particles is provided within the axon.

3.2.4 Bulk reservoir with finite diffusion rates

Model

Lipowsky *et al.* [127, 148] have introduced a model for intracellular transport which describes more accurately the situation in the axon than the model by Parmeggiani *et al.* mentioned above, i.e., it exhibits particle conservation and does not imply infinite diffusion rates in the bulk reservoir. The model has a three-dimensional geometry with discretized space. Particles hop between nodes of a cubic lattice with spacing l which corresponds to the step size of the molecular motor on a filament, i.e., 8 nm for kinesins on MTs. As in the previous models, MTs are represented by a linear arrangement of lattice nodes while all other nodes represent the cytoplasmic reservoir. The MT nodes differ from the non-MT nodes by the hopping rules of the particles. While the hopping of MT-bound particles follows the same rules as in the previous model, unbound particles undergo an unbiased random walk on a discrete three-dimensional lattice while interacting with each other via hard-core exclusion (figure 3.4). Because of the cubic lattice structure, every MT site can be reached from four reservoir nodes and the ratio of the hopping rates from these four sites to the MT and back, i.e., the attachment and detachment rates, determines the affinity of a particle to the MT. Thus, the model always has conservation of particles and the hopping between reservoir nodes determines the strength of diffusion.

This model includes more features of intracellular transport than the previously presented models by explicitly considering a three-dimensional geometry within which a filament is placed, so that different cellular environments can be modeled.

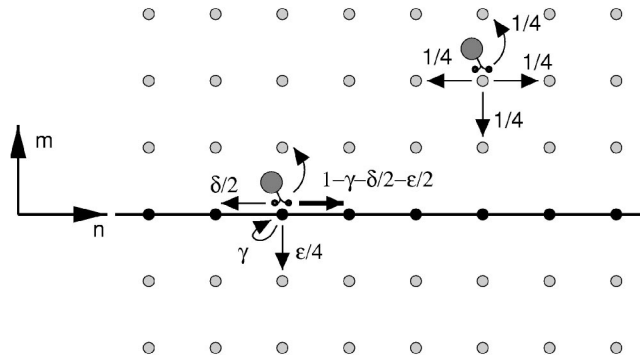


Figure 3.4: Model with explicit consideration of the bulk reservoir taken from [149]. Particles hop between neighboring nodes on a cubic lattice, where the filament is represented as a line of black nodes and the bulk reservoir by grey nodes. Hopping within the bulk reservoir is unbiased, but hopping to and away from filament sites depend on the attachment and detachment rates. Please note that the notation of the rates in this figure does not correspond to the notation in this thesis. Reprinted with permission from T. M. Nieuwenhuizen, S. Klumpp, R. Lipowsky, Phys. Rev. E 69, 061911, 2004. ©2004 by the American Physical Society.

This reduces the degree of abstraction, making it simpler to verify experimentally and hence increases the significance of this model's behavior. Consequently, Lipowsky *et al.* [127] tune the system by deriving hopping rates from real experiments and test the outcome of different geometries.

Although directed motion on the single-particle level can only occur along the filament, there is a strong co-localization of particles on the filament and in the cytoplasmic surroundings [127, 150]. Jam-like accumulations of particles on the filament thus lead to density gradients in the bulk reservoir generating a diffusive current $J_u \equiv -D_u \nabla \rho_u$ where the index u refers to unbound particles and D_u to the effective diffusion rate of particles. For the stationary state in closed geometries, this current equals the current along the filament which is strongly affected by collective effects as traffic jams occur generically because of the high affinity for the filament. The time evolution of some quantities of this model are discussed in [148, 149]. These are of lesser importance in the context of this thesis as the interest lies on efficient stationary transport states.

Stationary state configurations with different boundary conditions

In the stationary state of a closed system with reflecting boundaries, most of the particles accumulate at the plus end of the filament so that the length of this jam is determined by the total number of particles. In the case of very few particles, the jam is only a boundary effect at the MT plus end but already for intermediate densities, the filament is overcrowded and the jam extends through the whole system. As no

further hopping can then be done along the filament, particles cannot be driven to the plus end anymore. In consequence, there is also no more density gradient in the bulk reservoir which might have led to diffusive currents at lower densities. The number of particles in the system will consequently regulate the jam length and also the current which exhibits an optimum for the latter quantity at jam lengths which are shorter than the system length.

In a follow-up work [151], the same model was applied to a cylindrical geometry with a single filament on its axis and different boundary conditions in axial direction. For periodic boundary conditions, translational invariance and the finite radius of the cylinder lead to radial, i.e., perpendicular to the filament, equilibrium making the system very easy to solve under a mean field description. It turns out that the mean field approach is actually exact in this particular case.

In the case of open boundary conditions, one recovers the phase diagram of the TASEP (figure 3.2) with the only modification that the transitions might be slightly shifted depending on the couplings between filament and bulk reservoir [152]. This can again be understood by the presence of radial equilibrium⁵ which causes the density of unbound motor at a given horizontal position along the cylinder axis to be determined by the density of bound motors on the filament. This latter quantity is governed by the densities at the boundaries.

When coupling the filament only diffusively to the boundary reservoirs at both ends, the diffusive particle current to and from the boundary reservoirs determine the current which can occur along the filament. Depending on the choice of parameters, it is with these boundary conditions indeed possible to completely suppress the maximal-current phase which exists if there is no diffusive region at the filament ends.

A mixed choice of an open boundary at the minus end of the filament and a closed boundary at the plus end has been made in [153]. This choice mimics the situation in an axon more accurately with the closed end being the synapse and the open end the attachment to the cell body from which a constant density of molecular motors is provided. It was shown in that work that the density on the filament in the stationary state either approaches zero or one far from the open end, i.e., either the long tube is empty or all transport is blocked due to a jam extending through the whole system. The transition between these two states obviously depends on the strength of the diffusion which drives particles back to the open end against the preferential motion of particles on the filament. Müller *et al.* concluded in the article that additional regulatory mechanisms are necessary in order to maintain efficient transport in long tube-like geometries as the axon at intermediate densities.

Enhanced diffusion on filament networks

So, it is known from these works that the diffusion rate plays an important role for the occurrence of jams on the filament. In the crowded intracellular environment, diffu-

⁵Actually, radial equilibrium does not hold in the boundary layers.

sion cannot be considered to be very efficient when comparing the spacings of the axonal MT network (≈ 26 nm, section 2.4.1) to common vesicle sizes (≈ 100 nm [154]). Klumpp and Lipowsky used the framework of the three-dimensional lattice gas to show that certain arrangements of filaments lead to non-directed diffusive movements which can be used for transport over large distances and exhibit very large diffusion coefficients compared to passive diffusion in the absence of filaments [155]. This diffusive motion is driven by phases of directed transport along individual MTs and is thus dependent on the active stepping of individual motors. Klumpp and Lipowsky therefore refer to this phenomenon by the term *active diffusion* as the overall motion is undirected due to the uncoordinated attachment to filaments of different orientation. They show this type of motion not to depend on the diffusion coefficients in the cytoplasm surrounding the filaments.

Klumpp and Lipowsky discuss the relevance of this enhanced diffusion for several technical applications, but it may also play a role in dendritic transport. Dendrites are also very elongated with a parallel MT network. But in contrast to axons, dendritic MTs are not uniformly oriented so that the structure of the MT network might indeed enhance the transport of intracellular cargo. However, the same is not true for axons which have an almost uniformly oriented MT network (see section 2.4.1).

Summing up the results from this class of models, the predicted influence of a finite diffusivity in the cytoplasm is confirmed and generally leads to a co-localization of diffusing (unbound) particles and bound particles which step along the filament. Nevertheless, transport states similar to those of the previous models (sections 3.2.1 & 3.2.3) can also be found.

This class of models by Lipowsky *et al.* already contains very important features of intracellular transport by replicating the microscopic moves of motors and the geometry within which intracellular transport occurs. The model can of course still be extended in order to approach a realistic description. An example would be the inclusion of multiple filaments and a special consideration of the mechanochemical cycle of the molecular motors. While the effect of multiple filaments is ambiguous [156], a tuning of the mechanochemical cycle can increase the transport capacity of the model due to a modification of the collective effects [157].

3.2.5 Defects

Several defects can occur in intracellular transport leading to position-dependent properties of the molecular motors. The example par excellence is the influence of tau proteins which bind to MTs and influence the properties of kinesin and dynein motors in different ways (section 2.3). Transport models with spatial disorder can thus give some more insight into the consequences of these defects.

It has been shown for several stochastic lattice gases that inhomogeneities induced for example by defects may give rise to the formation of macroscopic high-density regions which depend on the defect [158–160]. Single defects in the bulk can therefore modify the properties of a finite fraction of the system.

Due to the basic structure of the transport models presented in this chapter, three different types of site-wise defects can be imagined which are related to the transport along the filament [161]: 1. A stepping defect which reduces the step rate p along the filament; 2. an unbinding defect which increases the detachment rate ω_d from that filament site to the bulk reservoir; 3. a binding defect which hinders the attachment (rate ω_a) of a particle to the filament site carrying that defect.

The influence of a single stepping defect in the transport model with infinite diffusion rates (section 3.2.3) was studied in [162] and for multiple stepping defects in [163]. While the phases of the defect-free system still persist, new states arise in which the system is subdivided into parts by the defects, leading to phases which are characterized by the coexistence of different domains.

In a generic way, stepping defects and unbinding defects decrease single-motor properties as the run-length along the filament or the velocity. In a system with periodic boundary conditions, the current along the filament in systems with many motors is negatively affected by stepping defects but may increase for unbinding defects at high enough particle densities. This is possible due to the reduction of the density of bound particles on the filament [161]. If this density is too high, jams form which block the current. Unbinding defects effectively decrease the number of particles on the filament, thus decreasing the tendency to form jams on the filament.

Binding defects on the other hand do not affect collective motion of particles much if not present at almost all sites [161, 164]. This result might in fact add to the understanding of the failure of axonal transport at abnormal tau concentrations while moderate tau concentrations are not deleterious (section 2.4.2). Since tau has important stabilizing functions for MTs, it is desirable that its action as binding defect on kinesins does not affect the overall transport properties if tau is not expressed at extreme concentrations.

The consequences of site-wise defects in the models of this section have been studied for single motors. If one considers intracellular cargo to be carried by teams of molecular motors [86, 90], these defects might indeed serve to regulate the motion of individual cargos as hypothesized in [67] (see also section 2.4.2).

3.3 Bidirectional transport

The extension of a stochastic lattice gas to bidirectional transport represents a further increase in complexity. In the following, two species of particles will be considered, one moving in positive direction along the lattice, the other in negative direction according to their 'charge'. Consequently, the two species will be referred to as positive and negative particle species, respectively. In models with exclusion interaction, the very basic problem in modeling two species of particles which move in opposite directions is how to overcome situations in which the next site is blocked by a particle of opposite charge. Indeed, in most of the models for bidirectional transport, the bypassing mechanism determines most of the system's properties.

In the present section, different lattice gas models are presented which lead to bidi-

rectional transport. The original TASEP with two particle species can obviously not describe bidirectional transport without other than the exclusion interaction as no current can be sustained in either direction. The following models are grouped with respect to the mechanism by which particles of opposite charge can effectively bypass each other.⁶

3.3.1 Site-exchange models

Several TASEP-like models have been proposed in which explicit site-exchange of particles is considered [166, 167]. For simplicity, the two particle species obey symmetric hopping rules under the constraint of hard-core exclusion but are also able to exchange sites with a reduced rate q . The hopping moves between two adjacent sites on the one-dimensional lattice (or filament) are given by

$$+0 \xrightarrow{p} 0+, \quad 0- \xrightarrow{p} -0, \quad +- \xrightarrow{q} -+, \quad (3.17)$$

where $+/-$ refers to a positive/negative particle and 0 to a vacancy on the lattice. The rate of the transition is given above the corresponding arrow. The conventional choice for the rates is $1 = p > q$, so that site exchanges occur on a longer time scale than unhindered motion. Models defined by the hopping rules in (3.17) are symmetric under exchange of particle species and inversion of the lattice.

Two-species TASEP with open boundaries

Evans *et al.* consider a single one-dimensional lattice with open boundary conditions and the hopping rules of the particles as described above [166, 168]. The first and the last site are coupled to the boundary reservoirs in an analogous way to the single-species TASEP from section 3.2.1:

$$\text{Site } i = 1 : \quad 0 \xrightarrow{\alpha} +, \quad - \xrightarrow{\beta} 0, \quad (3.18)$$

$$\text{Site } i = L : \quad 0 \xrightarrow{\alpha} -, \quad + \xrightarrow{\beta} 0. \quad (3.19)$$

In a mean field treatment, the currents of the two species along the filament are

$$J_+ = \rho_{b,i}^+(1 - \rho_{b,i+1}^+ - (1 - q)\rho_{b,i+1}^-), \quad J_- = \rho_{b,i}^-(1 - \rho_{b,i+1}^+ - (1 - q)\rho_{b,i+1}^-), \quad (3.20)$$

where the index b refers to the particles being bound to the filament and the index i to the site on the filament. Due to the open boundary conditions, equations (3.20) are complemented by the currents at the boundaries:

$$J_+ = \alpha(1 - \rho_{b,1}^+ - \rho_{b,1}^-) = \beta\rho_{b,L}^+, \quad J_- = \alpha(1 - \rho_{b,L}^+ - \rho_{b,L}^-) = \beta\rho_{b,L}^-. \quad (3.21)$$

⁶Please note that a TASEP involving two particle species has first been considered by Derrida *et al.* [159, 165]. Their model includes first-class and second-class particles moving in the same preferential direction. Since this model does not describe bidirectional transport, it will not be treated here.

For $q = 1$, the equations in (3.20) decouple in the bulk and the system can effectively be described by two one-species TASEPs with modified entrance rates since the two species only interact via the boundaries. Because the phase diagram of the single-species TASEP is well-known, the phase diagram of the two-species TASEP can easily be derived. While a low-density phase and the maximal-current phase still exist with symmetric properties, two new phases were hypothesized to occur in the low β -region which exhibit spontaneous symmetry-breaking and have unequal currents for the positive and the negative particle species: A HD/LD-phase and a LD/LD-phase occur in which the density profiles of the two species are qualitatively different and cannot be transformed one into the other by symmetry operations. A qualitatively similar behavior was predicted for $q < 1$. However, the existence of the LD/LD-phase has been disputed and might effectively be an artifact from a mean field treatment and a finite-size effect in MC simulations which is not present in the limit of infinite system sizes [169–171].⁷

For finite lattice lengths, the system flips between the two states belonging to the symmetry-broken HD/LD-phase. The flipping between states occurs on times which scale proportionally to $\exp(L)$, hence leading to true symmetry breaking in the thermodynamic limit. This is different from the behavior of the single-species TASEP on the coexistence line $\alpha = \beta < 1/2$: On the coexistence line, a low-density and a high-density region also coexist but they both have the same current and are therefore connected by a conserved domain wall (or shock) which diffuses through the system. The time for the shock to pass from one end of the system to the other and thus to flip the whole system is given by the diffusive scale L^2 which is significantly faster than found here for the symmetry-broken phases of the two-species TASEP.

Two-species TASEP with periodic boundary conditions

A system which follows the same rules as above but has periodic boundary conditions is not very interesting if $q = 1$. All permitted configurations occur at equal probability and thus, no non-trivial phenomena emerge. This can easily be understood because, as mentioned above already, a particle does not differentiate between a vacancy or a particle of the other species if $q = 1$. Without boundaries, the species therefore do not interact at all and every species on its own behaves like a single-species TASEP.

But the same is not true for $q < 1$, i.e., if the two species act reciprocally as defects for the other species. Since an oppositely charged particle acts as obstacle, jams (or clusters) build up through which the particles diffuse on longer time scales. These jams may eventually become macroscopic (section 3.2.5). Since particles have lower velocity within the domains of high particle density, the current in the whole system is controlled by the rate q as this rate determines the flux of particles out of the cluster. The current has to balance in the whole system in the stationary state. One

⁷The absence of the LD/LD-phase for infinite system sizes has also been stated for a very similar model in which the two species do not interact at all within the bulk but only on the two boundary sites [172].

consequently has a density-dependent state (and thus a current-density relation) with only little finite-size effects [173]. In fact, there is a typical size of the jams (or clusters) l_p^* which can be calculated [174] so that there is no macroscopic clustering in the limit of infinite system sizes $L \rightarrow \infty$ and finite-size effects should become negligible for $L > l_p^*$. In contrast to this result, it has been hypothesized from Monte Carlo simulations that in a similar quasi-one-dimensional system with two parallel lattices, i.e., $2 \times L$ sites, the model does exhibit phase separation [173]. The stationary state would then consist of three different blocks which are almost uniformly composed of positive particles, negative particles or vacancies, respectively, each occupying a finite fraction of the infinite system. However, this does not appear to be the case when applying a conjectured criterion for condensation in one-dimensional driven systems [175, 176] which later has found some support by high precision MC simulations in this particular case [177].

A similar discussion about the existence of a phase transition has been led for the so-called AHR model⁸ [167, 179]. As the previous model, the AHR model is defined by (3.17) on a ring, i.e., with periodic boundary conditions. But additionally, positive and negative particles may exchange sites against their preferential direction: $- + \xrightarrow{p} +-$. For $q < p$, a pure phase is found for the stationary state in which a block of positive particles is left of a block of negative particles which is left of a block of vacancies. The three blocks are almost immobile with flip times which increase exponentially with L such that they are pinned at infinite system sizes. This model thus exhibits true phase separation in this regime even under periodic boundary conditions which can be considered to be an interesting result as it spontaneously breaks translational invariance.⁹ The controversy was however about the behavior for $q > p$: In the original paper [179], the authors subdivide this part of the parameter space into two different phases: 1. A *mixed* phase with two non-homogenous blocks of particles and a block of vacancies which is no longer pure. Fluctuations in the blocks preserve translational invariance in this phase which corresponds to Bose-Einstein condensation in coordinate space. 2. A *disordered* phase with no ordering and no macroscopic structures. Using Yang-Lee Theory [181], Arndt showed that there is a second-order phase transition between the mixed and the disordered phase at least in finite systems [182]. It was subsequently proven for a grand-canonical setup that the block of the mixed phase might become as large as 10^{70} sites but is nevertheless a finite-size effect and does not exist in the thermodynamic limit [183]. As a consequence, the region of the parameter space $q > p$ would be only one single phase. This result was supported by the same criterion which excluded phase separation in the model by Korniss *et al.* treated above [175].

⁸The name of the model comes from the names of the authors (Arndt, Heinzel and Rittenberg) of the first publication in which it appeared [167], although other very similar models were published almost at the same time [173, 178]

⁹The existence of a symmetry-breaking phase-separated state could also be shown to hold in a related model by Evans *et al.* [178, 180].

There are two things to notice from the discussions of these models: 1. Introducing a second particle species may induce highly non-trivial effects and permit the appearance of phase transitions which are not boundary-controlled. 2. The formed structures may be excessively large without being macroscopic in the thermodynamic limit. The discussions about the existence of true phase transitions in the thermodynamic limit make clear that this question is hard to answer from MC simulations with finite system sizes and mean field approaches. It is thus reasonable to be cautious when making statements about phase transitions in such complicated systems as those which will be considered in this thesis.

As for the purpose of modeling intracellular transport, these models are less suitable despite their interesting properties. A site-exchange between oppositely charged particles is impossible in the case of molecular motors which have an overlapping binding site on the MT (section 2.3). The site-exchange proposed in this model can therefore only be a coarse-grained description of a complex sequence of moves of the motors involving detachment, diffusion, attachment and/or side steps on the filament. The details of this sequence will determine the exact properties of such a bidirectional transport model. It is therefore more appropriate to consider models which explicitly capture the individual moves needed to bypass particles of the other species. Models of this kind will be treated in the following.

3.3.2 Multi-lane models

The models presented in this section do not explicitly allow for exchanges of position of neighboring particles. On a single lane, oppositely charged particles would therefore mutually block each other and the whole system comes to a standstill with current zero. In order to have a more interesting behavior, possibilities to bypass obstacles on the filament have to be provided. This is done in the following by extending the one-dimensional lattice to a quasi-one-dimensional lattice, i.e., the models have several one-dimensional lattices arranged in parallel. Particles are then allowed to hop between these sub-lattices according to the model-specific rules.

Two-species ASEP on a two-dimensional lattice

The first model without site-exchange of particles was introduced by Schmittmann *et al.* [184]. Two species of particles hop on a square lattice with dimensions $L_x \times L_y$. In contrast to all previous models, the preferential hopping direction of the particles is determined by an external field E parallel to the x -axis which drives the particles according to their species or ‘charge’. The difference is that steps against the preferential direction imposed by the driving field are possible, like in the case of the ASEP, while the previous models correspond to an infinite driving field $E = \infty$. In the absence of a field $E = 0$ or at infinite temperature, particles of the two species are indistinguishable and hop randomly on the periodically closed lattice, leading to a homogenous distribution of both particle species and holes. For a finite field $E > 0$, a first-order transition toward a phase-separated state can be observed at least

in finite systems above a critical density of particles depending on the field strength $\rho = 2\rho^+ = 2\rho^- > \rho_{\text{crit}}(E)$. This phase is characterized by a compact strip of particles perpendicular to the field direction while the rest of the lattice is essentially empty. One thus has again a phase with spontaneously broken symmetry. Since this configuration emerges due to a mutual blocking of the particles, the current drastically decreases at the transition from the disordered to the phase-separated phase. The critical particle density $\rho_{\text{crit}}(E)$ is a decreasing function of the field strength E with the limit $\rho_{\text{crit}} \rightarrow 0$ for $E \rightarrow \infty$ in the limit of infinite system sizes $L_x, L_y \rightarrow \infty$. Since no steps against the driving force are possible in this limit, there is an absorbing state for $\rho > 0$ which is reached as soon as the particles get jammed on the whole height of the lattice, i.e., on every individual sublattice in y -direction.

Two-species TASEP coupled to a diffusive lane

For my diploma thesis [185], I developed a quasi-one-dimensional model for bidirectional transport. The model was inspired by the class of models introduced by Klumpp *et al.* (see section 3.2.4) and will serve as starting point for the models presented in chapter 4. The results of this model which were published in my diploma thesis and the subsequent publication [186] will therefore be presented in a bit more detail than the results of the other models of this section.

The model consists of two parallel one-dimensional lattices with periodic boundary conditions (figure 3.5). While one lattice represents the filament along which transport is carried out, the other mimics a diffusive environment in which no directed transport takes place. This corresponds to the cytoplasm which surrounds the microtubules and within which axonal cargos diffuse if not attached to one of the MTs. As in all models of this chapter, particles interact via hard-core exclusion on the filament along which they hop in preferential direction with rate p . On the diffusive lattice, particles hop in both directions with equal rate D and do not interact with each other such that a single site on the diffusive lattice can be occupied by multiple particles at the same time. Particle exchanges between the two lattices occur at rate ω_a and ω_d , corresponding to attachment and detachment moves to and from filament, respectively.

Whereas the motivation for the hopping rules on the filament has been discussed in section 3.2, the particular choice of the diffusive lattice needs some clarification: As discussed in section 3.2.4, diffusion of axonal cargo in the cytoplasm is limited due to the size of the cargo and to the confinement imposed by the amount of structures present in the axon. After detachment from the filament, an organelle might therefore not be able to diffuse away from the filament in radial direction. Consequently, a single diffusive lattice is considered to be sufficient to represent the whole cytoplasm. Nevertheless, the limitation of diffusion in the longitudinal direction is not yet included into the model, so that the model allows multiple particles to occupy the same site on the diffusive lattice. Therefore, organelles do not feel the local density of axonal cargo and can pass in front of each other if they are not attached to the filament. The model consequently overestimates this bypassing in the narrow

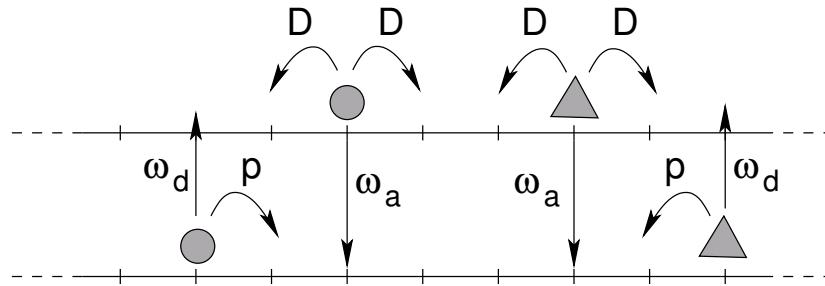


Figure 3.5: Two-species TASEP coupled to a diffusive lane. The model consists of two periodically closed one-dimensional lattices. The lower lattice serves as track for directed motion of the two oppositely charged particle species which interact via hard-core exclusion on this lane. The upper lane is a diffusive environment with no biased motion and absent of any interaction between particles.

environment and the results are likely to underestimate the jamming in a real system with strong spatial confinement.¹⁰

The generic result of this model is that a huge cluster is formed which absorbs almost all the particles of the system. This effect is due to the highly inefficient bypassing of obstacles on the filament. A particle which encounters an obstacle such as a cluster of particles on the filament would have to detach to the diffusive lane and then diffuse over the obstacle in order to re-attach to the filament on the other side. Being unbiased, the diffusive motion is much more likely to be stopped at the proximal end of the cluster where the particle started its random walk and not at the distant end. Several cycles of detachment, diffusion and re-attachment will therefore be needed before the particle finally succeeds in reaching the other side of the obstacle. In presence of a large cluster, the current in the system is therefore limited by the diffusive transport. This bypass mechanism gets the more inefficient the longer the obstacle is, causing more and more particles to diffuse in the region parallel to the jam. This means that a cluster on the filament is extremely stable as the flux of particles leaving the cluster decreases with increasing cluster size. The growth of the cluster is therefore only limited by the total number of particles present in the system.

This cluster formation does not depend on the density but on the number of particles as only a limited number of particles is necessary to form a nucleating cluster which will then start to grow indefinitely (figure 3.6). It therefore has been reasoned in [186] that the model exhibits macroscopic clustering at any finite density $\rho_{\text{tot}}^+ = \rho_{\text{tot}}^- > 0$ in the limit of infinite system sizes $L \rightarrow \infty$. This question will again be addressed in section 4.2.

The mutual blocking of particles is accompanied by a large build-up of correlations as can be seen by the failure of the mean field approximation for low detachment

¹⁰In [187], the effect of a larger cytoplasmic environment was considered by us. We reasoned that this only modifies the attachment rate ω_a in this model with the attachment rate depending inverse quadratically on the radius of the cytoplasmic environment perpendicular to the transport filament.

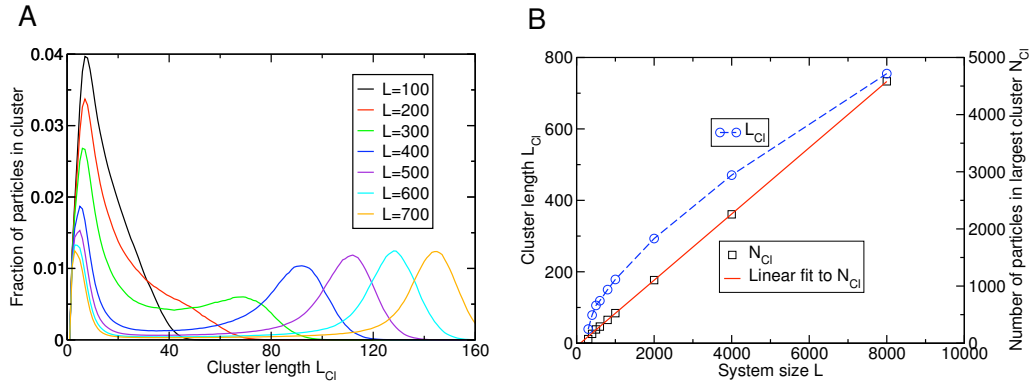


Figure 3.6: Cluster properties a two-species TASEP with a diffusive lane at density $\rho_{tot}^+ = \rho_{tot}^- = 0.3$ for different system sizes. (A) The fraction of all particles in a cluster of length L_{CI} is shown. Above a certain system length, the formation of a large cluster occurs absorbing almost all particles of the system, indicated by a peak at large values of L_{CI} . (B) The length of the largest cluster L_{CI} grows sub-linearly with the system size whereas the number of particles in the cluster N_{CI} is proportional to the system size, indicating the accumulation of particles in the reservoir above the cluster.

rates in figure 3.7. The data shown is for low densities in a relatively small system so that a large cluster does not form, but in the increasing part at low values of r , there are several small clusters with very few particles which block each other. The exchange processes between pairs of oppositely charged particles therefore determine the behavior of the system for high filament affinity, i.e., low ratio of detachment to attachment rate.

High values of the diffusion rate D decrease the tendency to form macroscopic clusters and actually totally suppress it in the limit $D \rightarrow \infty$, underlining the importance that the particles in the diffusive lane have some sort of memory of their last site of attachment to the filament. Keeping track of the horizontal position even for detached particles has further implications as will become apparent in chapter 5.

The effect of multiple transport filaments in parallel has also been considered by enlarging the model to have several subsystems as in figure 3.5 put next to each other. Particles may change from one subsystem to the other either via the diffusive lanes or by moves from filament to filament. Counter-intuitively, this coupling of multiple filaments has turned out to promote the formation of clusters although additional ways for the bypassing of obstacles are available. The moves from subsystem to subsystem transport locally high densities from one filament to the other, leading to a system which is blocked on all filaments at approximately the same horizontal position.

Taken together, these results indicate that a simple bypassing mechanism via a diffusive lane does not help in making bidirectional transport efficient and overcoming the blocking of particles of opposite charge on the filament. In real systems, the con-

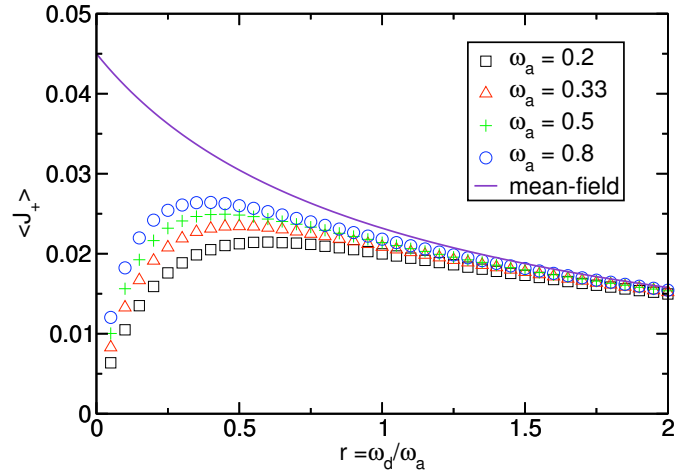


Figure 3.7: Average current in a two-species TASEP with a diffusive lane. The data shown is for a system of length $L = 1000$ and density $\rho_{\text{tot}}^+ = \rho_{\text{tot}}^- = 0.05$. The mean field solution (indigo solid line) fails for low detachment rates ω_d where the bypass mechanism via the diffusive lane is highly inefficient and strong correlations are able to build up due to the formation of small, but stable clusters.

sequences should be even worse, since these systems are open at their ends so that the growth of clusters is not limited by the number of particles in the system as is the case for the periodically closed system which was considered here.

Additional particle-particle interactions

A solution to the problem of blocked particles in bidirectional transport in one dimension has been proposed by Klumpp and Lipowsky [188] in a two-species version of the models treated in section 3.2.4. The hopping rules for both particle species are the same as those shown in figure 3.3 but with periodic boundary conditions. Additionally, particles cannot step onto the next site if it is occupied, regardless of the species of the particle on the next site. As seen with the previous model, this type of situation generically leads to jamming on the filament. Klumpp and Lipowsky resolve this issue by introducing an additional interaction between particles which modifies the attachment and detachment rates along the filament (figure 3.8). A particle has a higher probability of binding to a site if the next site in stepping direction is occupied by a particle of the same species. In this case, the attachment rate is increased by a factor q . At the same time, the detachment rate from that site is divided by q . If the next site is occupied by a particle of the opposite species, the detachment rate is enhanced by a factor q and the attachment is reduced by a factor $1/q$. The interaction is symmetric for both particle species and thus locally modulates the affinity of the particles to the filament.

The motivation for the addition of attractive and repulsive particle-particle inter-

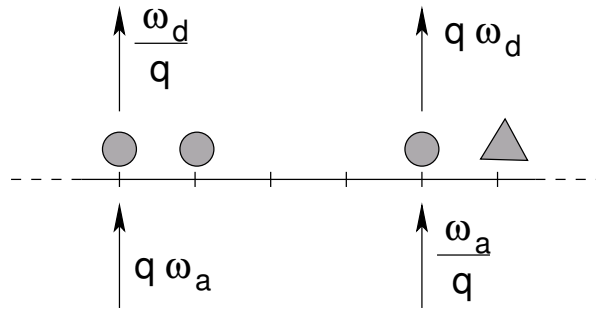


Figure 3.8: Particle-particle interactions in a two-species TASEP. The attachment (detachment) rate increases (decreases) by a factor q if the next site is occupied by a particle of the same species. In the case of a particle of the opposite species, detachment is enhanced and attachment is de-favored.

action comes from the decoration experiments mentioned in section 2.3.1 in which kinesin motors have been shown to attach preferentially in the vicinity of already attached kinesins. In the model presented in this section, this concept is generalized to apply for both particle species which are furthermore supposed to repulse each other reciprocally.

The central result of that model is that it comes to spontaneous symmetry breaking for $q > q_{crit}$, represented by a state in which one particle species is completely excluded from the filament. This sort of lane formation is a priori expected to cause a considerable difference in the currents of particles which is carried by a single filament. If one considers the possibility of multiple filaments in the system, one could find efficient transport in both directions as the transport in the two directions can be supported by two different sets of filaments.¹¹

This interesting lane formation effect was considered in the specific model in [188] for a reservoir with infinite diffusion rates (see section 3.2.3), but was supposed to persist also under a more explicit consideration of the bulk reservoir like in section 3.2.4.

The proposition of particle-particle interactions which make bidirectional transport efficient even under volume exclusion of the driven particles is very appealing since it proposes a very easy solution to achieve long-range transport by local interactions. Moreover, it should be possible to design experiments with molecular motors and microtubules which demonstrate lane formation if the interactions between molecular motors are strong enough.

For these reasons, a closer examination of the lane formation transition and its dependence on the type of reservoir as well as the interaction with lattice dynamics will be carried out in chapter 5.

¹¹We shall see later that it is not necessarily the case for this model that lane changing makes transport efficient, but still the possibility to obtain lane formation is an interesting effect.

3.4 Chapter summary

In the present chapter, several stochastic lattice gas models have been presented which are useful in elucidating the properties of intracellular transport in a quasi-one-dimensional system such as the axon. All models are derived from the prototypical TASEP. The non-equilibrium property of these models leads to a very rich phenomenology with several non-trivial phenomena. These phenomena include boundary-induced phase transitions but also spontaneous symmetry breaking in systems with periodic boundary conditions.

Additional effects arise when considering two species of particles which move in opposite directions along the filament. Due to the exclusion interaction on the filament, mechanisms have to be added to the models which allow the system to resolve a situation in which particles mutually block each other on the filament. It is therefore not surprising that these two-species models frequently exhibit phases with large clusters. If the exchange mechanism of the particles is efficient enough, the clustered state disappears and is replaced by a homogenous state which is characterized by a considerably increased current compared to the clustered state.

Applied to intracellular transport, it can be derived from the results of these models that the organization of intracellular transport in axons is all but simple. Very basic setups including only directed motion along the filament and diffusion are not able to reach efficient transport regimes so that an additional ingredient to the models is needed in order to explain why axonal transport does work properly in the real system. Finding an appropriate model which includes the basic features of the motion of molecular motors along MTs and exhibits efficient transport in both directions would then allow to further investigate on certain defects leading to the breakdown of axonal transport.

Chapter 4

Efficient transport in intracellular transport models I – Lattice dynamics

4.1 Chapter introduction

As has become clear from the two previous chapters, despite some success in unidirectional transport, existing models for bidirectional transport usually fail to explain the observed efficiency of axonal transport and exhibit spontaneous symmetry breaking in the form of clustering instead. A naturally arising question therefore is: What are the minimal prerequisites in order to maintain bidirectional stochastic transport of interacting particles in small volumes if site exchange on the track is not possible? As a possible answer to this question, the present chapter will propose a mechanism which leads to an efficient transport regime (section 4.3). But, since the models of this chapter are all extensions of the bidirectional transport model previously introduced by us [186], and already described in the previous chapter, we shall first pursue the study of this model beyond what had been done in my diploma thesis. The aim will be to show that this model really does exhibit macroscopic clustering at any finite density (section 4.2). It is only in section 4.3 that one of the main result of this thesis will be presented, i.e., a mechanism for efficient transport based on lattice dynamics.

4.1.1 Basic model

The starting point for all transport models which are presented in this chapter is the model from [186] which will be referred to as *basic model* and to which several elements are added in the subsequent sections. Though this model was already presented in section 3.3.2 and illustrated in figure 3.5, we recall its definition here in order to make this chapter self-contained. The basic model consists of two parallel one-dimensional lattices with L equidistant sites each. The model has periodic boundary conditions in the direction of the individual lattices. Two species of particles with opposite preferential moving direction or ‘charge’ hop on the two lattices. The local occupation states of the sites on the lower lattice (or *filament*) are given by b_i^\pm , where the plus/minus sign refers to the particle species or charge and i to the site on the lattice so that $i = 1, \dots, L$. The variable name b has been chosen with respect to the particles being bound to the MT filament which the lower lattice is supposed to represent in this model. Since motor proteins have overlapping binding sites (section 2.3),

the particles which represent them have to interact via hard-core exclusion. The occupation variable of the filament can thus only take the values $b_i^\pm = 0, 1$ with the additional constraint $b_i^+ + b_i^- \leq 1$ for all i . In the upper lane (or *reservoir*), the particles do not interact, implying that the local occupation states can take any non-negative value $u_i^\pm \in \mathbb{N}_0$, where the variable u stems from the modeled unbound molecular motors in this upper lane. This setup is motivated by the quasi-one-dimensional geometry of axons although it largely simplifies the real structure.

The dynamics is symmetric for both particle species and depend only on the present configuration, thus fulfilling the Markov property. Positively charged particles on the filament hop with rate p to the next-neighbor site in positive direction along the lattice, i.e., toward increasing values of i with site L being the left neighbor of site 1. Negatively charged particles correspondingly hop with the same rate p toward decreasing values of i . If the target site is already occupied by another particle, a hopping move is rejected to respect the hard-core exclusion interaction. Along the reservoir lattice, particles of both species hop with identical rate D to the right and to the left. Particles switch from the reservoir to the filament at rate ω_a if the target site on the filament is vacant. Detachment from the filament toward the reservoir occurs at rate ω_d and is always possible. The moves of the particles are presented in figure 3.7. In a more formal way, the system is defined by its master equation (3.1) from which the following set of equations can be derived which define the evolution of the system:

$$\begin{aligned} \frac{\partial \langle b_i^\pm \rangle}{\partial t} = & p [\langle b_{i-1}^\pm (1 - b_i^+ - b_i^-) \rangle - \langle b_i^\pm (1 - b_{i+1}^+ - b_{i+1}^-) \rangle] \\ & + \omega_a \langle u_i^\pm (1 - b_i^+ - b_i^-) \rangle - \omega_d \langle b_i^\pm \rangle, \end{aligned} \quad (4.1)$$

$$\begin{aligned} \frac{\partial \langle u_i^\pm \rangle}{\partial t} = & D [\langle u_{i-1}^\pm \rangle + \langle u_{i+1}^\pm \rangle - 2 \langle u_i^\pm \rangle] \\ & - \omega_a \langle u_i^\pm (1 - b_i^+ - b_i^-) \rangle + \omega_d \langle b_i^\pm \rangle. \end{aligned} \quad (4.2)$$

Since the dynamics conserves the number of particles of each species, the total densities of particles ρ_{tot}^\pm , defined as the total number of particles in the system divided by the system length L , stays constant. Furthermore, the densities of particles on the filament and in the reservoir have to add up to the total density:

$$\rho_{\text{tot}}^\pm = \rho_b^\pm + \rho_u^\pm. \quad (4.3)$$

Results for the stationary state of this model are presented in section 3.3.2.

4.1.2 Simulation method

Despite the rather simple formulation of the model, an analytical treatment of models like the one presented above is difficult. A direct approach to (4.1) and (4.2) is very challenging as all quantities depend on higher-order correlations. An approximative mean field treatment with a product state approximation is much easier to handle

but fails in the presence of strong correlations. Since we focus here on a model which generically exhibits clustering, strong correlations are generically present so that the insight which can possibly be gained from a mean field approximation is rather limited.

A numerical approach to the problem, on the other hand, is rather straightforward thanks to the Markov property of the system and allows to examine the model's properties. *Monte Carlo (MC) simulations* are the standard choice for this purpose and the procedure applied in this thesis will shortly be presented here according to [189]. MC simulations can be applied if a state can be described by a finite number of variables, i.e., if the configuration vector \mathbf{q} in (3.1) does not have infinite dimension. Furthermore, MC simulations rely on discrete time steps. In case a system with continuous time is simulated, the time step Δt has to be chosen small enough so that the sum of probabilities of transitions out of a state in (3.2) does not exceed unity:

$$\sum_{\mathbf{q}'} p(\mathbf{q} \rightarrow \mathbf{q}') < 1 \iff \Delta t < \left(\sum_{\mathbf{q}'} \omega(\mathbf{q} \rightarrow \mathbf{q}') \right)^{-1}. \quad (4.4)$$

The simulation itself is a sequence of states of which every single state is created by a transition from the previous state, thus building a Markov chain of states. For non-equilibrium systems as those considered in this thesis, the transitions within the Markov chain follow the dynamical rules given by the model definition so that the created chain of states represents a possible evolution of the system.

For the stochastic lattice gases considered here, the update scheme from time t to $t + \Delta t$ is as follows: First, a particle is chosen at random with the help of computer-generated pseudo-random numbers.¹ In a second step, the allowed local transitions, i.e., moves of the chosen particle, are determined as a function of the current state and the corresponding probabilities are determined according to (3.2). These probabilities subdivide the unit interval $[0, 1]$ into several intervals of lengths which are given by the probabilities: $[0, p_1], [p_1, p_1 + p_2], \dots, [\sum_{k=1}^M p_k, 1]$ for M local transitions. The last interval corresponds to the possibility that no transition is chosen if the transition probabilities do not sum up to one. A pseudo-random number between zero and one then chooses a local transition by the interval within which it lies. The chosen move is carried out if the resulting configuration is allowed in the sense that it does not violate any exclusion principles.

This procedure is repeated as many times as there are particles in the system so that – on average only – every particle is updated. After that, the so-called *Monte Carlo sweep* is complete and the system has passed from time t to $t + \Delta t$. Since the particles are updated randomly, this algorithm corresponds to the *random sequential update* addressed in section 3.1.2. Physical quantities such as averages or fluctuations of occupation densities or currents can then easily be deduced from recording of the appropriate local states after completed sweeps.

¹As random number generator, the algorithm *ran2()* from the *Numerical Recipes* [190] was used throughout all simulations.

4.2 Macroscopic clustering

Before introducing and discussing mechanisms which make bidirectional transport efficient in the basic model, the clustering properties of the basic model will be examined with respect to the question whether the observed clustering of particles is macroscopic or whether the system will appear homogenous in the limit of infinite system sizes $L \rightarrow \infty$.

4.2.1 Previous results

In [186], we already reasoned that the system shows true phase separation by applying a condensation criterion by Kafri *et al.* [175] which relies on mapping of the considered systems to the zero-range process (ZRP) (reviewed for example in [191]). The criterion subdivides the system into domains containing accumulations of n particles. These domains exchange particles and in the case of true phase separation, the system undergoes a coarsening process with coalescence of small domains to form a single macroscopic cluster. If smaller domains exchange more particles with the rest of the system in a given time interval than larger domains, coarsening should occur.

The criterion is based on the steady state currents J_n out of domains of size n in an assumed asymptotic form:

$$J_n = J_\infty \left(1 + \frac{b}{n^\sigma} \right). \quad (4.5)$$

According to [175], there are three different possibilities to observe phase separation: If domain currents are of the form in (4.5) and the exponent is $\sigma < 1$, phase separation always occurs, while the system is always homogenous for $\sigma > 1$. At exactly $\sigma = 1$, the additional condition $b > 2$ has to be fulfilled for phase separation to occur above a critical density. Lastly, phase separation can be observed for any scaling if the asymptotic current $J_\infty = 0$, although this might be difficult to assess in a finite system with finite currents for J_n .

For the basic model, the steady state currents as well as the length of the largest cluster have been measured at constant particle densities $\rho_{\text{tot}} = 2\rho_{\text{tot}}^+ = 2\rho_{\text{tot}}^-$ but varying system size L . Because the basic model conserves the current, the average current in the system has to equal the current of the domain represented by the largest cluster of particles, since this cluster is very long-lived and determines the system's behavior. A fit of the data points for domains $n > 250$ can be seen in figure 4.1. For the data considered here, one has $b/n^\sigma \gg 1$ so that (4.5) can be reduced to $J_n \approx J_\infty b/n^\sigma$. In the fitting procedure, it is therefore very difficult to obtain separate values for J_∞ and b with a good accuracy. As a consequence, only the product $K = J_\infty b$ of the two quantities will be considered, yielding final values $K = 0.0620 \pm 0.0002$ and $\sigma = 0.029 \pm 0.004$.

σ is clearly below one, thus indicating macroscopic clustering. It is, however, difficult to evaluate J_∞ individually and might in fact be conceivable that $J_\infty = 0$. This possibility is intuitively supported by the idea that the current in the clustered system

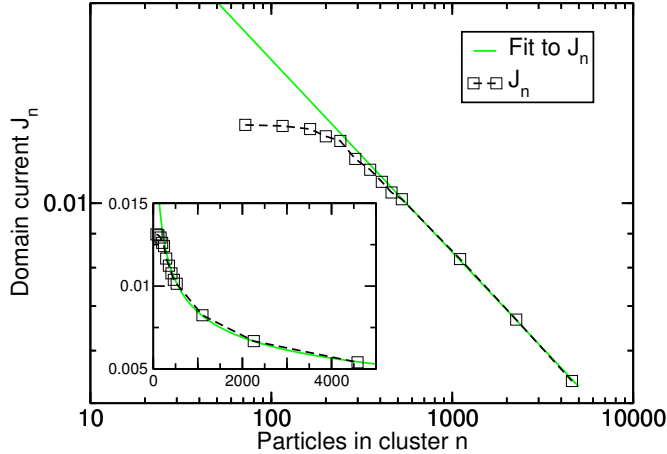


Figure 4.1: Domain current in the basic model (log-log plot). Data shown is from systems with total particle density $\rho_{\text{tot}}^{\pm} = 0.3$ and varying system size L . The black squares show the measures of the average current in the system in function of the average number of particles in the biggest cluster of the system. The green solid line is a fit of the function $J_n = J_{\infty} b/n^{\sigma}$. The inset shows the same data with linear axes.

is created by particles which diffuse over the cluster and reach the end of this cluster (see section 3.3.2). For infinitely long clusters, the probability of a diffusing particle starting at one end to reach the other end of the cluster tends to zero, resulting in a vanishing domain current J_{∞} for infinite domains. Whatever the true value of J_{∞} may be, in both cases, $J_{\infty} = 0$ or $J_{\infty} > 0$ with $\sigma < 1$, the conclusion is the existence of macroscopic clustering in the system.

4.2.2 General idea

In this section, another approach is proposed in order to give some evidence for macroscopic clustering in the basic model. Like the previous approach, the idea relies on the ZRP but this time in its two-species version [192]. The ZRP is defined by a one-dimensional lattice of L sites on which particles hop to neighboring sites with rates which depend only on the occupation of the starting site, hence having a zero-range interaction. In the two-species version considered here, one species hops only in the positive direction along the lattice while the other species hops in negative direction. The hopping rates are homogenous for the whole system and given by $u(n, m)$ for positive and $v(n, m)$ for negative particles where n and m are the number of positive and negative particles respectively which are currently occupying the starting site.

Since it is possible under certain conditions to determine exactly if the two-species ZRP has condensation of particles [192], the idea here is to attempt a sort of mapping of the basic model to a two-species ZRP. The mapping attempted here is not equivalent to the usual mapping between ZRP and TASEP [191] which is already expressed by the fact that it is not exact, i.e., it is not possible to get from the ZRP back to the ba-

sic model as will be seen below. The ‘mapping’ is thus only an approximation in the hope not to modify qualitatively the condensation behavior. This approach has the advantage that as soon as the hopping rates of the corresponding two-species ZRP are determined, deciding on the condensation criterion becomes very easy and is not subject to any major approximations.

The mapping consists in identifying clusters of particles in the basic model which will then be put on a single site in the two-species ZRP. In other words, the spatial extension of the cluster is neglected. After this mapping, a cluster of N_{Cl} particles appears as a single site being occupied by N_{Cl} particles and the current out of a cluster (also called cluster outflux) corresponds to the particle hopping rates $u(n, m)$ and $v(n, m)$ of positive and negative particles respectively. Within this framework, it is rather simple to answer the question if the system condenses into a single macroscopic cluster.

Since an approximate description of the hopping rate $u(n, m)$ of a particle is needed, the current out of a cluster is measured for various number of particles in the cluster in order to obtain a lot of data points in the n - m -plane. It is sufficient to do so for the rate $u(n, m)$ of positive particles because the basic model is symmetric under exchange of particle species and hence $v(m, n) = u(n, m)$. The approach is as follows: For a given total density of particles ρ_{tot} , several combinations of the individual particle concentrations ρ_{tot}^+ and ρ_{tot}^- are simulated and the composition of the largest cluster as well as the current in the system are recorded. With the assumption that the largest cluster controls the whole system, the current out of the cluster is known by current conservation and the hopping rates $u(n, m)$ can be deduced.

4.2.3 Numerical data

The numerical data shown in this section comes from simulations which have been carried out for four different system sizes $L = 1000, 2000, 4000, 8000$ and total particle densities $\rho_{\text{tot}} = 0.4, 0.5, 0.6, 0.7, 0.8, 0.9, 1$. The set of parameters for the particle dynamics is given by $p = 1, D = 0.33, \omega_{\text{d}} = 0.02$ and $\omega_{\text{a}} = 0.33$ which recovers the finite processivity of molecular motors by allowing on average $p/\omega_{\text{d}} = 50$ steps before detachment of particles. Also, the high affinity of molecular motors for the filament is respected due to $\omega_{\text{a}}/\omega_{\text{d}} \gg 1$.²

Cluster composition

As explained in the previous section, numerical data on the composition of the largest cluster as well as on the cluster outflux of each species was recorded. A typical set of data for a given total density of $\rho_{\text{tot}} = 1$ in a system of $L = 2000$ is shown in figure 4.2. The different data points have been obtained for different ratios of positive and negative particles with ρ_{tot} kept constant. Please note that half of the points have been obtained simply by performing a particle species exchange.

²A discussion of biologically relevant parameter values can be found in [186].

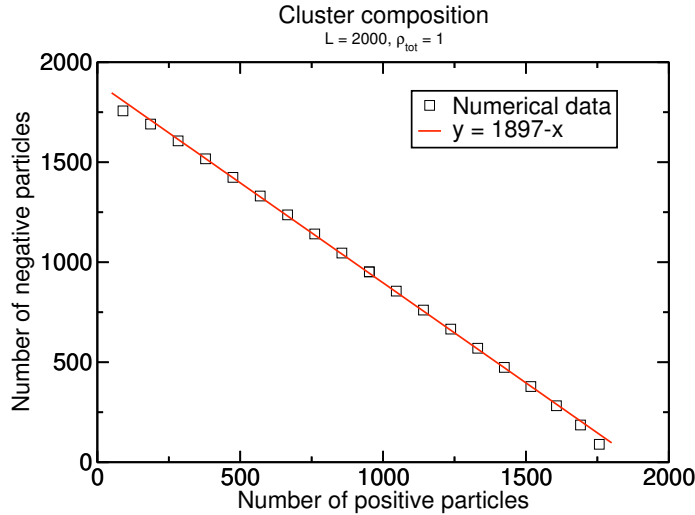


Figure 4.2: Composition of largest cluster for a system of size $L = 2000$ and total density $\rho_{\text{tot}} = 1$. Data points from left to right are for an increasing fraction of positive particles in the system. The red line is a linear fit to the shown data.

The data points lie on a straight line with the exception of the first and last points. These points correspond to the most de-balanced particle concentrations ($\rho_{\text{tot}}^+ = 0.05, \rho_{\text{tot}}^- = 0.95$ and $\rho_{\text{tot}}^+ = 0.95, \rho_{\text{tot}}^- = 0.05$) under which the cluster is extremely dynamic. This is a finite size effect as the number of particles involved in the cluster is extremely low for one of the species at these two points. Fluctuations of this number of particles may therefore lead to a dissolution of the cluster when there are no particles of one of the two species. The rest of the points can nicely be fitted by a linear function with slope -1 , indicating that the total number of particles in a cluster N_{Cl} is independent of the ratio of available positive and negative particles but is governed only by the total number of available particles $\rho_{\text{tot}}L$. Other choices of the parameters L and ρ_{tot} always reveal the same linear relation with unit slope.

Cluster outflux

For the estimate of the current out of a cluster, the average current of positive particles in the system is taken. Because of conservation of current, the two currents need to balance so that this quantity corresponds to the current out of the largest cluster. For the mapping on a two-species ZRP, we are interested in the hopping rates $u(n, m)$ and $v(n, m)$ of individual particles. Consequently, the cluster outflux is divided by the number of particles of the corresponding species in order to give an estimate of the hopping rates.

A representative plot of this data ($L = 2000, \rho_{\text{tot}} = 1$) is shown in figure 4.3. Note that all the data points are at constant total density of particles $\rho_{\text{tot}} = \rho_{\text{tot}}^+ + \rho_{\text{tot}}^-$. For very high numbers of positive particles, there are consequently very few negative

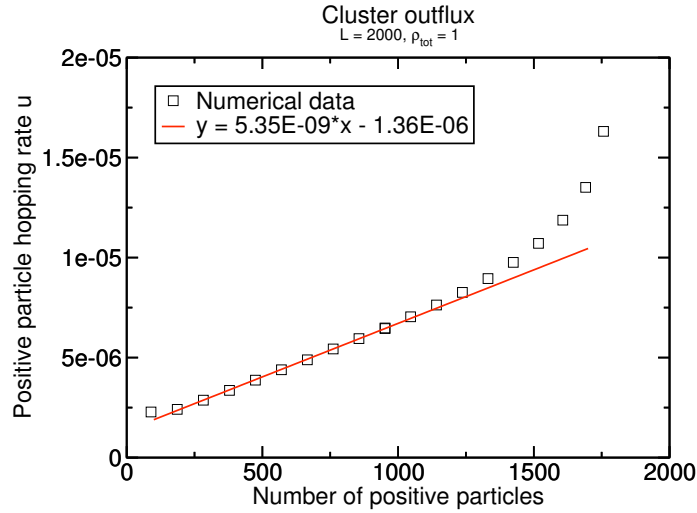


Figure 4.3: Positive particle current in a system of size $L = 2000$ and total density $\rho_{\text{tot}} = 1$. Data points from left to right are for an increasing fraction of positive particles in the system. The red line is a linear fit to the first half of the shown data.

particles which by the same reasoning as for the composition of clusters above leads to this deviation from the straight line. For more higher numbers of positive particles, there are less negative particles such that a variation in their number has a bigger impact on cluster properties such as the outflux of positive particles. This regime is irrelevant for the limit of infinite systems due to the high abundance of particles at any finite density $\rho_{\text{tot}}^{\pm} > 0$. Apart from this dynamic regime which will be discarded, the hopping rate $u(n, m)$ seems to depend linearly on the number of positive particles n . The increase of the hopping rate is plausible as there are less opposing negative particles the more positive particles contribute to the cluster. It is however not easy to determine why the increase is linear as the hopping rate $u(n, m)$ is a result of the structure of the cluster which varies non-trivially with a variation of the composition of the particles.

4.2.4 ZRP hopping rates

The deduction of the corresponding two-species ZRP hopping rates has to be done on the basis of the numerical data reported on in the last section, i.e., cluster composition and the corresponding currents. The data shown in figure 4.3 suggests a hopping rate of the form:

$$u(n, m) = D \cdot n + E. \quad (4.6)$$

The parameters D and E depend on the choice of L and ρ_{tot} and thus on the total number of particles in the cluster $N_{\text{Cl}} = n + m$. For a complete description of the

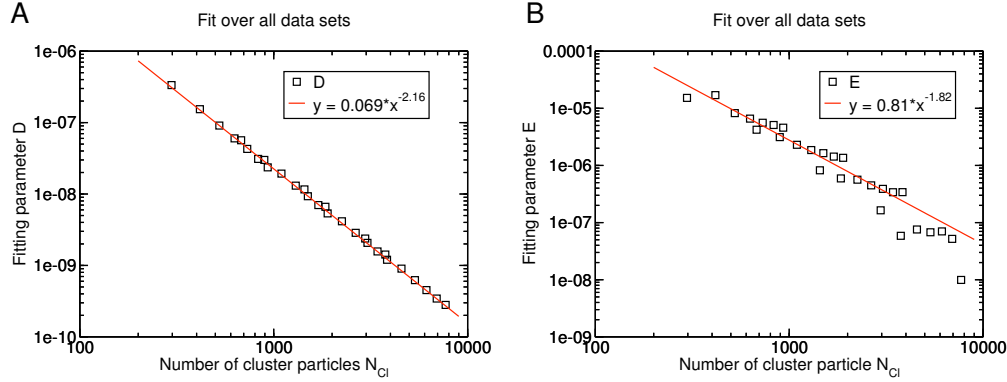


Figure 4.4: Dependence of the fitting parameters (A) D and (B) E on the number of cluster particles $N_{Cl} = n + m$. The red lines are algebraic fits to the shown data.

hopping rate, it is therefore necessary to determine the dependence of these parameters on N_{Cl} .

Plotting the values of D and E for all combinations of ρ_{tot} and L as a function of the number of particles in the cluster N_{Cl} gives figure 4.4. Whereas the data for D (figure 4.4 A) clearly indicates an algebraic decay at increasing number of particles in the cluster (or high occupation numbers of a site in the ZRP image), the data is less meaningful for the parameter E (figure 4.4 B). This parameter was also subject to much larger uncertainties in the fitting process than the parameter D . But the overall impression of a decreasing value of E with increasing particle number nevertheless persists.

Under the assumption of an algebraic decay for both parameters, the general form for the hopping rate in (4.6) reads:

$$u(n, m) = A \frac{n}{(n + m)^\gamma} + B \frac{1}{(n + m)^\delta}. \quad (4.7)$$

The corresponding hopping rate for negative particles $v(n, m)$ obeys the same expression with n and m interchanged because of the symmetry of the model under particle exchange:

$$v(n, m) = u(m, n). \quad (4.8)$$

4.2.5 Condensation criterion

Factorized steady state

The expression (4.7) shall now be used to determine if the two-species ZRP with these rates exhibits clustering. In [192], it is demonstrated that one needs

$$\frac{u(n, m)}{u(n, m - 1)} = \frac{v(n, m)}{v(n - 1, m)} \quad (4.9)$$

in order to have a factorized steady state of the two-species ZRP. Equation (4.7) obviously does not fulfill this condition. Another approximation has therefore to be made to obtain a suitable form of (4.7).

Approximation of the hopping rates

We are looking for a controlled approximation of the hopping rates which assumes a factorized steady state in the following. A simple approximation is to choose only the first term of (4.7):

$$\tilde{u}(n, m) := A \frac{n}{(n+m)^\gamma}. \quad (4.10)$$

One clearly has $\tilde{u}(n, m) < u(n, m)$ for all choices of n, m . The approximation thus reduces the hopping rates and the crucial question is whether smaller or bigger occupation numbers are reduced more strongly. A stronger reduction of the hopping rates of small occupation numbers reduces the system's tendency to condense as smaller clusters would then become more stable at the expense of large ones. The ratio of the approximated and the original hopping rate gives:

$$\frac{\tilde{u}(n, m)}{u(n, m)} = \frac{1}{1 + \frac{B}{An}(n+m)^{\gamma-\delta}}. \quad (4.11)$$

Considering the asymptotic limit of infinite n, m at constant ratio $\alpha = n/(n+m)$, one obtains:

$$\frac{\tilde{u}(n, m)}{u(n, m)} = \frac{1}{1 + \frac{B}{A\alpha}(n+m)^{\gamma-\delta-1}} \quad (4.12)$$

$$\xrightarrow[\frac{n}{m} = \text{const.}]{n, m \rightarrow \infty} \begin{cases} 0, & \text{for } \gamma > \delta + 1 \\ \frac{1}{1 + \frac{B}{A\alpha}}, & \text{for } \gamma = \delta + 1 \\ 1, & \text{for } \gamma < \delta + 1. \end{cases} \quad (4.13)$$

This result means that for $\gamma > \delta + 1$, the hopping rates of large occupation numbers are drastically reduced compared to smaller occupation numbers. A natural consequence is that the system will have a stronger tendency towards macroscopic clustering (or condensation) than the original one. In the other two cases ($\gamma \leq \delta + 1$), the hopping rates for bigger arguments n, m are less or equally affected by the approximation as the rates for smaller arguments. This is equivalent to a system which at best condenses as easily as the original system.

The numerical results shown in figure 4.4 suggest that the considered system falls into one of the last two cases ($\gamma = 2.16, \delta = 1.82$). The error on these values is too big to make a final statement about the validity of this assumption, but the given value of δ rather seems to underestimate the slope of the data shown in figure 4.4 B. However, there can be no certainty that the assumption $\gamma \leq \delta + 1$ really is correct.

Single-site weights

As can easily be verified, hopping rates as in (4.10) with (4.8) satisfy the constraint for a factorized steady state (4.9). Following the procedure in [192], we now can first calculate the single-site weights, then the generating function and deduce from there the condensation behavior.

In the considered factorized steady state, the single-site weights $f(n, m)$ are given by [192]

$$f(n, m) = \prod_{i=1}^n [\tilde{u}(i, m)]^{-1} \prod_{j=1}^m [\tilde{v}(0, j)]^{-1}, \quad (4.14)$$

which gives

$$f(n, m) = \prod_{i=1}^n \frac{(i+m)^\gamma}{Ai} \prod_{j=1}^m \frac{j^\gamma}{Aj} \quad (4.15)$$

$$= \frac{1}{A^{m+n} n! m!} \left(\frac{(n+m)!}{m!} \right)^\gamma \quad (4.16)$$

$$= \frac{[(n+m)!]^\gamma}{n! m!} \frac{1}{A^{m+n}}. \quad (4.17)$$

Generating function

The grand-canonical generating function of the two-species ZRP is defined as

$$F(z, y) = \sum_{n=0}^N \sum_{m=0}^M z^n y^m f(n, m), \quad (4.18)$$

where z and y correspond to the grand-canonical fugacities of positive and negative particles, respectively. From this function, the particle densities $\rho_{\text{tot}}^+ = N/L$ and $\rho_{\text{tot}}^- = M/L$ can be calculated [192]:

$$\rho_{\text{tot}}^+ = z \frac{\partial}{\partial z} \ln F(z, y) \quad \rho_{\text{tot}}^- = y \frac{\partial}{\partial y} \ln F(z, y). \quad (4.19)$$

These equations are the saddle point equations of the generating function (4.18). These equations require that z and y be less than or equal to the radii of convergence of (4.18) in order for $F(z, y)$ to exist.

The radii of convergence of the generating function for both z and y actually is zero in the limit $N, M, L \rightarrow \infty$. For a demonstration, the extreme case $y = 0$ is considered in which the radius of convergence of $z = 0$ should be largest:

$$F(z, 0) = \sum_{n=0}^N z^n \frac{(n!)^\gamma}{n!} \frac{1}{A^n} = \sum_{n=0}^N \frac{(n!)^{\gamma-1}}{A^n} z^n = \sum_{n=0}^N a_n z^n. \quad (4.20)$$

By applying the ratio test, the radius of convergence r of the power series (4.20) can be calculated:

$$r = \lim_{n \rightarrow \infty} \left| \frac{a_n}{a_{n+1}} \right| = \lim_{n \rightarrow \infty} A \left(\frac{n!}{(n+1)!} \right)^{\gamma-1} = A \cdot \lim_{n \rightarrow \infty} (n+1)^{1-\gamma}. \quad (4.21)$$

The radius of convergence thus can be either zero or infinite depending on the value of the exponent γ . Since the numerics indicate a value which is well above 1 (figure 4.4), the radius of convergence vanishes, i.e., the generating function does not exist for any point other than $(z = 0, y = 0)$. According to (4.19), the generating function thus only converges for zero density $\rho_{\text{tot}}^+ = \rho_{\text{tot}}^- = 0$. The two-species ZRP defined by the hopping rates (4.10) hence condenses all particles onto a single site.

4.2.6 Discussion

Under the assumption of the correctness of the approximations, this result implies that the basic model exhibits condensation at any non-zero density in the limit $L \rightarrow \infty$ which is the intuitively expected result discussed in section 4.2.1. Two important approximations were needed to obtain this result: First, the information of the spatial extent of particle clusters had to be eliminated for the inexact mapping to the two-species ZRP. While the current out of the largest cluster can well be identified by the average current in the system, it is less clear if this loss of information has a considerable impact on the condensation properties. The approach is however similar to a successful treatment of a model for car traffic [193]. There, all spatial information on the length of car clusters on the road was also discarded. The system nevertheless exhibited the same phase transition from a disordered to a jammed phase as a modified TASEP with very similar rules for passing of cars and random hopping rates of cars [194].

Second, the hopping rates had to be modified to allow for a factorized steady state of the two-species ZRP. This approximation appears less crucial as it was shown that for the observed parameter ranges, it actually decreases the tendency toward condensation. Lastly, the numerical data has been obtained for particle numbers which range over less than two decades. It cannot be excluded that extending the results to larger systems reveals different finite size effects.

In total, the result is in line with the formerly published result in [186], proposing that the basic model phase separates into one macroscopic cluster and an almost empty rest of the system in the limit of infinite system sizes. However, the finite size corrections considerably affected the system in the considered ranges, making the analysis subject to errors.

4.3 Transport on a dynamic lattice

4.3.1 Motivation

As presented in the previous part, generic problems occur when considering bidirectional transport on a static lattice if particles interact via exclusion. Meanwhile, axonal transport is very efficient although it is bidirectional and molecular motors exclude each other from MT binding sites. So far, there is only the model by Klumpp and Lipowsky [188] (section 3.3.2) which proposes a mechanism to bring theory closer to reality. Their approach includes species-dependent interactions which lead to an efficient self-organized state providing stable transport. This mechanism will be addressed in chapter 5. In the present section, a completely different type of mechanism will be presented which can lead to efficient bidirectional transport on a single track through consideration of the filament dynamics. This extension of the model has been inspired by the experimentally observed dynamics of the cytoskeleton (see section 2.4.1). In fact, the MTs on which molecular motors move are themselves highly dynamic, due to nucleation, polymerization and depolymerization, which occur on time scales similar to those involved in motor transport and are thus likely to interfere with the motor dynamics. Beyond the interest for intracellular traffic, the present section gives an example where a dynamically driven jammed phase is hindered by the lattice dynamics. The basic results of this section have partly been published by us in [195].

4.3.2 Model definition

The model is a modified version of the basic model presented in section 4.1.1 (figure 3.5). As a new feature we add some lattice dynamics for the lower lane, i.e., some sites are eliminated and recreated. The diffusive upper lane remains unchanged. On the lower lane, particles can only occupy a site if this binding site exists. The attachment moves (rate ω_a) are consequently rejected if the binding site has been eliminated. Additionally, a particle will automatically switch to the upper lane if it makes a forward step (rate p) onto an eliminated site or if the site which is currently occupied by the particle is eliminated.

Different types of lattice dynamics are considered (section 4.3.5) with a strong focus on a very simple uncorrelated choice of dynamics. This dynamics consists of eliminating randomly a site of the filament with rate k_d and recreating eliminated sites with rate k_p (figure 4.5) where the indices are reminiscent of the processes of MT polymerization and depolymerization. The state of the filament lattice is given by the local lattice states τ_i which take the value zero if site i is eliminated and one if the site exists. Since the lattice dynamics is uncorrelated and not influenced by the particle dynamics, the evolution of the lattice state τ_i can be easily expressed as:

$$\frac{\partial \langle \tau_i \rangle}{\partial t} = k_p (1 - \langle \tau_i \rangle) - k_d \langle \tau_i \rangle. \quad (4.22)$$

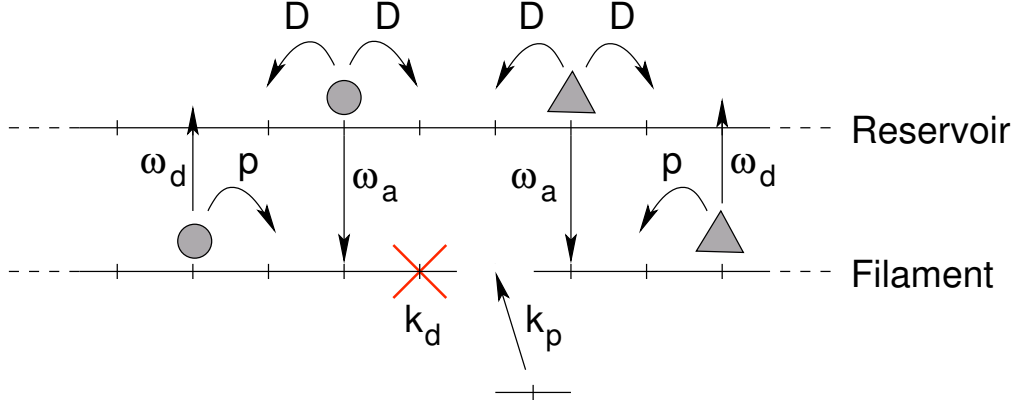


Figure 4.5: Basic model of section 4.1.1 with additional lattice dynamics on the filament. In the realization shown here, a filament site is eliminated at rate k_d and recreated at rate k_p .

In the stationary state, one therefore has a homogenous density of filament sites given by $\langle \tau_i \rangle = k_p / (k_p + k_d)$. Equations (4.1) and (4.2) are modified according to the additional moves caused by the lattice dynamics:

$$\begin{aligned} \frac{\partial \langle b_i^\pm \rangle}{\partial t} = & p [\langle b_{i-1}^\pm (1 - b_i^+ - b_i^-) \tau_i \rangle - \langle b_i^\pm (1 - b_{i+1}^+ - b_{i+1}^-) \tau_{i+1} \rangle - \langle b_i^\pm (1 - \tau_{i+1}) \rangle] \\ & + \omega_a \langle u_i^\pm (1 - b_i^+ - b_i^-) \tau_i \rangle - \omega_d \langle b_i^\pm \rangle - k_d \langle b_i^\pm \rangle, \end{aligned} \quad (4.23)$$

$$\begin{aligned} \frac{\partial \langle u_i^\pm \rangle}{\partial t} = & D [\langle u_{i-1}^\pm \rangle + \langle u_{i+1}^\pm \rangle - 2 \langle u_i^\pm \rangle] + p \langle b_i^\pm (1 - \tau_{i+1}) \rangle \\ & - \omega_a \langle u_i^\pm (1 - b_i^+ - b_i^-) \tau_i \rangle + \omega_d \langle b_i^\pm \rangle + k_d \langle b_i^\pm \rangle. \end{aligned} \quad (4.24)$$

For the stationary state, i.e., for the time derivatives set to zero, some insight on the mechanism introduced by the lattice dynamics can be gained if one assumes translational invariance and uses a mean field approximation. The mean field approximation is expressed by a factorization of correlation functions $\langle \sigma_i \sigma_j \rangle = \langle \sigma_i \rangle \langle \sigma_j \rangle$ and the translational invariance postulates that the averages do not depend on the site i . Defining $\rho_b^\pm := \langle b^\pm \rangle$ and $\rho_u^\pm := \langle u^\pm \rangle$, equations (4.23) and (4.24) hence reduce to

$$\omega_a \frac{k_p}{k_p + k_d} \rho_u^\pm (1 - \rho_b^+ - \rho_b^-) = \left(\omega_d + p \frac{k_d}{k_p + k_d} + k_d \right) \rho_b^\pm. \quad (4.25)$$

This mean field equation describes the equilibrium between the two lattices, i.e., between the filament and the reservoir. The left side gives the flux of particles attaching to the filament from the reservoir, while the right side is the flux away from the filament. Equation (4.25) also illustrates clearly the effect of the lattice dynamics on the particles as one can define effective detachment and attachment rates

$$\omega_{a,\text{eff}} := \omega_a \frac{k_p}{k_p + k_d}; \quad \omega_{d,\text{eff}} := \omega_d + p \frac{k_d}{k_p + k_d} + k_d, \quad (4.26)$$

so that the mean field equation of the basic model with a static lattice is recovered. The effective attachment rate is thus lowered by the lattice dynamics while the effective detachment rate is increased. The global effect is that the particles have a lower effective affinity to the filament. Considering only a lower affinity to the filament has been shown to reduce but not eliminate the tendency of cluster formation [186]. In combination with the conservation of mass, $\rho_{\text{tot}}^{\pm} = \rho_{\text{b}}^{\pm} + \rho_{\text{u}}^{\pm}$, it is possible to find a solution to (4.25) and calculate the current along the filament $J_{\text{b}}^{\pm} = \rho_{\text{b}}^{\pm}(1 - \rho_{\text{b}}^{+} - \rho_{\text{b}}^{-})$. This has also been done in [186] and turned out to provide wrong results as a consequence of neglecting all correlations.

The results presented on this model therefore come from numerical simulations as presented in section 4.1.2 and have been obtained over at least 10^6 MC sweeps for the same parameter set as in section 4.2: $p = 1$, $D = 0.33$, $\omega_{\text{d}} = 0.02$ and $\omega_{\text{a}} = 0.33$. Again, $p \gg \omega_{\text{d}}$ is chosen in order to capture the processivity of molecular motors. The polymerization is fixed at $k_{\text{p}} = 1$ if not stated otherwise and k_{d} is usually varied in order to observe the effects of the lattice dynamics with $k_{\text{d}} = 0$ corresponding to a static lattice. The density of particles is fixed at $\rho_{\text{tot}} = 2\rho_{\text{tot}}^{+} = 2\rho_{\text{tot}}^{-} = 1$ in order to have clustering on static lattices in numerically accessible system lengths.

4.3.3 Phase transition to a homogenous state

Suppression of clusters

The effect of the lattice dynamics on the collective behavior of the particles is investigated by varying the parameter k_{d} . The basic model with the static lattice corresponds to $k_{\text{d}} = 0$ and an increase of k_{d} causes a stronger and stronger lattice dynamics. As reported above, the lattice dynamics varies the effective affinity of the particles to the filament by changing the fraction of holes $k_{\text{d}}/(k_{\text{p}} + k_{\text{d}})$ in the filament. A first consequence of considering a dynamic lattice is the suppression of large clusters³ which become less and less dominant on increasing k_{d} until they disappear completely and the system becomes homogenous (figure 4.6 A). This disappearance of the large cluster is accompanied by a transition from a size-dependent to a size-independent state (figure 4.6 B).

The degree of homogeneity can be estimated by comparison with a mean field approximation addressed in the last section. Indeed, above the transition, particles are well-dispersed over the whole system and are much less correlated than in the static filament case (figure 4.7). Below the transition, a big cluster is formed and the mean field approximation obviously has to fail. Above the transition, the mean field prediction still overestimates the current although the two get closer due to the reduced affinity (figure 4.8). This indicates that clusters made of a few particles still play an important role. It is only for strong lattice dynamics that the mean field solution regains validity.

³Here, a cluster is defined as any accumulation of particles on the filament with only single isolated vacancies. Other definitions have been tested previously showing that the identification of the large cluster is very robust with regard to the cluster definition [185].

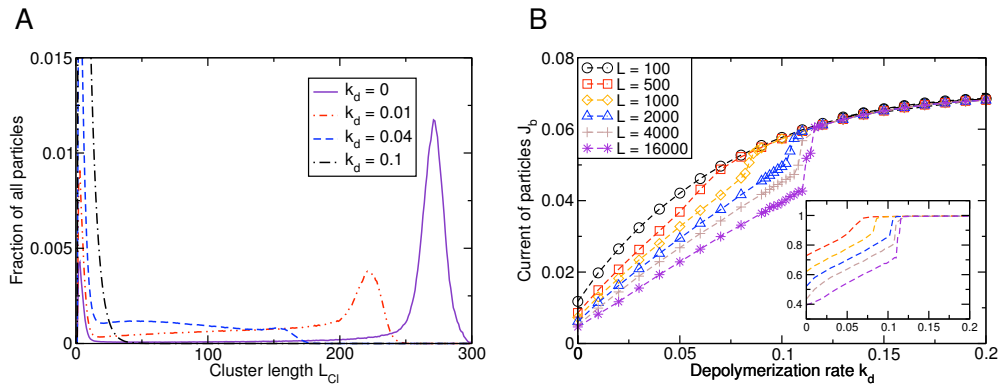


Figure 4.6: Cluster distribution and (B) current in the basic model with additional lattice dynamics. (A) The cluster distribution shows the fraction of all particles in the system which are found in a cluster of a given size L_{Cl} . (B) The current of positive particles bound to the filament J_b is shown for different system sizes L as a function of the depolymerization rate k_d . Since both particle species behave symmetrically, the current of negative particles takes an identical form. The inset shows the same data divided by the current in the smallest system $L = 100$.

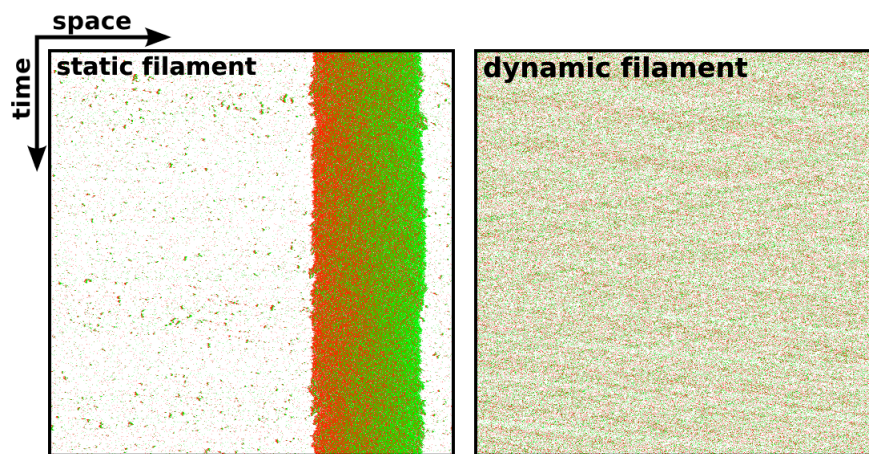


Figure 4.7: Space-time plots on a static and a dynamic filament. Every line in the images corresponds to the configuration of the filament lattice in a system of length $L = 1000$ with positive particles in red and negative particles in green. Vacant lattice sites are white. The static lattice plot has been recorded at $k_d = 0$ and the dynamic lattice plot at $k_d = 0.2$.

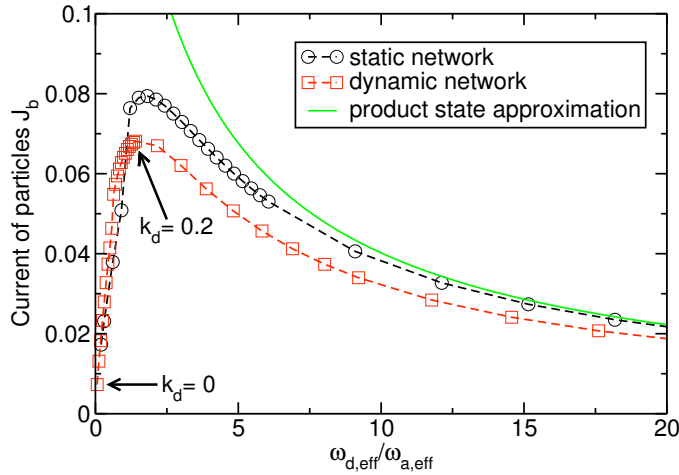


Figure 4.8: Comparison of the current of positive particles along the filament for static and dynamic lattices. The figure shows the current as a function of the ratio of effective detachment and effective attachment rates $\omega_{d,\text{eff}}/\omega_{a,\text{eff}}$. The value on the horizontal axis thus corresponds to the inverse of the particles' affinity to the filament. Data for a static lattice (black circles), a dynamic lattice (red squares), and the mean field solution (green line) are shown for a system size of $L = 1000$. For the static lattice, the effective rates correspond to the actual rates: $\omega_{a,\text{eff}} = \omega_a$ and $\omega_{d,\text{eff}} = \omega_d$. The variation of the effective rates is achieved by tuning the detachment rate ω_d in the static network case and by tuning the depolymerization rate k_d in the dynamic network case. The arrows indicate the parameters at which the space-time plots of figure 4.7 have been recorded.

When the depolymerization rate k_d is increased, first the current along the filament (symmetric for both particle species) increases, too. However, it should be noted that, if k_d is too high, binding sites become increasingly sparse and particles have fewer segments on which they can contribute to the total current in the system. Hence, the current of each particle species along the filament disappears for $k_d \rightarrow \infty$ and k_p constant. This behavior entails the existence of an optimal value for k_d (not seen on figure 4.6 B) at which the current is maximized. In this optimal regime with not too many holes in the filament, blocking situations with at least two particles of different species still occur frequently. As a consequence, the maximum currents that were obtained are about one third of the flux in a comparable single-species system [151], which is nevertheless a great improvement compared to the static filament case.

In fig. 4.9, simulation results for the optimal depolymerization rate $k_{d,\text{max}}(k_p)$ maximizing the flux are drawn as a function of the polymerization rate. The maximum flux $J_b(k_p, k_{d,\text{max}}(k_p))$ is shown as a function of k_p . One can see that the gain in transport capacity is obtained for a wide range of values of the polymerization rate k_p – an observation which supports the general validity of the results. Furthermore, the fraction of eliminated filament sites $k_d/(k_p + k_d)$ in the optimal regime decreases with increasing polymerization rate k_p as the optimal value $k_{d,\text{max}}$ saturates. This indicates

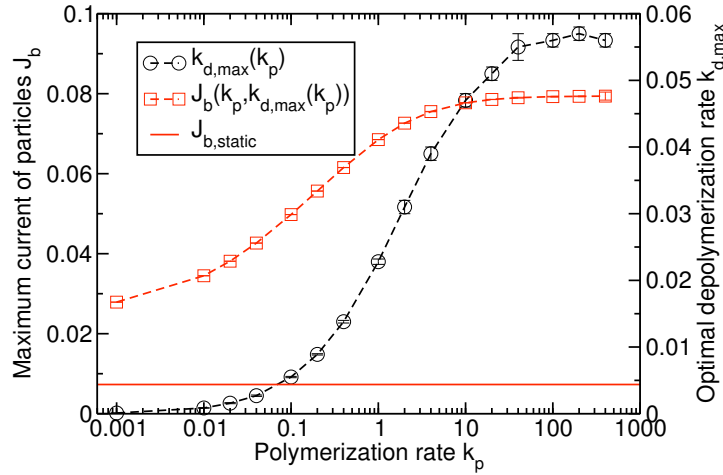


Figure 4.9: Maximum current $J_b(k_p, k_{d,\max}(k_p))$ (red squares) and optimal depolymerization rate $k_{d,\max}(k_p)$ (black circles) at given polymerization rates k_p in a system of size $L = 1000$. For comparison, the flux in a system with a static lattice is drawn as a solid red line. Note that the horizontal axis is in logarithmic scale and, therefore, both quantities seem to saturate at high polymerization rates.

that the optimal flux depends on the time interval a site persists rather than on the delay after which it is recreated.

Nature of the transition

The results presented above show that lattice dynamics can hinder the formation of structures which span over a considerable part of a finite system. Looking at figure 4.6 B, it can be noted that the depolymerization rate $k_{d,\text{crit}}(L)$ at which the system transits from the clustered to the homogenous state seems to shift to bigger values for larger system sizes L . Before stating that the observed transition causes the system to have a finite current even for $L \rightarrow \infty$, the limit $\lim_{L \rightarrow \infty} k_{d,\text{crit}}$ has to be determined. In case this critical depolymerization rate diverges for infinite systems, the system will still have a macroscopic cluster and the lattice dynamics does not make transport efficient in infinite systems. One is thus interested in the nature of the transition.

A typical record of the current along the filament of one particle species can be seen in figure 4.10 A. The system oscillates between the homogenous and the clustered configuration at the shown choice of parameters near the transition $k_{d,\text{crit}}$. This can be seen by the bimodal distribution of the current along the filament, in which the larger currents correspond to a homogenous configuration. For configurations with a large cluster, the current is significantly lower as the cluster blocks a part of the current. The transitions between homogenous and clustered configurations are very abrupt as they occur on a much shorter time scale than the persistence of the system in one of those states. For long enough simulation times, many of the oscillations

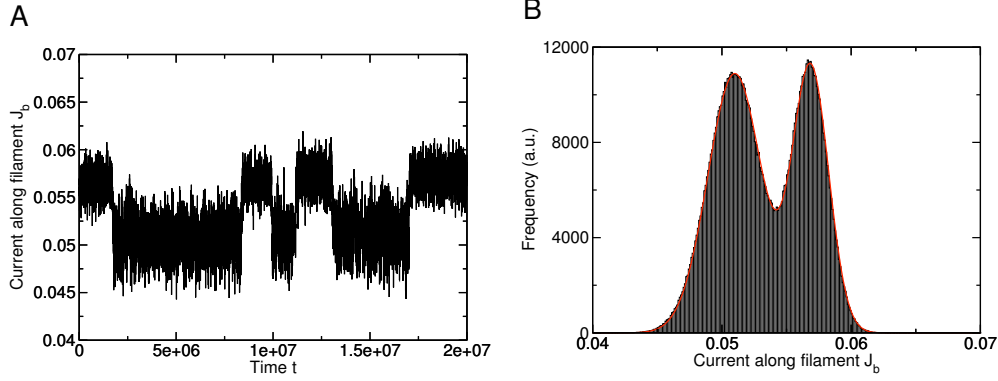


Figure 4.10: Time evolution of current along the filament. (A) The graph shows the current of positive particles along the filament J_b^\pm recorded over time in a system of size $L = 1600$ and at depolymerization rate $k_d = 0.099$ after a transient time allowing the system to reach its steady state. (B) Histogram of the current distribution for the data shown on the left part of the figure in black. The red line is a fit by the sum of two gaussian distributions with parameters $\mu_1 = 0.051, \sigma_1 = 0.0021$ and $\mu_2 = 0.057, \sigma_2 = 0.0014$ and respective pre-factors $A_1 = 56.8$ and $A_2 = 39.1$.

between the two states can be observed and a histogram over the recorded values of the current can be created (figure 4.10 B). This histogram can be fitted very well by the sum of two gaussians:

$$f(J_b) = \frac{A_1}{\sqrt{2\pi}\sigma_1} \exp\left(-\frac{1}{2}\left(\frac{J_b - \mu_1}{\sigma_1}\right)^2\right) + \frac{A_2}{\sqrt{2\pi}\sigma_2} \exp\left(-\frac{1}{2}\left(\frac{J_b - \mu_2}{\sigma_2}\right)^2\right). \quad (4.27)$$

If this distribution function is fitted for different values of k_d , the critical depolymerization rate $k_{d,crit}$ at which the transition takes place can be determined: The point of coexistence is given by the equality of the prefactor $A_1 = A_2$ and defines $k_{d,crit}$ [196].

The problem with the presented procedure is that the time spent in either the homogenous or clustered state grows very quickly with the system size L so that only very few transitions can be observed for reasonable simulation times. In addition to the low number of transitions, the memory of the initial configuration becomes stronger so that the initial choice might influence the state of the system over a longer transient time than acceptable. As a consequence, $k_{d,crit}$ can only be determined for small systems as shown in figure 4.11. The data does not even extend over one order of magnitude and any conclusion has to be handled with a lot of care. In fact, from a plot with linear axes (inset of figure 4.11), the functional dependence of $k_{d,crit}$ on L is hard to tell as the curvature is extremely low. By contrast, in a plot with a logarithmic horizontal axis, the data appears linear, suggesting a scaling of the form $k_{d,crit}(L) = A \cdot \ln(L) + B$. A fitting procedure provides the parameters $A = 0.031$ and $B = -0.132$.

For our model, a logarithmic scaling would mean that the phase transition which is observed in figure 4.6 B does not persist in the limit $L \rightarrow \infty$ but diverges infinitely

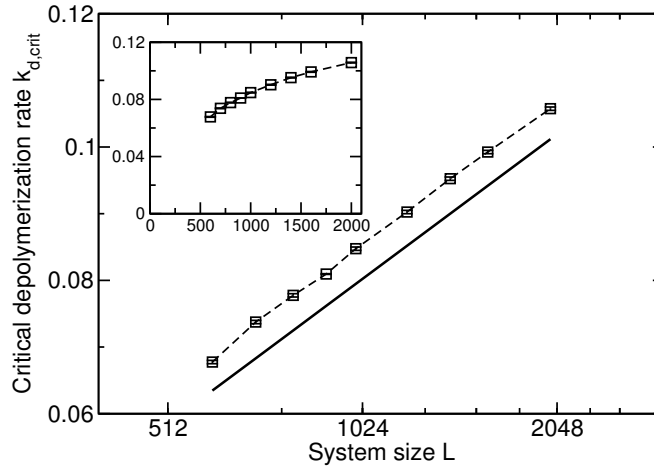


Figure 4.11: Critical depolymerization rate $k_{d,crit}$ as a function of the system size L . The data has been produced as described in the main text. The main plot has a logarithmic horizontal axis while the inset is linear on both axis. The solid black line is a guide to the eye with slope 0.031.

slowly. The dissolution of nascent clusters as shown in figure 4.6 *A* would therefore not be efficient enough in an infinite system to cause a homogenous state which depends solely on the density of particles and represents an efficient transport state with finite current.

In summary, there is a transition in finite systems which works actively against structure formation and which may not persist in the thermodynamic limit as the critical rate diverges, although the divergence is infinitely slow. It will be shown in the following, however, that the lattice dynamics introduces another effect which prevents the formation of macroscopic structures.

4.3.4 Constraints on maximum cluster lengths

Approach

Although it was not possible to exclude with certainty from numerical simulations that the transition to a homogenous state persists for infinite systems, the following calculations will show that no macroscopic structures can exist for $L \rightarrow \infty$ if $k_d > 0$, i.e., the system is homogenous in this limit. The idea relies entirely on the stationary state of the transport lattice so that the particles are completely discarded from the presentation in the current section.

The lattice dynamics creates holes in the filament, thus subdividing the whole lattice into several segments of different lengths. This naturally puts a constraint on the cluster length if a cluster is understood as an accumulation of particles on the filament with only isolated vacancies as is the case here. Other cluster definitions will

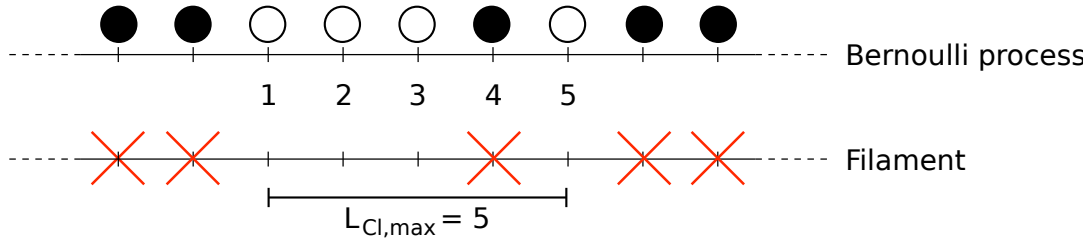


Figure 4.12: Schematic representation of a segment of the transport lattice without any particles. Eliminated binding sites are marked by a red cross. Because of the cluster definition, a cluster on this segment cannot be longer than $L_{Cl,max} = 5$ as eliminated binding sites cannot be occupied by particles. $L_{Cl,max}$ therefore represents the maximum possible cluster length on this segment. On the upper part of the figure is the corresponding Bernoulli process in which a white ball is placed on a site with probability p and a black ball is chosen with probability $q = 1 - p$.

be addressed further below. The maximum cluster length $L_{Cl,max}$ which can exist on a given segment is therefore determined by the distance between two pairs of neighboring holes (see figure 4.12). This length $L_{Cl,max}$ is obviously an upper bound for the actual cluster length L_{Cl} that will be found on the segment so that the clustering properties of the system are limited by the distribution of the maximum cluster lengths.

The distribution of the maximum cluster lengths $L_{Cl,max}$ will be derived by a mapping of the lattice configuration to a simple Bernoulli process. In this mapping, the transport lattice corresponds to a Bernoulli process with the site i being the i -th Bernoulli trial in the process. The state of lattice site i is described by a stochastic variable X_i taking values 0 and 1 if the lattice site has been eliminated or exists, respectively. An existing lattice site is hence mapped to a success (= white ball) in the Bernoulli trial and an eliminated site is mapped to failure (= black ball). In the stationary state of the lattice, the success and failure probabilities p and $q = 1 - p$ are given by:⁴

$$P(X_i = 1) = \frac{k_p}{k_d + k_p} =: p \quad \text{and} \quad P(X_i = 0) = \frac{k_d}{k_d + k_p} =: q. \quad (4.28)$$

The idea is to calculate from these basic properties the distribution of maximum cluster lengths $P(L_{Cl,max})$. In other words: What is the probability that between two pairs of holes or eliminated sites on the lattice, there are exactly $L_{Cl,max}$ sites of which only isolated ones are eliminated. In the language of the Bernoulli process, one wants to determine the probability for a sequence of $L_{Cl,max}$ Bernoulli trials during which two black balls have never been drawn consecutively.

⁴Please note that we apply the standard nomenclature of Bernoulli processes, i.e., the success probability is p , although p is used for the forward hopping rate in the rest of this thesis. Since there are no particles involved in the current section, this should not lead to confusion.

Boundary conditions

Several stochastic variables are fixed by the boundary conditions imposed by the fact that we are interested in the probability for a segment of exactly $L_{\text{Cl,max}}$ sites. Starting from two consecutive failures in trials -1 and 0 , the first trial has to be a success ($X_1 = 1$) in order to start the sequence with the desired properties. Since the sequence is supposed to end after $L_{\text{Cl,max}}$ trials, the two subsequent trials have to fail ($X_{L_{\text{Cl,max}}+1} = 0, X_{L_{\text{Cl,max}}+2} = 0$). For the same reason as for X_1 , one also has $X_{L_{\text{Cl,max}}} = 1$.

Auxiliary function

The inner part of the sequence extending from trial 2 to $L_{\text{Cl,max}} - 1$ is a random sequence of successes and failures with the constraint that two subsequent trials may not fail. In order to formulate this condition, the auxiliary function $F(\{X_i\})$ is introduced:

$$F(\{X_i\}_{i=2}^{L_{\text{Cl,max}}-1}) = \prod_{i=2}^{L_{\text{Cl,max}}-2} 0^{(1-X_i)(1-X_{i+1})}, \quad (4.29)$$

with $\{X_i\}_{i=2}^{L_{\text{Cl,max}}-1}$ denoting the sequence of stochastic variables $X_2, X_3, \dots, X_{L_{\text{Cl,max}}-1}$. This form takes advantage of the conventional definition $0^0 = 1$. A factor in the product takes the value 1 if at least one of the two stochastic variables X_i, X_{i+1} is equal to one, i.e., if not both are failures. If this is fulfilled for all pairs of stochastic variables, the product as a whole is one so that one has $F = 1$. On the other hand, if $X_i = 0$ and $X_{i+1} = 0$ for one of the factors, then the whole product vanishes and $F = 0$. The auxiliary function therefore indicates if a sequence of stochastic variables fulfills the desired condition by taking the value 1.

Distribution of maximum cluster lengths

With the preliminaries of the previous subsections, the desired probability can be formulated as

$$\begin{aligned} & P(L_{\text{Cl,max}}) \quad (4.30) \\ & := P\left(X_1 = 0 \cap X_{L_{\text{Cl,max}}} = 0 \cap X_{L_{\text{Cl,max}}+1} = 1 \cap X_{L_{\text{Cl,max}}+2} = 1 \cap F(\{X_i\}_{i=2}^{L_{\text{Cl,max}}-1}) = 1\right) \\ & = P(X_1 = 0) \cdot P(X_{L_{\text{Cl,max}}} = 0) \cdot P(X_{L_{\text{Cl,max}}+1} = 1) \cdot P(X_{L_{\text{Cl,max}}+2} = 1) \\ & \quad \cdot P\left(F(\{X_i\}_{i=2}^{L_{\text{Cl,max}}-1}) = 1\right). \end{aligned}$$

For the last equality, the independence of the stochastic variables in the Bernoulli process was used. With the exception of the last probability, this expression is trivial. The last factor expresses the probability *not* to have two or more failures in a row in a

Bernoulli process with parameter p . This probability can conveniently be written as

$$P\left(F\left(\{X_i\}_{i=2}^{L_{\text{Cl,max}}-1}\right) = 1\right) = \sum_{\{X_i\}_{i=2}^{L_{\text{Cl,max}}-1}} P\left(\{X_i\}_{i=2}^{L_{\text{Cl,max}}-1}\right) \cdot F\left(\{X_i\}_{i=2}^{L_{\text{Cl,max}}-1}\right). \quad (4.31)$$

This equation simply is a weighted counting of all possible outcomes of the process. If a result is not allowed because it has two or more subsequent failures, the auxiliary function returns 0 and eliminates the contribution of that result. In the other case, it takes the value 1 and the result is counted according to its probabilistic weight given by

$$P\left(\{X_i\}_{i=2}^{L_{\text{Cl,max}}-1}\right) = \prod_{i=2}^{L_{\text{Cl,max}}-1} p^{X_i} q^{1-X_i} = p^{\sum_{i=2}^{L_{\text{Cl,max}}-1} X_i} q^{L_{\text{Cl,max}}-2-\sum_{i=2}^{L_{\text{Cl,max}}-1} X_i}, \quad (4.32)$$

so that it is now possible to compute (4.31). In order to alleviate the notation and to emphasize the generality of the calculation for a Bernoulli process with N draws and parameter p , the index i is reduced by one and the end of the sequence is taken to be at $N = L_{\text{Cl,max}} - 2$.

The sequence

$$A_N := P\left(F\left(\{X_i\}_{i=1}^N\right) = 1\right) \quad (4.33)$$

is the sequence of probabilities for no more than one failures in a row if a Bernoulli trial is repeated N times. This sequence obeys the recursion relation:

$$A_N = p \cdot A_{N-1} + pq \cdot A_{N-2}. \quad (4.34)$$

Proof:

$$\begin{aligned} A_N &= \sum_{\{X_i\}_{i=1}^N} P\left(\{X_i\}_{i=1}^N\right) \cdot F\left(\{X_i\}_{i=1}^N\right) \\ &= \sum_{\{X_i\}_{i=1}^N} p^{\sum_{i=1}^N X_i} q^{N-\sum_{i=1}^N X_i} \prod_{i=1}^{N-1} 0^{(1-X_i)(1-X_{i+1})} \\ &= \sum_{\{X_i\}_{i=1}^{N-1}} p^{\sum_{i=1}^{N-1} X_i} q^{N-1-\sum_{i=1}^{N-1} X_i} \prod_{i=1}^{N-2} 0^{(1-X_i)(1-X_{i+1})} \sum_{X_N=0}^1 p^{X_N} q^{1-X_N} 0^{(1-X_{N-1})(1-X_N)} \\ &= \sum_{\{X_i\}_{i=1}^{N-1}} P\left(\{X_i\}_{i=1}^{N-1}\right) \cdot F\left(\{X_i\}_{i=1}^{N-1}\right) \cdot \left(p + q \cdot 0^{(1-X_{N-1})}\right) \\ &= p \cdot A_{N-1} + q \cdot \sum_{X_{N-1}=0}^1 0^{1-X_{N-1}} \sum_{\{X_i\}_{i=1}^{N-2}} P\left(\{X_i\}_{i=1}^{N-1}\right) \cdot F\left(\{X_i\}_{i=1}^{N-1}\right) \\ &= p \cdot A_{N-1} + pq \cdot \sum_{\{X_i\}_{i=1}^{N-2}} P\left(\{X_i\}_{i=1}^{N-2}\right) \cdot F\left(\{X_i\}_{i=1}^{N-2}\right) \\ &= p \cdot A_{N-1} + pq \cdot A_{N-2} \end{aligned}$$

The second term is obtained for $X_{N-1} = 1$ which is the only choice for which this term does not vanish in the third last line. The starting values of this sequence can be found by counting configurations:

$$A_1 = 1 \quad \text{and} \quad A_2 = 1 - q^2. \quad (4.35)$$

Equation (4.34) with (4.35) can be solved:

$$A_N = -\frac{q \left(p + \sqrt{p^2 + 4qp} \right) \left(-\frac{2qp}{p - \sqrt{p^2 + 4qp}} \right)^N}{\sqrt{p^2 + 4qp} \left(p - \sqrt{p^2 + 4qp} \right)} - \frac{q \left(-p + \sqrt{p^2 + 4qp} \right) \left(-\frac{2qp}{p + \sqrt{p^2 + 4qp}} \right)^N}{\sqrt{p^2 + 4qp} \left(p + \sqrt{p^2 + 4qp} \right)}. \quad (4.36)$$

The base of the exponentiation in the second term is always negative but its absolute value is smaller than the base of the first term. For $N \gg 1$, the sequence A_N is consequently dominated by its first term (figure 4.13 A):

$$A_N \xrightarrow{N \rightarrow \infty} C_1 \cdot \exp(-N/C_2) \quad (4.37)$$

with

$$C_1 := -\frac{q \left(p + \sqrt{p^2 + 4qp} \right)}{\sqrt{p^2 + 4qp} \left(p - \sqrt{p^2 + 4qp} \right)} \quad (4.38)$$

$$C_2 := \left[\ln \left(-\frac{p - \sqrt{p^2 + 4qp}}{2qp} \right) \right]^{-1}. \quad (4.39)$$

The parameter C_2 represents the characteristic decay length of the probability not to have two or more failures in a row given the probabilities p and $q = 1 - p$. For low values of q , this length decays almost inversely quadratically⁵ (figure 4.13 B).

Connection to transport model

With this result, it is now possible to explicitly state the probability (4.30) to have a maximal cluster length of exactly $L_{Cl,max}$ for $L_{Cl,max} \geq 2$:

$$P(L_{Cl,max}) = q^2 \cdot p^2 \cdot \left[-\frac{q \left(p + \sqrt{p^2 + 4qp} \right) \left(-\frac{2qp}{p - \sqrt{p^2 + 4qp}} \right)^{L_{Cl,max}-2}}{\sqrt{p^2 + 4qp} \left(p - \sqrt{p^2 + 4qp} \right)} - \frac{q \left(-p + \sqrt{p^2 + 4qp} \right) \left(-\frac{2qp}{p + \sqrt{p^2 + 4qp}} \right)^{L_{Cl,max}-2}}{\sqrt{p^2 + 4qp} \left(p + \sqrt{p^2 + 4qp} \right)} \right] \quad (4.40)$$

$$\approx q^2 \cdot p^2 \cdot C_1 \cdot \exp(-(L_{Cl,max} - 2)/C_2). \quad (4.41)$$

⁵A better approximation is $C_2 = p^{-2} \frac{1+2.5p}{1+1.5p}$.

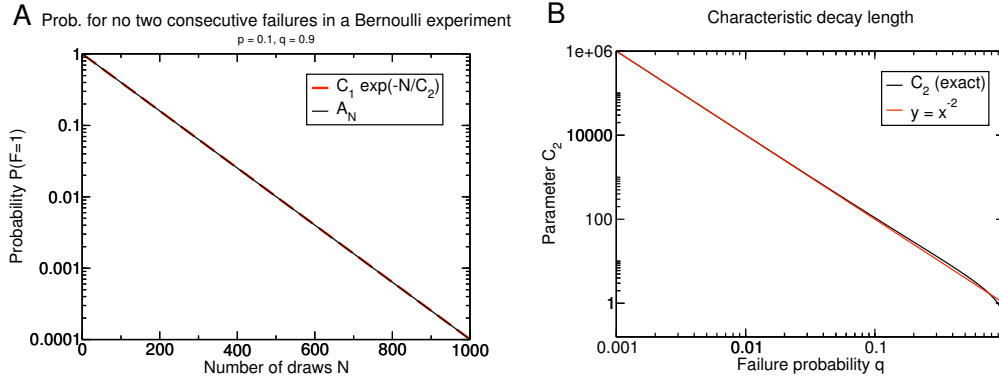


Figure 4.13: Properties of the conditioned Bernoulli process. (A) Probability for no two consecutive failures in a Bernoulli process which is repeated N times for $p = 0.1$. The exact result (4.36) is the solid black line, the dashed red line is an exponential approximation which neglects the second term of the exact solution. (B) Characteristic decay length (4.39) in black. For comparison, the inverse of a parabola $y = q^{-2}$ has been added to the graph (red line).

For completeness, two special cases have to be added: A maximum cluster length of $L_{\text{Cl,max}} = 1$ has not been considered so far, its probability is:

$$P(L_{\text{Cl,max}} = 1) = q^2 \cdot p. \quad (4.42)$$

The second case which deserves attention is if the pair of holes in the lattice (i.e., failures in the Bernoulli process) is followed by at least one additional hole. In that case, the pair of holes is not directly followed by a potential cluster segment and is consequently not covered by the expression above. The probability for this to happen is

$$P(\text{hole}) = q. \quad (4.43)$$

As a confirmation of the considerations above, the normalization

$$P(\text{hole}) + \sum_{k=1}^{\infty} P(L_{\text{Cl,max}} = k) = 1, \quad (4.44)$$

was numerically verified for $p \in [0, 1]$.

The probability for long maximum cluster lengths thus decays exponentially for $q > 0$ which is equivalent to $k_d > 0$, i.e., for a dynamic lattice. This means that at any given strength of the lattice dynamics, the appearance of large clusters becomes exponentially unlikely. This effect will be perceivable for all system sizes as soon as the number of particles in the system is bigger than the characteristic maximum cluster length as expressed by (4.39). For much larger system sizes, the system will thus appear homogenous. This transition to a homogenous appearance can be noticed

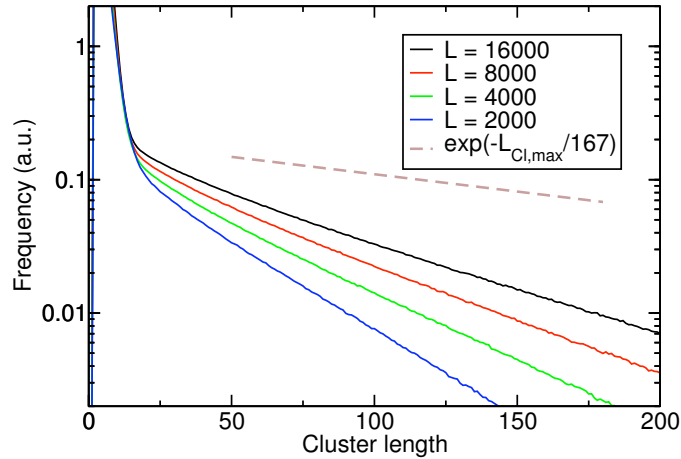


Figure 4.14: Comparison of cluster length decay and maximum cluster length decay. The solid lines are the tails of the cluster length distributions as measured in simulations with different system sizes L . The lattice dynamics were given by $k_p = 1$ and $k_d = 0.08$, i.e., close to but still below the dynamical transition described in section 4.3.3. The brown dashed line has the same decay as the distribution of maximum cluster lengths $L_{Cl,max}$ at the given parameters of the lattice dynamics. The characteristic length scale is $C_2(k_p = 1, k_d = 0.08) \approx 167$ for these parameters.

at lower depolymerization rates k_d for larger system sizes L as these permit larger structures. This indicates that the type of cluster inhibition described here is qualitatively different from the one presented in section 4.3.3 where the transition towards a homogenous state actually shifted positively with the system length L .

There are consequently two different effects which limit the cluster sizes in different regimes. In the finite systems considered in section 4.3.3, the decay of maximum cluster lengths is indeed much slower than the actual decay of the cluster size distribution (figure 4.14). As explained above, the distribution of maximum cluster lengths is only an upper bound since the particle dynamics does not necessarily cause every segment of a given length $L_{Cl,max}$ to really be populated by enough particles to form a cluster of the same length. This also explains why the decay of the cluster length distributions is more important for smaller systems: Because smaller systems have fewer particles at the same density, there are less particles to form larger clusters which thus become increasingly unlikely the smaller the system is.

It can be concluded that the limitation of maximum cluster lengths does not trigger the transition which is observed in finite systems but that dynamical effects play a more important part and that the effects leading to homogenous states are qualitatively different in finite and infinite systems.

Furthermore, the lattice is itself dynamic and not frozen in one particular configuration so that additional effects may arise due to the alteration of the lattice. A segment of a given maximum cluster length might not even exist long enough to allow

a cluster to form on that segment. It can be shown that longer segments have short survival times before they decompose into smaller segments. Since the derivation of this result is somewhat lengthy and the result rather intuitive, it is not shown here but can be found in appendix A instead.

Generalized cluster definition

The results of this section have been derived for a plausible, but still arbitrary definition of clusters. In principle, it cannot be derived from the absence of such defined macroscopic clustering that there will be no macroscopic structures. For example, it is conceivable that a huge accumulation of particles forms which spans over several neighboring segments although they are separated by at least two holes in the lattice. The filament itself would, of course, be subdivided into several segments, but the particles may heavily populate the bulk reservoir at those sites, hence still giving the overall picture of a macroscopic structure.

Fortunately, the important property of the maximum cluster length distribution, namely the exponential decay, seems to remain if the cluster definition is generalized in the following way: Instead of allowing only isolated vacancies on the filament in a cluster, a cluster is now defined to have at most $k - 1$ adjacent vacancies and is consequently bounded on both sides by k vacancies at least. The derivation procedure for this case is identical to the case $k = 2$ treated above, although it becomes lengthier due to the higher number of terms and will not be carried out here.

First, the auxiliary function (4.29) is generalized:

$$F_k(\{X_i\}_{i=1}^N) = \prod_{i=1}^{N-k+1} 0 \prod_{l=0}^{k-1} (1 - X_{i+l}), \quad (4.45)$$

which then leads with the same steps as before to the recursion relation

$$A_N = p \cdot \sum_{i=1}^k q^{i-1} A_{N-i}. \quad (4.46)$$

The starting values are:

$$A_l = 1, \quad \text{for } 1 \leq l \leq k - 1; \quad A_k = 1 - q^k. \quad (4.47)$$

This recursion can be solved for any given choice of p and k , always returning an exponentially decreasing sequence. The involved characteristic length scale increases with increasing k at constant p .

Although it is not possible to write the solution of A_N for a general value k , a

general expression for the generating function $G_k(z)$ can be given:

$$G_k(z) := \sum_{i=1}^{\infty} A_i z^i = \frac{Q_k(z)}{R_k(z)} \quad (4.48)$$

$$Q_k(z) = z \left[\sum_{i=0}^{k-2} p^i z^i + (1-p)p^{k-1} z^{k-1} \right] \quad (4.49)$$

$$R_k(z) = 1 - (1-p) \sum_{i=1}^k p^{i-1} z^i. \quad (4.50)$$

This form has not been derived exactly but deduced by guessing from the form of $G_k(z)$ for low values of k . Afterwards, it was verified algebraically that (4.48) actually describes the generating function $G_k(z)$ for values $1 \leq k \leq 1000$, suggesting that the result holds generally which will be assumed here. The sequence element A_N can consequently be determined for any k by derivation of the generating function:

$$A_N = \frac{1}{N!} \left. \frac{d^N G_k}{dz^N} \right|_{z=0}. \quad (4.51)$$

Even if the given form of the generating function was not true for the unverified cases $k > 1000$, the values $k \leq 1000$ should be fairly enough for the reasoning below.

These observations suggest that the exponential distribution of segments persists even for this generalized cluster definition. Macroscopic structures can only exist in the infinite system if particles are able to bridge the gap between neighboring segments of the lattice by high occupation of the bulk reservoir. Since motion is undirected in the bulk reservoir, the invariant particle dynamics determines the spreading of particles in the bulk reservoir and therefore the escape rate of particles out of a big accumulation of particles. The argument here is that, for long enough sequences of holes in the lattice which separate two segments, no persistent accumulation of particles can exist in the bulk reservoir between the segments. If diffusion is high, particles spread quickly and do not localize strongly enough about clusters on the filament in order to maintain them [185] and for low diffusion rates, particles in the bulk reservoir are not able to diffusively hop across k sites in order to bridge two long lattice segments via the reservoir if k is large enough. The result would be isolated islands of particles which form around long segments of lattice sites and which have a characteristic length scale determined by the decay of the maximum cluster length distribution.

Since this reasoning is based on intuitive arguments, a validation would be desirable. However, a validation is difficult because large system sizes would have to be simulated to make sure that one is below the transition reported on in section 4.3.3 but still has an accessible characteristic cluster length decay.

4.3.5 Different lattice dynamics

So far, the results for bidirectional transport on a dynamic lattice have been obtained for very simple lattice dynamics which does not resemble a realistic MT dynamics as presented in section 2.2.2. A random elimination of binding sites would translate to a breaking of MT filaments and the recreation of binding sites to gluing two MT parts together. Both processes are not dominant in MT dynamics if they occur at all. This particular choice of lattice dynamics has been made because of its simplicity and because a realistic dynamics of the axonal MT network is very complicated. So far, there is not even a quantitative model for axonal MTs including the interactions between shorter and longer axonal MTs as proposed in the *Cut-and-run* model (section 2.4.1).

We claim that the main result of section 4.3.3, i.e., the phase transition to a density-dependent state with efficient transport in a finite system is independent of the exact choice of lattice dynamics. As a support of this claim, different lattice dynamics have also been examined. After the simple lattice dynamics of the previous sections, an occupation-dependent variant was implemented in which a site is eliminated with rate k_d *only* if that site is occupied by a particle. This choice corresponds to molecular motors putting strain on the MT filament and thus increasing the chance of depolymerization if they are bound to the MT. Although some kinesins are known to act as depolymerizing agents by a similar mechanism (section 2.3.1), these MT-depolymerizing kinesins are not responsible for intracellular long-range transport. Therefore, this choice of lattice dynamics is also rather an illustration that the transition is not dependent on the choice of lattice dynamics than a modeling of realistic interactions.

In the mean field picture, the dependence of the depolymerizing step on site occupation changes the average value of the binding site variable to

$$\langle \tau_i \rangle = \frac{k_p}{k_p + (\rho_b^+ + \rho_b^-)k_d}, \quad (4.52)$$

modifying the mean field equation (4.25) accordingly.

It turns out that the results are qualitatively the same as obtained for the first type of lattice dynamics. The main difference is that the flux in the homogenous phase is higher than in the first scenario. In this phase, when a motor is moving freely, it encounters less holes than in the case of the simple lattice dynamics, as empty sites cannot be eliminated anymore. Processive runs along the filament are thus less frequently interrupted. By contrast, in the clustered phase, there is almost no difference to the first scenario as the transport capacity is limited by the large clusters, where all filament sites are occupied by particles anyway. The transition to a density-dependent efficient state is maintained if one generalizes the occupation-dependent lattice dynamics by requiring that a higher number of particles has to accumulate in order to put enough strain on the filament to break.

Finally, a third kind of dynamics is considered, resembling treadmilling of filaments (section 2.2.2). Although this type of motion is actually of minor importance in axons, it is a bio-inspired type of dynamics and as individual binding sites are

eliminated after some time, a qualitative similar behavior is expected and indeed obtained. The treadmilling filaments were modeled in a simplified way by considering regularly spaced holes in the lower lane which propagate synchronously but stochastically through the system. The aforementioned transition toward efficient transport is still observed. It is to be noted that, since the holes move only in one direction, the two species of particles are affected differently. The fluxes of both species therefore depend on the moving direction along the filament, though they are of the same order. For both species, there is a considerable increase of the flux and a maximum current comparable to the one in the previous scenarios is reached.

4.3.6 Discussion

To summarize, a model for bidirectional transport on a one-dimensional dynamic lattice coupled to a confined diffusion reservoir was presented in this section. While on a static lattice persistent clusters form which inhibit efficient transport, the counter-intuitive effect is found that the transient suppression of filament sites dramatically *enhances* the transport capacity. Indeed, the inhibition of large clusters leads to a transition toward a homogenous state characterized by efficient transport in the sense that the state is density-dependent and the current will be finite also in very large systems. This is a new mechanism in the phenomenology of dynamic phase transitions. This transition separates a size-dependent (jammed) state from a density-dependent one. It is robust in the sense that it is obtained for quite different types of lattice dynamics. The actual transport capacity of the system rather depends on the optimal lifetime of a binding site than on the details of the filament dynamics. The lifetime has to be short enough in order to avoid jam formation and long enough in order to direct the transport.

The numerical data suggests that the point of transition diverges infinitely slowly with increasing system sizes so that the transition might not be present in the infinite system. Even if this turns out to be correct, no macroscopic clustering will be observed in the limit $L \rightarrow \infty$ as the steady state of the lattice introduces a characteristic length scale into the system which is independent of the particle dynamics and which inhibits any macroscopic structures. The infinite system therefore also presents a finite current on a dynamic lattice even if the dynamic phase transition is not observed anymore.

Some more insight could be gained from an analysis similar to the one found in [197] for the symmetric motion of non-interacting particles in fluctuating energy landscapes. However, note that here the effective ‘potential’ landscape emerges spontaneously from the particle jamming.

4.4 Chapter conclusion

The examination of the models in this chapter yields the general result that it is not trivial to observe bidirectional transport of particles which move along the same

track. For the type of models considered here, there is indeed some indication that bidirectional transport does not persist in the thermodynamic limit (section 4.2). This property is fortunately lost in the case of a dynamic transport lattice (section 4.3). Instead, two effects occur which effectively inhibit the appearance of macroscopic structures and therefore create a finite current even in large or infinite systems. First, lattice dynamics inhibits the formation of large clusters by frequently driving particles which are blocked by other particles to the bulk reservoir. Second, the steady state under lattice dynamics subdivides the lattice into multiple segments with a characteristic length which is independent of the total system size. While the former mechanism is visible in finite system and considerably increases the current along the filament, there is numerical evidence that the transition between the clustered and the homogenous state diverges with increasing system size. For extremely long or infinite systems, the latter mechanism will therefore be responsible for limiting the size of particle accumulation in those cases.

In summary, the lattice dynamics has been introduced and proposed as a possible mechanism to overcome the failure of transport which generically occurs for bidirectionally moving particles on a single filament.

Finally, it is worth to discuss the relevance of the model results for axonal transport. In view of the results for bidirectional transport on static lattices, which generically leads to jamming, it is rather surprising, but of course necessary, that transport in these real one-dimensional axonal structures would be at all stable and efficient. This is all the more surprising given that the model overestimates the diffusivity of the detached particles, which should be reduced in real systems due to the size and interactions of the vesicles in the cytoplasm. These results give strong evidence that additional effects must come into play in order to stabilize motor driven transport in axons and reduce the tendency to form large particle clusters. The mechanism suggested in this chapter is based on the fact that the filament dynamics limits the size of particle clusters. A more detailed modeling of motor driven transport in axons is difficult since the experimental findings concerning the motor interactions and the MT dynamics are so far incomplete and subject to interpretation: while it is well established that the plus ends of MTs undergo polymerization events toward the synapse, the path length of the growing plus ends as well as the dynamics of the minus ends are not known yet. Besides the robustness of the results with respect to the lattice dynamics details, the importance of the lattice dynamics is supported by experimental results on transport in axons, where the strong correlation between MT dynamics and vesicle transport has been demonstrated [100] (see also section 2.4.2).

An alternative mechanism for efficient bidirectional transport, lane formation as proposed by Klumpp and Lipowsky [188], will be treated in the following chapter and will be shown to be influenced by the lattice dynamics.

Chapter 5

Efficient transport in intracellular transport models II – Lane formation

5.1 Chapter introduction

The present chapter treats a second mechanism which possibly leads to efficient transport. The idea is to add interactions to the model which cause a self-organized state with the characteristic property that the system demixes and individual filaments (or protofilaments) are occupied by particles of a single species only. This lane formation eliminates the mutual blocking of two particles of opposite charge which is the cause for the inefficient transport properties of the basic model on the static lattice (section 4.1.1). If all the particles on the filament hop in the same direction, these encounters do not occur anymore and the system effectively is in a state with a single species. In order to have efficient *bidirectional* transport, one then obviously needs more than one filament so that there are some filaments carrying transport in one and some filaments carrying transport in the other direction.

Lane formation is known from different systems such as driven colloids [198], dusty plasmas [199], ions within two-dimensional membranes [200], granular matter [201] or pedestrian traffic [202] and is usually associated to an important increase of flux along the direction of the formed lanes. These systems have in common that lane formation occurs due to local interactions causing the agents of the model to self-organize in this efficient form. For intracellular transport, lane formation of molecular motors could not be shown experimentally yet, but the interactions leading to lane formation would also have to be local as there is no evidence for any mechanism which would be able to globally regulate that molecular motors only attach to filaments carrying the transport in the appropriate direction. Lane formation therefore has to occur due to local interactions, e.g., between molecular motors. This chapter will examine two different types of interactions between particles which lead to lane formation under certain conditions and regard the influence lattice dynamics has on them.

In a first part, species-dependent particle-particle interactions are examined which have formerly been proposed by Klumpp and Lipowsky [188] (see also section 3.3.2). It is shown that 1. lane formation is not necessarily connected to an efficient transport state and 2. the lane formation mechanism in this specific model relies on a property of the particle reservoir which turns out to be unrealistic if one wants to apply the

results to systems with limited diffusion such as intracellular transport. In the second part of the paper, an alternative model with different particle-particle interactions is introduced which – under certain conditions – leads to lane formation even at limited diffusion. Besides, it is established for both models that a dynamic underlying lattice as considered in chapter 4 enhances the transport efficiency either by reducing the impact of clusters or by promoting lane formation.

In order to allow a better comparison of the different interactions considered, all shown data of the current will be presented in figures with vertical axes which end at $J_b = 0.25$. An inset will additionally show the same data on a smaller scale if necessary.

5.2 Attractive/repulsive particle-particle interactions

In this section, the model by Klumpp and Lipowsky [188] will be discussed for different assumptions for the bulk reservoir with respect to the robustness of the results. Furthermore, the influence of a dynamic lattice will be investigated.

5.2.1 Model definition

The model treated in this section has the same structure as the basic model of section 4.1.1 with a filament and a reservoir. Particles of the two species obey the same hopping rules as before on the filament. The considered set of parameters for the particle dynamics is $p = 1$, $\omega_a = 0.1$ and $\omega_d = 0.01$ which again recovers the basic feature of molecular motors as kinesin or dynein (section 2.3) and is the same set of parameters as in [188]. We examine different reservoirs which are defined below in the corresponding sections. Particle densities are denoted by ρ_{tot}^{\pm} and defined as number of particles divided by the system length. The index refers to the particle species. The quantity ρ_b denotes the density of bound particles on the filament and ρ_u the density of particles in the reservoir.

The decoration experiments addressed in section 2.3.1 showed that motors of the kinesin finally are mutually attracted by each other on the filament. This motivates the assumption of a general attractive interaction between molecular motors of the same species. This experimental fact was first considered by Klumpp and Lipowsky [188] in a modification of the above-presented basic model by consideration of detachment and attachment rates that depend on the next neighbor in the stepping direction of the particle: If the next site in moving direction is occupied by a particle of the same species, the detachment rate is lowered by a factor $1/q$ whereas the attachment to that site is enhanced by a factor q . If the next site is occupied by a particle of the opposite species, the detachment is enhanced by a factor q and attachment is lowered by a factor $1/q$ (see figure 3.8). In all other cases, the rates remain unchanged.

We will also consider the influence of the dynamics of the underlying lattice in this chapter. The same type of lattice dynamics as in chapter 4 will be considered: a site of

the lattice is randomly eliminated at rate k_d and recreated at rate k_p . The polymerization rate is fixed at $k_p = 1$ in order to reduce the number of free parameters. Indeed, it was shown in chapter 4 that transport features were more sensitive to k_d than to k_p . A discussion of this simple choice of lattice dynamics can be found in section 4.3.5.

While in chapter 4 the effect of the lattice dynamics alone was considered, this chapter shall explore how it combines with the effects of particle-particle interactions. However, in the next section, only the case of a static lattice will be considered, and the consequences of the attractive interaction introduced by [188] shall be studied in a more complete way than it was done before. In particular, several types of reservoirs will be considered and shown to have a strong influence on transport.

5.2.2 Static lattice

Infinite diffusion rate

If particles interact via the interactions of figure 3.8 on a static lattice, lane formation is observed in a grand-canonical setup [188]. In this section, we briefly present some new results obtained with this model in order to discuss the efficiency of the lane formation mechanism. Two different types of reservoirs will be discussed which we refer to as *grand-canonical* and *canonical*. Both have in common that particles in the reservoir do not have any spatial coordinate and can attach to any empty site along the lattice. This corresponds to an infinite diffusion rate in the surroundings of the lattice as presented and discussed for the one-species model in section 3.2.3. However, in the canonical setup, we limit the total density of particles $\rho_{\text{tot}}^{\pm} = \rho_b^{\pm} + \rho_u^{\pm}$, while the grand-canonical reservoir has a constant density of $\rho_u = 2\rho_u^+ = 2\rho_u^- = 0.1$. Attachment to empty sites on the lattice occurs at rate $\rho_u^{\pm} \cdot \omega_a$.

Lane formation occurs in the grand-canonical setup if the interaction strength q exceeds a critical value q_{crit} . This effect is illustrated in the space-time plots in figure 5.1. With increasing interaction strength, the size of the mini-jams in the system coarsens until one particle species completely takes over the system at q_{crit} so that all particles move in the same direction.

The transition manifests itself by a dramatic increase of the magnetization which is defined as the difference in the densities of the two particle species divided by the total density of particles on the filament $m = (\rho_b^+ - \rho_b^-)/(\rho_b^+ + \rho_b^-)$. This quantity takes the value one for completely demixed subsystems, i.e., under lane formation and is zero equal numbers of particles of both species on the filament.¹ The currents of the two species along the filament exhibit a bifurcation at the transition: while one species dominates the filament and moves in a TASEP-like fashion, the excluded species does not participate in transport at all for $q > q_{\text{crit}}$ (figure 5.2).

Two remarks can be made from the data shown in figure 5.2. First, the current does not exhibit strong finite-size effects as the structures (jams) below the transition are smaller than the typical system size and then dramatically increase in size

¹Please note that this is a different definition than the one used in [188].

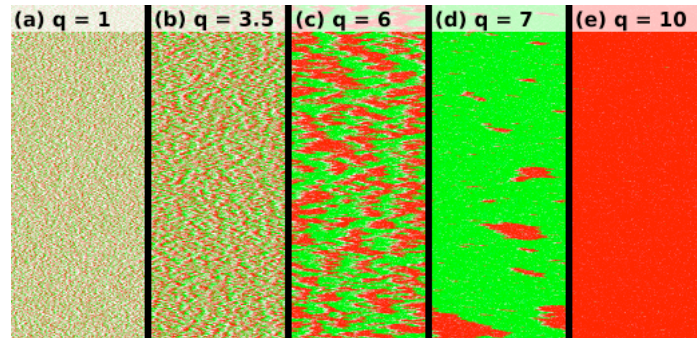


Figure 5.1: Space-time plots of the filament with a grand-canonical reservoir on a static filament. Every line is a snapshot of the filament of length $L = 400$ for different interaction strengths: (A) $q = 1$, (B) $q = 3.5$, (C) $q = 6$, (D) $q = 7$, (E) $q = 10$. Red dots represent particles moving to the right, green dots are particles moving to the left, white dots are vacancies on the filament.

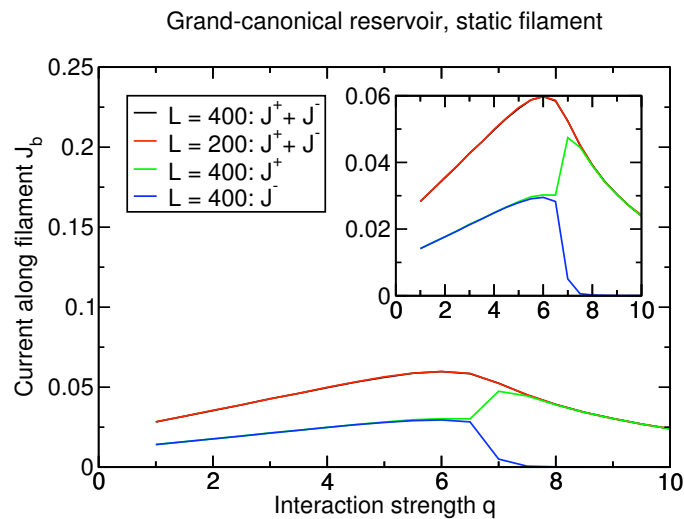


Figure 5.2: Current along a static filament of the dominant (green) and excluded (blue) particle species. The sum of both currents is shown black and red for systems of size $L = 400$ and $L = 200$ with a grand-canonical reservoir. All graphs displaying the current in this chapter will have a vertical axis going to $J_b = 0.25$. The inset then always shows the same data on a more appropriate scale of the vertical axis if necessary.

near the transition. Second and more important, although the difference in current between the two species is very large above the transition, indicating that lane formation has occurred, transport is actually less efficient than just at the onset of lane separation. This can be seen by the sum of the currents (black and red line in figure 5.2) which corresponds to the current of a single species in a system with two filaments, of which each is dominated by a different species. The interesting feature is that, above the transition, the current actually decreases although the encounters of oppositely charged particles are less frequent. This decrease is instead caused by the filament being overcrowded, as can be seen in figure 5.1. The density on the filament is close to one and although all particles move in the same direction, most of the attempted steps are rejected because of the lack of vacancies. The stronger the interactions between particles, the more the situation worsens. Consequently, the current continues to decrease for increasing interaction strengths, since the particles have an ever-increasing affinity to the filament and the number of vacancies thus decreases with increasing q .

Now, the reservoir is modified and chosen not to allow for an infinite number of particles anymore. Instead, the number of positive (negative) particles N^+ (N^-) in the system is fixed and the consequences on the transport properties are observed. Besides, more than only one track on which particles can walk is considered here. In contrast to the grand-canonical setup with constant reservoir densities, choosing more than one filament becomes important since lane formation would be hindered otherwise. In a system with only one filament, the species which is excluded from the filament becomes dominant in the reservoir and therefore tends to destroy the lane formed by the other species. Putting two (or more generally any pair number of) filaments in a system resolves this issue. This is an appropriate approach as in the biological situation, one typically has several filaments in parallel. In the systems studied in the following, the transport along two filaments is examined.

Density and particle number are related through $N^\pm = \rho_{\text{tot}}^\pm \times L \times \#\text{filaments}$, still with equal densities $\rho_{\text{tot}} = 2\rho_{\text{tot}}^+ = 2\rho_{\text{tot}}^-$ of the two species. Note that ρ_{tot} can be greater than one as it counts the total number of particles (including those in the reservoir), divided by the number of filament sites. In the following, we shall consider the case of two filaments only.

The behavior of the system is qualitatively different for densities $\rho_{\text{tot}} = 2\rho_{\text{tot}}^+ = 2\rho_{\text{tot}}^- \geq 1$ and $\rho_{\text{tot}} < 1$ since in the latter case, there are not enough particles to completely fill both filaments with a single particle species each. The results are illustrated in figure 5.3. For the magnetization, it is interesting to see, that the transition still takes place, even at very low total particle densities. The fewer particles are present in the system, the higher the interaction between particles has to be in order to induce polarization. For $\rho_{\text{tot}} = 1$, there are exactly as many particles of one species in the system as there are sites on a single filament and lane formation is extremely stable in this case since there are enough particles to mediate the interaction at best but not too many to avoid that particles frequently attach to the ‘wrong’ filament on which the species is not dominant. For densities $\rho_{\text{tot}} > 1$, the latter effect is not avoided anymore

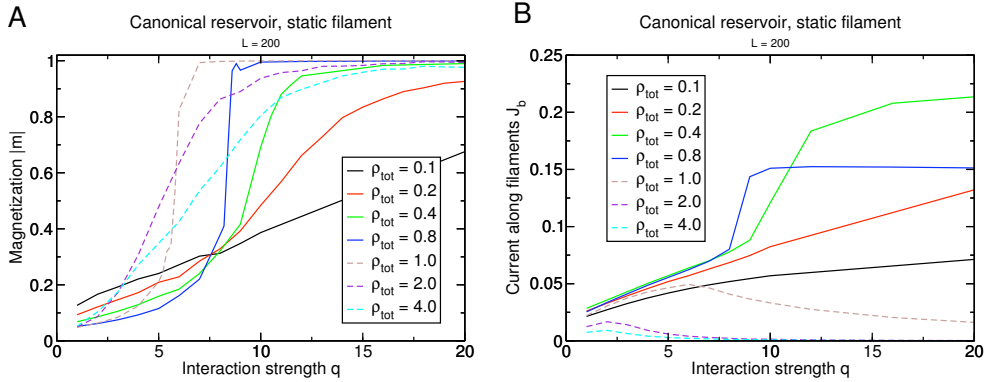


Figure 5.3: (A) Magnetization of the filaments and (B) current along both filaments of positive particles in the canonical setup with a static filament for system size $L = 200$ and different densities ρ_{tot} . Full lines are for densities $\rho_{\text{tot}} < 1$ and dashed lines are for densities $\rho_{\text{tot}} \geq 1$.

as the reservoir cannot be emptied. There are always many particles of both species in the reservoir left which interfere with the existing lanes such that the transition to the lane formation state is hindered.

The current also reflects these two regimes: For $\rho_{\text{tot}} < 1$, the current increases monotonously with increasing interaction strength. At the lane formation transition, the current jumps toward a value very close to the current of the one-species TASEP, which is the upper bound for the current on the filament (figure 5.4). For densities $\rho_{\text{tot}} \geq 1$, the behavior is distinctively different as the curves for the current have much more similarity with those found in the grand-canonical setup and decrease with further increasing interaction.

On the basis of these observations, we are able to draw an approximative phase diagram (figure 5.5). For this, the system was considered to be phase separated at magnetization $|m| \geq 0.8$ where a distinction is made between two different phase-separated regimes depending on the current at infinite interaction strength as explained above. In terms of the transport capacity, only *phase-separated I* can be considered to be an efficient state, as the current in *phase-separated II* does not reach very high values due to the overcrowding of the filament as discussed above.

In total, one can draw the conclusion that for low densities, the dominating effect of the interaction is to induce lane formation which leads to very good values of the current but necessitates strong particle-particle interactions. For high densities or a grand-canonical reservoir, the interaction additionally impedes lane formation and rather leads to a regulation of the density on the filament. Since this density is very high, it allows only for little transport along the filament.

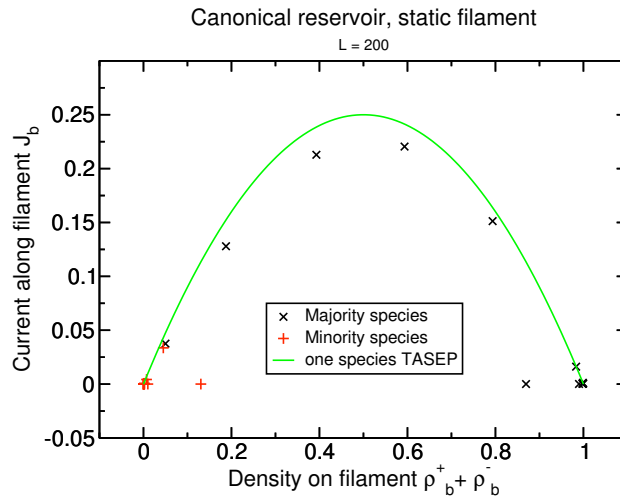


Figure 5.4: Comparison of the current in a one-species TASEP (green line) and the recorded current along one given filament in the two-species system with a canonical reservoir and a static lattice at $q = 20$ (which ensures that lane formation has occurred for most densities shown in figure 5.3 A). The dominating particle species is shown as black crosses, the other species as red plus signs. Following the black crosses from left to right along the green parabola, the total density of particles increases from $\rho_{\text{tot}} = 0.1$ to $\rho_{\text{tot}} = 4.0$. The value for $\rho_{\text{tot}} = 8.0$ is far from the TASEP solution as lane formation is not complete. Please note that there are equal numbers of black and red crosses but that the latter are clustered around the origin.

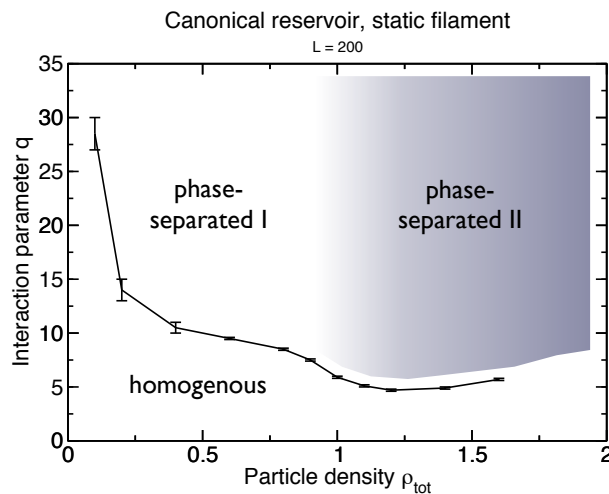


Figure 5.5: Phase diagram of a system with a canonical reservoir, where $|m| \geq 0.8$ is taken as the criterion for lane separation. The phase-separated state is subdivided into two different regions (I and II). In the first region, the current reaches a constant and large value for high interaction while the current decreases in region II, because the filament is overcrowded although completely polarized.

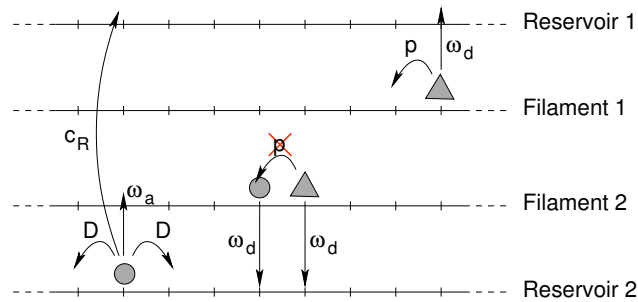


Figure 5.6: Sketch of the system with two filaments and explicit positions in the reservoir. In addition to the moves explained for the model with an infinite diffusion rate above, a coupling between the two reservoirs is introduced by allowing particles to jump from one reservoir to the other at rate c_R .

Finite diffusion rate

The results are very different when considering such a reservoir that detached particles diffuse within a crowded and confined environment which allows only for very limited diffusive motion. Like in the basic model (section 4.1.1), we add a second lane which represents the reservoir. The diffusion rate is fixed at $D = \omega_a = 0.1$. Two identical subsystems with a filament and a reservoir each are considered (figure 5.6) for the same reasons as explained above. Particles can hop from one reservoir to the other by conserving their longitudinal position at rate c_R . This corresponds to diffusion in transverse direction. The diffusion in both directions along the reservoir lattices is chosen to be equal to the attachment rate, i.e., $D = c_R = \omega_a = 0.1$. The two filament lattices are not directly coupled by particle moves in this model.

Without the particle-particle interactions defined in section 5.2.1, this model has been shown to generically form a single big cluster which contains almost all of the particles in the system (sections 3.3.2 & 4.2 and [186]). The existence of this big cluster is a clear indicator for an inefficient state since it blocks most of the transport.

If particle-particle interactions are included, we see that the finite diffusion rate in the reservoir inhibits even partial demixing of the particles into the different subsystems (figure 5.7 A). Although lane formation is suppressed by the limited diffusion, the current (figure 5.7 B) is enhanced by the interaction, though a single big cluster is still present in the system. The increase in the current is caused by the reduced time which blocked particles spend in front of each other and the fact that, in low density regions, particles of a given species are more likely to have nearest neighbors of the same species.

5.2.3 Dynamic lattice

In this section, the interest lies in the impact that a dynamic lattice as defined in section 5.2.1 and examined in chapter 4 has on the considered particle-particle inter-

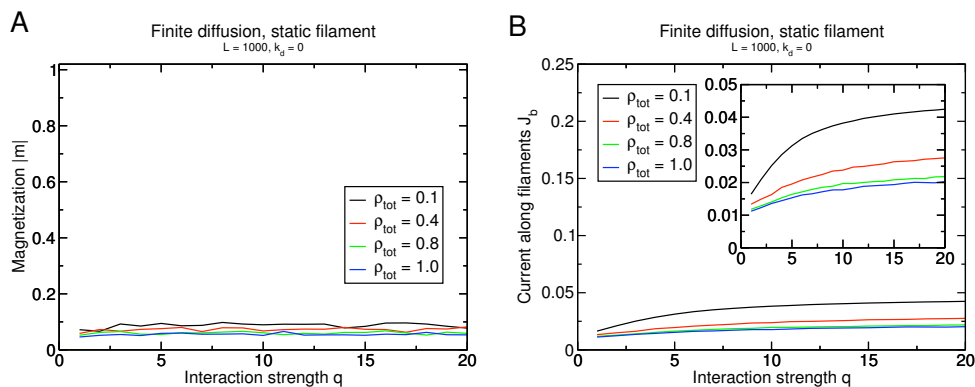


Figure 5.7: (A) Magnetization of the filaments and (B) current along both filaments of positive particles in the setup with a finite diffusion rate and a static filament for system size $L = 1000$ and different densities ρ_{tot} .

actions. We focus, first, on the lane formation mechanism that exists at least in the case of an infinite diffusion rate in the reservoir, and, second, on the overall transport efficiency. We again discriminate between reservoirs with infinite and finite diffusion rates.

Infinite diffusion rate

Eliminating lattice sites reduces the effectiveness of the particle-particle interaction since it is next-neighbor and cannot reach across holes in the filament. As a consequence, the transition is shifted to higher values of q with increasing depolymerization rate k_d as can be seen in figure 5.8 A. For a very dynamic lattice, there seems to be no transition toward lane formation at all.

However, although lane formation is hindered by the lattice dynamics, it positively affects the current of the system (figure 5.8 B). By pushing particles to the reservoir when a lattice site is eliminated, the lattice dynamics keeps the density on the filament low enough so that particles have enough space in front of them to move. Thus, extreme densities that were strongly limiting the current in the case of a static lattice are avoided here.

The results shown in figure 5.8 are obtained for the grand-canonical reservoir but are qualitatively the same for a canonical setup at high densities. For densities $\rho_{\text{tot}} < 1$, the current on the static lattice is already close to optimal (figure 5.3 B) and so there is little space for improvement. Actually, the lattice dynamics corrupts these states by shifting the transition to higher values of q and making the phase separation less stable.

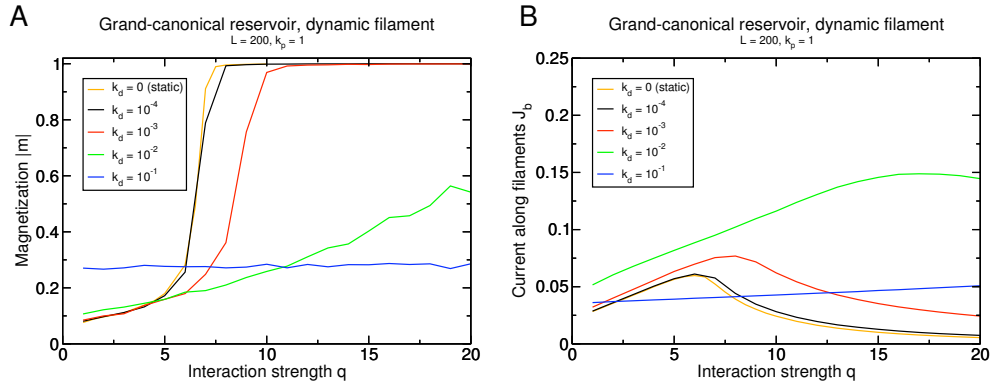


Figure 5.8: (A) Magnetization of the filaments and (B) current along both filaments of positive particles in the grand-canonical setup on a dynamic lattice of size $L = 1000$. The lattice dynamics suppresses lane formation and improves the current if the lattice dynamics is not too strong.

Finite diffusion rate

In the model with finite diffusion rates in the reservoir, there is no lane formation on the static lattice and the same remains true if a lattice dynamics at any strength is added. But as has already been reported in chapter 4, a dynamic lattice is capable of dramatically increasing the current along the lattice and reaching an efficient state by dissolving large clusters. This effect is obviously also present in this system and the strength of the interaction only has very little impact on the current on the dynamic lattice.

The increase of current due to the attractive interaction on the dynamic lattice is of the same order as the one observed on the static lattice (figure 5.7) and represents only a small fraction of the increase due to lattice dynamics: In a system of density $\rho_{\text{tot}} = 1$ and length $L = 1000$, the maximum current increase caused by the lattice dynamics is almost ten-fold, whereas the particle-particle interactions do not even double the current in the system.

5.2.4 Summary

An overview of the results of this section with its multiple scenarios is shown in table 5.1 with the color of the cell indicating if lane formation is possible.

In summary, particle-particle interactions which modify the attachment and detachment rates of particles depending on the occupation of the neighboring sites can lead to lane formation for reservoirs with an infinite diffusion rate only. In this case, although the number of encounters of particles of different species is reduced, the throughput of particles is extremely low in systems with a large number of particles. This is due to overcrowding of the lattice caused by the strong attractive interactions in lane-separated systems. The fact that lane formation mechanism is dependent on

	Static lattice	Dynamic lattice
Infinite diffusion rate, grand-canonical reservoir	High density on filament => no efficient current	Transition is suppressed for strong lattice dynamics, current increase only due to lattice dynamics
Infinite diffusion rate, canonical reservoir	Very high transport capacity for low total densities only	Transition is suppressed for strong lattice dynamics, current increase only due to lattice dynamics
Finite diffusion rate	Transport capacity improves slightly with stronger interaction	Increase of the transport capacity due to lattice dynamics

Table 5.1: Overview of results for attractive/repulsive particle-particle interactions. As a function of the two dimensions *type of reservoir* and *lattice dynamics*, the most important results on the lane formation are given. A green cell indicates that lane formation occurs whereas the inverse is true for a red cell. The text in the cell gives additional information on the phenomenology.

an infinite diffusivity around the transport lattice is a major drawback for the relevance of this type of interaction for the axon.

Independently from the particle-particle interaction, the lattice dynamics was shown to improve the current along the filament for all three types of reservoir. Actually, it has a positive effect whenever current is hindered by a (possibly local) high density. The lattice dynamics dominate the behavior of the system in the sense that the lane formation disappears for strong lattice dynamics whereas for strong particle-particle interactions, the effect of the lattice dynamics remains visible.

5.3 Lane change through steric interactions

In this section, we propose another type of particle interaction, which is capable of inducing lane formation even for finite diffusion rates in the reservoir.

5.3.1 Model definition

As we are interested in lane formation at a finite diffusion rate, only the reservoir with a finite diffusion rate will be treated here. Particles obey the same hopping rules as depicted in figure 5.6, i.e., they hop into a preferential direction along the filaments and hop with equal rates in both directions in the reservoirs. In order to keep the model simple, we consider again only two filaments and the two associated reservoirs. Exchanges between reservoirs or reservoir and filament occur with the same rates as before. The particles still interact via hard-core exclusion on the filament but

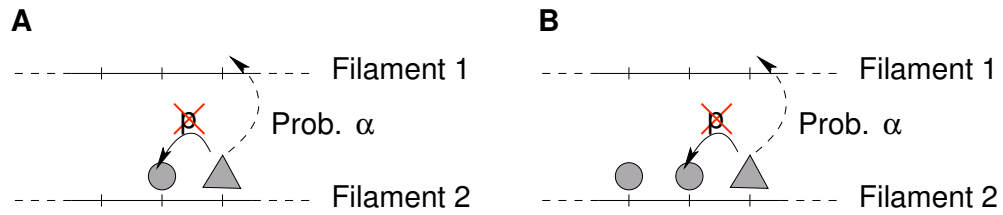


Figure 5.9: Lane changes through steric interactions. A particle may change onto the neighboring filament with filament α if it encounters (A) one or (B) two particles of the other species. The reservoirs are not shown.

instead of modifying attachment and detachment, we consider the following interaction between particles: If a particle's step along the filament is rejected because the target site is occupied by a particle of the opposite species, the particle switches to the other filament with probability α provided the site at the same longitudinal position is empty on the other filament (figure 5.9 A). We shall refer to this interaction as the 'single obstacle' interaction in the following.

So far, there is no experimental data showing a similar behavior of molecular motors. However, the only known experiments on interactions between molecular motors are the decoration experiments for kinesins addressed in section 5.2.1 which was shown to be rather implausible as a cause for possible lane formation. Here, the idea is that opposed motors push against each other and thus might exert a force pushing a motor to the side, therefore making it possible to switch directly between filaments or protofilaments without detaching in between. This effect might be even more pronounced if one thinks of the relatively large cargos carried by the molecular motors. Alternatively, this can also be the hypothesized ability of molecular motors to step to the side when encountering obstacles (see section 2.3).

We shall also consider a variant of this interaction where the particle may only switch from one filament to the other with probability α if it encounters *two* particles of the opposite species on the two next sites in stepping direction (figure 5.9 B). This mechanism will be referred to as the 'two obstacles' interaction.

5.3.2 Static lattice

'Single obstacle' interaction

On a static lattice, changing lanes in front of a single particle of opposite species does not lead to dramatic effects. In particular, no lane formation is observed although the absolute magnetization of the filament slightly increases. This effect competes with the reservoir change rate c_R which tends to mix the system and destroys any phase separation between the two subsystems. At $c_R = D = 0.1$, no effect of the additional particle-particle interaction is visible at any probability α .

Nevertheless, there is a small effect for decoupled reservoirs at $c_R = 0$. The increase of the magnetization is stronger the fewer particles we have in the system, but even

for densities as low as $\rho_{\text{tot}} = 0.1$, the magnetization does not exceed $|m| < 0.3$. It is noteworthy that at the system size $L = 1000$ considered here, there is no important clustering at this low density. In a clustered system with higher particle density, absolute increases in magnetization are almost negligible: For $\rho_{\text{tot}} = 1$, the magnetization passes from $|m| = 0.047$ at $\alpha = 0$ to $|m| = 0.0784$ at $\alpha = 1$.

In the same way, the current does not improve much with this ‘single obstacle’ interaction. The clustered systems remain clustered and exhibit a maximal gain of their current of 25% while starting from an extremely low value because of the existence of the large cluster.

‘Two obstacles’ interaction

If we consider a stronger condition for filament changes as shown in figure 5.9 *B*, lane formation is obtained much more easily compared to the ‘single obstacle’ interaction and occurs at any density with decoupled reservoirs, i.e., $c_R = 0$. The current of particles along each filament is consequently very high and close to the optimal value found in a one-species TASEP. The interaction is asymmetric in the sense that a single particle changes the filament if opposed to two particles of opposite charge while the single particle cannot induce any lane change on the two particles. As a consequence, a particle species which is only slightly dominant on one filament can push more and more particles from the minority species to the other filament. Ultimately, complete lane formation is observed.

As discussed in the last section, the lane formation competes with the mixing through the reservoirs. If the reservoir coupling c_R is increased, the magnetization is lowered at some point and lane formation disappears (figure 5.10 *A*). The onset of remixing the separated lanes occurs at lower couplings c_R for higher densities as in these cases, more particles are continuously transported to the reservoir belonging to the ‘wrong’ filament. For $c_R = D = 0.1$, the system is completely mixed at any density.

The current increases by one order of magnitude if lane formation occurs (figure 5.10 *B*) and is very close to the optimal value in the one-species TASEP.

5.3.3 Dynamic lattice

‘Single obstacle’ interaction

If the possibility to perform filament changes is combined with lattice dynamics, the system’s tendency toward lane formation is increased (figure 5.11 *A*). A system of density $\rho_{\text{tot}} = 0.4$ reaches complete lane formation at $k_d = 0.1$. However, at this value of the depolymerization rate k_d , the basic model without filament changes does not exhibit a large cluster anymore, but is in a homogenous state with very small structures and thus already has improved transport properties (see section 4.3.3).

The enhanced lane formation can be understood in the following way: In order to separate into a lane formation state, filament changes of particles are necessary which

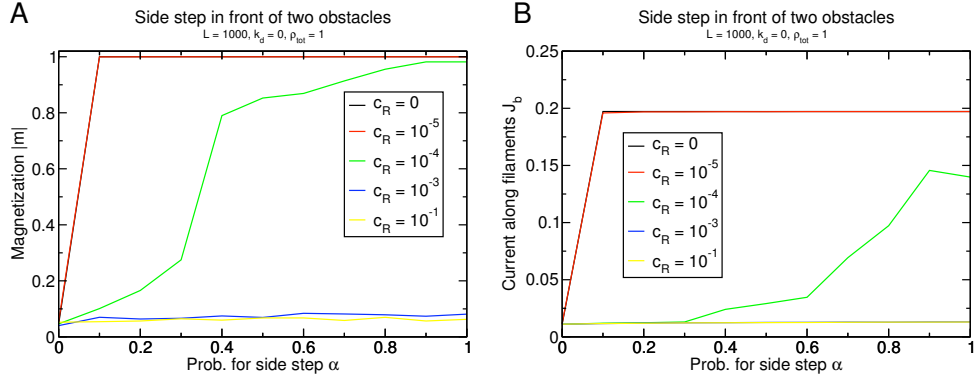


Figure 5.10: (A) Magnetization of the filaments and (B) current along both filaments of positive particles on a static lattice with the ‘two obstacle’ interaction. The reservoir coupling inhibits lane formation. Systems with lane formation show a close-to-optimal current which is one order of magnitude higher than in the mixed case.

can only occur if particles of different species meet. Consequently, more lane changes are induced if there are more interfaces between positive and negative particles. In a clustered system, almost all the particles are accumulated in the cluster so that there are only very few interfaces. The lattice dynamics, though, inhibits the formation of large clusters and instead distributes the particles more homogeneously over the whole system leading to many very small clusters. This effectively increases the number of interfaces between positive and negative particles and thus favors lane changes and lane formation. The above-mentioned effect that holes in the lattice decrease the effectivity of a next-neighbor particle-particle interaction seems to be overcompensated by the increase in interfaces due to the dissolution of the big cluster.

The strength of the lattice dynamics that is needed to form lanes depends on the particle density, e.g., a system of density $\rho_{tot} = 1$ does not exhibit complete lane formation at any lattice dynamics (figure 5.11 C) while a system of density $\rho_{tot} = 0.1$ forms lanes at very low lattice dynamics (not shown).

Again, the current is more strongly affected by the lattice dynamics than by the additional particle-particle interaction as can be seen in figure 5.11 B,D: The higher the lattice dynamics, the higher the overall position of the current curves. In particular, for the completely lane separated system at $\rho_{tot} = 0.4$ for $\alpha > 0$, the current increases by 40% due to the lane formation, but more than quadruples because of the lattice dynamics (figure 5.11 B). This impression is strengthened by the observation that similar gains due to the dynamic lattice are obtained even if no lane formation occurs (figure 5.11 D). The values of the current for $\rho_{tot} = 1$ are remarkable since they are rather close to the maximum current of $1/4$ that would be found in a one-species TASEP, although encounters between particles of different species are still frequent in our model even at important lattice dynamics.

These results have so far been obtained at decoupled reservoirs $c_R = 0$. The influence of the reservoir coupling c_R is shown in figure 5.12 for a dynamic lattice. Al-

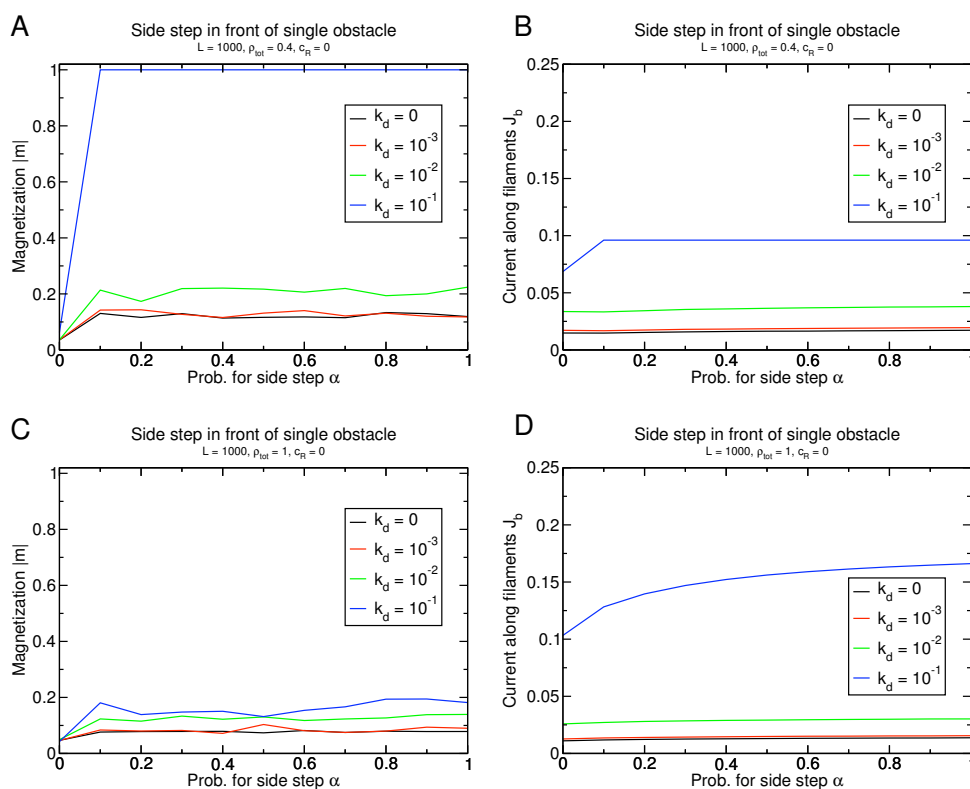


Figure 5.11: (A,C) Magnetization of the filaments and (B,D) current of one particle species along both filaments in a system of length $L = 1000$ with decoupled reservoirs $c_R = 0$, for a density (A,B) $\rho_{\text{tot}} = 0.4$ or (C,D) $\rho_{\text{tot}} = 1$ and ‘single obstacle’ interaction. For $\rho_{\text{tot}} = 0.4$, the enhancement of lane formation by the lattice dynamics is obvious (A), while it is hardly existent for $\rho_{\text{tot}} = 1$ (C). Lattice dynamics have a stronger impact on the current than the lane formation as currents in (B,D) are comparable although only one of the systems exhibits lane formation.

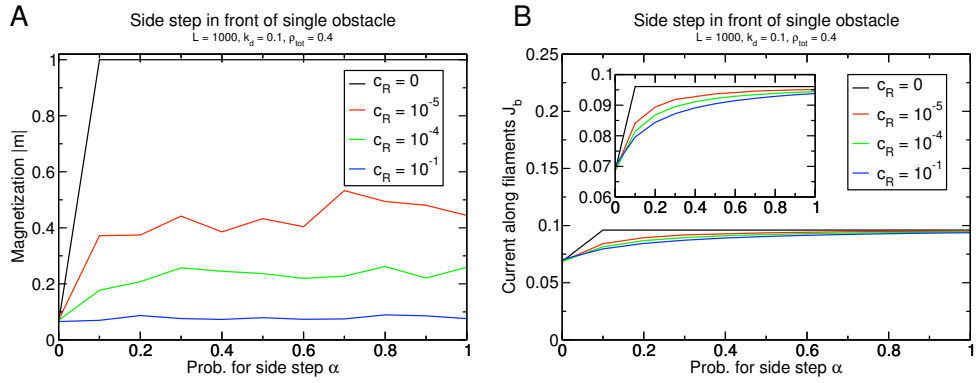


Figure 5.12: (A) Magnetization of the filaments and (B) current of one particle species along both filaments in a system of length $L = 1000$ at density $\rho_{\text{tot}} = 0.4$. The different curves correspond to different reservoir couplings which acts against lane formation induced by the ‘single obstacle’ interaction.

ready an extremely small reservoir coupling inhibits lane formation (figure 5.12 A). If diffusion in longitudinal and transverse direction are equal, i.e., $c_R = D = 0.1$, the lane formation effect disappears almost completely. However, the current is only marginally affected (figure 5.12 B) and reaches almost identical values for all reservoir couplings at $\alpha = 1$. This once more confirms that the lattice dynamics is dominant in determining the transport capacity of the system. The fact that all curves show a similar increase for increasing α is an indicator for the more efficient resolution of encounters of particles of opposite species.

‘Two obstacles’ interaction

As for the ‘single obstacle’ interaction, the lattice dynamics also improve the lane formation mechanism by increasing the number of interfaces between oppositely charged particles for the ‘two obstacles’ interaction (figure 5.13 A). The influence of the lattice dynamics and the competition with the reservoir coupling c_R on the magnetization and on the lane formation remains qualitatively unchanged compared to the ‘single obstacle’ case.

There is nevertheless an interesting difference for the value of the current in the systems with lane formation: For the most dynamic lattices $k_d = 0.1$, the current in the separated system can sometimes be lower than in demixed or even mixed systems at lower lattice dynamics (blue and green line in figure 5.13 B). In these cases, the lattice dynamics actually inhibits any further improvement of the current by eliminating too many sites of the filament along which no transport can happen. This effect is the more pronounced, the lower the density of particles is.

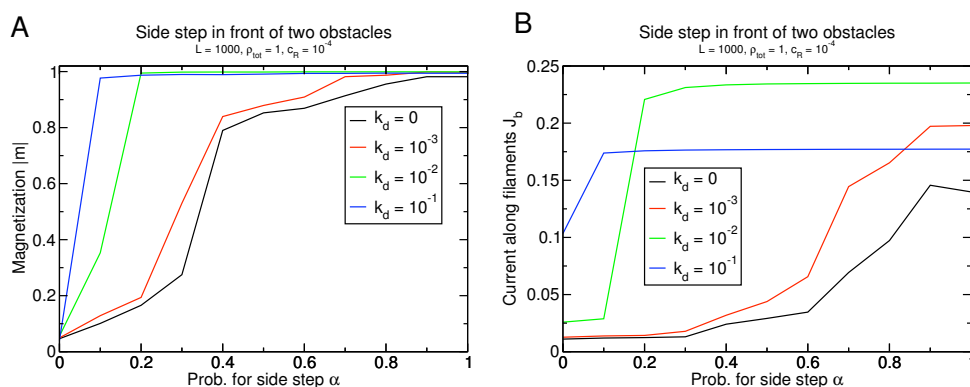


Figure 5.13: (A) Magnetization of the filaments and (B) current along both filaments of positive particles on a dynamic lattice with the ‘two obstacles’ interaction and reservoir coupling $c_R = 10^{-4}$. The lattice dynamics enhance lane formation in only partially demixed systems and have an important impact on the current.

	Static lattice	Dynamic lattice
‘Single obstacle’ interaction	Very small increase of magnetization and current	Lane formation only for low reservoir coupling, high transport capacity with lane formation
‘Two obstacle’ interaction	Lane formation only for low reservoir coupling, high transport capacity with lane formation	Lane formation only for low reservoir coupling, high transport capacity with lane formation

Table 5.2: Overview of results for lane formation through direct filament changes. As a function of the two dimensions *type of interaction* and *lattice dynamics*, the most important results on the lane formation are given. A green cell indicates that lane formation occurs whereas the inverse is true for a red cell. The text in the cell gives additional information on the phenomenology.

5.3.4 Summary

Again, the most important results of this section are summarized in table 5.2.

The proposed interaction which eventually induces filament changes of the particles has been shown to lead to lane formation under special conditions. In general, three factors determine the possibility of lane formation: 1. A higher particle density ρ_{tot} decreases the tendency to form separate lanes for both species (in contrast to what was observed for the interaction of section 5.2). 2. The reservoir coupling c_R suppresses lane formation by mixing partially phase-separated subsystems (already true for the interaction of section 5.2). This mixing is very efficient as the rates needed to inhibit lane formation are several orders of magnitude smaller than all the other rates in the system. 3. Lattice dynamics promote lane formation by increasing the number of contacts between positive and negative particles. We therefore have two effects leading to higher currents, one of which (lattice dynamics) improves the other (lane formation).

Considering the current, lane separated states can obviously be considered as efficient transport states. They have a high throughput of particles and because of the absence of large structures, no finite-size effects are present, so that we have a density-dependent state. This property is necessary to have finite current in very long systems. However, we have shown that the effect of lattice dynamics on the current has a much larger amplitude than the proposed side stepping mechanism.

5.4 Chapter conclusion

In the present chapter, two different types of particle-particle interactions in a quasi one-dimensional lattice gas with oppositely charged particle species were presented. Both types of interactions lead to lane formation under certain conditions. The robustness of these phase-separated states and their transport capacity was explored. An efficient transport state was supposed to be characterized by a system size-independent (= density-dependent) state with a finite current that compares to the current in a one-species TASEP serving as a benchmark.

The first type of interaction which was introduced by Klumpp and Lipowsky [188] affects the affinity to the filament in the vicinity of other particles. The lane-separated states that are found (only for infinite reservoir diffusion) exhibit a density-dependent current but many of these states also have extremely high densities on the filament so that the actual current of bound particles is rather low compared to an optimal regime. This is in particular the case for open systems (grand-canonical reservoir), or for closed systems with high enough densities (canonical reservoir). Lower densities do lead to very efficient states which compare well to the one-species TASEP. The conclusion is that lane formation does not necessarily imply efficient transport although this can be the case.

Lane formation in this system was only possible for an infinite diffusion rate in the reservoir. With regard to an application of these concepts to real transport processes

as intracellular transport, this is a very strong assumption as the interior of a cell is very crowded and considering the typical sizes of vesicles and organelles, diffusion should be very limited as mentioned earlier. In the case of finite diffusion rates, no lane formation is observed and the interaction plays a minor role in improving the current, compared to the much more positive impact of lattice dynamics.

In the second type of interaction which have been considered, particles hop to the neighboring filament when they meet an oppositely charged motor. Although this model is in principle able to exhibit lane formation at finite longitudinal diffusion, the lane-separated state is extremely sensitive to diffusion between reservoirs, i.e., in transverse direction. This is in sharp contrast to the first interaction model which actually needed infinite diffusion rates to exhibit lane formation. The difference comes from the nature of the particle-particle interaction. Any demixing in the first scenario has to be carried out through the reservoir whereas particles directly switch from one filament to the other and do not need the reservoir to form lanes in the second scenario.

Furthermore, it was considered that the underlying lattice itself can undergo some dynamics, through the random polymerization/depolymerization of filament units. We have studied the influence of a dynamic lattice on the transport efficiency. In almost all cases (i.e., for almost all types of reservoirs and particle interactions), we found that the lattice dynamics improves the efficiency of transport. Actually, there was only one case in which the lattice dynamics does not improve the current in the system: if the system forms lanes at low total particle density ρ_{tot} , with an infinite diffusion rate in the reservoir, then lattice dynamics worsens a state which is already close to optimal transport. However, an infinite diffusion rate in the reservoir is not expected to be relevant for transport in real cells. In all other cases, the benefits from lattice dynamics as described in chapter 4 were still valid also when combined with particle-particle interactions.

On the other hand, the lattice dynamics modifies the lane formation mechanism for both types of interaction scenarios. While in the first scenario, lane formation is shifted to stronger interactions, lattice dynamics still improve the transport in the system by lowering the density on the filament in the inefficiently crowded states. The second lane formation mechanism was indeed enhanced by the lattice dynamics as it relies on direct contacts between particles of opposite species which are increased by the dissolution of clusters.

With respect to the question of what makes bidirectional transport in axons as efficient as it is, we can summarize our results in the following way: The mechanisms treated here indicate that lane formation in a real system should only be possible if the axon is compartmentalized such that there diffusing particles cannot reach other filaments than the one in their direct neighborhood. Since it cannot be totally excluded that other interactions between motors lead to lane formation which is less sensitive to system parameters, there is an urgent need for more data on particle-particle interactions which could possibly be acquired by statistical exploitation of *in vitro* experiments involving many motors. Then again, the lattice dynamics always has a positive effect on the transport in the relevant models with a finite diffusion

rate and even enhances the effectivity of one of the lane formation mechanisms proposed in this chapter. Our conclusion is that no matter how and if lane formation is achieved, the microtubule dynamics will still heavily influence the transport capacity and possibly also the lane formation mechanism.

Chapter 6

Modeling of microtubule dynamics

6.1 Chapter introduction

The particular dynamic regime of MTs (section 2.2.2), the *dynamic instability*, makes these semi-flexible bio-polymers an interesting object of study. The frequent switching between a polymerizing and a depolymerizing state allows the cell to quickly reorganize its MT network in order to adapt to an ever-changing environment. Since the MT network also plays a role in supporting the cell shape, the MT dynamics have to be finely tuned in order to allow for many contacts between cell membrane and cytoskeleton which can rapidly be modified if needed. A static cytoskeleton would not be able to fulfill this function and, as was shown in chapter 4, MTs under continuous reconstruction are actually better transport tracks than static ones. The regulation of MT dynamics and their dynamic instability therefore play a crucial role in the cell's survival.

In the present chapter, we will review very briefly some existing models of MT dynamics which point out different consequences arising from the biological situation (section 6.2). After that, a new model for MT dynamics will be presented in section 6.3 which includes aging effects thus contributing to the understanding of the regulation of the MT network in the cell.

6.2 Existing models

There is an extreme abundance of models of MT dynamics which, for lack of space, are impossible to cover here in as much detail as these works would deserve. Instead, we focus here on the basic structure of this model class and discuss certain mechanisms which are able to regulate the length of MTs *in vivo*. The last part of this short overview treats models which, considering the hydrolysis of a GTP cap, are able to reproduce the characteristics of dynamic instability instead of postulating them.

Since the total number of models cited is intentionally kept very low, we refer to the introduction of Margolin *et al.* [203] for further references. There, a very succinct (and consequently also partial) overview of the field is given which can serve as starting point for a more complete review of MT models.

6.2.1 Two-state model

The first models of MT dynamics described the MT as a two-state system which switches between growth and shrinkage [204–206]. In the simplest version, these models are characterized by four rates: the growth rate ν_g , the shortening rate ν_s , the rescue rate ν_r and the catastrophe rate ν_c . This set of parameters is sometimes extended by a fifth parameter c which gives the concentration of free tubulin and may be used as argument of some of the other rates. The MT is treated as a one-dimensional chain of l subunits to which subunits can be added and removed at the plus end.

Assuming a constant concentration of free tubulin, the concentration c can be neglected in this simple model and the master equation of the probabilities $p_{\pm}(l, t)$ to observe a filament at length l in the growing or shrinking state far from any boundary is given by [206]:

$$\frac{\partial p_+(l, t)}{\partial t} = \nu_g p_+(l-1, t) - \nu_g p_+(l, t) - \nu_c p_+(l, t) + \nu_r p_-(l, t) \quad (6.1)$$

$$\frac{\partial p_-(l, t)}{\partial t} = \nu_s p_-(l+1, t) - \nu_s p_-(l, t) + \nu_c p_+(l, t) - \nu_r p_-(l, t). \quad (6.2)$$

In this representation, the plus sign in the index denotes the growing state and the minus sign the shrinking state. Space is discretized in a natural way as MTs possess with the tubulin dimer a well-defined structural unit.

This model presents a phase transition between bounded and unbounded growth with the transition taking place at

$$\nu_s \nu_c = \nu_g \nu_r. \quad (6.3)$$

The MT length distribution in the bounded growth phase is exponentially decaying with mean

$$\langle l \rangle \approx \frac{\nu_g \nu_s}{\nu_s \nu_c - \nu_g \nu_r}, \quad (6.4)$$

while in the unbounded growth regime, the average length grows linear over time as

$$\langle l \rangle = \frac{\nu_g \nu_r - \nu_s \nu_c}{\nu_c + \nu_r} t. \quad (6.5)$$

Including the spatially and temporally varying concentration of free tubulin dimers, dynamical states can be created in which two populations of MTs exist simultaneously: While one population exhibits unbounded growth, a second one is trapped at finite MT lengths because of a lack of free tubulin which has been consumed by the first population [206]. This result thus shows that collective effects influence the MT network and may play a role in regulation of the cytoskeleton.

6.2.2 Length regulation

Microtubules *in vivo* can obviously not grow infinitely due to the lack of intracellular space and a finite amount of tubulin. But the bounded growth case also does not describe appropriately the MT network, as MT length distributions in cells are usually not exponentially decaying (e.g., [12]). Some sort of length regulation must therefore be present, leading to long MTs which are able to span a considerable part of the system.

The approach of section 6.2.1 has been extended in [207] by explicitly accounting for tubulin which is consumed and released during polymerization and depolymerization. In small volumes with a limited total concentration of tubulin, this leads to a stationary state with finite average MT length. Furthermore, the distribution of MT lengths is non-exponential. This form of length regulation due to a lack of tubulin was argued to be of importance in cells with small compartments such as axons. Additionally, length fluctuations of individual MTs are larger the smaller the cell compartment is. Consequently, strongly confined MTs would appear more dynamic, supporting the idea of a dynamic axonal MT network.

Alternatively, a length regulation can be introduced into this class of models by explicitly considering the cell boundary, i.e., imposing a maximum filament length l^* so that $l \leq l^*$ as in [208]. As a result of this cut-off at l^* , the distribution of MT lengths is exponential, but increasing instead of decreasing toward the cell boundary. This model variant thus explains why most MTs reach the cell membrane. The model which is presented in section 6.3 is derived from [208] and the consequences from the boundaries will therefore also be addressed in that section.

The action of MT-severing proteins such as katanin has been introduced into the two-state model in [209] by considering randomly occurring severing events. The MT is then split into two with the newly exposed plus end being in the shrinking state. This modification could also be shown to lead to a finite average MT length with non-exponential length distributions. Interestingly, the severing does not increase the total number of MTs although the average MT length decreases.

Another mechanism for filament length regulation has been proposed in [210]. This model considers a treadmilling filament, i.e., the filament loses subunits at its minus end while subunits are added at the plus end. Although this is probably of more relevance for actin filaments than for MTs, the proposed mechanism is conceptually interesting as it exhibits length regulation under free growth conditions and involves a form of aging, similar to what happens in our model of the next section: Subunits in the filament have at each time step a certain probability to be occupied by a protein which increases the depolymerization rate of that subunit if exposed at the minus end. Older subunits, i.e., those subunits which are polymerized for a longer time, therefore have a higher probability to carry that destabilizing protein so that very old subunits disappear very quickly from the minus end. The length regulation hence acts by removing old subunits. As a result, three different regimes can be found depending on the parameter including one which exhibits a sharply peaked unimodal distribution which is indicative for a self-regulated filament length.

6.2.3 GTP cap

A different class of models does not postulate switching between a growing and a shrinking state, but instead allows individual subunits to always be added to or removed from the plus end. Additionally, the presence of a GTP cap (section 2.2.2) is considered. Subunits which are added always carry a GTP and have low (or vanishing) probability to depolymerize from the plus end. The GTP then hydrolyzes to GDP at a certain rate after the subunit has polymerized. The hydrolysis event modifies the subunit's kinetics, which is considered to have a higher probability of being removed if it is exposed at the plus end and is bound to GDP instead of GTP.

These models are thus mesoscopic in the sense that there is no state variable describing the filament as a whole as with the growing and shortening state in the two-state model. Nevertheless, these models exhibit macroscopically observable behavior by reproducing long periods of persistent growth and shrinkage which is characteristic for the dynamic instability of MTs [203,211–213]. The rescue and catastrophe rates assumed above (section 6.2.1) are in these models observables which follow from the kinetics of the tubulin subunits with GDP or GTP.

From a phenomenological point of view, a growing MT has several subunits which are bound to GTP at the plus end. This so-called GTP cap has an average length which is determined by the rate of hydrolysis of GTP to GDP. Since the hydrolysis is a stochastic process, the front between GTP and GDP diffuses within the filament relative to the plus end. If the front arrives at the plus end, a GDP subunit is exposed and catastrophe is likely to occur, i.e., the filament starts to lose subunits. Since these events depend on the diffusion of the shock front, the observed rate of catastrophes scales as n^{-2} if n is the average length of the GTP cap [203]. That model is also able to reproduce the same effects of a cell boundary and a limited tubulin supply as reported above for the two-state model. For unconstrained systems, the two regimes of bounded and unbounded growth can also be recovered [212].

A success of these models has to be seen in the explanation of the dependence of the catastrophe rate ν_c on the concentration of free tubulin [203,213], since this dependence cannot be explained by simple intuitive reasoning without considering the hydrolysis of the GTP cap.

Different models of hydrolysis have been examined, e.g., spontaneous hydrolysis [203,212,213], induced hydrolysis [211] and vectorial hydrolysis [211], and compared to experimental data in order to gain a better understanding of the still unclear nature of the GTP (discussed, e.g., in [203]). Although many experimental details could be explained with the different models, no single valid picture of GTP hydrolysis so far emerges from these models.

6.3 Theoretical modeling of aging effects in microtubule dynamics

6.3.1 Motivation

In this section, we aim at providing a model of MT dynamics which allows one to distinguish between a scenario in which a modification of the dynamic instability is caused by a rescue factor that effectively co-polymerizes with tubulin or a rescue factor that binds preferentially at the plus end of the MTs. In this context, *dynamical inclusion* refers to the rescue factor being introduced because of the dynamics of the filament, i.e., by being built into the MT at growth. *Structural recognition* on the other hand means that the rescue factor is added to the tip because of its property of being the end of the MT. For a few +TIPs, e.g., Stu2 in budding yeast [214] or the kinesin-14 Kar3p [215], experiments indicate that they find the MT plus end by structural recognition. Evidence for dynamic inclusion in other cases is mentioned below.

The motivation for our investigation comes from the interaction of MTs with certain +TIPs which are able to enhance rescues and therefore stabilize MTs (section 2.2.3). It will be shown that the different scenarios for plus end tracking lead to different filament properties, thus allowing one to discriminate between the two scenarios with appropriate experimental data.

The distinction between the two scenarios can be made by the presence or absence of aging effects in the survival probabilities of MTs. This kind of aging has to be distinguished from the observed correlation between age and MT stability under the action of a destabilizing agent such as nocodazole [22]. Instead, we refer to aging as a modification of the dynamic instability leading to different behavior of the MT over time. Technically, aging manifests itself by an autocorrelation function which depends on absolute times and not only on time differences. In this case, this can be translated to the time dependence of the filament's properties. For this, we present a stochastic model for MT dynamics whose key ingredients are the consideration of the cell boundary and a dynamical modification of the dynamic instability by means of a binding site to which a rescue-enhancing +TIP such as the CLIP-170-EB1 complex can bind at high frequency (section 2.2.3). We show that dynamical inclusion of such a binding site inevitably leads to aging whereas structural recognition of the plus end would not entail any aging effects. In a dynamical inclusion scenario, an MT ages at the cell membrane as no further rescue factors can be added to the tip if the MT is constrained by the finite cell geometry. The probability of being rescued on depolymerization decreases drastically and the risk of complete depolymerization increases, an effect which we will refer to as *aging* in the following. Our results thus demonstrate that the molecular mechanism of microtubule formation is intimately connected with aging.

We investigate the dynamics of MTs in a finite volume, which is relevant for the *in vivo* situation and might give new insights by predicting aging of MTs under dynamic modifications of the dynamic instability. The model and its results have been published in [216].

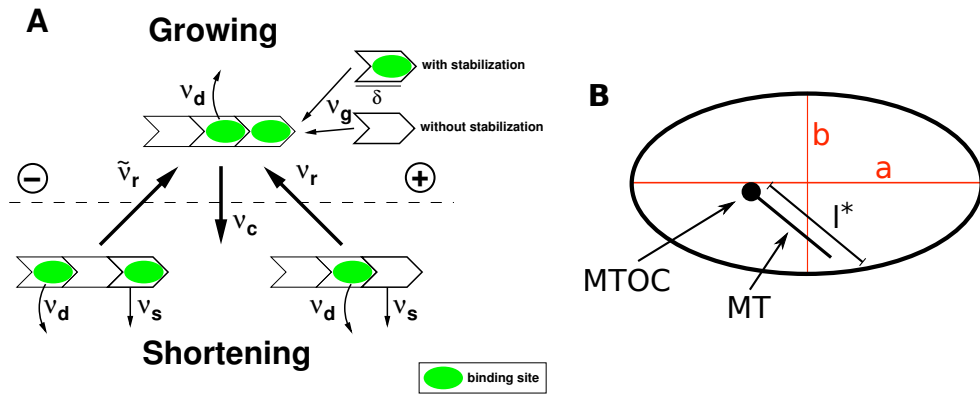


Figure 6.1: Schematic representation of the model. (A) The filament is built from individual subunits of length δ and can be either in the growing or in the shortening state. In the growing state, a subunit is added at a rate ν_g to the plus end of the filament. Depending on the scenario, the added subunit carries a binding site for a rescue-enhancing +TIP or not. Transitions to the shortening state happen with rate ν_c . In this state, the filament loses subunits from its plus end at rate ν_s regardless of the possible existence of a binding site. However, the switching back to the growing state depends on the presence of a binding site for the +TIP on the last subunit at the plus end and may happen with rate $\tilde{\nu}_r$ or ν_r depending on the state of the last subunit. At any time, a +TIP binding site disappears from the filament at rate ν_d . Boundary effects enter because reaching the cell boundary stops any growth and thus prevents the addition of binding sites for +TIPs. The distance between MTOC and cell boundary determines the length ratios between +TIP-decorated and undecorated parts of the MT. (B) The cell is an ellipse with half-axes a and b . From the MTOC, a MT grows in a random direction toward the cell boundary. The distance between the MTOC and the cell boundary in the current growth direction determines the maximum length l^* of that MT.

6.3.2 Model

The basis of our model relies on the phenomenological description of dynamic instability, whose motion in the bulk is usually characterized by four parameters: growth velocity, shortening velocity, rescue (= transition from depolymerization to polymerization) frequency and catastrophe (= transition from polymerization to depolymerization) frequency [11]. Accordingly, the model consists of a linear filament (MT) of individual subunits (tubulin dimers) which is either in the growing or the shrinking state. Depending on its state, a tubulin dimer of length δ is added to or removed from the tip of the filament such that the growth and shortening rates ν_g and ν_s are obtained. Switching of states is stochastic with rescue frequency ν_r and catastrophe frequency ν_c (figure 6.1 A).

The model cell has a predefined geometry, an ellipse with half-axes a, b , within which the origin of nucleating MTs (MT organizing center = MTOC) is chosen (figure 6.1 B). A MT grows in a random direction from the MTOC, thus determining the

maximum distance to the boundary l^* . The filament follows the bulk dynamics as described above until it reaches the boundary where switching to the shrinking state is induced with a probability p_{ind} . This probability describes experimental observations [46] which indicate that a MT filament pauses at the boundary, but that these pauses are too short to be caused by the stochastic switching which is characteristic for the dynamic instability. An ensemble of such filaments is used to determine the stationary distribution of filament states.

The influence of a rescue factor like the binding site for a +TIP is included in the model in the following way: A tubulin dimer that is added to the tip of a growing filament leads to the appearance of the binding site as the tubulin ring is complete and closes along the seam (section 2.2.2). +TIPs are then assumed to bind at such high frequency to these binding sites that the filament is considered to possess modified dynamic instability parameters as long as the binding sites exist. The binding site disappears with rate ν_d as the corresponding part of the microtubule grows older. After the vanishing of the binding site, the +TIP can no longer bind. As for the filament dynamics, the presence of the +TIP only affects the rescue frequency as has been shown in the case of CLIP-170 [46]. Thus, if the MT tip is decorated with a binding site, a rescue occurs with frequency $\tilde{\nu}_r (> \nu_r)$.

More formally, the dynamics can be formulated by representing a configuration of an existing filament in the following way:

$$|\dots -- + -- + \dots > \dots| \quad (6.6)$$

$$\text{or } |\dots -- + -- + \dots < \dots| \quad (6.7)$$

The vertical bars represent the system boundaries. The $>$ and $<$ symbols are at the tip of the filament and show the direction of tip motion: $>$ for filament growth and $<$ for filament shortening. The ‘plus’ sign stands for a tubulin subunit which has an associated binding site for a rescue-enhancing +TIP, while the ‘minus’ sign illustrates a subunit without binding site.

The local dynamics are then defined by the following moves.

1. Disappearance of a binding site:

$$|\dots + \dots \lesseqgtr \dots| \quad \Longrightarrow \quad |\dots - \dots \lesseqgtr \dots| \quad \text{rate } \nu_d \quad (6.8)$$

where \lesseqgtr is simply a compact way to denote the shortening and the growing state at the same time.

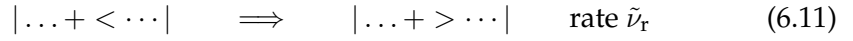
2. Switching from growing to shortening state (catastrophe):

$$|\dots > \dots| \quad \Longrightarrow \quad |\dots < \dots| \quad \text{rate } \nu_c \quad (6.9)$$

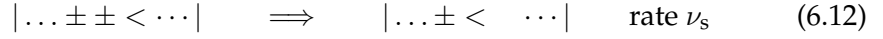
3. Switching from shortening to growing state (rescue) in absence of a binding site at the tip:

$$|\dots - < \dots| \quad \Longrightarrow \quad |\dots - > \dots| \quad \text{rate } \nu_r \quad (6.10)$$

4. Switching from shortening to growing state (rescue) in presence of a binding site at the tip:

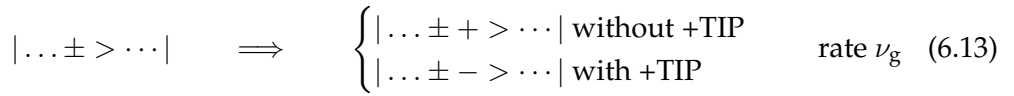


5. Shortening by one subunit:



with \pm being a subunit either with or without an associated binding site for a +TIP.

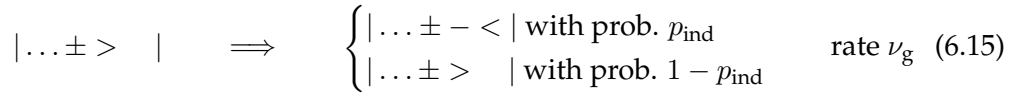
6. Growth by one subunit:



7. At the left boundary, the filament immediately switches to the growing state after losing its last subunit:



8. The right boundary stops filament growth and may induce catastrophe:



The behavior at the boundary, especially the addition of a subunit when undergoing boundary-induced catastrophe, may seem peculiar but was chosen in order to recover exactly the model in [208] if we consider the scenario without dynamical inclusion of the +TIP and $p_{\text{ind}} = 1$. This last site on which rescues can never occur does not contribute much to the overall behavior in a system of several thousand sites as considered here.

In accordance with [208], the fundamental length unit δ by which a filament grows or shrinks is chosen to be $8 \text{ nm}/13 \approx 0.6 \text{ nm}$, reflecting the length of 8 nm of a single tubulin dimer and the fact that a MT typically consists of 13 protofilaments that are arranged in parallel. Thirteen subunits therefore have to be added to elongate the filament by 8 nm.

We compare the results of this model with a model in which the binding sites are not dynamically included into the filament, i.e., filament rescues cannot be enhanced by +TIPs. The model does not explicitly take into account a realistic value for the stoichiometry of +TIP association to polymerized tubulin [217], since we make here a qualitative prediction about the aging effects occurring whenever the MT dynamics is altered by a dynamically, i.e., only in the growing phases, introduced rescue factor.

6.3.3 Methods

Simulation method

For the simulation of this model, a standard Monte Carlo algorithm was implemented: The sum of the rates of all possible moves in the current state was calculated before choosing one of these moves via tower sampling [189]. When the filament depolymerized completely to length zero, the new growth direction was drawn from a uniform distribution, and the resulting maximum filament length l^* was determined and kept constant until the new filament depolymerized again. The cell geometry including the position of the MTOC was kept constant throughout the whole simulation.

Distribution of active plus ends

Active plus ends were defined as MT ends that were either growing or shrinking, similar to [46]. In our model, pausing filaments can only exist at the cell boundary where MTs have their maximum length if $p_{\text{ind}} < 1$ was chosen. In this case, the filament paused before depolymerizing and consequently, the boundary site at l^* was excluded from the measurements of MT length distributions as filaments at maximum length would not be identified as being active. All other MT lengths were classed into a histogram with five bins that represent 20% of the maximum length l^* each (see figure 6.4).

Shortening lengths and aging behavior

Shortening lengths were determined as the distance between the site on which catastrophe occurred and the site on which the filament was rescued. If the filament depolymerized completely, the rescue site was taken to be at the origin. The threshold of experimental measurements was $0.18 \mu\text{m}$ [46] which corresponds to approximately 300δ . Since experimental measurements below this value were not possible, we excluded shortening events of less than 300 subunits from our statistics. The same applies to the excursions used to determine the aging behavior: If the excursions away from the cell boundary were below the experimentally detectable threshold, the counter for boundary hits was not increased.

Catastrophe and rescue frequency

Whenever a MT switched from growing to shrinking (shrinking to growing), a catastrophe (rescue) event was scored if the event did not take place at one of the boundary sites. The sum was then divided by the total simulated time.

Parameter	Simulation value
Growth rate ν_g	600 s^{-1}
Shortening rate ν_s	1000 s^{-1}
Catastrophe rate ν_c	0.003 s^{-1}
Rescue rate without CLIP-170 ν_r	0.024 s^{-1}
CLIP-170 dissociation rate ν_d	0.15 s^{-1}
Prob. of boundary-induced cat. p_{ind}	5×10^{-4}

Table 6.1: Standard set of parameters derived from experimental data.

6.3.4 Choice of parameters

The microtubule dynamics is determined by seven parameters. Approximate values for the four fundamental parameters of dynamic instability (growth and shortening rate, catastrophe and rescue rate in absence of CLIP-170) can be derived from [46]. Growth and shortening rates are with respect to the addition and removal of a single subunit of length δ , respectively.

The rate at which the +TIP binding site vanishes can be inferred from the observation that fluorescing CLIP-170 or EB1 comet tails usually have lengths of 1 to 3 μm . Assuming a first-order stochastic process, the average time spent on the MT is thus around 6 s which is consistent with estimations in [48] and with comet tails that disappear about 5 s after MT growth has stopped as observed in [12].

The probability of boundary-induced catastrophe p_{ind} is difficult to determine as there is little experimental data. Nevertheless, experimental trajectories of MTs without CLIP-170 [46] show that MT tips pause at the boundary before undergoing catastrophe. In combination with the growth rate one obtains the value of p_{ind} shown in table 6.1.

The remaining parameter – rescue frequency in presence of the binding site $\tilde{\nu}_r$ – determines the experimentally observed rescue frequency in presence of CLIP-170. As mentioned above, the true stoichiometry of +TIP association with polymerized tubulin is not considered, so that $\tilde{\nu}_r$ was chosen in order to obtain the correct observed overall rescue frequency under the influence of CLIP-170 of 0.17 s^{-1} [46]. This leads to values of $\tilde{\nu}_r$ which are about 100 times bigger than ν_r , but which are still a lower bound for the real value, since it can be assumed that very rapid sequences of catastrophe and rescue were not observable in the experiments even though they are counted in our simulations. These nano-depolymerization events have already been observed in another MT model [218].

6.3.5 Steady state solution without +TIPs

Since we are particularly interested in the effects the existence of the dynamically introduced binding site has on MTs, we also examine the case where no binding sites occur if a new tubulin subunit is added to the filament. The complete set of master equations for the steady state probabilities for the filament being in the growing or

shortening state with length l that have to be solved are:

$l = 0$:

$$\frac{\partial p_+(0, t)}{\partial t} = \nu_s p_-(1, t) - \nu_g p_+(0, t) \quad (6.16)$$

$$p_-(0, t) = 0 \quad (6.17)$$

$1 \leq l < l^* - 1$:

$$\frac{\partial p_+(l, t)}{\partial t} = \nu_g p_+(l-1, t) - \nu_g p_+(l, t) - \nu_c p_+(l, t) + \nu_r p_-(l, t) \quad (6.18)$$

$1 \leq l < l^*$:

$$\frac{\partial p_-(l, t)}{\partial t} = \nu_s p_-(l+1, t) - \nu_s p_-(l, t) + \nu_c p_+(l, t) - \nu_r p_-(l, t) \quad (6.19)$$

$l = l^* - 1$:

$$\frac{\partial p_+(l^* - 1, t)}{\partial t} = \nu_g p_+(l^* - 2, t) - \nu_g p_{\text{ind}} p_+(l^* - 1, t) \quad (6.20)$$

$$- \nu_c p_+(l^* - 1, t) + \nu_r p_-(l^* - 1, t) \quad (6.21)$$

$l = l^*$:

$$p_+(l^*, t) = 0 \quad (6.22)$$

$$\frac{\partial p_-(l^*, t)}{\partial t} = \nu_g p_{\text{ind}} p_+(l^* - 1, t) - \nu_s p_-(l^*, t) \quad (6.23)$$

where $p_+(l, t)$ and $p_-(l, t)$ are the probabilities for the filament to be in the growing or shortening state respectively at time t with tip position l .

These equations are only slightly modified compared to those treated in [208]. Consequently, solving for the steady state solution, i.e., setting the derivatives to zero, can be done straightforwardly in the same way. The solution reads:

$$p_+(l) = \begin{cases} A \times a^l & \text{for } 0 \leq l < l^* - 1 \\ A \times a^{l^* - 1} \left(\frac{1 + \frac{\nu_c}{\nu_g}}{p_{\text{ind}} + \frac{\nu_c}{\nu_g}} \right) & \text{for } l = l^* - 1 \\ 0 & \text{for } l = l^* \end{cases} \quad (6.24)$$

$$p_-(l) = \begin{cases} 0 & \text{for } l = 0 \\ A \times \frac{\nu_g}{\nu_s} a^{l-1} & \text{for } 1 \leq l < l^* \\ A \times \frac{\nu_g}{\nu_s} a^{l^* - 1} p_{\text{ind}} \left(\frac{1 + \frac{\nu_c}{\nu_g}}{p_{\text{ind}} + \frac{\nu_c}{\nu_g}} \right) & \text{for } l = l^* \end{cases} \quad (6.25)$$

with

$$a = \frac{1 + \frac{\nu_r}{\nu_s}}{1 + \frac{\nu_c}{\nu_g}} \quad (6.26)$$

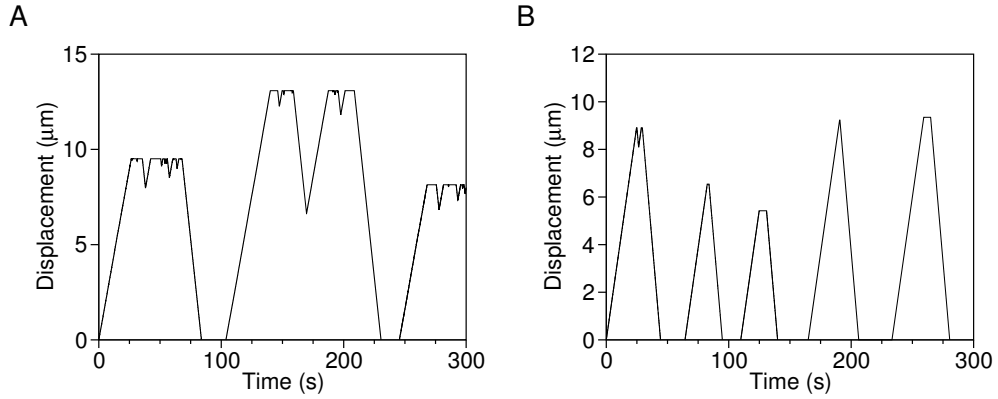


Figure 6.2: Life history plots of simulated MTs (A) with and (B) without +TIPs. If binding sites for a rescue-enhancing +TIP are added under growth (A), the MTs show dynamic instability at the cell boundary with frequent rescues. Without this effect (B), the MTs depolymerize completely after a short contact with the cell boundary. MT lifetimes are mostly determined by the time needed for polymerization to the cell boundary and depolymerization back to the MTOC. The geometry for the simulations was an ellipse of half-axes $a = 19.2 \mu\text{m}$, $b = 6.6 \mu\text{m}$ with the MTOC being $1.2 \mu\text{m}$ off the center of the ellipse in x - and in y - direction which are representative parameters for the cell geometry discussed in [46].

and A being a normalization constant such that $\sum_{l=0}^{l^*} [p_+(l) + p_-(l)] = 1$. These results have been used in order to check the numerical simulations that serve to produce the results in the spatial disorder case in the presence of CLIP.

The stationary probability for the tip position therefore is exponentially increasing in the bulk toward the cell boundary. For biologically relevant parameters (see table 6.1), the value of a is close to one so that the increase is not very dramatic. In any case, most of the probability mass is accumulated in the growing state at site $l^* - 1$ if the cell boundary induces catastrophe with a probability $p_{\text{ind}} < 1$.

In the dynamical inclusion scenario, the system exhibits spatial disorder which renders an analytical treatment very challenging. Instead, we performed extensive Monte Carlo simulations to obtain statistics of a large number of microtubules over their entire lifetime.

6.3.6 Simulation results

Increased lifetime and geometry dependence

The addition of binding sites for the +TIP at polymerization of tubulin leads to persistent growth up to the cell boundary where frequent switching between growth and shortening is observed (figure 6.2 A) before a filament eventually depolymerizes completely. Typical lifetimes are in the order of several minutes as observed in experiments [219]. If there are no binding sites for the +TIPs and the filament therefore

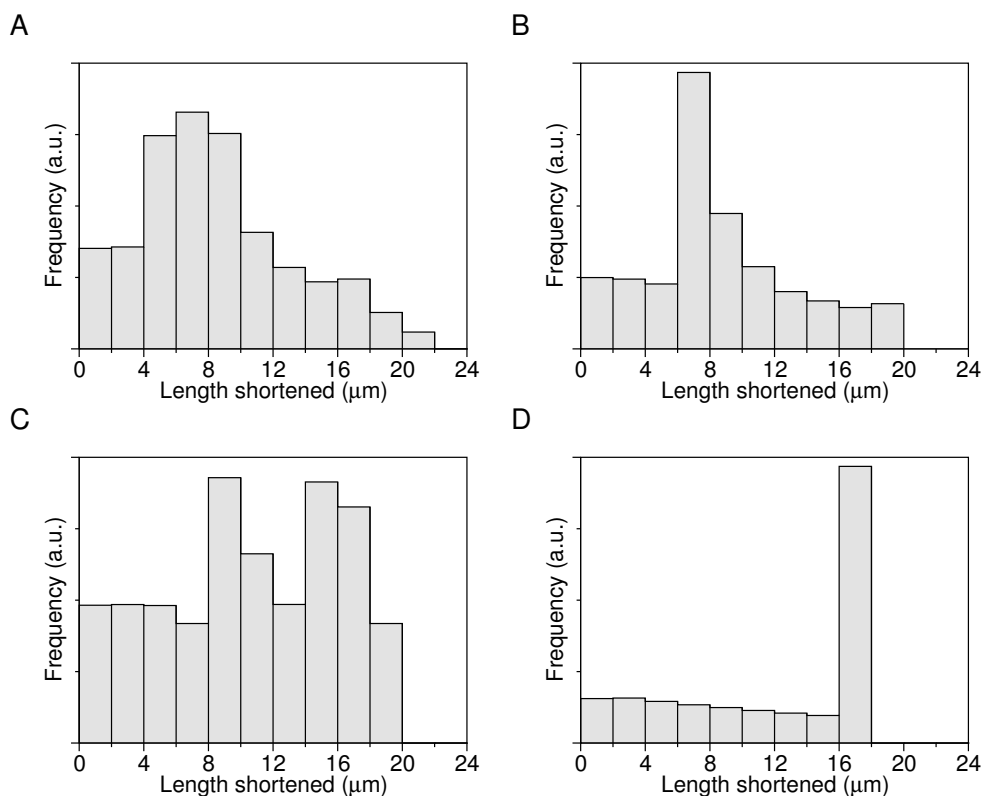


Figure 6.3: Examples for distributions of shortening lengths in absence of binding sites for different geometries. With the same set of dynamic parameters, very different distributions are obtained depending on the geometry. Reproducing the distribution experimentally determined in [46] is thus a question of finding the correct geometry. Chosen geometries were an ellipse with half-axes $a = 19.2 \mu\text{m}$, $b = 6.6 \mu\text{m}$ ((A) MTOC at $(1.2 \mu\text{m}, 1.2 \mu\text{m})$ off the center or (B) MTOC at the center), (C) an ellipse with half-axes $a = 18 \mu\text{m}$, $b = 12 \mu\text{m}$ (MTOC at $(0 \mu\text{m}, 3 \mu\text{m})$), and (D) a circle of radius $r = 18 \mu\text{m}$ (MTOC at the center).

cannot be rescued rapidly, MTs are very unstable and depolymerize entirely after a short sojourn time at the boundary (figure 6.2 B). This behavior has been anticipated as switches from the growing to the shrinking state and vice versa are rare with respect to the growing and shrinking times resulting from the typical distance between MTOC and cell boundary. The cell geometry thus has a big impact on the results in the absence of binding sites for the +TIP. Hence, the length distribution of shortening episodes (definition in section 6.3.3) is mainly an indicator for the shape of the cell rather than for the MT dynamics. Indeed, simulations with different geometries reveal very different distributions of shortening lengths (figure 6.3). Nevertheless, the qualitative behavior is conserved over a wide range of geometric parameters and rescaled quantities as those presented in figure 6.4 correlate well with experiments.

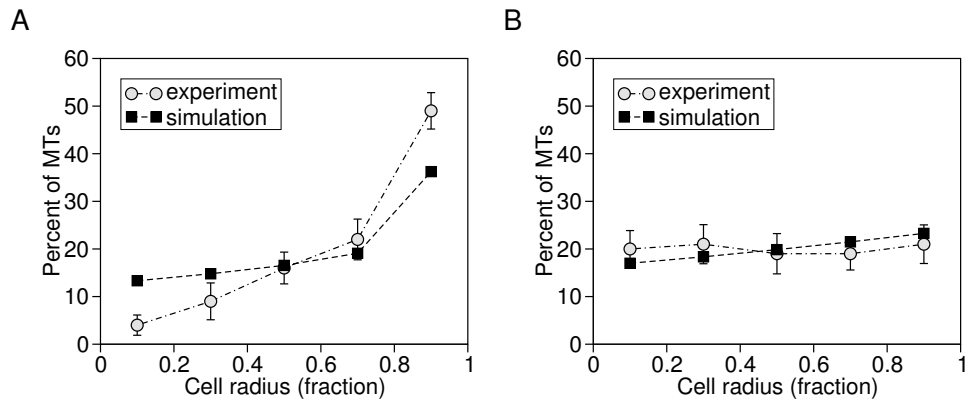


Figure 6.4: Histograms of the distribution of active plus ends along the cell radius (comparison with experiment). (A) After correction for paused MTs (definition in section 6.3.3), the simulation results still show an increased number of active MT ends near the boundary if the rescue-enhancing +TIP is included. (B) In absence of +TIP binding sites, the distribution of active MT ends increases only very slowly toward the boundary. As in the experiment, MT lengths are rescaled with the cell radius in the corresponding direction of the filament. These dimensionless lengths are robust to variations in cell shape while the absolute ones are not (not shown). Experiments [46] were performed on CHO-K1 and COS-7 cells injected with Cy-3 labeled tubulin; the experimental data was provided to us by Y. Komarova. Details on the experimental methods can be found in [46].

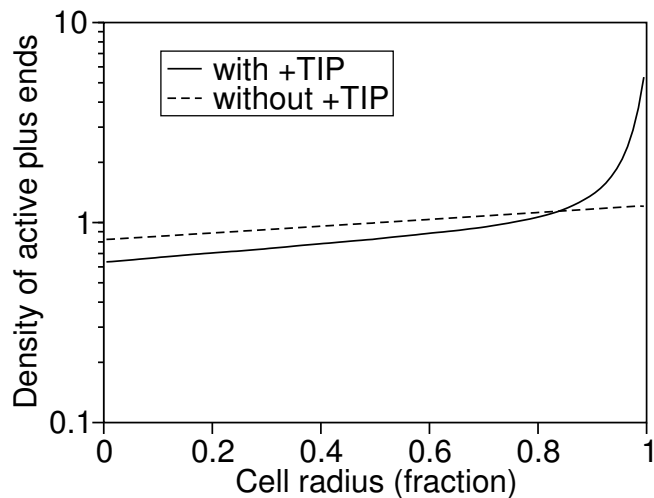


Figure 6.5: Distribution of active plus ends along the cell radius with (solid line) and without (dashed line) enhancement of rescues through vanishing binding sites for a +TIP. The data is the same that has been used to plot the histogram in figure 6.4. The plot is semi-logarithmic, thus indicating that the increase of active MT plus ends toward the cell boundary is not part of an exponential distribution.

Distribution of MT lengths

Figure 6.4 shows the distribution of active plus ends, i.e., MTs that are not pausing (definition in section 6.3.3), with respect to the fraction of the cell radius at which they are located. In contrast to alternative interpretations of the MT length distribution [12, 46, 208], our simulations indicate a very slow increase in the bulk with a stronger than exponential accumulation of MT ends at the cell boundary (figure 6.5). In an experimental setup, the number of short filaments is systematically underestimated, since the tips are located near the MTOC in a dense environment where they can scarcely be resolved [12]. These difficulties obviously do not exist in a theoretical model which explains the higher values of short MT lengths in our model compared to the experimental data (figure 6.4 A). The qualitative behavior is not affected by this shortcoming of the experimental method. In the absence of +TIP binding sites, the distribution of active MT ends is almost flat (figure 6.4 B) and thus corresponds well with the experimental data. In appendix B, simulation data is presented for a more complicated cell geometry which has been derived from experimental images of cells. Results are qualitatively the same as for the modeled ellipse.

Aging of MTs

The presence of a binding site for a +TIP which increases the rescue frequency leads to a qualitatively different behavior of the MT dynamics: The association of a rescue factor with the growing plus end leads to observable aging at the cell boundary. This is because no further binding site can be added to the MT tip once it has stopped at the boundary while the older ones continuously vanish from the filament (see figure 6.6). This reduces the probability of rescue after a boundary-induced catastrophe. In consequence, the MT ages while resting at the boundary, resulting in a shorter remaining lifetime.

In order to visualize this, the plot in figure 6.7 A shows the probability that a MT filament has not yet completely depolymerized at $t - t_N$ seconds after hitting the boundary for the N -th time at time t_N , where ‘hitting the boundary’ means the contact between filament and cell boundary after an excursion away from the cell boundary which is larger than the experimental threshold (see section 6.3.3). Younger MTs, i.e., those with smaller N , have at all times higher survival probabilities. We chose the number of boundary hits instead of the time after the first contact with the boundary as longer excursions away from the boundary and back to it occur. During these excursions, the filament does not age, since new binding sites are added to the tip. In contrast to these results, the absence of binding sites eliminates the aging behavior which means that all MTs show the very same behavior regardless of the time spent at the boundary. This is portrayed in figure 6.7 B which shows identical curves for different values of N .

Depending on the parameters of the rescue factor dynamics, the aging effects observed in figure 6.7 can be much stronger and depend mainly on the rate ν_d at which the binding site vanishes and the rescue rate in presence of the +TIP $\tilde{\nu}_r$. In figure 6.8,

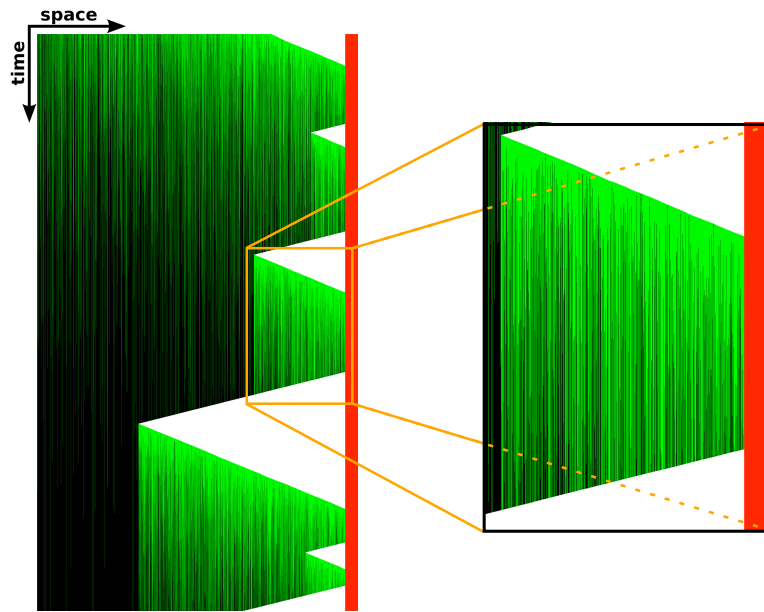


Figure 6.6: Evolution of a filament during the simulation. Similar to a kymograph, every line corresponds to the tip of a MT which nucleated on the left and polymerizes toward the cell boundary on the right shown in red. +TIPs are shown in green and can be seen to slowly dissociate over time, thus causing the filament to be rescued less frequently.

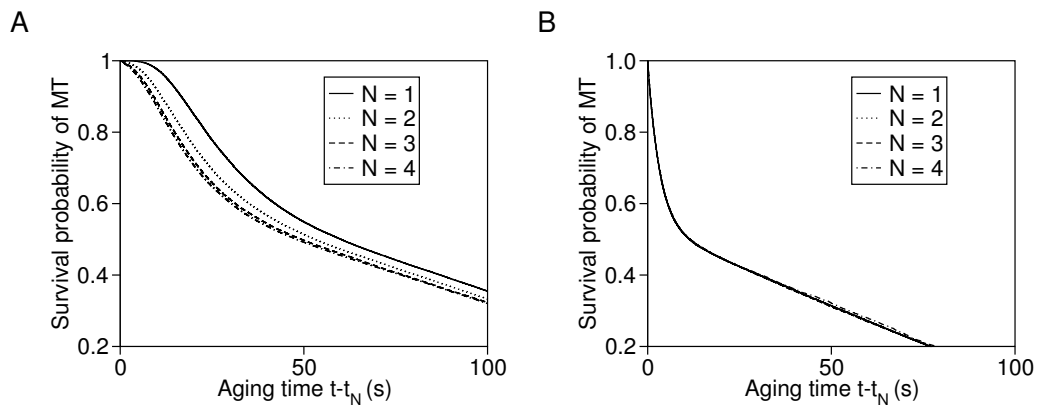


Figure 6.7: Survival probability of an MT of maximum length $l^* = 18 \mu m$ after boundary contact. (A) A dynamically introduced binding site for a rescue-enhancing +TIP induces aging of the MT. The survival probability of an MT after it hit the cell boundary for the N -th time at the time t_N is lower for higher values of N . (B) Without the positive effect on the rescue frequency, all MTs show the same behavior regardless of their past, i.e., the number of collisions with the cell boundary. Consequently, all curves collapse.

the survival probability of an MT is plotted for different combinations of these two parameters in order to elucidate their influence on the aging behavior.

At constant binding site rescue rate $\tilde{\nu}_r$, stronger aging effects can be observed if the dissociation rate ν_d is decreased (figure 6.8 *B,C,D*). Moreover, the dissociation rate ν_d controls the time scale which is relevant for the survival probability. Dividing the dissociation rate by a factor of ten, increases the time scale of the filament's lifetime also by about a factor of ten. Since the presence of +TIP binding sites prevents depolymerization, their dissociation rate is necessarily the relevant parameter for the destabilization of a MT.

A variation of the binding site rescue rate $\tilde{\nu}_r$ is also able to alter considerably the aging behavior (figure 6.8 *A,C,E*) as the survival times also increase if $\tilde{\nu}_r$ increases. For very high values of $\tilde{\nu}_r$, the number of boundary contacts seems to be irrelevant for the survival probability after the second boundary contact (figure 6.8 *E,F*). Because of the high probability of being rescued very close to the boundary, the part of the MT which is decorated by binding sites gets smaller and smaller as new subunits are only added to a limited region at the boundary. Once the filament retracts further away from the boundary, almost no more binding sites are left which is then also the case for all following contacts with the boundary.

6.4 Chapter conclusion

Cytoskeletal dynamics constitute one of the fundamental processes in the cell which shows generic non-equilibrium behavior. Here, we focus on the changes of the dynamic instability of MTs under the action of a rescue-enhancing +TIP, in which case boundary-induced catastrophes are frequently observed. Our results indicate that the actual quantitative results are strongly influenced by the cell geometry. First, the boundary effects induce a stationary distribution of MT lengths that is not exponentially decaying, as for example in [206]. In particular, the number of MTs in contact with the cell membrane is drastically increased such that the ability of interaction between the cytoskeleton and the cell membrane is enhanced. Second, quantitative parameters like the distribution of shortening lengths or MT lengths depend strongly on the exact shape of the cell boundary. Nevertheless, the qualitative behavior is conserved over a wide range of geometric parameters and correlates with experimental results, yielding astonishingly good results although several details of the cellular processes have been neglected.

We have shown that dynamical inclusion of a +TIP binding site into the MT filament will lead to aging phenomena, which means that quantities such as remaining lifetime of the filament or the average extent of a shortening episode depend on its past. In contrast to this model of dynamic addition of binding sites to the MT, models in which plus end tracking is assured by the recognition of a structural feature at the plus end would not lead to observable aging as recruitment of new +TIPs would happen for as long as a plus end exists and does not depend on addition of tubulin subunits during growth phases. The existence of aging thus allows one to discrimi-

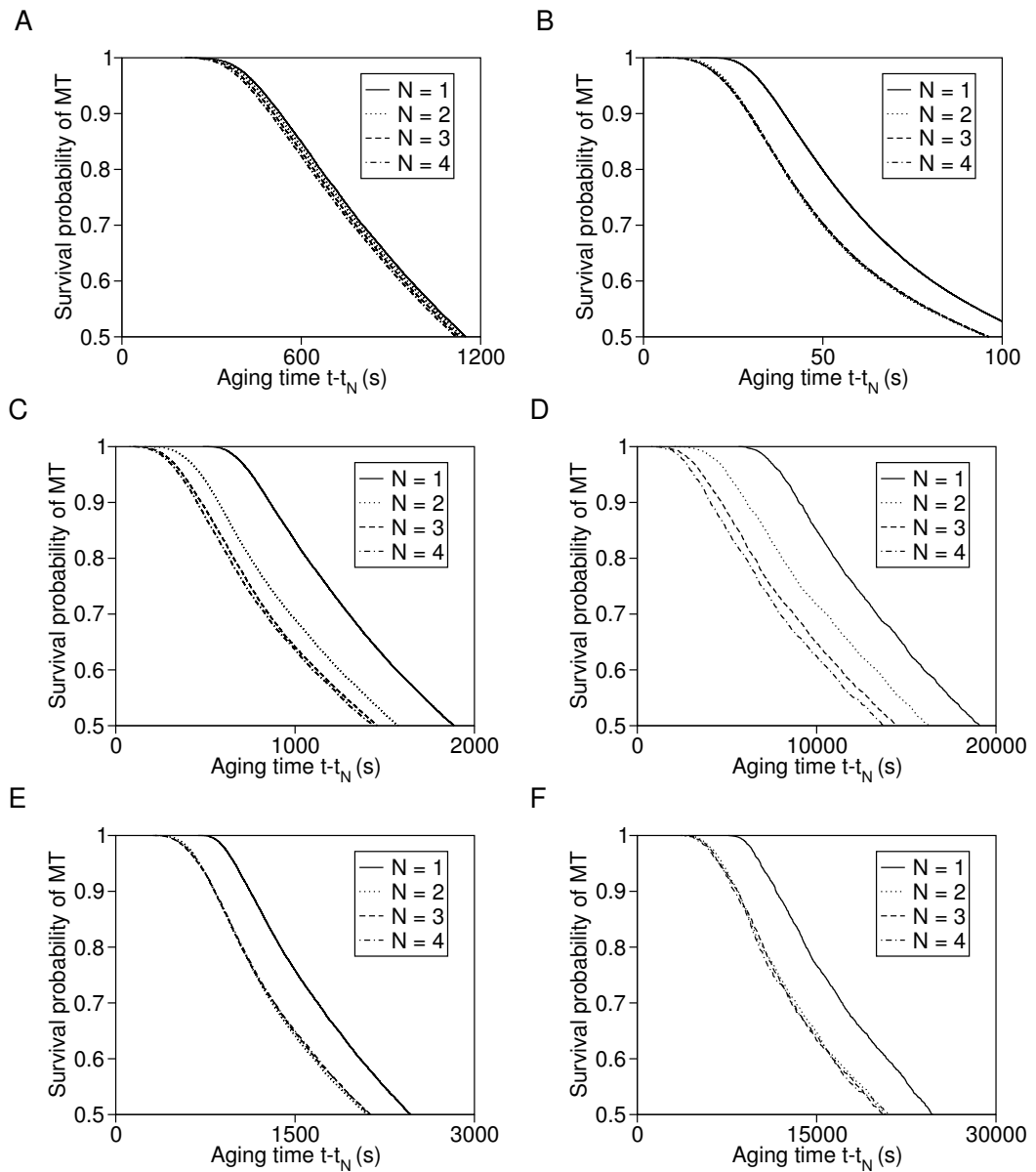


Figure 6.8: Survival probability of MT after boundary contact with altered rescue factor dynamics. In order to better illustrate the effect of aging through dynamical interaction, the same curves as in figure 6.7 A are plotted for different parameters of the CLIP-170 dynamics: (A) $\tilde{\nu}_r = 3.5 \text{ s}^{-1}$, $\nu_d = 10^{-2} \text{ s}^{-1}$; (B) $\tilde{\nu}_r = 40 \text{ s}^{-1}$, $\nu_d = 1.5 \cdot 10^{-1} \text{ s}^{-1}$; (C) $\tilde{\nu}_r = 40 \text{ s}^{-1}$, $\nu_d = 10^{-2} \text{ s}^{-1}$; (D) $\tilde{\nu}_r = 40 \text{ s}^{-1}$, $\nu_d = 10^{-3} \text{ s}^{-1}$; (E) $\tilde{\nu}_r = 400 \text{ s}^{-1}$, $\nu_d = 10^{-2} \text{ s}^{-1}$; (F) $\tilde{\nu}_r = 400 \text{ s}^{-1}$, $\nu_d = 10^{-3} \text{ s}^{-1}$. Note the difference in time scales on the horizontal axis.

nate between these scenarios.

In a general way, aging of MTs will indicate the presence of a mechanism similar to the one presented in this chapter: the rescue-enhancing factor is dynamically introduced into a growing MT and then slowly disappears from the filament thus leaving a destabilized filament behind if the MT stops its growth. For example, the frequently addressed GTP cap might fall into the same class of mechanism as GTP-remnants in the filaments have been proposed to be caused by slow hydrolysis and to be responsible for rescues [16]. Thus, we expect aging of filaments to be observable *in vivo* whether it is due to the GTP cap or the interaction with a rescue-enhancing +TIP. Furthermore, our results show that a dynamical inclusion leads to destabilization of static filaments over time. In this way, the cell is provided with the ability to adapt its shape to the environment.

To summarize, the model offers a possibility to experimentally confirm whether the inclusion of a rescue factor is mediated by a dynamical interaction with the filament or a structural recognition of the MT plus end. Namely, the macroscopic effect of microscopic aging should manifest itself in a reduced remaining lifetime of the filament. This quantity is experimentally accessible, sufficient statistics provided. Another quantity which can serve to identify the mechanism might be the length of excursions away from the cell boundary which should become larger as the filament ages.

Chapter 7

Conclusion & Outlook

In this thesis, stochastic models for two different intracellular processes were investigated: bidirectional transport along axonal microtubules and the dynamics of microtubules. In the part on bidirectional transport, we were particularly interested in the transport capacity determined by the stationary current in periodically closed systems. For the microtubule dynamics, the focus was on the consequences of a rescue factor which is dynamically added to the tip of the microtubule in growth phases.

Motivated by bidirectional transport in axons, we tried to answer the question how the transport can efficiently be organized if both types of motors (anterogradely and retrogradely moving ones) use the same MTs for their motion. The encounters of oppositely charged motors together with the very confined axonal environment were shown to lead to clustering (or jam formation) in our basic model for bidirectional transport. The cluster absorbs almost all particles in the system and controls the current of particles in the whole system, making transport extremely inefficient.

First of all, we attempted to show that the clustering observed in numerical simulations also persists in the limit of infinite system sizes. This was done by a mapping to the two-species zero-range process describing the particle exchange between clusters and neglecting the spatial extent of the cluster in the basic model. With an additional assumption on the value of a fitting parameter, it was possible to show macroscopic clustering for the infinite system. This result holds in the limit of the assumptions of which discarding the spatial information on the cluster certainly is the most restricting one. Nevertheless, we regard the result as valid since simulations did not leave the slightest doubt that the system will form a large cluster if enough particles are present. This result served as motivation for the subsequent investigations which were led by the question what kind of process can prevent this clustering.

In a first approach, the dynamics of the transport lattice were proposed as possible solution, representing the central result of this thesis. Applying a simple choice of lattice dynamics eventually leads to a dissolution of the large cluster in finite systems, thus eliminating the blocking structure. As a consequence, the particles are redistributed over the whole system which assumes then a homogenous state with a density-dependent current. This transition exists for different types of lattice dynamics and relies on the finite lifetime of binding sites. It should be underlined that this result is rather counter-intuitive at first: it is by destroying the road on which transport takes place that the transport capacity is improved. This result is of inter-

est first for the field of non-equilibrium physics, as we have evidenced a new type of dynamic transition driven by the dynamics of the underlying lattice. From the biological point of view, the existence of this transition is compelling as it underlines the possibly crucial role played by the dynamics of the microtubule network for the transport through the axon. Unfortunately, the structure and dynamics of the axonal MT network are not known in enough detail to be modeled more realistically. In particular, current knowledge suggests that a part of the axonal MT population is very stable and might in fact persist for a very long time. On the other hand, we see the basic relation between efficient intracellular transport and microtubule dynamics confirmed by the experiments by Shemesh and Spira [100] in which the failure of axonal transport coincides with a stabilization of the MT network.

The question whether the discovered transition will actually be visible in the living cell is tightly linked to the amplitude of the lattice dynamics which is needed to reach the homogenous state. The finite size examination of the transition showed that the critical depolymerization rate shifts positively with the system size, probably to infinity. The conclusion is that for the infinite system, probably no lattice dynamics at any strength will be capable of dissolving nascent clusters. However, real systems may be long but are always finite, so that the transition might indeed exist in cells. A final answer cannot be given as long as a more quantitative description of real axonal transport is missing.

As for the clustering behavior in the limit of infinite system sizes, it was shown that macroscopic structures cannot persist in that limit even though the lattice dynamics might in fact no longer be able to hinder clustering. Instead, a stationary state property of the lattice induces a length scale equivalent to that for the decay of the cluster distribution. The exponential decay of this quantity was shown to be robust with respect to different cluster definitions. This shows that besides the dissolution of clusters, a second cluster limiting mechanism exists. While this result is of theoretical interest, its implications are marginal for axonal transport.

So far, the model did not take into account that the amount of tubulin in the cytoplasm is limited and that the transport of small MTs through the axon depends to a great extent on the existing MT network. On the path to a more complete model which extends our understanding of the relation of MT dynamics and axonal transport, it seems natural in a next step to include the transport of tubulin. An alteration of axonal transport by modified lattice dynamics will have a feedback on the lattice dynamics as the supply of tubulin or new MT parts might be disrupted.

Apart from adding another feature of the real system and thus bringing the model closer to reality, an extension in this direction might also be able to elucidate the open question of the fate of axonal MTs when they are not growing. Present live-cell imaging techniques can only show growing plus ends and transported small MTs which usually move anterogradely so that the observed tubulin transport is only unidirectional, while it is unclear how tubulin is transported back to the soma if it is at all. This question could be addressed by a model which keeps track of the local amount of tubulin in its different forms. It would thus elucidate if degradation and/or diffusion are sufficient to reach a stationary state or if additional mechanisms

have to exist which are not observed with current experimental techniques.

As an alternative mechanism to reach an efficient bidirectional transport state, we picked up the idea of self-organized lane formation and investigated two different types of interactions possibly exhibiting this phenomenon.

A local modification of the particles' affinity to the filament in the vicinity of other particles was confirmed to lead to lane formation in systems with infinite diffusion in the bulk reservoir. For finite diffusion, however, no lane formation could be observed although the proposed interaction was able to increase the current along the filament especially in systems with low density. Furthermore, it was shown that for those systems which exhibited lane formation, the number of particles was decisive for the efficiency of the transport after lane formation: The increased affinity to the filament next to particles of the same species leads to extreme occupation densities on the filament; the resulting lack of vacant binding sites limits the current if too many particles are present in the system. On the other hand, for low or medium total densities of particles, TASEP-like currents could be reached. However, the necessary interaction strength increased considerably in these cases.

In combination with a lattice dynamics, it was shown that the transition toward lane formation is shifted to stronger particle-particle interactions with increasing lattice dynamics, while increasing the improvement of the transport capacity nevertheless.

As for the relevance for axonal transport, the conclusion to draw from this model is that lane formation does not occur as soon as a somewhat realistic reservoir around the MT is considered. In other words, no efficient transport can be achieved due to the proposed local variation of the affinity to the filament if molecular motors do not diffuse infinitely fast within the axon.

Consequently, we investigated another type of interaction that relies on an assumed steric interaction between oppositely charged particles which may push each other to neighboring filaments. In contrast to the previous proposition, this type of interaction leads to lane formation with a very high transport capacity if diffusion is *low*. We also saw that lattice dynamics promotes lane formation in this case due to the dissolution of large clusters.

This scenario is consequently more realistic than the previous one in that it exhibits lane formation in low diffusion environments. However, the mechanism is so extremely sensitive to the rate of diffusion that it is difficult to estimate if diffusion in the axonal cytoplasm is weak enough to allow for lane formation by this mechanism.

In total, it is difficult to draw a conclusion from the investigation of these two mechanisms as lane formation could in principle be observed, but depends on some major conditions which are not necessarily fulfilled in the real system. Nonetheless, the overall picture emerges that lattice dynamics in the proposed form dominates the lane formation mechanisms as the latter are significantly affected by the former. The variation in the transport capacity also seems to be influenced much more strongly by lattice dynamics than by additional particle-particle interactions.

The existence of the assumed particle-particle interactions or modifications thereof

will have to be shown by experiments, before a statement about possible lane formation can be made. The only case where this could be done so far was for an attractive interaction between kinesins [63–65]. But the reported interaction strength appears slightly too low to induce lane formation if compared to the first mechanism treated here. Further experiments might reveal more features of the way molecular motors interact so that a refinement of the model will be possible in the future. A more direct way would be to observe a spatial separation of motor species and deduce the particle-particle interactions from the conditions under which this separation breaks down. However, a success of this approach is unlikely at the moment as microscope techniques are not able to resolve the distances of several tens of nanometers between axonal MTs, to name only one challenge.

The last part of this thesis was devoted to a model of microtubule dynamics in a non-circular model cell. The model included the action of a rescue factor which is built into the filament at the MT tip upon growth and thus addresses to the question of the plus-end tracking mechanisms of the +TIP protein family. Interesting results appear due to combination of this process with the finite geometry of the cell such that MTs were limited in their maximal length. While not only reproducing experimentally determined rescaled distributions of MT tips, we were also able to show that quantities such as the shortening lengths of MTs depend strongly on the shape of the cell. Considering the consequences of the dynamical inclusion of the rescue factor, it was shown that the distribution of plus ends increases faster than exponentially near the cell boundary. This is a refinement of the conclusions drawn from experiments with limited resolution [12].

Additionally, MTs which are stabilized by a dynamically included rescue factor exhibit aging, i.e., their dynamical properties change over time as they are paused near the boundary. The effect is easy to understand since the filament constantly loses the rescue factor due to its dissociation from the filament but new rescue factors can only be added while growing. It therefore makes a difference if a filament arrives at the boundary for the first time or if it comes back for the n -th time after excursions of the tip away from the boundary. In the latter case, the filament arrives with fewer rescue factors at the boundary such that it has a higher probability of complete depolymerization afterwards.

The exploitation of simulation results was intentionally kept close to the analysis of the experiment in [46], for example considering a threshold for the detection of MT tip excursions. As a consequence, aging should also be detectable in experiments by measuring the proposed quantity, i.e., measuring the survival probability at a given time after the n -th contact with the cell boundary. Alternatively, one could measure the extent of excursions away from the boundary after several contacts with the boundary. The drawback of both propositions is obviously the requirement of good statistics. With new tracking techniques, we are confident that it nevertheless should be possible to observe an effect if the assumption about the dynamical inclusion is correct. This would then allow to exclude other proposed plus-end tracking mechanisms as for example the hitchhiking model.

The discovered aging effect is not limited to the detection of plus-end tracking mechanisms of +TIPs, but also adds to the understanding of the GTP cap as the addition of GTP is conceptually close to the dynamical inclusion proposed in our model. Experiments have shown that islands of GTP can be found inside polymerized MTs [16]. Better statistics provided, this result could also be cross-checked against our model of microtubule dynamics by considering quantities like the distribution of the sizes of these GTP islands. As different hypotheses about the hydrolysis of GTP exist, modifications of the present model could possibly contribute to the discussion in this area of MT dynamics.

On a more global view, the results from this thesis are to be seen as early steps in the development of a realistic model for axonal transport with the ultimate goal of explaining the failure of transport in certain neuronal diseases. Therefore, a combination of the knowledge gained from the different parts of this thesis is desirable. Although the qualitative differences of MT dynamics in axons and in other cells are not extreme, the network structure in the axon appears much more complicated. A deeper understanding of the consequences brought about by the crosslinks and the transport of MT parts along the already existing MT network would be necessary in a next step. We see this as the crucial point for an ensuing refinement of the bidirectional transport model. A fully validated model could then be used in order to investigate mechanisms that are underlying clinically relevant transport defects in nerve cells [114,119].

Appendix A

Dynamics of maximum cluster lengths

The maximum cluster lengths in the bidirectional transport model on a dynamic lattice are constantly modified as addressed at the end of section 4.3.4. In this appendix, the time during which certain maximal cluster lengths persist, i.e., the time that a cluster would have to build up on the segment before it is changed by the lattice dynamics is determined. The presentation follows the Bernoulli process picture used in the main text although here, dynamical processes are considered, corresponding to the changes of the outcome of a Bernoulli trial at a certain rate. A black ball is hence exchanged by a white ball at rate k_p and a white ball gets replaced by a black ball at rate k_d .

A.1 Rates of length change

A segment might change its length through addition of a black ball on a site whose neighboring site is already occupied by a black ball or by taking away a black ball which is part of the 'barrier' between two segments. In the first case, there is division of the segment into two segments, the latter corresponds to fusion of two segments. Rates for these changes are derived in the following.

A.1.1 Fusion of segments

The governing rate for the fusion of two segments is the polymerization rate k_p at which a black ball might be replaced by a white ball and reduce the length of the barrier H below 2 (figure A.1). The length of the barrier H (= number of black balls on adjacent sites) determines the different possible transitions, which in turn depend on the position n of the black ball which is replaced. The corresponding rates will be labeled $\omega(L_1, L_2 \rightarrow L_3)$ and give the total rate at which the transition of the argument takes place. The argument of the rate ω consists of the segment lengths left of the arrow which are transformed to segments of the length on the right side of the arrow. This notation will be kept throughout the following and the number of arguments may change depending on the considered transition.

$H = 2$:

$$n = 1, 2 : \quad \omega(L_1, L_2 \rightarrow L_1 + L_2 + 2) = k_p. \quad (\text{A.1})$$

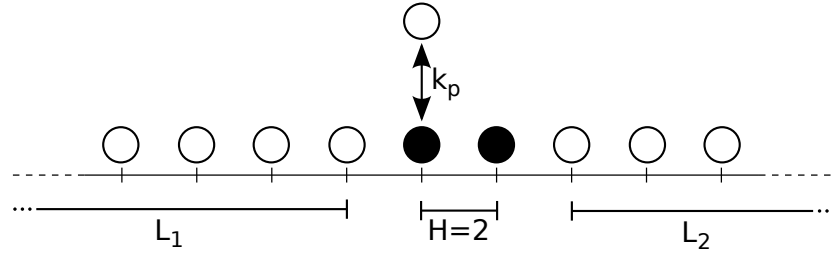


Figure A.1: Fusion of two adjacent segments of length L_1 and L_2 which are separated by a barrier of H black balls. If one of the black balls is replaced by a white ball, the segments are not separated by at least two black balls anymore and the criterium for the segment definition is not fulfilled. Note that the segments L_1 and L_2 are shown to be completely occupied by white balls although they might contain isolated black balls.

$H = 3$:

$$n = 1 : \quad \omega(L_1, L_2 \rightarrow L_1 + 1, L_2) = k_p \quad (\text{A.2})$$

$$n = 2 : \quad \omega(L_1, L_2 \rightarrow L_1 + L_2 + 3) = k_p \quad (\text{A.3})$$

$$n = 3 : \quad \omega(L_1, L_2 \rightarrow L_1, L_2 + 1) = k_p. \quad (\text{A.4})$$

$H \geq 4$:

$$n = 1 : \quad \omega(L_1, L_2 \rightarrow L_1 + 1, L_2) = k_p \quad (\text{A.5})$$

$$n = 2 : \quad \omega(L_1, L_2 \rightarrow L_1 + 2, L_2) = k_p \quad (\text{A.6})$$

$$3 \leq n \leq H - 2 : \quad \omega(L_1, L_2 \rightarrow L_1, 1, L_2) = k_p \quad (\text{A.7})$$

$$n = H - 1 : \quad \omega(L_1, L_2 \rightarrow L_1, L_2 + 2) = k_p \quad (\text{A.8})$$

$$n = H : \quad \omega(L_1, L_2 \rightarrow L_1, L_2 + 1) = k_p. \quad (\text{A.9})$$

A.1.2 Splitting of segments

Replacing a white by a black ball next to another black ball splits an existing segment or at least reduces its length. The addition of a black ball corresponds to the depolymerization of a lattice site at rate k_d which is therefore the rate at which these transitions happen. The possible transitions obviously depend on the length of the segment L_1 and on the configuration of the segment, i.e., which sites are already occupied by a black ball. Therefore, in addition to the rates, the probabilities with which the corresponding local configuration occurs will be given. In this context, it is worth to recall that the very last site on both sides of the segment are occupied by white balls by definition. Addition of balls to the lattice that do not modify the segment length are not mentioned. n gives the site within the segment, on which a ball is placed.

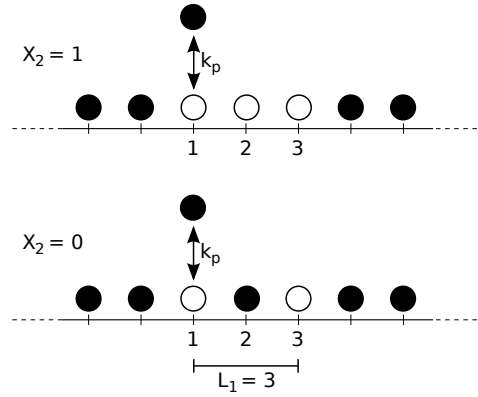


Figure A.2: Modification of a segment of length $L_1 = 3$ by exchange of a white ball on the first site. Depending on the occupation of the second site, the resulting segment takes length 2 or 1. The system is symmetric for inversion of the coordinate and the same transitions therefore occur at the right boundary for site 3.

$L_1 = 1$: The only site of the segment is occupied by a white ball by definition and the segment vanishes if the white ball is replaced by a black one.

$$n = 1 : \quad P(X_1 = 1) \cdot \omega(1 \rightarrow \emptyset) = 1 \cdot k_d. \quad (\text{A.10})$$

$L_1 = 2$: Both sites are occupied by white balls and either one can be exchanged, thus reducing the segment length by 1.

$$n = 1, 2 : \quad P(X_1 = 1) \cdot \omega(2 \rightarrow 1) = 1 \cdot k_d. \quad (\text{A.11})$$

$L_1 = 3$: The exchange of the ball on the middle site does not result in a change of the segment length. For the replacement of a ball on the first site, two cases have to be considered depending on the configuration of site 2 (figure A.2). The situation on site 3 is symmetric to site 1.

$$n = 1, 3 : \quad P(X_1 = 1, X_2 = 1, X_3 = 1) \cdot \omega(3 \rightarrow 2) = p \cdot k_d \quad (\text{A.12})$$

$$P(X_1 = 1, X_2 = 0, X_3 = 1) \cdot \omega(3 \rightarrow 1) = q \cdot k_d. \quad (\text{A.13})$$

$L_1 = 4$: The segment length may change by addition of a black ball to any site under certain conditions, see figure A.3. The problem is again symmetric under the transformation $n \leftrightarrow L_1 + 1 - n$.

$$n = 1, 4 : \quad P(X_1 = 1, X_2 = 1) \cdot \omega(4 \rightarrow 3) = p \cdot k_d \quad (\text{A.14})$$

$$P(X_1 = 1, X_2 = 0) \cdot \omega(4 \rightarrow 2) = q \cdot k_d \quad (\text{A.15})$$

$$n = 2, 3 : \quad P(X_1 = 1, X_2 = 1, X_3 = 0) \cdot \omega(4 \rightarrow 1, 1) = q \cdot p \cdot k_d. \quad (\text{A.16})$$

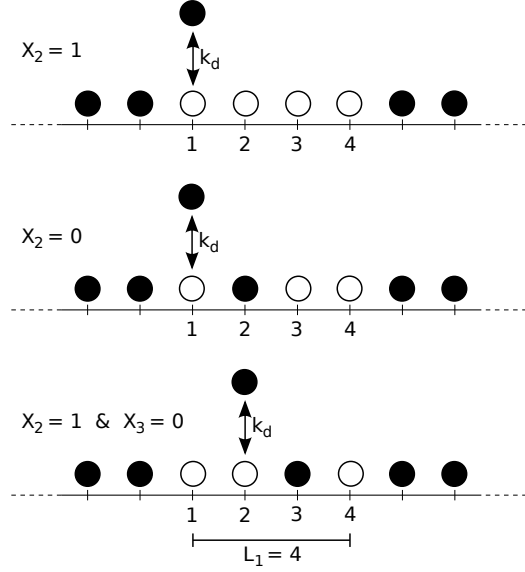


Figure A.3: Modification of a segment of length $L_1 = 4$ by addition of a black ball. Only the moves which lead to a change in the segment composition are shown and the symmetric transitions at the right boundary are not drawn.

$L_1 \geq 5$: All other cases can be treated at once. The procedure is the same as before with the same symmetry arguments. For convenience, the segment is divided into the boundary which consists of the two sites at the left and right boundary of the segment, respectively (figure A.4 (Left)) and the bulk of the segment which extends from site 3 to site $L_1 - 2$ (figure A.4 (Right)).

Boundary: $n = 1, 2, L_1 - 1, L_1$

$$n = 1, L_1 : \quad P(X_1 = 1, X_2 = 1) \cdot \omega(L_1 \rightarrow L_1 - 1) = p \cdot k_d \quad (\text{A.17})$$

$$P(X_1 = 1, X_2 = 0) \cdot \omega(L_1 \rightarrow L_1 - 2) = q \cdot k_d \quad (\text{A.18})$$

$$n = 2 : \quad P(X_1 = 1, X_2 = 1, X_3 = 0) \cdot \omega(L_1 \rightarrow 1, L_1 - 3) = q \cdot p \cdot k_d \quad (\text{A.19})$$

$$n = L_1 - 1 : \quad P(X_{L_1-2} = 0, X_{L_1-1} = 1, X_{L_1} = 1) \cdot \omega(L_1 \rightarrow L_1 - 3, 1) = q \cdot p \cdot k_d. \quad (\text{A.20})$$

Bulk: $3 \leq n \leq L_1 - 2$

$$P(X_{n-1} = 0, X_n = 1, X_{n+1} = 0) \cdot \omega(L_1 \rightarrow n - 2, L_1 - (n + 1)) = q^2 \cdot p \cdot k_d \quad (\text{A.21})$$

$$P(X_{n-1} = 1, X_n = 1, X_{n+1} = 0) \cdot \omega(L_1 \rightarrow n - 1, L_1 - (n + 1)) = q \cdot p^2 \cdot k_d \quad (\text{A.22})$$

$$P(X_{n-1} = 0, X_n = 1, X_{n+1} = 1) \cdot \omega(L_1 \rightarrow n - 2, L_1 - n) = q \cdot p^2 \cdot k_d. \quad (\text{A.23})$$

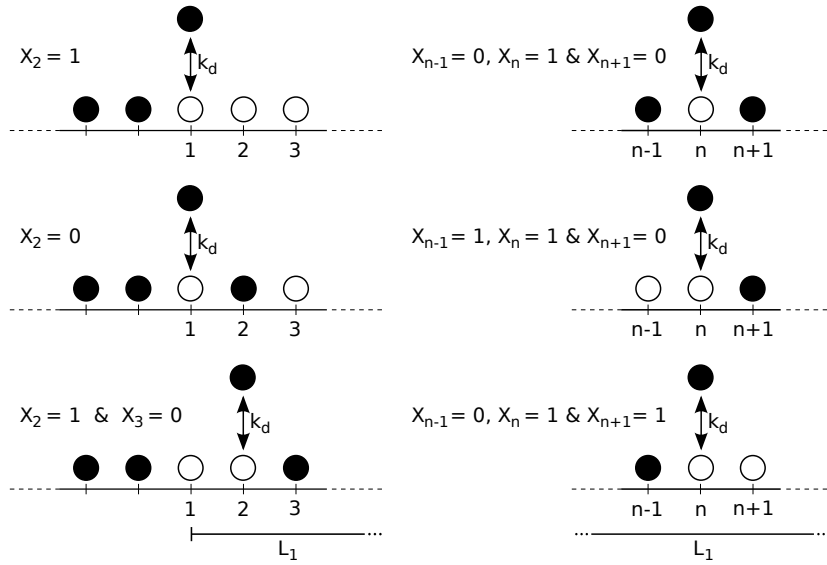


Figure A.4: Modification of a segment of length $L_1 \geq 5$ by addition of a black ball. Only the moves which lead to a change in the segment composition are shown for the boundary sites (*left*) and the bulk of the system (*right*).

A.2 Flux of probability mass

With the identified transitions, one is in principle able to formulate the master equation for the segment lengths $L_{Cl,max}$. This will not be done here because of the complicated nature of the transitions involving a different number of arguments. The steady state solution of the master equation is already known anyway as it was derived in section 4.3.4.

Instead, the flux of probability mass away from a given segment length is determined and some results are derived. This will be done separately for the fusion and splitting of segments, as the first leads to longer segments and the latter to shorter segments. By calculating both fluxes separately, the net flux from a certain segment length toward higher or shorter segment lengths can be determined.

A.2.1 Flux towards higher lengths

The flux of probability mass to higher segment lengths is denoted $j^+(L_{Cl,max} \rightarrow \cdot)$. Since the fusion transitions always involve a second segment, a sum over all lengths of the second segment has to be taken and the result then multiplied by two in order to account for the permutation of the two segments. In the following, all rates from (A.1)–(A.9) with the probabilities for a certain barrier length H and second segment length to occur are summed while excluding those transitions that leave the length of the first segment L_1 unchanged, i.e., (A.4) & (A.7)–(A.9).

$$\frac{j^+(L_1 \rightarrow \cdot)}{P(L_{\text{Cl,max}} = L_1)} = 2 \sum_{L_2=1}^{\infty} \sum_{k=2}^{\infty} \frac{P(L_{\text{Cl,max}} = L_2)}{1-q} P(H = k) \cdot \omega(L_1, L_2 \rightarrow L_1 + \cdot, \cdot) \quad (\text{A.24})$$

$$= 2 \sum_{L_2=1}^{\infty} \frac{P(L_{\text{Cl,max}} = L_2)}{1-q} \left[P(H = 2) \cdot 2k_p \right. \\ \left. + P(H = 3) \cdot 2k_p + \sum_{k=4}^{\infty} P(H = k) \cdot 2k_p \right] \quad (\text{A.25})$$

$$= 4k_p \sum_{k=2}^{\infty} q^{k-2} p \quad (\text{A.26})$$

$$= 4k_p. \quad (\text{A.27})$$

The segment length distribution $P(L_{\text{Cl,max}} = L_2)$ is divided by $1 - q$ which is the normalization in (4.44) if one excludes the probability $P(\text{hole})$ which is taken care of by explicitly summing over the probability for all barrier lengths $P(H = k)$. For equation (A.26), the normalization in (4.44) and the distribution of barrier lengths $P(H = k) = q^{k-2}p$ was used.

The derivation of this result appears to be a bit over-complicated: An existing segment will simply grow if one of the four black balls constituting the two pairs of barriers on the boundaries is taken away, leading to a total rate of $4k_p$. This consequently confirms the validity of the derivation.

A.2.2 Flux towards shorter lengths

The flux from a segment of given length towards shorter lengths $j^-(L_1 \rightarrow \cdot)$ is created exclusively by black balls which replace white balls next to at least one other black ball. We proceed in the same way as before with the additional notation $P(L_1 \rightarrow L'_1, L'_2)$ which stands for the probability that the segment has a local configuration which allows the transition. These are the probabilities given in equations (A.10)–(A.23) as factor in front of the rates ω .

$$\frac{j^-(L_1 \rightarrow \cdot)}{P(L_{\text{Cl,max}} = L_1)} = \sum_{n=1}^{L_1} P(L_1 \rightarrow L_1 - \cdot, \cdot) \cdot \omega(L_1, L_2 \rightarrow L_1 - \cdot, \cdot) \quad (\text{A.28})$$

Since the number of possible transitions depends on the length of the segment L_1 , the flux has to be calculated separately for the different cases.

$L_1 = 1$:

$$\frac{j^-(1 \rightarrow \emptyset)}{P(L_{\text{Cl,max}} = 1)} = k_d. \quad (\text{A.29})$$

$L_1 = 2$:

$$\frac{j^-(2 \rightarrow 1)}{P(L_{\text{Cl,max}} = 2)} = 2k_d. \quad (\text{A.30})$$

$L_1 = 3$:

$$\frac{j^-(3 \rightarrow \cdot)}{P(L_{\text{Cl,max}} = 3)} = 2(q \cdot k_d + p \cdot k_d) = 2k_d. \quad (\text{A.31})$$

$L_1 = 4$:

$$\frac{j^-(4 \rightarrow \cdot)}{P(L_{\text{Cl,max}} = 4)} = 2(p + q + p \cdot q)k_d = 2(1 + p \cdot q)k_d. \quad (\text{A.32})$$

$L_1 \geq 5$:

$$\frac{j^-(L_1 \rightarrow \cdot)}{P(L_{\text{Cl,max}} = L_1)} = 2(q + p + p \cdot q)k_d + \sum_{n=3}^{L_1-2} (q^2 \cdot p + 2 \cdot q \cdot p^2)k_d \quad (\text{A.33})$$

$$= 2(1 + p \cdot q)k_d + (L_1 - 4)q \cdot p(1 + p)k_d \quad (\text{A.34})$$

$$= [2 + (L_1 - 2)q \cdot p + (L_1 - 4)q \cdot p^2] k_d. \quad (\text{A.35})$$

Again, this result has a very intuitive form and reassures us of the correctness of our reasoning, as every term in the last equation describes a local three-site state by a product of the probability for that local state and the possible number of the corresponding three-site states in the whole system.

A.2.3 Balance of fluxes

The previous results indicate that a segment of a given length transforms into a larger segment at a constant rate whereas the inverse process is length dependent. There will therefore be a distinguished segment length at which the flux of probability mass toward higher and toward shorter segment lengths is equal. For longer (shorter) segments, the probability flux towards shorter (longer) segments exceeds the flux in the opposite direction. Therefore, the segment length at which the two fluxes are equal plays the role of a characteristic length scale L_{char} similar to (4.39).

$$j^+(L_{\text{char}} \rightarrow \cdot) = j^-(L_{\text{char}} \rightarrow \cdot) \quad (\text{A.36})$$

$$\Leftrightarrow 4k_p = [2 + (L_{\text{char}} - 2)q \cdot p + (L_{\text{char}} - 4)q \cdot p^2] k_d \quad (\text{A.37})$$

$$\Leftrightarrow L_{\text{char}} = \frac{2(2q^3 - q^2 + q - 1)}{q^2(q - 1)} \quad (\text{A.38})$$

$$\Leftrightarrow = 2 \left[\frac{1}{q^2} + 1 + \frac{q}{q - 1} \right] \quad (\text{A.39})$$

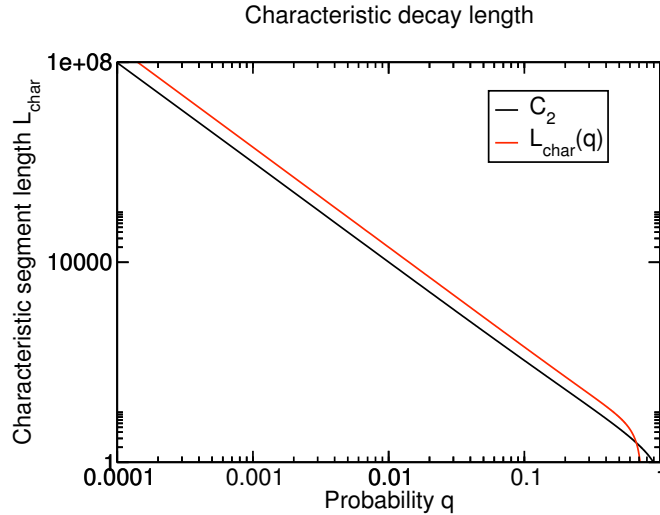


Figure A.5: Comparison of characteristic segment lengths as determined by the steady state distribution in (4.39) (black line) and the segment dynamics in (A.39) (red line). Both decay as q^{-2} and differ only by a factor 2 for low values of q .

This characteristic length scale actually decays quadratically for small values of q which is the same behavior as determined for (4.39) (figure A.5). This is again reassuring as both length scales have been obtained by completely different considerations but still yield the same behavior.

A.3 Survival times of segments

The expression in (A.35) enables us to estimate the average time before a segment is split by depolymerization if it is not fused with a neighboring segment before. From (A.39), it is known from which segment length on the splitting of segments dominates over the fusion of segments. In this case, the waiting time for splitting of an individual segment is the interesting time scale and is given by (after eliminating p and k_d from the expression):

$$\frac{P(L_{Cl,max} = L_1)}{j^-(L_1 \rightarrow \cdot)} = \frac{1}{k_p} \left[2 \frac{q}{1-q} + (L_1 - 2)q^2 + (L_1 - 4)q^2(1-q) \right]^{-1}. \quad (\text{A.40})$$

This ‘time before shortening’ is plotted in figure A.6. All the curves have in common that toward shorter segment lengths, the time before shortening is almost constant and then crosses over to an algebraic decay for longer segments with exponent -1 . This means that the appearance of very long segments is not only exponentially unlikely (4.41) but these segments also decompose extremely quickly into shorter segments if they occur. Note that the characteristic segment lengths (4.39) all lie in the decaying regions of the plots in figure A.6. This property does not depend on the

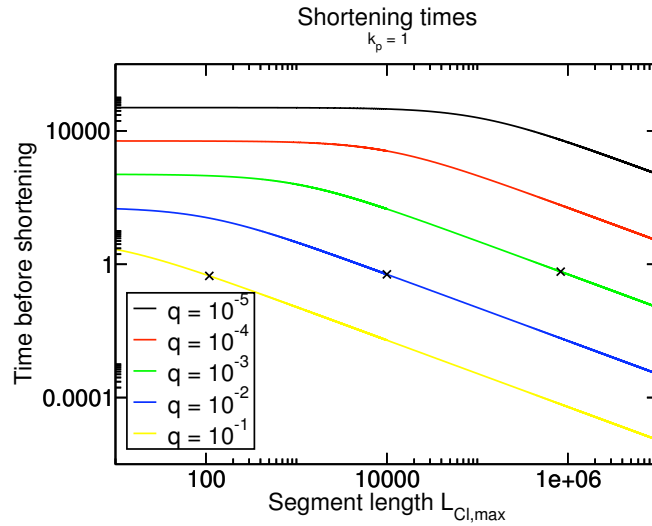


Figure A.6: Time before shortening for different values of q and $k_p = 1$. All curves show a constant and a decaying ($\propto L_{Cl,max}^{-1}$) regime. The black crosses indicate the characteristic length scale (4.39) for the corresponding value of q .

intensity of the dynamics: If $q > 0$, there will always be this decaying regime and long segments will disappear in no time. This effect is obviously stronger, the higher the value of q , thus preventing the formation of particle clusters which have similar lengths as the maximum cluster lengths $L_{Cl,max}$.

Appendix B

Simulated microtubule distribution on a real cell geometry

In order to verify that the results presented in figures 6.4 and 6.5 are generic and do not depend on the geometry chosen for the simulations, we extracted the shape of a real cell which was shown in figure 4 B in [46]. The cell boundary was by hand approximated with a sequence of Bézier curves and the MTOC identified as the point of highest MT concentration. The resulting geometry can be seen in figure B.1.

We then ran our simulations on this more complex geometry and reproduced figures 6.4 and 6.5 which are shown below as figures B.2 and B.3. The distribution of active plus ends with respect to the distance to the cell boundary is virtually unchanged. The higher slope in the scenario without a +TIP is mostly caused by the large radius of the cell in figure B.1.

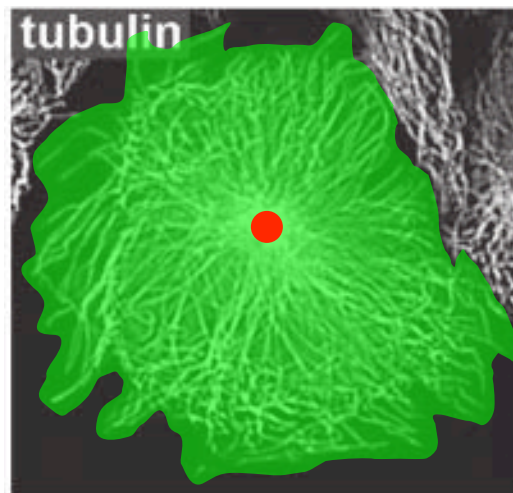


Figure B.1: Approximation of real cell geometry. The cell is shown in green and the MTOC in red. The background is a microscopic image published as figure 4 B in [46].

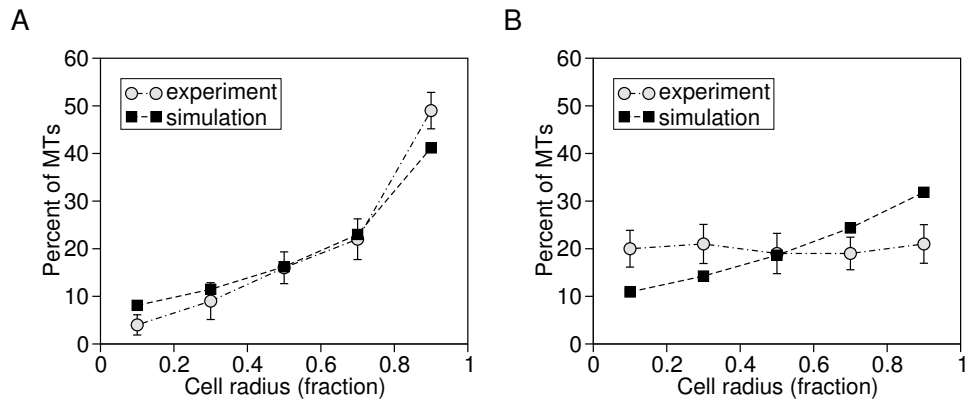


Figure B.2: Histograms of the distribution of active plus ends in a real cell geometry with (A) and without (B) rescue-enhancing +TIP. These figures correspond to figure 6.4 in the main text.

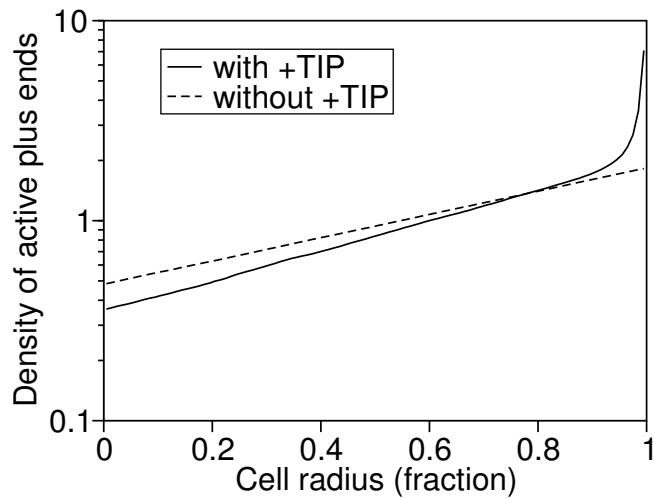


Figure B.3: Distribution of active plus ends along the cell radius in a real cell geometry with (solid line) and without (dashed line) enhancement of rescues through vanishing binding sites for a +TIP. The data is the same that has been used to plot the histograms in figure B.2. This figure corresponds to figure 6.5.

Own publications

Publications related to this thesis

M. Ebbinghaus and L. Santen. Theoretical modeling of aging effects in microtubule dynamics. *Biophys. J.*, 100:832, 2011.

M. Ebbinghaus, C. Appert-Rolland, and L. Santen. Particle interactions and lattice dynamics: Scenarios for efficient bidirectional stochastic transport? *arXiv.org*:1103.3658, 2011.

M. Ebbinghaus, C. Appert-Rolland, and L. Santen. Bidirectional transport on a dynamic lattice. *Phys. Rev. E*, 82:040901(R), 2010.

M. Ebbinghaus, C. Appert-Rolland, and L. Santen. Bidirectional traffic on microtubules. In *Proceedings of the ACRI2010 Conference, Lecture Notes in Computer Science*, New York, 2010 (to appear).

M. Ebbinghaus and L. Santen. A model for bidirectional traffic of cytoskeletal motors. *J. Stat. Mech.*, P03030, 2009.

Other publication

M. Ebbinghaus, H. Grandclaude, and M. Henkel. Absence of logarithmic scaling in ageing behaviour of the 4D spherical model. *Eur. Phys. J. B*, 63:85, 2008.

Bibliography

- [1] C. P. McKay. What is life—and how do we search for it in other worlds. *PLoS Biol.*, 2:1260, 2004.
- [2] E. Schrödinger. *What is Life?* Cambridge University Press, 1992.
- [3] B. Alberts, A. Johnson, J. Lewis, M. Raff, K. Roberts, and P. Walter. *Molecular Biology of the Cell*. Taylor and Francis, 4th edition, 2002.
- [4] A. Raj and A. van Oudenaarden. Nature, nurture, or chance: Stochastic gene expression and its consequences. *Cell*, 135:216, 2008.
- [5] S. Klumpp and T. Hwa. Stochasticity and traffic jams in the transcription of ribosomal RNA: Intriguing role of termination and antitermination. *Proc. Natl. Acad. Sci.*, 105:18159, 2008.
- [6] G. E. Briggs and J. B. S. Haldane. A note on the kinetics of enzyme action. *Biochem. J.*, 19:338, 1925.
- [7] H. Qian and X. S. Xie. Generalized haldane equation and fluctuation theorem in the steady-state cycle kinetics of single enzymes. *Phys. Rev. E*, 74:010902(R), 2006.
- [8] K. Kruse, J. F. Joanny, F. Jülicher, J. Prost, and K. Sekimoto. Asters, vortices, and rotating spirals in active gels of polar filaments. *Phys. Rev. Lett.*, 92:078101, 2004.
- [9] A. Akhmanova and M. O. Steinmetz. Tracking the ends: a dynamic protein network controls the fate of microtubule tips. *Nature Rev. Mol. Cell Biol.*, 9:309, 2008.
- [10] T. Mitchison and M. Kirschner. Dynamic instability of microtubule growth. *Nature*, 312:237, 1984.
- [11] R. A. Walker, E. T. O'Brien, N. K. Pryer, M. F. Soboeiro, W. A. Voter, H. P. Erickson, and E. D. Salmon. Dynamic instability of individual microtubules analyzed by video light microscopy: Rate constants and transition frequencies. *J. Cell Biol.*, 107:1437, 1988.
- [12] Y. A. Komarova, I. A. Vorobjev, and G. G. Borisy. Life cycle of MTs: persistent growth in the cell interior, asymmetric transition frequencies and effects of the cell boundary. *J. Cell Sci.*, 115:3527, 2002.

- [13] R. A. Walker, S. Inoué, and E. D. Salmon. Asymmetric behavior of severed microtubule ends after ultraviolet-microbeam irradiation of individual microtubules in vitro. *J. Cell Biol.*, 108:931–937, 1989.
- [14] T. David-Pfeuty, H. P. Erickson, and D. Pantaloni. Guanosinetriphosphatase activity of tubulin associated with microtubule assembly. *Proc. Natl. Acad. Sci.*, 74:5372, 1977.
- [15] S. C. Schuyler and D. Pellman. Microtubule “plus-end-tracking proteins”: The end is just the beginning. *Cell*, 105:421–424, 2001.
- [16] A. Dimitrov, M. Quesnoit, S. Moutel, I. Cantaloube, C. Poüs, and F. Perez. Detection of GTP-tubulin conformation in vivo reveals a role for GTP remnants in microtubule rescues. *Science*, 322:1353, 2008.
- [17] H.-W. Wang and E. Nogales. Nucleotide-dependent bending flexibility of tubulin regulates microtubule assembly. *Nature*, 435:911, 2005.
- [18] C. Walsh. *Posttranslational Modification of Proteins: Expanding Nature’s Inventory*. Roberts and Co. Publishers, 1st edition, 2005.
- [19] P. W. Baas and M. M. Black. Individual microtubules in the axon consist of domains that differ in both composition and stability. *J. Cell Biol.*, 111:495, 1990.
- [20] H. T. Idriss. Man to trypanosome: The tubulin tyrosination/detyrosination cycle revisited. *Cell Mot. Cytoskel.*, 45:173, 2000.
- [21] E. W. Dent and F. B. Gertler. Cytoskeletal dynamics and transport in growth cone motility and axon guidance. *Neuron*, 40:209, 2003.
- [22] J. C. Bulinski and G. G. Gundersen. Stabilization of post-translational modification of microtubules during cellular morphogenesis. *Bioessays*, 13:285, 1991.
- [23] M. W. Kirschner. Microtubule assembly and nucleation. *Int. Rev. Cytol.*, 54:1, 1978.
- [24] B. R. Brinkley. Microtubule organizing centers. *Annu. Rev. Cell Biol.*, 1:145, 1985.
- [25] A. Desai and T. J. Mitchison. Microtubule polymerization dynamics. *Annu. Rev. Cell Dev. Biol.*, 13:83, 1997.
- [26] C. E. Oakley and B. R. Oakley. Identification of gamma-tubulin, a new member of the tubulin superfamily encoded by mipA gene of *A. nidulans*. *Nature*, 338:662, 1989.
- [27] B. R. Oakley. γ -tubulin. In J. S. Hyams and C. W. Lloyd, editors, *Microtubules*, page 33. Wiley-Liss., 1994.
- [28] Y. Zheng, M. L. Wong, B. Alberts, and T. Mitchison. Nucleation of microtubule assembly by a gamma-tubulin-containing ring complex. *Nature*, 378:578, 1995.

-
- [29] M. Moritz, M. B. Braunfeld, J. W. Sedat, B. Alberts, and D. A. Agard. Microtubule nucleation by gamma-tubulin-containing rings in the centrosome. *Nature*, 378:638, 1995.
- [30] T. J. Mitchison. Polewards microtubule flux in the mitotic spindle: evidence from photoactivation of fluorescence. *J. Cell Biol.*, 109:637, 1989.
- [31] V. I. Rodionov and G. G. Borisy. Microtubule treadmilling in vivo. *Science*, 275:215, 1997.
- [32] R. Bernhardt and A. Matus. Light and electron microscopic studies of the distribution of microtubule-associated protein 2 in rat brain: A difference between dendritic and axonal cytoskeletons. *J. Comp. Neurol.*, 226:203, 1984.
- [33] L. I. Binder, A. Frankfurter, and L. I. Rebhun. The distribution of tau in the mammalian central nervous systems. *J. Cell Biol.*, 101:1371, 1985.
- [34] S. A. Lewis, I. E. Ivanov, G.-H. Lee, and N. J. Cowan. Organization of microtubules in dendrites and axons is determined by a short hydrophobic zipper in microtubule-associated proteins. *Nature*, 342:498, 1989.
- [35] J. Al-Bassam, R. S. Ozer, D. Safer, S. Halpain, and R. A. Milligan. MAP2 and tau bind longitudinally along the outer ridges of microtubule protofilaments. *J. Cell Biol.*, 157:1187, 2002.
- [36] R. A. Santarella, G. Skiniotis, K. N. Goldie, P. Tittmann, H. Gross, E. M. Mandelkow, E. Mandelkow, and A. Hoenger. Surface-decoration of microtubules by human tau. *J. Mol. Biol.*, 339:539, 2004.
- [37] D. N. Drechsel, A. A. Hyman, M. H. Cobb, and M. W. Kirschner. Modulation of the dynamic instability of tubulin assembly by the microtubule-associated protein tau. *Mol. Biol. Cell*, 3:1141, 1992.
- [38] G. Drewes, A. Ebnet, and E. M. Mandelkow. MAPs, MARKs and microtubule dynamics. *Trends Biochem. Sci.*, 23:307, 1998.
- [39] K. J. Rosenberg, J. L. Ross, H. E. Feinstein, S. C. Feinstein, and J. Israelachvili. Complementary dimerization of microtubule-associated tau protein: Implications for microtubule bundling and tau-mediated pathogenesis. *Proc. Natl. Acad. Sci.*, 105:7445, 2008.
- [40] A. Samsonov, J. Z. Yu, M. Rasenick, and S. V. Popov. Tau interaction with microtubules in vivo. *J. Cell Sci.*, 117:6129, 2004.
- [41] L. Qiang, W. Yu, A. Andreadis, M. Luo, and P. W. Baas. Tau protects microtubules in the axon from severing by katanin. *J. Neurosci.*, 26:3120, 2006.
- [42] N. Galjart and F. Perez. A plus-end raft to control microtubule dynamics and function. *Curr. Opin. Cell Biol.*, 15:48, 2003.
-

- [43] P. Carvalho, J. S. Tirnauer, and D. Pellman. Surfing on microtubule ends. *Trends in Cell Biol.*, 13:229–237, 2003.
- [44] E. E. Morrison. Action and interactions at microtubule ends. *Cell. Mol. Life Sci.*, 64:307, 2007.
- [45] A. Akhmanova and C. C. Hoogenraad. Microtubule plus-end-tracking proteins: mechanisms and functions. *Curr. Opin. Cell Biol.*, 17:47–54, 2005.
- [46] Y. A. Komarova, A. S. Akhmanova, S. Kojimo, N. Galjart, and G. G. Borisy. Cytoplasmic linker proteins promote microtubule rescue in vivo. *J. Cell Biol.*, 159:589, 2002.
- [47] Y. Komarova, G. Lansbergen, N. Galjart, F. Grosveld, G. G. Borisy, and A. Akhmanova. EB1 and EB3 control CLIP dissociation from the ends of growing microtubules. *Mol. Biol. Cell*, 16:5334, 2005.
- [48] P. Bieling, L. Laan, H. Schek, E. L. Munteanu, L. Sandblad, M. Dogterom, D. Brunner, and T. Surrey. Reconstitution of a microtubule plus-end tracking system in vitro. *Nature*, 450:1100, 2007.
- [49] P. Bieling, S. Kandels-Lewis, I. A. Telley, J. van Dijk, C. Janke, and T. Surrey. CLIP-170 tracks growing microtubule ends by dynamically recognizing composite EB1/tubulin-binding sites. *J. Cell Biol.*, 183:1223, 2008.
- [50] K. A. Dragestein, W. A. van Cappellen, J. van Haren, G. D. Tsibidis, A. Akhmanova, T. A. Knoch, F. Grosveld, and N. Galjart. Dynamic behavior of GFP-CLIP-170 reveals fast protein turnover on microtubule plus ends. *J. Cell Biol.*, 180:729, 2008.
- [51] R. Dixit, B. Barnett, J. E. Lazarus, M. Tokito, Y. E. Goldman, and E. L. F. Holzbaur. Microtubule plus-end tracking by CLIP-170 requires EB1. *Proc. Natl. Acad. Sci.*, 106:492, 2009.
- [52] L. Peris, M. Thery, J. Fauré, Y. Saoudi, L. Lafanechère, J. K. Chilton, P. Gordon-Weeks, N. Galjart, M. Bornens, L. Wordeman, J. Wehland, A. Andrieux, and D. Job. Tubulin tyrosination is a major factor affecting the recruitment of capgly proteins at microtubule plus ends. *J. Cell Biol.*, 174:839, 2006.
- [53] Y. Komarova, C. O. De Groot, I. Grigoriev, S. Montenegro Gouveia, E. L. Munteanu, J. M. Schober, S. Honnappa, R. M. Buey, C. C. Hoogenraad, M. Dogterom, G. G. Borisy, M. O. Steinmetz, and A. Akhmanova. Mammalian end binding proteins control persistent microtubule growth. *J. Cell Biol.*, 159:691, 2009.
- [54] R. D. Vale and R. J. Fletterick. The design plan of kinesin motors. *Annu. Rev. Cell Dev. Biol.*, 13:745, 1997.

- [55] M. Schliwa and G. Woehlke. Molecular motors. *Nature*, 422:759, 2003.
- [56] R. Vale and R. A. Milligan. The way things move: Looking under the hood of molecular motor proteins. *Science*, 288:88, 2000.
- [57] A. N. Fehr, C. L. Asbury, and S. M. Block. Kinesin steps do not alternate in size. *Bipolys. J.*, 94:L20, 2008.
- [58] A. Seitz and T. Surrey. Processive movement of single kinesins on crowded microtubules visualized using quantum dots. *EMBO J.*, 25:267, 2006.
- [59] S. Ray, E. Meyhöfer, R. A. Milligan, and J. Howard. Kinesin follows the microtubule's protofilament axis. *J. Cell Biol.*, 121:1083, 1993.
- [60] S. M. Block, C. L. Asbury, J. W. Shaevitz, and M. J. Lang. Probing the kinesin reaction cycle with a 2D optical force clamp. *Proc. Natl. Acad. Sci.*, 100:2351, 2003.
- [61] A. Yildiz, M. Tomishige, A. Gennerich, and R. D. Vale. Intramolecular strain coordinates kinesin stepping behavior along microtubules. *Cell*, 134:1030, 2008.
- [62] K. Dreblow, N. Kalchishkova, and K. J. Böhm. Kinesin passing permanent blockages along its protofilament track. *Biochem. Biophys. Res. Comm.*, 395:490, 2010.
- [63] A. Vilfan, E. Frey, F. Schwabl, M. Thormählen, Y.-H. Song, and E. Mandelkow. Dynamics and cooperativity of microtubule decoration by the motor protein kinesin. *J. Mol. Biol.*, 312:1011, 2001.
- [64] E. Muto, H. Sakai, and K. Kaseda. Long-range cooperative binding of kinesin to a microtubule in the presence of ATP. *J. Cell Biol.*, 168:691, 2005.
- [65] W. H. Roos, O. Campàs, F. Montel, G. Woehlke, J. P. Spatz, P. Bassereau, and G. Cappello. Dynamic kinesin-1 clustering on microtubules due to mutually attractive interactions. *Phys. Biol.*, 5:046004, 2008.
- [66] A. Seitz, H. Kojima, K. Oiwa, E. M. Mandelkow, Y. H. Song, and E. Mandelkow. Single-molecule investigation of the interference between kinesin, tau and MAP2c. *EMBO J.*, 21:4896, 2002.
- [67] R. Dixit, J. L. Ross, Y. E. Goldman, and E. L. F. Holzbaur. Differential regulation of dynein and kinesin motor proteins by tau. *Science*, 319:1086, 2008.
- [68] A. Desai, S. Verma, T. J. Mitchison, and C. E. Walczak. Kin I kinesins are microtubule-destabilizing enzymes. *Cell*, 96:69–78, 1999.
- [69] C. A. Moores, M. Yu, J. Guo, C. Beraud, R. Sakowicz, and R. A. Milligan. A mechanism for microtubule depolymerization by KinI kinesins. *Molecular Cell*, 9:903–909, 2002.

- [70] D. Tan, A. B. Asenjo, V. Mennella, D. J. Sharp, and H. Sosa. Kinesin-13s form rings around microtubules. *J. Cell Biol.*, 175:25–31, 2006.
- [71] J. R. Kardon and R. D. Vale. Regulators of the cytoplasmic dynein motor. *Nat. Rev. Mol. Cell Biol.*, 10:854, 2009.
- [72] N. Mizuno, A. Narita, T. Kon, K. Sutoh, and M. Kikkawa. Three-dimensional structure of cytoplasmic dynein bound to microtubules. *Proc. Natl. Acad. Sci.*, 104:20832, 2007.
- [73] Z. Wang, S. Khan, and M. P. Sheetz. Single cytoplasmic dynein molecule movements: Characterization and comparison with kinesin. *Biophys. J.*, 69:2011, 1995.
- [74] S. L. Reck-Peterson, A. Yildiz, A. P. Carter, A. Gennerich, N. Zhang, and R. D. Vale. Single-molecule analysis of dynein processivity and stepping behavior. *Cell*, 126:335, 2006.
- [75] R. Mallik, B. C. Carter, S. A. Lex, S. J. King, and S. P. Gross. Cytoplasmic dynein functions as a gear in response to load. *Nature*, 427:649, 2004.
- [76] M. P. Singh, R. Mallik, S. P. Gross, and C. C. Yu. Monte carlo modeling of single-molecule cytoplasmic dynein. *Proc. Natl. Acad. Sci.*, 102:12059, 2005.
- [77] Z. Wang and M. P. Sheetz. One-dimensional diffusion on microtubules of particles coated with cytoplasmic dynein and immunoglobulins. *Cell Struct. Funct.*, 24:373, 1999.
- [78] J. L. Ross, K. Wallace, H. Shuman, Y. E. Goldman, and E. L. F. Holzbaur. Processive bidirectional motion of dynein-dynactin complexes in vitro. *Nat. Cell Biol.*, 8:562, 2006.
- [79] J. P. Caviston and E. L. F. Holzbaur. Microtubule motors at the intersection of trafficking and transport. *TRENDS in Cell Biol.*, 16:530, 2006.
- [80] N. Mizuno, S. Toba, M. Edamatsu, J. Watai-Nishii, N. Hirokawa, Y. Y. Toyoshima, and M. Kikkawa. Dynein and kinesin share an overlapping microtubule-binding site. *EMBO J.*, 23:2459, 2004.
- [81] M. Vershinin, J. Xu, D. S. Razafsky, S. J. King, and S. P. Gross. Tuning microtubule-based transport through filamentous maps: The problem of dynein. *Traffic*, 9:882, 2008.
- [82] R. H. Miller and R. J. Lasek. Cross-bridges mediate anterograde and retrograde vesicle transport along microtubules in squid axoplasm. *J. Cell Biol.*, 101:2181, 1985.

- [83] A. Ashkin, K. Schütze, J. M. Dziedzic, U. Euteneuer, and M. Schliwa. Force generation of organelle transport measured *in vivo* by an infrared laser trap. *Nature*, 348:346, 1990.
- [84] R. Mallik, D. Petrov, S. A. Lex, S. J. King, and S. P. Gross. Building complexity: An *in vitro* study of cytoplasmic dynein with *in vivo* implications. *Curr. Biol.*, 15:2075, 2005.
- [85] J. Beeg, S. Klumpp, R. Dimova, R. S. Gracià, E. Unger, and R. Lipowsky. Transport of beads by several kinesin motors. *Biophys. J.*, 94:532, 2008.
- [86] S. Klumpp and R. Lipowsky. Cooperative cargo transport by several molecular motors. *Proc. Natl. Acad. Sci.*, 102:17284, 2005.
- [87] M. A. Welte. Bidirectional transport along microtubules. *Curr. Biol.*, 14:R525, 2004.
- [88] C. Kural, H. Kim, S. Syed, G. Goshima, V. I. Gelfand, and P. R. Selvin. Kinesin and dynein move a peroxisome *in vivo*: A tug-of-war or coordinated movement? *Science*, 308:1469, 2005.
- [89] S. Ma and R. L. Chisholm. Cytoplasmic dynein-associated structures move bidirectionally *in vivo*. *J. Cell Sci.*, 115:1453, 2002.
- [90] M. J. I. Müller, S. Klumpp, and R. Lipowsky. Tug-of-war as a cooperative mechanism for bidirectional cargo transport by molecular motors. *Proc. Natl. Acad. Sci.*, 105:4609, 2008.
- [91] Susan Standring, editor. *Gray's Anatomy: The Anatomical Basis of Clinical Practice*. Churchill Livingstone, 40th edition, 2008.
- [92] P. W. Baas, J. S. Deitch, M. M. Black, and G. A. Banker. Polarity orientation of microtubules in hippocampal neurons: Uniformity in the axon and nonuniformity in the dendrite. *Proc. Natl. Acad. Sci.*, 85:8335, 1988.
- [93] A. Brown, Y. Li, T. Slaughter, and M. M. Black. Composite microtubules of the axon: quantitative analysis of tyrosinated and acetylated tubulin along individual axonal microtubules. *J. Cell Sci.*, 104:339, 1993.
- [94] W. Yu and P. W. Baas. Changes in microtubule number and length during axon differentiation. *J. Neurosci.*, 14:2818, 1994.
- [95] J. Chen, Y. Kanai, N. J. Cowan, and N. Hirokawa. Projection domains of MAP2 and tau determine spacings between microtubules in dendrites and axons. *Nature*, 360:674, 1992.
- [96] P. W. Baas and F. J. Ahmad. The plus ends of stable microtubules are the exclusive nucleating structures for microtubules in the axon. *J. Cell Biol.*, 116:1231, 1992.

- [97] Y. Li and M. M. Black. Microtubule assembly and turnover in growing axons. *J. Neurosci.*, 16:531, 1996.
- [98] M. Stiess, N. Maghelli, L. C. Kapitein, S. Gomis-Rüth, M. Wilsch-Bräuninger, C. C. Hoogenraad, I. M. Tolić-Nørrelykke, and F. Bradke. Axon extension occurs independently of centrosomal microtubule nucleation. *Science*, 327:704, 2010.
- [99] T. Stepanova, J. Slemmer, C. C. Hoogenraad, G. Lansbergen, B. Dortland, C. I. De Zeeuw, F. Grosveld, G. van Cappellen, A. Akhmanova, and N. Galjart. Visualization of microtubule growth in cultured neurons via the use of EB3-GFP (End-Binding Protein 3-Green Fluorescent Protein). *J. Neurosci.*, 23:2655–2664, 2003.
- [100] O. A. Shemesh and M. E. Spira. Paclitaxel induces axonal microtubules polar reconfiguration and impaired organelle transport: implications for the pathogenesis of paclitaxel-induced polyneuropathy. *Acta Neuropathol.*, 119:235, 2010.
- [101] P. W. Baas, A. Karabay, and L. Qiang. Microtubules cut and run. *TRENDS in Cell Biol.*, 15:518, 1995.
- [102] F. J. Ahmad, W. Yu, F. J. McNally, and P. W. Baas. An essential role for katanin in severing microtubules in the neuron. *J. Cell Biol.*, 145:305, 1999.
- [103] F. J. Ahmad and P. W. Baas. Microtubules released from the neuronal centrosome are transported into the axon. *J. Cell Sci.*, 108:2761, 1995.
- [104] P. W. Baas. Microtubules and axonal growth. *Curr. Opin. Cell Biol.*, 9:29, 1997.
- [105] K. A. Myers, Y. He, T. P. Hasaka, and P. W. Baas. Microtubule transport in the axon: Re-thinking a potential role for the actin cytoskeleton. *Neuroscientist*, 12:107, 2006.
- [106] F. J. Ahmad, Y. He, K. A. Myers, T. P. Hasaka, F. Francis, M. M. Black, and P. W. Baas. Effects of dynactin disruption and dynein depletion on axonal microtubules. *Traffic*, 7:524, 2006.
- [107] P. W. Baas, C. V. Nadar, and K. A. Myers. Axonal transport of microtubules: the long and short of it. *Traffic*, 7:490–498, 2006.
- [108] L. Wang and A. Brown. Rapid movement of microtubules in axons. *Curr. Biol.*, 12:1496, 2002.
- [109] Y. Ma, D. Shakiryanova, I. Vardya, and S. V. Popov. Quantitative analysis of microtubule transport in growing nerve processes. *Curr. Biol.*, 14:725, 2004.
- [110] P. Paggi and R. J. Lasek. Axonal transport of cytoskeletal proteins in oculomotor axons and their residence times in the axon terminals. *J. Neurosci.*, 7:2397, 1987.

- [111] A. Karabay, W. Yu, J. M. Solowska, D. H. Baird, and P. W. Baas. Axonal growth is sensitive to the levels of katanin, a protein that severs microtubules. *J. Neurosci.*, 24:5778, 2004.
- [112] M. M. Black, T. Slaughter, S. Moshiach, M. Obrocka, and I. Fischer. Tau is enriched on dynamic microtubules in the distal region of growing axons. *J. Neurosci.*, 16:3601, 1996.
- [113] A. D. Cash, G. Aliev, S. L. Siedlak, A. Nunomura, H. Fujioka, X. Zhu, A. K. Raina, H. V. Vinters, M. Tabaton, A. B. Johnson, M. Paula-Barbosa, J. Avila, P. K. Jones, R. J. Castellani, M. A. Smith, and G. Perry. Microtubule reduction in Alzheimer's disease and aging is independent of tau filament formation. *Am. J. Path.*, 162:1623, 2003.
- [114] G. B. Stokin, C. Lillo, T. L. Falzone, R. G. Brusch, E. Rockenstein, S. L. Mount, R. Raman, P. Davies, E. Masliah, D. S. Williams, and L. S. B. Goldstein. Axonopathy and transport deficits early in the pathogenesis of Alzheimer's disease. *Science*, 307:1282, 2005.
- [115] P. W. Baas and L. Qiang. Neuronal microtubules: when the MAP is the roadblock. *TRENDS in Cell Biol.*, 15:183, 2005.
- [116] B. Trinczek, A. Ebnet, E.-M. Mandelkow, and E. Mandelkow. Tau regulates the attachment/detachment but not the speed of motors in microtubule-dependent transport of single vesicles and organelles. *J. Cell Sci.*, 112:2355, 1999.
- [117] E.-M. Mandelkow, E. Thies, B. Trinczek, J. Biernat, and E. Mandelkow. MARK/PAR1 kinase is a regulator of microtubule-dependent transport in axons. *J. Cell Biol.*, 167:99, 2004.
- [118] A. Yuan, A. Kumar, C. Peterhoff, K. Duff, and R. A. Nixon. Axonal transport rates *In Vivo* are unaffected by tau deletion or overexpression in mice. *J. Neurosci.*, 28:1682, 2008.
- [119] O. A. Shemesh, H. Erez, I. Ginzburg, and M. E. Spira. Tau-induced traffic jams reflect organelles accumulation at points of microtubule polar mismatching. *Traffic*, 9:458–471, 2008.
- [120] F. Keime-Guibert, M. Napolitano, and J.-Y. Delattre. Neurological complications of radiotherapy and chemotherapy. *J. Neurol.*, 245:695, 1998.
- [121] R. Fazio, A. Quattrini, A. Bolognesi, G. Bordogna, E. Villa, S. Previtali, N. Canal, and R. Nemni. Docetaxel neuropathy: a distal axonopathy. *Acta Neuropathol.*, 98:651, 1999.
- [122] N. G. van Kampen. *Stochastic processes in physics and chemistry*. Elsevier, 3rd edition, 2007.

- [123] A. Schadschneider. Traffic flow: a statistical physics point of view. *Phys. A*, 313:153, 2002.
- [124] D. Chowdhury, L. Santen, and A. Schadschneider. Statistical physics of vehicular traffic and some related systems. *Phys. Rep.*, 329:199, 2000.
- [125] C. Appert-Rolland, H. J. Hilhorst, and G. Schehr. Spontaneous symmetry breaking in a two-lane model for bidirectional overtaking traffic. *J. Stat. Mech.*, P08024, 2010.
- [126] C. MacDonald, J. Gibbs, and A. Pipkin. Kinetics of biopolymerization on nucleic acid templates. *Biopolymers*, 6:1, 1968.
- [127] R. Lipowsky, S. Klumpp, and T. M. Nieuwenhuizen. Random walks of cytoskeletal motors in open and closed compartments. *Phys. Rev. Lett.*, 87:108101, 2001.
- [128] K. Nishinari, Y. Okada, A. Schadschneider, and D. Chowdhury. Intracellular transport of single-headed molecular motors KIF1A. *Phys. Rev. Lett.*, 95:118101, 2005.
- [129] N. Rajewsky, L. Santen, A. Schadschneider, and M. Schreckenberg. The asymmetric exclusion process: Comparison of update procedures. *J. Stat. Phys.*, 92:151, 1998.
- [130] P. Meakin, P. Ramanlal, L. M. Sander, and R. C. Ball. Ballistic deposition on surfaces. *Phys. Rev. A*, 34:5091, 1986.
- [131] B. Derrida, M. R. Evans, V. Hakim, and V. Pasquier. Exact solution of a 1D asymmetric exclusion model using a matrix formulation. *J. Phys. A: Math. Gen.*, 26:1493, 1993.
- [132] G. Schütz and E. Domany. Phase transitions in an exactly soluble one-dimensional exclusion process. *J. Stat. Phys.*, 72:277, 1993.
- [133] B. Derrida, E. Domany, and D. Mukamel. An exact solution of a one-dimensional asymmetric exclusion model with open boundaries. *J. Stat. Phys.*, 69:667, 1992.
- [134] R. A. Blythe and M. R. Evans. Nonequilibrium steady states of matrix product form: A solver's guide. *J. Phys. A: Math. Theor.*, 40:R333, 1997.
- [135] J. Krug. Boundary-induced phase transitions in driven diffusive systems. *Phys. Rev. Lett.*, 67:1882, 1991.
- [136] M. Ha and M. den Nijs. Macroscopic car condensation in a parking garage. *Phys. Rev. E*, 66:036118, 2002.

- [137] D. A. Adams, B. Schmittmann, and R. K. P. Zia. Far-from-equilibrium transport with constrained resources. *J. Stat. Mech.*, P06009, 2008.
- [138] L. J. Cook and R. K. P. Zia. Feedback and fluctuations in a totally asymmetric simple exclusion process with finite resources. *J. Stat. Mech.*, P02012, 2009.
- [139] A. Parmeggiani, T. Franosch, and E. Frey. Phase coexistence in driven one-dimensional transport. *Phys. Rev. Lett.*, 90:086601, 2003.
- [140] M. R. Evans, R. Juhász, and L. Santen. Shock formation in an exclusion process with creation and annihilation. *Phys. Rev. E*, 68:026117, 2003.
- [141] C. Schiffmann, C. Appert-Rolland, and L. Santen. Shock-dynamics of two-lane driven lattice gases. *J. Stat. Mech.*, P06002, 2010.
- [142] R. Juhász and L. Santen. Dynamics of an exclusion process with creation and annihilation. *J. Phys. A: Math. Gen.*, 37:3933, 2004.
- [143] A. Parmeggiani, T. Franosch, and E. Frey. Totally asymmetric simple exclusion process with Langmuir kinetics. *Phys. Rev. E*, 70:046101, 2004.
- [144] R. Wang, R. Jiang, M. Liu, J. Liu, and Q.-S. Wu. Effects of Langmuir kinetics of two-lane totally asymmetric exclusion processes in protein traffic. *Int. J. Mod. Phys. C*, 18:1483–1496, 2007.
- [145] P. Pierobon, E. Frey, and T. Franosch. Driven lattice gas of dimers coupled to a bulk reservoir. *Phys. Rev. E*, 74:031920, 2006.
- [146] K. Luby-Phelps, D. L. Taylor, and F. Lanni. Probing the structure of cytoplasm. *J. Cell Biol.*, 102:2015, 1986.
- [147] S. Popov and M. Poo. Diffusional transport of macromolecules in developing nerve processes. *J. Neurosci.*, 12:77, 1992.
- [148] T. M. Nieuwenhuizen, S. Klumpp, and R. Lipowsky. Walks of molecular motors in two and three dimensions. *Europhys. Lett.*, 58:468, 2002.
- [149] T. M. Nieuwenhuizen, S. Klumpp, and R. Lipowsky. Random walks of molecular motors arising from diffusional encounters with immobilized filaments. *Phys. Rev. E*, 69:061911, 2004.
- [150] S. Klumpp, T. M. Nieuwenhuizen, and R. Lipowsky. Self-organized density patterns of molecular motors in arrays of cytoskeletal filaments. *Biophys. J.*, 88:3118, 2005.
- [151] S. Klumpp and R. Lipowsky. Traffic of molecular motors through tube-like compartments. *J. Stat. Phys.*, 113:233, 2003.
- [152] K. Tsekouras and A. B. Kolomeisky. Parallel coupling of symmetric and asymmetric exclusion processes. *J. Phys. A: Math. Theor.*, 41:465001, 2008.

- [153] M. J. I. Müller, S. Klumpp, and R. Lipowsky. Molecular motor traffic in a half-open tube. *J. Phys.: Condens. Matter*, 17:S3839, 2005.
- [154] D. S. Forman, K. J. Lynch, and R. S. Smith. Organelle dynamics in lobster axons: anterograde, retrograde and stationary mitochondria. *Brain Res.*, 412:96, 1987.
- [155] S. Klumpp and R. Lipowsky. Active diffusion of motor particles. *Phys. Rev. Lett.*, 95:268102, 2005.
- [156] D. Chowdhury, A. Garai, and J.-S. Wang. Traffic of single-headed motor proteins KIF1A: Effects of lane changing. *Phys. Rev. E*, 77:050902(R), 2008.
- [157] S. Klumpp, Y. Chai, and R. Lipowsky. Effects of the chemomechanical stepping cycle on the traffic of molecular motors. *Phys. Rev. E*, 78:041909, 2008.
- [158] S. A. Janowsky and J. L. Lebowitz. Finite-size effects and shock fluctuations in the asymmetric simple-exclusion process. *Phys. Rev. A*, 45:618, 1992.
- [159] B. Derrida, S. A. Janowsky, J. L. Lebowitz, and E. R. Speer. Microscopic-shock profiles: Exact solution of a non-equilibrium system. *Europhys. Lett.*, 22:651, 1993.
- [160] K. Mallick. Shocks in the asymmetry exclusion model with an impurity. *J. Phys. A: Math. Gen.*, 29:5375, 1996.
- [161] Y. Chai, R. Lipowsky, and S. Klumpp. Transport by molecular motors in the presence of static defects. *J. Stat. Phys.*, 135:241, 2009.
- [162] P. Pierobon, M. Mabilia, R. Kouyos, and E. Frey. Bottleneck-induced transitions in a minimal model for intracellular transport. *Phys. Rev. E*, 74:031906, 2006.
- [163] P. Greulich and A. Schadschneider. Disordered driven lattice gases with boundary reservoirs and Langmuir kinetics. *Phys. Rev. E*, 79:031107, 2009.
- [164] H. Grzeschik, R. J. Harris, and L. Santen. Traffic of cytoskeletal motors with disordered attachment rates. *Phys. Rev. E*, 81:031929, 2010.
- [165] B. Derrida, S. A. Janowsky, J. L. Lebowitz, and E. R. Speer. Exact solution of the totally asymmetric simple exclusion process: Shock profiles. *J. Stat. Phys.*, 73: 813, 1993.
- [166] M. R. Evans, D. P. Foster, C. Godrèche, and D. Mukamel. Spontaneous symmetry breaking in a one dimensional driven diffusive system. *Phys. Rev. Lett.*, 74: 208, 1995.
- [167] P. F. Arndt, T. Heinzl, and V. Rittenberg. Stochastic models on a ring and quadratic algebras. the three-species diffusion problem. *J. Phys. A: Math. Gen.*, 31:833, 1998.

- [168] M. R. Evans, D. P. Foster, C. Godrèche, and D. Mukamel. Asymmetric exclusion model with two species: Spontaneous symmetry breaking. *J. Stat. Phys.*, 80:69, 1995.
- [169] P. F. Arndt, T. Heinzel, and V. Rittenberg. First-order phase transitions in one-dimensional steady states. *J. Stat. Phys.*, 90:783, 1998.
- [170] M. Clincy, M. R. Evans, and D. Mukamel. Symmetry breaking through a sequence of transitions in a driven diffusive system. *J. Phys. A: Math. Gen.*, 34:9923, 2001.
- [171] D. W. Erickson, G. Pruessner, B. Schmittmann, and R. K. P. Zia. Spurious phase in a model for traffic on a bridge. *J. Phys. A: Math. Gen.*, 38:L659, 2005.
- [172] E. Pronina and A. B. Kolomeisky. Spontaneous symmetry breaking in two-channel asymmetric exclusion processes with narrow entrances. *J. Phys. A: Math. Theor.*, 40:2275, 2007.
- [173] G. Korniss, B. Schmittmann, and R. K. P. Zia. Long-range order in a quasi one-dimensional non-equilibrium three-state lattice gas. *Europhys. Letters*, 45:431, 1999.
- [174] C. Godrèche and S. Sandow. Unpublished, 1998.
- [175] Y. Kafri, E. Levine, D. Mukamel, G. M. Schütz, and J. Török. Criterion for phase separation in one-dimensional driven systems. *Phys. Rev. Lett.*, 89:035702, 2002.
- [176] G. M. Schütz. Critical phenomena and universal dynamics in one-dimensional driven diffusive systems with two species of particles. *J. Phys. A: Math. Gen.*, 36:R339, 2003.
- [177] I. T. Georgiev, B. Schmittmann, and R. K. P. Zia. Anomalous nucleation far from equilibrium. *Phys. Rev. Lett.*, 94:115701, 2005.
- [178] M. R. Evans, Y. Kafri, H. M. Koduvely, and D. Mukamel. Phase separation in one-dimensional driven diffusive systems. *Phys. Rev. Lett.*, 80:425, 1998.
- [179] P. F. Arndt, T. Heinzel, and V. Rittenberg. Spontaneous breaking of translational invariance in one-dimensional stationary states on a ring. *J. Phys. A: Math. Gen.*, 31:L45, 1998.
- [180] M. R. Evans, Y. Kafri, H. M. Koduvely, and D. Mukamel. Phase separation and coarsening in one-dimensional driven diffusive systems: Local dynamics leading to long-range hamiltonians. *Phys. Rev. E*, 58:2764, 1998.
- [181] C. N. Yang and T. D. Lee. Statistical theory of equations of state and phase transitions. I. Theory of condensation. *Phys. Rev.*, 87:404, 1952.

- [182] P. F. Arndt. Yang-lee theory for a nonequilibrium phase transition. *Phys. Rev. Lett.*, 84:814, 2000.
- [183] N. Rajewsky, T. Sasamoto, and E. R. Speer. Spatial particle condensation for an exclusion process on a ring. *Phys. A*, 279:123–142, 2000.
- [184] B. Schmittmann, K. Hwang, and R. K. P. Zia. Onset of spatial structures in biased diffusion of two species. *Europhys. Lett.*, 19:19, 1992.
- [185] M. Ebbinghaus. Stochastische Modelle für bidirektionalen Transport in beschränkten Geometrien. Master’s thesis, Universität des Saarlandes, 2008.
- [186] M. Ebbinghaus and L. Santen. A model for bidirectional traffic of cytoskeletal motors. *J. Stat. Mech.*, P03030, 2009.
- [187] M. Ebbinghaus, C. Appert-Rolland, and L. Santen. Bidirectional traffic on microtubules. In *Proceedings of the ACRI2010 Conference*, Lecture Notes in Computer Science. New York, 2010. (to appear).
- [188] S. Klumpp and R. Lipowsky. Phase transitions in systems with two species of molecular motors. *Europhys. Letters*, 66:90–96, 2004.
- [189] W. Krauth. *Statistical Mechanics: Algorithms and Computations*. Oxford University Press, 2006.
- [190] W. H. Press, S. A. Teukolsky, W. T. Vetterling, and B. P. Flannery. *Numerical Recipes: The Art of Scientific Computing*. Cambridge University Press, 3rd edition, 2007.
- [191] M. R. Evans and T. Hanney. Nonequilibrium statistical mechanics of the zero-range process and related models. *J. Phys. A: Math. Gen.*, 38:R195, 2005.
- [192] M. R. Evans and T. Hanney. Phase transition in two species zero-range process. *J. Phys. A: Math. Gen.*, 36:L441, 2003.
- [193] I. Ispolatov and P. L. Krapivsky. Phase transition in a traffic model with passing. *Phys. Rev. E*, 62:5935, 2000.
- [194] J. Krug and P. A. Ferrari. Phase transitions in driven diffusive systems with random rates. *J. Phys. A: Math. Gen.*, 29:L465, 1996.
- [195] M. Ebbinghaus, C. Appert-Rolland, and L. Santen. Bidirectional transport on a dynamic lattice. *Phys. Rev. E*, 82:040901(R), 2010.
- [196] R. A. Blythe. An introduction to phase transitions in stochastic dynamical systems. *J. Phys.: Conf. Ser.*, 40:1, 2006.
- [197] A. Nagar, S. N. Majumdar, and M. Barma. Strong clustering of noninteracting, sliding passive scalars driven by fluctuating surfaces. *Phys. Rev. E*, 74:021124, 2006.

- [198] J. Dzubiella, G. P. Hoffmann, and H. Löwen. Lane formation in colloidal mixtures driven by an external field. *Phys. Rev. E*, 65:021402, 2002.
- [199] H. M. Thomas, D. D. Goldbeck, T. Hagl, A. V. Ivlev, U. Konopka, G. E. Morfill, H. Rothermel, R. Sütterlin, and M. Zuzic. Complex plasmas under microgravity conditions: Parabolic flights. *Phys. Scr.*, T89:16, 2001.
- [200] R. R. Netz. Conduction and diffusion in two-dimensional electrolytes. *Europhys. Lett.*, 63:616, 2003.
- [201] S. B. Santra, S. Schwarzer, and H. Herrmann. Fluid-induced particle-size segregation in sheared granular assemblies. *Phys. Rev. E*, 54:5066, 1996.
- [202] D. Helbing, P. Molnár, I. J. Farkas, and K. Bolay. Self-organizing pedestrian movement. *Environ. Plan. B: Plan. Des.*, 28:361, 2001.
- [203] G. Margolin, I. V. Gregoret, H. V. Goodson, and M. S. Alber. Analysis of a mesoscopic stochastic model of microtubule dynamic instability. *Phys. Rev. E*, 74:041920, 2006.
- [204] T. L. Hill and Y.-D. Chen. Phase changes at the end of a microtubule with a GTP cap. *Proc. Natl. Acad. Sci.*, 81:5772, 1984.
- [205] P. M. Bayley, M. J. Schilstra, and S. R. Martin. A simple formulation of microtubule dynamics: quantitative implications of the dynamic instability of microtubule populations *in vivo* and *in vitro*. *J. Cell Sci.*, 93:241, 1989.
- [206] M. Dogterom and S. Leibler. Physical aspects of the growth and regulation of microtubule structures. *Phys. Rev. Lett.*, 70:1347, 1993.
- [207] A. Janulevicius, J. van Pelt, and A. van Ooyen. Compartment volume influences microtubule dynamic instability: A model study. *Biophys. J.*, 90:788, 2006.
- [208] B. S. Govindan and W. B. Spillman, Jr. Steady states of a microtubule assembly in a confined geometry. *Phys. Rev. E*, 70:032901, 2004.
- [209] S. H. Tindemans and B. M. Mulder. Microtubule length distributions in the presence of protein-induced severing. *Phys. Rev. E*, 81:031910, 2010.
- [210] C. Erlenkämper and K. Kruse. Uncorrelated changes of subunit stability can generate length-dependent disassembly of treadmilling filaments. *Phys. Biol.*, 6:046016, 2009.
- [211] H. Flyvbjerg, T. E. Holy, and S. Leibler. Stochastic dynamics of microtubules: A model for caps and catastrophes. *Phys. Rev. Lett.*, 73:2372, 1994.
- [212] T. Antal, P. L. Krapivsky, and S. Redner. Dynamics of microtubule instabilities. *J. Stat. Mech.*, L05004, 2007.

- [213] L. Brun, B. Rupp, J. J. Ward, and F. Nédélec. A theory of microtubule catastrophes and their regulation. *Proc. Natl. Acad. Sci.*, 106:21173, 2009.
- [214] M. van Breugel, D. Drechsel, and A. Hyman. Stu2p, the budding yeast member of the conserved Dis1/XMAP215 family of microtubule-associated proteins is a plus end-binding microtubule destabilizer. *J. Cell Biol.*, 161:359, 2003.
- [215] L. R. Sproul, D. J. Anderson, A. T. Mackey, W. S. Saunders, and S. P. Gilbert. Cik1 targets the minus-end kinesin depolymerase Kar3 to microtubule plus ends. *Curr. Biol.*, 15:1420, 2005.
- [216] M. Ebbinghaus and L. Santen. Theoretical modeling of aging effects in microtubule dynamics. *Biophys. J.*, 100:(in print), 2011.
- [217] T. Manna, S. Honnappa, M. O. Steinmetz, and L. Wilson. Suppression of microtubule dynamic instability by the +TIP protein EB1 and its modulation by the CAP-Gly domain of p150Glued. *Biochemistry*, 47:779, 2008.
- [218] H. T. Schek III, M. K. Gardner, J. Cheng, D. J. Odde, and A. J. Hunt. Microtubule assembly dynamics at the nanoscale. *Curr. Biol.*, 17:1445, 2007.
- [219] E. Schulze and M. Kirschner. Microtubule dynamics in interphase cells. *J. Cell Biol.*, 102:1020, 1986.

Acknowledgments

On this last page, I would like to thank the people who helped me on my way to the completion of this PhD thesis:

First and foremost, I want to thank my two supervisors Cécile Appert-Rolland and Ludger Santen for their support, encouragement and scientific advice during my first steps in the world of research. In particular, I benefited greatly from performing my research in two different countries with two different research cultures. I am very grateful that they haven given me this opportunity, despite the organizational and administrative hazards.

I would also like to thank my fellow co-workers Matthias Brust, Philip Greulich, Olaf Leidinger, Otto Pulkkinen, Joachim Rambeau, Christof Schäfer and Ines-Kristin Weber for fruitful discussions on my work.

Both hosting institutions, the working group of Prof. Santen and the LPT at Paris-Sud University, have proven to be inspiring, warm and supportive environments that provided exceptional working conditions. I wish to thank all members of these two groups for making life at work that comfortable and trouble-free.

I also want to express my gratitude to Simona Helmsmüller, Philipp Ebbinghaus and Felix Ebbinghaus for their advice on no matter what topic and lately especially for proof-reading the manuscript of this thesis.

Finally, my thanks go to my parents for never leaving any doubt about their unre-served support and for sparking my interest in science.